Department of Physical and Macromolecular Chemistry

Faculty of Science

Charles University in Prague

PhD THESIS

New active systems for surface-enhanced Raman spectral probing of molecular and biomolecular species based on laser-ablated Ag nanoparticles and nanostructures

Karolína Šišková

Supervisors: Assoc.Prof. RNDr. Blanka Vlčková, CSc.

Prof. Pierre-Yves Turpin

Prague 2006

THESE DE DOCTORAT DE L'UNIVERSITE PARIS 6

Spécialité : Physico-chimie

Présentée par

Mlle **Karolína Šišková**

Pour obtenir le grade de

DOCTEUR de l'UNIVERSITE PARIS 6

Sujet de la thèse :

Elaboration de nouvelles nanostructures d'Argent, obtenues par ablation laser, pour caractériser des macro- et biomolécules par spectroscopie Raman exaltée par effet de surface

soutenue le 13 Decembre 2006

devant le jury composé de :

Mme Maître de conférence RNDr. Blanka Vlčková,CSc.	Directrice de thèse
M. Professeur Pierre-Yves Turpin	Directeur de thèse
M. Professeur Laurent Servant	Rapporteur
M. RNDr. Petr Štěpánek, DrSc.	Rapporteur
M. Maître de conférence RNDr. Marek Procházka, Ph.D.	Rapporteur
Mme Professeur Sophie Cribier	Examinateur
M. Professeur RNDr. Karel Procházka, DrSc.	Examinateur
M. Professeur RNDr. Jiří Vohlídal, CSc.	Examinateur

This work was elaborated in the frame of French-Czech PhD co-tutoring studies at the Department of Physical and Macromolecular Chemistry, Charles University in Prague, and at Université Pierre et Marie Currie, Paris VI, in Paris, and in BioMoCeTi UPMC/CNRS UMR 7033, in Evry, under the supervision of Assoc.Prof. RNDr. Blanka Vlčková, CSc. and of Prof. Pierre-Yves Turpin.

I guarantee that the work is original and only the literature listed in references was used.

Kateřina Šišková

Acknowledgment:

I would like to express my gratitude and my thanks to following persons:

Blanka Vlčková for her patient guidance of my Thesis and valuable discussions,

Pierre-Yves Turpin for his advice and worthwhile consultations in all aspects,

Jiřina Hromádková for measurements and pre-treating of TEM-images
(in Institute of Macromolecular Chemistry, ASCR, Heyrovsky Square, Prague 6, CR),

Alain Thorel *and* ***Arnaud Grosjean*** for HR-TEM measurements and valuable discussions
(in Centre des matériaux, UMR-CNRS 7633, Ecole des Mines de Paris, Evry, France),

Claire Fayet for TEM measurements
(in Service de Microscopie Electronique de l'IFR M 83 de Biologie Intégrative-CNRS-Paris VI, France),

Josef Štěpánek for worthwhile discussions,

Jiří Bok for updating program LabTolPb,

Vít Marek for calculations performed in program MatLab,

all members of research group BioMoCeTi settled in Evry,
all members of Dept. of Physical and Macromolecular chemistry Charles University in Prague, and
all members of Division of Biomolecular Physics, Institute of Physics
who helped me to solve various problems connected with this work,

my friends and *my family.*

For financial support I gratefully acknowledge:

French Foreign Affairs,
French Institute in Prague and
Le CROUS de Paris
for PhD co-tutoring support,

GACR grants 203/05/H001 and 203/04/0688.

« L'essentiel est invisible pour les yeux. »

Antoine de Saint-Exupéry : Le Petit Prince

(Folio, imprimé en France 2003, p. 76)

Content

Introduction

(1) Plasmonic metal nanoparticles

The unique tunable optical properties of plasmonic metal nanoparticles (NPs) and their assemblies are currently the subject of focused interest owing to their expansively growing applications in sub-wavelength optics [1], surface-enhanced Raman scattering (SERS) [2, 3], as well as chemical and biochemical sensors [4], hence, in general, these NPs are applicable in nanoscience and nanotechnologies [5].

The free-electron-like metal (e.g. Ag, Au, Cu and alkali) NP optics is based on localized surface plasmon resonances (LSPR) which represent collective oscillations of free electrons in the NP resonantly driven by the exciting radiation [6]. A majority of the above mentioned applications requires production of plasmonic NPs with desired LSPR [1,7].

The resonance frequency of isolated particles is affected by their size, shape (i.e. morphology) and optical constants of the particular metal together with the optical characteristics of the surrounding medium [8]; while in NP assemblies, interparticle distance is the major determining parameter [9].

In chemical preparations of plasmonic metal NPs, morphological characteristics are largely predetermined by the particular preparation procedure. On the contrary, the possibilities to control these characteristics are offered during preparations of plasmonic metal NPs by laser ablation (LA) [10] of a metal target in liquid ambient in combination with nanoparticle fragmentation (NF) [11] by the laser pulse impact.

The possibilities to control NP morphology by the parameters of laser pulse radiation employed in LA/NF, in particular by laser pulse duration, wavelength, energy and beam focusation have recently been intensively explored [11-76]. On the other hand, the effect of the presence of selected chemical species in the liquid ablation medium has been so far explored only marginally and has been mostly limited to simple ions [11-14]. There is thus a vast, yet unexplored potential in combining processes induced by pulse laser radiation during LA/NF with a specific molecular reactivity of selected molecular species. This approach can be one of the pathways to overcome a current problem in the production of chemically functionalized plasmonic metal NPs. It stems from the fact that the excellent chemical strategies of functionalized (capped) Ag and Au NP preparations (e.g. [15]) yield mostly NPs with sizes 2-6 nm, while those of sizes 20- 100 nm are required to provide largest LSPR in their functional assemblies, e.g. NP dimers [9].

One of the fields of plasmonics which could immediately benefit from the targeted preparations of plasmonic metal (and particularly of Ag) NPs by LA in chemically modified liquid ablation medium is SERS spectroscopy. This well-established analytical method [3, 77] is known for its potential ability of single molecule detection [78], nevertheless, in this Thesis, we are interested in the estimation of SERS spectral detection limit concentration value of a particular adsorbate (i.e. the detection of at least three characteristic SERS spectral bands of this adsorbate).

The following chapters of Introduction will deal with: (i) the mechanisms of LA, NF and the current state of research on this field; (ii) the description of the morphological and optical characteristics of NPs prepared by LA/NF process and the description of methodologies generally used for NPs properties determination; (iii) the brief explanation of the principles of SERS/SERRS phenomena and the most interesting applications of SERS and SERRS spectroscopy; (iv) some characteristics of molecules and biomolecules selected for SERS/SERRS spectral studies.

(2) Laser ablation and nanoparticles fragmentation

LA can be carried out in air and/or in liquid ambient. Principal differences between the mechanism of LA in each of these ambients have been found. The scope of this Thesis is focused on LA of a noble metal target (namely Ag) in liquid ambient. In the following chapters, the mechanism of LA of a metal target in air and in liquid ambient will be outlined and mutually compared. Subsequently, the attention will be focused on LA of noble metal targets in liquid ambient.

(2.1) Process of LA:

Laser ablation implies the removal of macroscopic amounts of matter from the surface of a solid material. During this process, the material must undergo a change of the fundamental state and a transformation into some volatile phase, e.g., a gas or a plasma [16].

The transition from the solid phase to the gas phase can occur in a stepwise process by the melting of the solid; under certain conditions, sublimation may occur, i.e., a direct transition between the solid phase and the gas phase; finally, laser radiation of sufficiently high intensity leads to ionization and transforms solid material into dense plasma [17] .

(2.2) Mechanism of LA in air:

Knowing the properties of a target material, one can try to establish the inter-correlation between the material properties and ablation efficiency. A sufficiently good correlation was found with the melting point temperature and material hardness [18]. Ablation efficiency is higher for metals with lower melting point temperature and hardness. This correlation was valid for three different regimes of interaction: ns, ps and fs, and for 1064, 532, 400 and 266 nm laser beam wavelengths [18].

In the same paper [18], it was shown that when the laser fluence was kept constant while the pulse duration was decreased, the optical electric field strength exceeded, at some point, the breakdown threshold of the material. Thus, plasma formation has been expected to become the dominant mode of laser ablation when the pulse duration was reduced. Analogous results, namely the best ablation efficiency obtained with a fs laser was reported also in [19, 20].

The interpretation of LA process on material energy states level:

The laser radiation interacts primarily with the electronic states of the valence and the conduction bands. The laser pulse width determines the time to deposit energy into these states. The deposited optical energy is subsequently redistributed over the various energy states of the system, mostly by carrier–carrier, carrier–phonon, and phonon–phonon interactions. The energy relaxation time t is the characteristic time to reach a thermal energy distribution, i.e., a Fermi–Dirac and a Bose–Einstein distribution for electrons and phonons, respectively. In metals and semiconductors, t is typically in the order of 10^{-12} to 10^{-11} s (1 to 10 ps). [16]

Other important time constants are the times for the transport of energy and mass. Energy transport can have a significant effect on the ablation threshold, which is the minimum energy fluence that must be supplied in order to remove material. The ablation threshold is expected to be higher in materials, in which the deposited energy is rapidly carried away from the surface and redistributed over a larger volume. Because ablation involves displacement of heavy particles, the ablation times are generally rather long, as they are determined by hydrodynamic and acoustic processes.

Two different regimes of laser–target interaction have been defined:

(1) A fs regime, where a laser pulse terminates before the energy is completely redistributed in the solid matter [21, 22]. It is likely that the energy is deposited in the matter without laser-plasma interaction resulting in a better ablation efficiency than the one in the ps and ns regimes.

(2) A ps-ns regime, where the pulse duration is of the same order or longer than the energy relaxation time. In this case, the irradiated volume heating is fast enough to vaporize the surface during the laser pulse, and plasma shielding can occur. The main result obtained in this case is a better efficiency with a ns pulse than with a ps pulse for the same wavelength and laser beam spots [18]. To explain this larger efficiency for a nanosecond case the following phenomena in the laser-matter interaction process should be taken into account:

- The hydrodynamic motion of the ablated matter during the laser pulse: the ablation should be considered as a dynamic process because the vaporization front moves into the solid matter during the pulse. Hence, both the ablated depth and the volume increase with the laser pulse duration increase [23].
- Laser pulse energy absorption in the dense near-surface plasma: the two main factors responsible for plasma absorption are: laser intensity and the plasma particle density. Both of them are larger in the case of ps pulse than in the ns pulse case. Thus, it can be concluded that for ps pulses the plasma absorption is larger and, consequently, the LA efficiency is lower [18].

(2.3) Mechanism of LA in liquid ambient:

A change of the ablation medium from air to a solvent (water and/or organic solvent) principally changes the LA efficiency. For example: in air, the craters generated by fs pulses are deeper and smaller in diameter than those generated by ns pulses [24]. A corona structure is observed on the edge of crater generated by ns pulses, while the edge of crater generated by fs pulses is smooth. The shape and the volume of the crater prepared in water in the case of ns ablation is similar to those of the crater prepared in air [24]. On the other hand, the shape and the volume of the craters prepared by fs pulses significantly changed with surrounding medium. The crater prepared by fs pulses in water is much shallower than that prepared in air [24]. Thus, the LA efficiency in water decreased in comparison to that performed in the air for fs pulses.

One possible explanation on the lowering of the ablation efficiency (in the case of fs ablation) caused by water presence will be energy transfer from the surface of the target to water. Since the electron-phonon energy relaxation and evaporation of matter in the fs ablation is a dark process, a lower temperature layer will be generated in the surface of target if the energy transfer occurs during the electron-phonon energy relaxation process.

Such cooling of the surface of target by water can be compensated by continuous irradiation of laser light in the case of ns ablation, because irradiation by a ns pulse continues during and after the electron-phonon energy relaxation.

On the other hand, if we assume that fs ablation is a direct solid-vapor transition, the energy transfer to water can be negligible and water will not provide the cooling effect. Thus, another possible explanation of the decrease in the ablation efficiency has been invented in [24]: the non-linear excitation of water near the focus

point induced by the high peak intensity of a fs pulse. The non-linear excitation of water will cause fluctuation of the refractive index of water. Consequently, the scattering of laser light can take place near the focus point, leading to a decrease in incident energy onto the surface of target. In fact, white-continuum emission from the focus point was observed when fs laser light was focused onto a target in water [24].

Tsuji et al. [25] have reported on an observation of ablation (by ns laser pulses) reactions, especially ejection events, occurring at the interface of metal target (Ag, Au) and water by means of microsecond time-resolved shadowgraphy. Two different ablation reactions at the metal target–water interface were observed in the shadowgraphs. One is a straight jet and the other is a bubble. The origin of the bubbles is ascribable to the generation of plasma which must contain atoms, molecules and ions of metal and water. Furthermore, they propose [25] that generation of the straight jet can be assigned to ejection of massive clusters and droplets of metal from a metal target (because the heavy clusters and droplets can penetrate a cage of solvent more efficiently than light plasma gas). On the assumption that the straight jet consists of massive clusters and droplets of metal, it can be considered as the main process of metal NPs formation. Larger nano-sized colloidal particles must be produced from the clusters and droplets in the jet via aggregation and cooling processes.

A similar hypothesis has been estimated by Yoo et al. [26]. They assume that the mass removal from metal target is mainly due to the ejection of massive clusters and droplets, while the contribution of plasma gas is small.

However, the temperature and pressure in water-confined plasma bubbles have been estimated to be more than 10^3 K and 10^9 Pa [27], respectively. Due to the high pressure and temperature, the surface of metal target can be ablated by plasma gas in the bubbles. It was shown that the enhancement of ablation efficiency in liquids compared to that in gas (for ns laser pulses) was due to such secondary ablation by plasma [28].

Moreover, very recently, Kabashin and Meunier [29] explained the two different distributions of NPs sizes (around 20 nm and 70 nm) prepared by fs LA on the basis of two different ablation mechanisms. One is direct ablation by laser light (radiation-mechanism) and the other is the secondary ablation by plasma (plasma-related mechanism). They note that the relative contribution of the plasma-related mechanism can be weakened or undetected by a decrease of laser energy during the experiment, leading to a reduction of the mean size of the NPs produced in deionized water. Thus, the energy decrease is accompanied with a decrease in the efficiency of NP production.

Results confirming the two mechanisms of LA by fs laser pulses were presented in [30].

(2.4) Role of NPs presence during LA:

Another characteristic factor influencing the LA process in the liquid medium is the presence of NPs [11, 31]. Unlike in air systems, the ablation of metals in a liquid medium results into the formation of metal particles. Resulting metal NPs are dispersed in the liquid ablation medium, forming a hydrosol (provided that the ablation medium is water), or an organosol (in an organic solvent). In all types of experimental setups reported, Fig. 1, the incident laser light has to pass through the NP sol prior to its impact on the metal target. The metal NPs can absorb the incident laser light of a particular wavelength, [Introduction, Section (3)].

The efficiency of the absorption of laser light of a particular wavelength depends on absorption spectra of the NP hydrosols. For example: based on the absorption spectra of the Ag hydrosols, the efficiencies of the absorption by Ag NPs at 355 and 532 nm must be higher than that at 1064 nm [32] due to the plasmon bands around 400 nm [Introduction, Section (3)]. The effective fluence of laser pulses (i.e. reaching the Ag target) is thus lower for pulses of 355 and 532 nm wavelength than for those of 1064 nm wavelength. Therefore, a lower efficiency of hydrosol formation is observed for 355 and 532 nm pulses than for those of 1064 nm. The difference in LA efficiency is more pronounced at higher laser fluences, since more metal NPs are produced.

In ref. 18, two processes of the laser pulse absorption by metal NPs are described. One process is "inter-pulse" absorption, in which particles produced by the earlier pulses stay in the laser light path and absorb the subsequently coming pulses. The other is "intra-pulse" absorption, in which particles produced by the earlier part of one pulse immediately absorb the photons of the later part of the same pulse. The latter process must be taken into account when the ns laser pulses are used for the ablation of metals because the ejection of the ablated matter begins on a ps time scale [18]. The relative contributions of the inter-pulse and intra-pulse absorptions to the ablation efficiency can be determined from the fact that the efficiency of the inter-pulse absorption increases with the accumulation of the particles, while that of the intra-pulse absorption is constant [31].

Furthermore, to reduce a possible "micro-concentration" effect caused by the localized NPs in the vicinity of the target surface, the stirring of solution was introduced [11, 31]. This stirring can, however, decrease ablation efficiency as it was reported by Procházka et al. [11]. Such a decrease of the ablation efficiency was explained in terms of the increased effect of the inter-pulse absorption by stired solutions because the NPs spread over the entire laser light path.

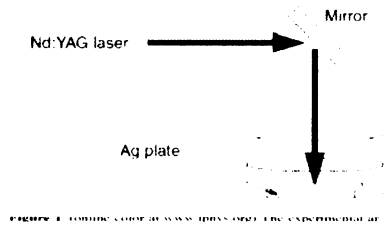

F. Hajiesmaeilbaigi et al., Laser Phys. Lett. 3, No. 5 (2006) p. 252.

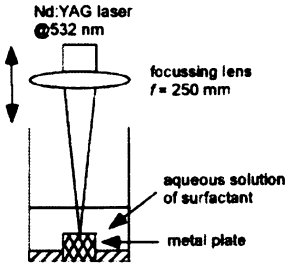

Mafune et al., J. Phys. Chem. B 104, No. 39 (2000) p. 9111.

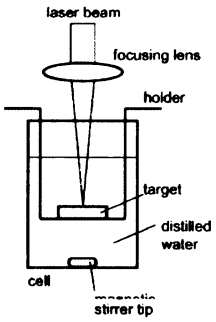

T. Tsuji et al., Applied Surface Science 202 (2002) p. 80.

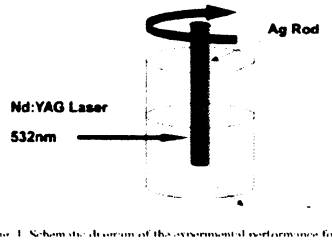

Y.-H. Chen et al.,Colloids and Surfaces A : Physicochem. Eng. Aspects 197 (2002) p. 133.

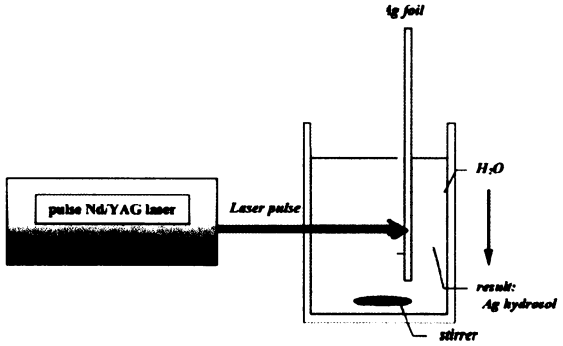

Šmejkal et al., Spectrochimica Acta Part A 59 (2003) p. 2321.

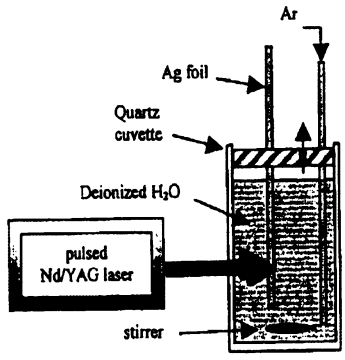

Pfleger et al., SPIE 5122 (2003) p. 198.

Fig. 1: Various experimental setups for laser ablation |

(2.5) Current state of research and parameters influencing LA process:

To summarize the published important and interesting information about LA of a metal target immersed in various types of liquid ambient, an overview of experimental studies on LA is provided in Table I. In addition, there are many theoretical simulations of LA. The seminal papers appear to be for example: reference 33 in which molecular dynamics simulations are employed to discuss dependence of mechanism of LA on the initial temperature and pulse duration [33]; ref. 34 demonstrating that the ablation process involves three different mechanisms as a function of deposited energy; [35] which provides an overview of the different modeling approaches available for LA and a detailed description of the interactions of ns pulses with a Cu target.

Furthermore, different factors which can influence NPs formation in the LA process will be clasified. First of all, the factors will be divided into four different groups: (a) physical, (b) chemical, (c) physico-chemical, and (d) technical parameters.

Physical parameters that affect the results of LA are the following: laser pulse duration [16, 18-20, 24, 36-39], laser pulse wavelength [18-20, 31, 40-45], energy per pulse and laser beam focusation [11, 31, 46-48] which defines the irradiated spot area. Energy per pulse is frequently related to the irradiated spot area and expressed in terms of fluence (in [J.cm^{-2}]) [11, 18, 19, 31, 40-42, 46, 49-59]

The basic chemical parameters of LA are the identity of the selected metal [16, 18-20, 25, 31, 38, 44, 50, 60, 61] and of the solvent [43, 44, 53, 58, 60]. Additional; but very important chemical parameters are the presence of simple ions [11-13, 48, 62] and/or more complex ions [14, 36, 45, 51, 55-58, 63-65], or even of

Table I: List of selected publications concerning laser ablation

Article	Pulse duration	Laser wavelength	repetition rate of pulses	energy in a pulse or fluence	Ablation time	Target	Medium	surfactant
Bae et al., Applied Surface Science 2002, 197-198	5 ns	1064 nm	10 Hz	6.4 J/cm²	5 min	Ag	water	NaCl
Brause et al., Applied Physics B, Laser and Optics 2002, 75, 711-716.	ns	532 nm 355 nm	10 Hz	100 mJ/pulse 130 mJ/pulse	30, 60 min 5-30 min	Ag	water	-
Burakov et al., Eur. Phys. J. Appl. Phys. 2005, 30, 107-112	ns	1064 nm 532 nm	10 Hz	50 mJ/pulse	8 min	Ag, Cu	water, acetone	-
Chen et al., Colloids and Surfaces A: Physicochem. Eng. Aspects 2002, 197, 133-139	5 ns	532 nm	10 Hz	120 mJ/pulse 60 mJ/pulse	10 min	Ag	water	SDS, CTAB
Compagnini et al., J. AppL. Phys. 2003, 94, 7874-7877	5 ns	532 nm	10 Hz	1-200 J/cm²	?	Au	liquid n-alkanes	
Hajiesmaeilbaigi et al., Eur. Phys. J. Appl. Phys. 2005, 30, 107-112	20 ns	1064 nm	5 Hz	50 - 80 mJ/pulse	5 - 20 min	Ag	water	-
Kabashin et al., J.Appl.Phys. 2003, 94, 7941-7943	110 fs	800 nm	1 kHz	400 J/cm²	20 min	Au	water	-
Kabashin et al., J. Phys. Chem. B 2003	110 fs	800 nm	1 kHz	max. 1 mJ/pulse	?	Au	water	α-CD, β-CD, γ-CD
Mafuné et al., J. Phys. Chem. B 2000, 104, 8333-8337	~10 ns	532 nm	10 Hz	<90 mJ/pulse	?	Ag	water	SDS
Mafuné et al., J. Phys. Chem. B 2000, 104, 9111-9117	~10 ns	532 nm	10 Hz	<90 mJ/pulse	?	Ag	water	SDS
Mafuné et al., J. Phys. Chem. B 2001, 105, 5114-5120	~5 ns	1064 nm	10 Hz	80 mJ/pulse	?	Au	water	SDS
Mafuné et al., J. Phys. Chem. B 2001, 105, 9050-9056	~5 ns	1064 nm	10 Hz	80 mJ/pulse	?	Au	water	SDS
Mortier et al., Chem. Phys. Lett. 2003, 382, 650-653	ns	1064 nm	50 Hz	5-15 mJ/pulse	10 min	Au	$CHCl_3$	CTAB

Table I: List of selected publications concerning laser ablation - continuation

Pfleger et al., Proceedings of SPIE 2003, 5122, 198-205	6 ns	1064nm	10 Hz	310 mJ/pulse	from 2 to 18 min	Ag	water	-
Prochazka et al., Anal. Chem. 1997, 69, 5103-5108	20 ns	1064 nm	10 Hz	10 mJ/pulse 20 mJ/pulse 30 mJ/pulse 30 mJ/pulse	240 min 90 min 30 min 15 min	Ag	water	- $NaNO_3$, NaCl
Pyatenko et al., ppl. Phys. A 2004, 79, 803-806.	10 ns	532 nm	10 Hz	50-340 mJ/pulse	30 s - 5 min	Ag	water	-
Semerok et al., Appl. Surf. Sci. 1999, 138-139, 311-314	4 ns 25 ps 18 ps 13 ps 150 fs	532 nm, 266 nm 1064 nm 532 nm 266 nm 400 nm	?	1-1000 J/cm²	?	Al, Cu, Mo, Fe, Pb, Ni	air	-
Simakin et al., Chem. Phys. Lett. 2001, 348, 182-186	20 ns	510.6 nm	15 kHz	10-30 J/cm²	?	Ag, Au	water	-
Simakin et al., Appl. Phys. A 2004, 79, 1127-1132	20 ns	510.6 nm	15 kHz	16-55 J/cm²	2 hours	Ag, Au, Ti	water, ethanol, $C_2H_4Cl_2$	only for EtOH addition of PVP
Srnova et al., Langmuir 1998, 14, 4666-4670	40 ps	1064 nm	1 Hz	40 mJ/pulse	30 min	Ag	water	NaCl, pht,
Sylvestre et al.,J. Phys. Chem. B, 2004; Vol. 108, pp 16864-16869	120 fs	800 nm	1 kHz	<1 mJ/pulse	?	Au	water	KCl, NaCl, NaOH, $NaNO_3$, N-propylamine
Sylvestre et al., Appl. Phys. A: Materials Science & Processing 2005, 80, 753-758	120 fs	800 nm	1 kHz	0.25 mJ/pulse	?	Au	water	-
Šmejkal et al., Spectrochim. Acta A 2003, 59, 2321-2329	6 ns	1064 nm	10 Hz	310 mJ/pulse	from 2 to 18 min	Ag	water	-
Šmejkal et al., Journal of Physics - accepted 2006	6 ns	1064 nm 532 nm 355 nm	10 Hz	0 - 27.5 mJ/mm² 0 - 21 mJ/mm² 0 - 15.5 mJ/mm²	5, 10, 20 min 20 min 30 min	Ag	water	-
Tarasenko et al.,Appl.Surf.Sci 2005, 247, 418-422	10 ns	532 nm 1064 nm	?	50 mJ/pulse	?	Ag	acetone water	-

Table I: List of selected publications concerning laser ablation - continuation

Tsuji et al., J.Photochem. Photobio. A: Chemistry 2001, 145, 201-207.	5-9 ns	1064 nm 532 nm 355 nm	10 Hz	900 mJ/cm² >12 mJ/cm²	10 min	Ag, Cu	water	-
Tsuji et al., Applied Surface Science 2002, 202, 80-85	ns	1064 nm 532 nm 355 nm	?	12-36 J/cm²	30 min	Ag	water	-
Tsuji et al., Applied Surface Science 2003, 206	120 fs	800 nm	10 Hz		30 min	Ag	water; air	-
	8 ns	800 nm	10 Hz	4 mJ/pulse				
Tsuji et al., Appl. Surf. Sci. 2004, 229, 365-371.	10 ns	1064 nm	?	18 J/cm²	-	Ag, Au, Si	water	-
von der Linde, Appl. Surf. Sci 2000, 154-155, 1-10	100-120 fs	620 nm	?	<plasma formation	?	Ti, Al, Au, GaAs	air	-
	5 ps	620 nm						
Zhao et al., Chemistry Letters 2003, 32, 602-603	120 fs	800 nm	1 kHz	0.5 mJ/pulse	<30 min	-	water	$HAuCl_4$
				0.36 mJ/pulse	<30 min	-	water	$HAuCl_4$, TiO_2
Zhu et al., Appl. Phys. Lett. 2001, 79, 1396	23 ns	248 nm	?	3.1 J/cm²	1000 pulses	Si	water	-

Note: CD = cyclodextrin; CTAB = cetyltrimethylamonnium bromide; pht = phtalazine; PVP = polyvinylpyrrolidione, SDS = sodium dodecylsulphate, ? = The information was not found throughout the article.

adsorbates (i.e. species which adsorb on NPs surface) [13, 53, 62, 66], these all are also involved in chemical parameters influencing LA process.

Furthermore, it seems to be important how the experimental setup is arranged. In general, several different arrangements have been employed in the published papers, and their overview is shown in Figure 1. The technical parameter which is closely related to the experimental arrangement is the possibility or impossibility to stir during LA.

The last type of parameter which are denoted in this Thesis as the physico-chemical ones has not been sufficiently evaluated in the literature so far. The particular parameter which, in this Thesis, has been investigated and found important, is the presence (or absence) of breaks (pauses) in the course of the LA process. LA has been mostly performed from several minutes to several hours without regular interruptions. In ref. 11, the LA process has been interrupted to perform SPE measurements and follow thus the progress of LA. Furthermore, Pyatenko et al. [52] tried to follow the LA process as a function of time (using sampling times of 30 s and/or 60 s) during a 5-min LA – Table I.

In the latest published article [42] the efficiency of NPs formation has been investigated as a function of various ablation times (durations). The experiments have been carried out separately in four different samples which might possibly cause the peculiar decrease of LA efficiency after 15 min, and its recovery after 20 min. Such problem is avoided when the step-wise LA is performed in one particular sample, and its progress is followed after each LA step. Therefore, this approach has been generally adopted in this Thesis. Furthermore, the importance of the presence of absence of breaks in LA process is demonstrated in this Thesis by a direct comparison of the outcome of LA of Ag target in water carried out with and without regular interruptions, using the same physical parameters in both experiments. Moreover, it is revealed in the Thesis that the influence of pauses during LA is even more complicated in the presence of agents, such as thiosulphate, in the aqueous ablation medium [Chapter 4.7]. On the basis of the fact that the physical factor (i.e. the presence or absence of the interruptions during LA process) has a particular role in the chemistry of the NPs formation, particularly in the presence of a chemical agent, it is classified in my Thesis as physico-chemical parameter.

In the literature, the effect of each particular parameter on NPs formation by LA in liquid ambient has mostly been evaluated on the basis of SPE spectra; nevertheless, different characteristics have been used. Many authors, like for example Mafuné et al. [55] have discussed the LA efficiency of Au colloid formation on the basis of the absorbance value at 200 nm (A_{200}). Similarly, Tsuji et al. [31] have used the A_{250} value for Ag NPs formation. Both values, A_{200} or A_{250}, correlate with an interband transition in Au or Ag, respectively, and, thus, they provide information about entire metal content in a colloid.

Other authors [11, 48] use the A_{max} values of a SPE band, nevertheless, they carefully discuss that one can do so only provided that a Lorenzian-shaped band is observed and the FWHM value does not change markedly during the LA/NF process.

The first elegant experimental evidence of the correspondence between the integrated area below a SPE curve and Ag content (in mg/l) has been given in ref. 32. In comparison to that, we have tried to use the approximate area (= A_{max}*FWHM) of a particular SPE band to prove the NPs formation efficiency [67].

In the very beginning of the Thesis [Chapter 1], the criterion of the selection of parameters for the LA efficiency evaluation will be discussed.

(2.6) Mechanism of LA in a surfactant:

In the experiments of Mafuné et al. [36], i.e. LA/NF performed in the presence of a surfactant, it has been shown that (1) the NPs are produced above a threshold laser power, (2) their number density increases proportionally with the laser power, and (3) their average size increases with an increase in the laser power and decreases with increase in the surfactant concentration. These findings have been explained in terms of dynamic formation mechanism. This mechanism implies a rapid formation of an embryonic silver particle and a consecutive particle growth in competition with termination of the growth due to surfactant coating on the particle. Let us consider the particle formation in a chronological order. Immediately after the laser ablation, a dense cloud of silver atoms is built over the laser spot of the metal plate. As the inter-atomic interaction is much stronger than the interaction between a silver atom and a surfactant molecule or a solvent molecule, silver atoms are aggregated as much as silver atoms are supplied. This initial rapid aggregation continues until silver atoms in the close vicinity are consumed almost completely. As a result, an embryonic silver particle forms in a region void of silver atoms (cavity). However, the supply of silver atoms outside the region through diffusion causes the particle to grow slowly even after the rapid growth ceases. In competition, the slow growth tends to be terminated by coating the particle surface with surfactant molecules, which diffuse through the solution toward the particle.

The surface coverage increases with the surfactant concentration and at extreme the surface is covered by a bilayer. Evidently, the NPs are resistant against re-aggregation when the particle surfaces are sizably charged and covered fully with the surfactant molecules; otherwise the NPs are prone to aggregation. It follows that the stability of a NP is affected by the coverage, or more practically, by the concentration of a surfactant [68].

(2.7) Additional irradiation of Ag NP sols by laser pulses:

In addition to that, a NP sol can be irradiated by laser pulses in the absence of a metal target [11]. In the case of irradiation of the sol by ns laser pulses, the sizes of NPs were found to be reduced during this process and the process itself has been dubbed nanoparticle fragmentation (NF) [11]. Further investigations have revealed that observation of NF during additional irradiation of NP sol (which manifests itself by size-reduction of the NPs) is strongly dependent on laser pulse duration. For example, Link et al. [37] have shown that while irradiation with ns pulses generally leads to NF, with fs pulses, this process is observed only for high energies per pulse.

Furthermore, not only the size, but also the shape of the particles has been found to change during additional irradiation. Such NP-reshaping from a non-spherical to a spherical shape has been clearly observed, e.g. during irradiation of Au nanorods (ellipsoidally shaped NPs) with fs pulses of lower energies (at which NF has not occurred). The mechanisms of processes leading to NP size-reduction and/or reshaping are discussed in [Introduction, Section (2.8)].

Finally, it has been noted that absorption of laser pulses during additional irradiation of NP sol by ns laser pulses proceeds analogously to inter-pulse absorption during LA [Introduction, Section (2.4)]. Therefore, NF occurs not only during the additional irradiation of a sol by ns laser pulses, but also during the process of LA itself (with ns laser pulses). To emphasize this point, the term LA/NF is used throughout this Thesis.

(2.8) Mechanisms of NP size-reduction and/or reshaping induced by laser pulses:

Several mechanisms of the laser-induced NP size-reduction and/or reshaping of (mostly chemically) pre-prepared NPs were described: (i) photo-melting (preparation of spherical NPs) [37, 54, 59], (ii) photo-fragmentation induced by multiphoton absorption [37, 54 , 59, 69], and (iii) photo-dissolution of NPs [70].

It appears important to distinguish between mechanisms occurring under ns, ps, or fs laser pulses irradiation. Nevertheless, only Kamat et al. [69] and Link et al. [37] compared mechanisms of the processes in the different time-regimes: ps with ns and fs with ns, respectively (Table II).

Link et al. observed Au-nanorods fragmentation under ns laser pulses, and under fs laser pulses, only at higher energies in a pulse, while at lower energies in a fs laser pulse, only melting occurred. They considered that the initial absorption heats the electrons within fs [71, 72]. This is then followed by electron-phonon relaxation processes in the 1-3 ps time domain [71, 72]. This leads to an increase in the metal atom kinetic energy and melting of the NPs. In the fs irradiation, this occured in the dark since the laser pulse width (100 fs) was shorter than the electron-phonon relaxation time (1-3 ps). In the nanosecond experiments, the hot molten NPs were continuously bathed with light from the ns laser pulse. The authors thus expect [37] that absorption of more photons by the hot lattice occurring in the ns experiment is what leads to an increase in the lattice internal energy and, consequently, to the NF. Furthermore, they have shown that by a sufficient increase of the fs-pulse energy, the mutiphoton ionization processes occur, and thus the NF has been observed at these pulse durations too [37].

The same result of NF with ns laser pulses was published by Kurita et al. [54, 59]. They ascribe the NP shape change to melting because the liquid droplet is spherical, and thus the nonspherical shape of original NPs is lost [59]. However, they consider that during a single laser pulse, one gold NP absorbs consecutively more than 1000 photons and is heated to its boiling point. When the temperature of the NP rises to the boiling point, atoms and/or small particles are ejected through vaporization [59]. As a result, the particle size is reduced. The amount of the ejected atoms and/or small particles depends on the absorbed laser energy. The maximum diameter is determined through the balance between the ejection of atoms and/or small particles through vaporization and the deposition of ejected atoms and/or small particles on the particle. Because the ejected atoms and/or small particles are very unstable in aqueous solution, they tend to agglomerate and/or deposit on the particles remaining in the solution.

In ref. 54, the occurrence of NF due to the presence of some cracks in the original NPs is mentioned.

Kamat et al. [69] have explained the photo-fragmentation of NPs by the following reactions:

$$(Ag)_n + 2h\nu \rightarrow (Ag)_n^+ + e_{aq}^- \qquad (1)$$

$$(Ag)_n^+ + e_{aq}^- \rightarrow (Ag)_n^* \qquad (2)$$

$$(Ag)_n^* \rightarrow (Ag)_{n-x} + xAg \qquad (3)$$

The photo-ejection of electrons (reaction 1) is an ultrafast biphotonic process and is completed within the laser-pulse duration of 18 ps. Although some of these ejected electrons undergo quick recombination (reaction 2), the rest will accumulate at or near the NP surface. The electrons that do not undergo photo-ejection are rapidly thermalized by electron-phonon scattering. The time scale for this process is around 1-3 ps [71, 72]. The energy deposited into the phonon modes is subsequently transferred to the surrounding medium on a 10-100 ps time scale [71]. The dumping of thermal energy into the solvent causes the change of dielectric function of the surrounding medium, which in turn, influences the plasmon resonance frequency of the silver nanoclusters. Electron ejection process, which is predominant at high laser excitation intensities, leads to the charging of the surface of the 50-60 nm diameter metal

Table II: List of selected publications concerning nanoparticle fragmentation

Article	Pulse duration	Laser wavelength	Repetition rate of pulses	Energy per pulse or fluence	NF time	Target
Bae et al., Applied Surface Science 2002, 197-198	7ns	355 nm	10 Hz	6.4 J/cm²	3 min	1064nm-LA Ag colloid in water and/or in NaCl
Brause et al., Applied Physics B, Laser and Optics 2002, 75, 711-716.	ns	532 + 355 nm 355 nm	10 Hz	100 + 130 mJ/pulse 130 mJ/pulse	60 + 60 min 5-25 min	citrate-reduced Ag colloid 532nm-LA Ag colloid
Burakov et al., Eur. Phys. J. Appl. Phys. 2005, 30, 107-112	ns	1064 nm 532 nm 1064 + 532 nm	10 Hz	0.35 - 5 J/pulse	1-8 min	1064nm-LA Ag colloid in water 1064nm-LA Ag colloid in acetone
Hajiesmaeilbaigi et al., Eur. Phys. J. Appl. Phys. 2005, 30, 107-112	20 ns	1064 and/or 532 nm 1064 + 532 nm	5 Hz	70, 38 mJ/pulse 70 + 38 mJ/pulse	5 min, 5 min 5 + 5 min	1064nm-LA Ag colloid in water
Kamat et al., J. Phys. Chem.B 1998, 102, 3123-3128	18 ps 6 ns	355, 532 nm 355 nm	10 Hz	2-3 mJ/pulse <10 mJ/pulse	3 min	citrate-reduced Ag colloid
Kurita et al., Appl. Phys. Lett. 1998, 72, 789-791	7 ns	532 nm	10 Hz	<60 mJ/pulse	5-60 min	citrate-reduced Au colloid
Link et al., J. Phys. Chem. A 1999, 103, 1165-1170.	100fs 7 ns	800 nm 800 nm	1 kHz 10 Hz	40 μJ/pulse 20 mJ/pulse	?	Au nanorods prepared electrochemically in micelles
Mafuné et al., J. Phys. Chem. B 2001, 105, 5114-5120	~5 ns	532 nm	10 Hz	50 mJ/pulse	60 min	1064nm-LA Au colloid in SDS
Mafuné et al., J. PHys. Chem. B 2001, 105, 9050-9056	~5 ns	532 nm	10 Hz	<400 mJ/pulse.cm²	5-40 min	1064nm-LA Au colloid in SDS
Mafuné et al., J. Phys. Chem. B 2002, 106, 7575-7577	ns	532 nm	10 Hz	320, 480 and/or 1200 mJ/pulse.cm²	?	1064nm-LA Au colloid in SDS
Mafuné et al., J. . PHys. Chem. B 2002, 106, 8555-8561	ns	532 nm	10 Hz	200, 400 and/or 800 mJ/pulse.cm²	?	1064nm-LA Au colloid in SDS
Mafuné et al., J. Am. Chem. Soc. Commun. 2003, 125, 1686-1687	ns	532 nm	10 Hz	2.2 J/pulse.cm²	?	a mixture of 1064nm-LA Au and Pt colloids
Mafuné et al., J. PHys. Chem. B 2003, 107, 12589-12596	ns	532 nm	10 Hz	5 J/pulse.cm²	20 min	a mixture of 1064nm-LA Au colloid in SDS and in water
Mafuné et al., Chem. Phys. Lett. 2003, 372, 199-204	ns	355 nm 532 nm	10 Hz	80 mJ/pulse	?	1064nm-LA Au colloid in SDS

Table II: List of selected publications concerning nanoparticle fragmentation - continuation

Pfleger et al., Proceedings of SPIE 2003, 5122, 198-205	6 ns	1064 + 532 nm	10 Hz	310 + 170 mJ/pulse	20 + 12 min	1064nm-LA Ag colloid in water and/or citrate-reduced Ag colloid
Šmejkal et al., Spectrochim. Acta A 2003, 59, 2321-2329	6 ns	1064 + 532 nm	10 Hz	310 mJ/pulse + 170 mJ/pulse	20 min + 12 min	1064nm-LA Ag colloid in water
Šmejkal et al., Appl. Phys. A 2004, 79, 1307-1309	6 ns	355, 532 and/or 1064 nm	10 Hz	85, 170 and/or 310 mJ/pulse	from 1 to 1800 pulses (3 min)	citrate-reduced Ag colloid
Takami et al., J. Phys. Chem. B 1999, 103, 1226-1232	7 ns	532 nm	10 Hz	14-800 mJ/cm²	5-120 min	citrate-reduced Au colloid
Tarasenko et al., Appl.Surf.Sci 2005, 247, 418-422	10 ns	266, 532 nm 400, 800 nm	10 Hz	100, 500 mJ/cm² 100, 600 mJ/cm²	5 min	1064nm-LA Ag colloid in acetone 532nm-LA Ag colloid in acetone

Note: SDS = sodium dodecylsulphate; ? = The information was not found throughout the article.

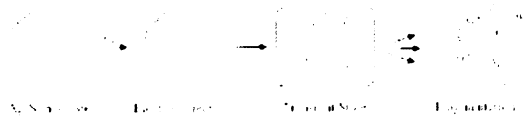

Fig. 2: Fragmentation of Ag cluster with laser excitation. A transient aggregate formed via the photoejection of electrons is consider to be a precursor for complete fragmetation of the particle take from [Kamat et al., J. Phys. Chem. B 102 (1998) p. 3123].

nanoclusters. This in turn causes them to disintegrate and form smaller-size particles (5-20 nm diameter) – as shown in Fig. 2.

The third possibility of NP reshaping is complete photo-dissolution followed by the reduction of Ag^+ ions with aqueous electrons to form smaller particles. This dissolution process, investigated in the earlier study of Linnert et al. [70], dominates only when photo-ejected electrons are scavenged with species such as N_2O.

(2.9) Parameters influencing NF of pre-prepared hydrosols with ns laser pulses:

In the previous [Section (2.8)], it has been shown that laser pulse duration is the key parameter affecting the mechanisms and outcome (size-reduction and/or reshaping of NPs) of additional irradiation of pre-prepared NP hydrosols by laser pulses. The affect of other parameters has been further investigated for irradiation by ns pulses, i.e. in the regime when size-reduction of the NP due to NF generally occurs (Table II). The wavelength of the laser pulses emerges as a key parameter affecting the efficiency and the rate of NF as well as the optical and morphological characteristics of resulting NPs [41-45, 73] because different sized particles can be excited at different laser excitation wavelengths. For instance, the NF of citrate-reduced Ag hydrosols [73], carried out with laser pulses of 1064, 532 and 355 nm wavelengths, has shown that the 532-nm pulses are the most efficient (from these three selected wavelengths) in the NF of the largely polydisperse Ag hydrosols containing spherical and ellipsoidal NPs together with nanowires. Tarasenko et al. [43], who performed NF under four different laser wavelengths (266 – 800 nm), have pointed out the fact that the work function of silver is about 4.3 eV and thus the photoemission of electrons is a monophotonic process for 266 nm laser excitation, while in the others (400, 532 and 800 nm) the contribution of multiphoton photoeffect should be taken into account (as described in previous section).

With respect to the mechanism of NF, a certain amount of energy is required, hence, there is a threshold fluence has to be achieved in order to that NF can proceed [43, 44, 55-57]. Furthermore, the time of irradiation has its proper role [43, 44, 54, 55, 59, 73] too.

Similarly to the chemical parameters affecting LA (see above), the choice of solvent [43, 44] and the presence of simple ions [12] and/or surfactant in the ablation ambient [14, 45, 55-57, 65] are important.

The effect of the surfactant presence has been exhaustively studied by Mafuné et al. and it is quite fascinating to follow their investigations. In 2001, they published their first results about the NF carried out with 532 nm pulses of a ns laser on the Au colloid pre-prepared by LA at 1064 nm in a surfactant [55, 65]. They have discussed their results in terms of the laser-assisted fragmentation of a parent NP and the aggregation of a product NP with atoms and small fragments, i.e. in an analogous manner as Kurita et al. [54, 59]. The only exception from the mechanism proposed by Kurita et al. is that the surfactant molecules were present in the solution, therefore, the growth by the aggregation was greatly retarded so that smaller NPs tended to be produced in a more concentrated surfactant solutions.

Furthermore, they discovered in ref. 55 that the smallest possible diameter of produced NPs decreased with the laser fluence increase, however, they showed that aggregation of the nanoparticles is not negligible when the laser fluence is very high [55]. Thus, to obtain well-dispersed NPs with a desired average size they have advised to tune properly the surfactant concentration and the laser fluence [56, 57].

In their next article [14], they investigated NF in various mutual ratios of Au-LA colloids prepared (a) in the absence and (b) in the presence of a surfactant. In the same year, 2003, they came out [74] with a new strategy how to prepare nanowebs (constructed by the platinum NPs with gold nanojoints) by choosing the wavelength of laser pulses and appropriate fluence, i.e. they irradiated a mixture of Pt and Au LA-prepared colloids and observed "nano-soldering".

Finally in ref. 45, they have tried to fragment gold NPs by excitation into Au interband transition by employing the 355-nm laser pulse irradiation. As a result, smaller nanoparticles (~2 nm) and clusters with sizes smaller than 20 Au atoms were produced by excitation of the interband transition in a sufficiently concentrated SDS (sodium dodecylsulphate) solution. Their observation exemplifies feasibility of the laser-induced size control for preparation of very small nanoparticles and clusters with a narrow size distribution, which are stabilized by weakly bound surfactant molecules.

The same group then has continued to study NF in the presence of DNA [75] and, very recently, they have employed the 532nm-irradiation of a pulse laser to protein degradation due to nanoplasma created by gold NPs [76].

(3) NPs properties and methodologies of their investigation

Metal NP, and the plasmonic metal NPs in particular, have quite unique optical properties. The interaction between a metal NP in a dielectric medium and electromagnetic radiation is briefly described below.

(3.1) Surface Plasmon Resonance (SPR):

Electromagnetic surface waves can propagate along the interface between conducting materials and a dielectric [79] over a broad range of frequencies, ranging from dc and radio frequencies up to the visible. The oscillation modes form an electromagnetic field coupled to the oscillations of conduction electrons and are called surface plasmon resonance (SPR). They are characterized by strong field enhancement at the interface, while the electric field vector decays exponentially away from the surface (in the nm range) [80]. When the dimensions of the conductor are reduced, boundary and surface effects become very important and the SPR becomes spacially localized, dubbed localized surface plasmon resonances (LSPR). The optical properties of small metal NPs are thus dominated by such a collective oscillation of conduction electrons in resonance with incident electromagnetic radiation [81-83] .

For many metals such as Pb, In, Hg, Sn, and Cd, the SPR frequency lies in the UV part of the spectrum and NPs do not display color effects [84]. Such small metal particles are also readily oxidized making SPR experiments difficult. On the other hand, the coinage elements (Cu, Ag, and Au) are exceptional. First they are more noble and form more air-stable sols. Second, LSPR wavelength falls into the visible part of the spectrum.

In simple terms, the LSPR can be viewed as follows: the electric field of the incoming radiation induces an oscilating dipole in the NP (considering a dipolar approximation), and there is a restoring force that tries to compensate it, so that a unique LSPR frequency matches this electron oscillation within the NP (Fig. 3). The resonance excitation of such dipole is also dubbed dipolar surface plasmon excitation.

The LSPR arises from the particular dielectric properties of the metals, thus, they can be modeled using the equations derived by Mie for the resolution of Maxwell equations for the absorption and scattering of electromagnetic radiation by small spheres [85] and their modification by Gans for ellipsoids [86].

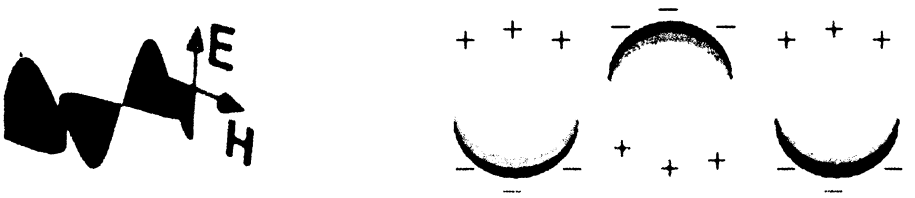

Fig. 3: Schematic drawing of the interaction of an electromagnetic radiation with a metal nanosphere. A dipole which oscillates in phase with the electric field of the incoming light is induced - taken from [Liz-Marzan, Langmuir 22 (2006) p. 32].

Apart from complete descriptions of the theory [6], the main equations can be found in various recent reviews [87-90]. For example, the conditions for light amplification by small metallic NPs can be defined from the resonance condition for Mie scattering (considering only the first term of Mie scattering matrix):

$$I_{Mie\ scattering} \approx \left| \frac{\varepsilon(\lambda) - \varepsilon_m}{\varepsilon(\lambda) + 2\varepsilon_m} \right|^2$$

where $I_{\text{Mie-scattering}}$ is the intensity of scattered light, ε_m is the relative permitivity (dielectric constant) of medium, and $\varepsilon(\lambda)$ is the relative complex permitivity (dielectric function) of a metal. In general, the dielectric function $\varepsilon(\lambda)$ determines the electrical properties of a material in electrodynamics as a function of the wavelength of the incident radiation λ. There are two parts of $\varepsilon(\lambda)$, the real part $\varepsilon_1(\lambda)$ and the imaginary part $\varepsilon_2(\lambda)$ (called the damping factor of the resonance):

$$\varepsilon(\lambda) = \varepsilon_1(\lambda) + i * \varepsilon_2(\lambda).$$

In optics, materials are characterized by their complex refractive index $N(\lambda)$ which also consists of two parts:

$$N(\lambda) = n(\lambda) + i * k(\lambda),$$

where $n(\lambda)$ is the real part (refractive index) and $k(\lambda)$ is the imaginary part (absorption index). For a particular material, the dielectric function $\varepsilon(\lambda)$ and the refractive index $N(\lambda)$ are related by the equation:

$$\varepsilon(\lambda) = N(\lambda)^2.$$

From the relations above, it follows that:

$$\varepsilon_1(\lambda) = n(\lambda)^2 - k(\lambda)^2 \quad \text{and} \quad \varepsilon_2(\lambda) = 2 * n(\lambda) * k(\lambda).$$

Finally, the resonance condition can be expressed as:

$I_{Mie\text{-}scattering} \to \infty$ if $\{\varepsilon(\lambda) + 2\varepsilon_m\} \to 0$, i.e. $\varepsilon_1(\lambda) = -2\varepsilon_m \wedge \varepsilon_2(\lambda) \to 0$.

The Mie resonance condition is thus fulfilled when the real part of the dielectric function of a metal is equal to the dielectric constant of the surrounding medium multiplied by the factor –2, and simultaneously the imaginary part of the dielectric function of the metal (which represents the resonance damping) is small. The wavelength of the

incident radiation at which the Mie resonance condition is fulfilled is dubbed the resonance wavelength, and is specific for each particular metal. For plasmonic metal (such as Ag and Au) spheres, the resonance wavelength is in the visible spectral region, and the Mie resonance is sharp (i.e. experiences a very small damping). For example, for small (ca 10 nm) spheres in water, the resonance wavelength is ~380 nm [84]. A real system constituted by small Ag NPs in water, is a Ag NP hydrosol.

(3.2) SPE band in UV-vis spectrum and its characteristics:

Fulfillment of the Mie (LSPR) condition manifests itself in both absorption and scattering of light by a small Ag NPs constituting a Ag NP hydrosol. The overall optical response of the hydrosol is expressed in terms of extinction (extinction = absorption + scattering) and is measured as a function of λ, giving rise to a surface plasmon extinction (SPE) spectrum. SPE spectra are routinely measured using UV-vis absorption spectrometers. Nevertheless, in the interpretation of the measured spectra, one has to take into account that, in the case of species for which scattering is not negligible, the absorbance values measured by the spectrometer are in fact the values of extinction. A typical SPE spectrum of a Ag hydrosol is shown and the significant parameters of the SPE band are marked in Fig. 4: (i) the position of the SPE band maximum (λ_{max}) which lies at 398 nm for the system shown in Fig. 4; (ii) the absorbance value at SPE band maximum (A_{max}); (iii) the full-width-at-half-maximum (FWHM).

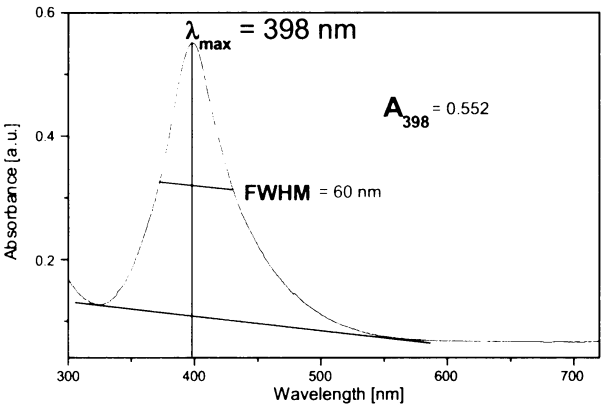

Fig. 4: The significant parameters of the main band in the SPE spectrum of a Ag hydrosol.

All these three parameters are related to NP sizes and shapes, particle size distribution (PSD), NP concentration, and aggregation state of a particular hydrosol.

(3.3) Factors affecting SPE band characteristics:

An overview of the factors influencing the SPE band characteristics is provided in refs 81-83, 91-93. The most important factors will be briefly discussed below.

Firstly, for polyhedral (near-spherical) and spherical particles an overall NP size increase induces the shift of λ_{max} to the long-wavelength region of spectrum (a red-shift of SPE band). On the contrary, a decrease of NP size leads to a blue-shift of SPE band (i.e. a displacement of λ_{max} toward the short-wavelength region of spectrum). Moreover, for larger NP not only the main SPE band originating from dipole excitations, but also a weaker 'second' SPE band (or shoulder) originating from quadrupole excitations may occur in UV-vis spectrum [8]. While the band arising from quadrupole excitations for a 60 nm silver NP occurs around 360 nm, as it has been calculated by Kelly et al. [8], the main SPE band for the same NP appears at approx. 425 nm – Fig. 5.

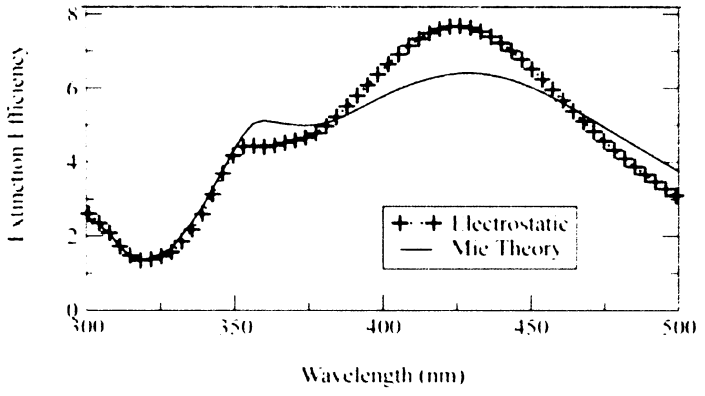

Fig. 5: The extinction efficiency for a 60 nm NP, including for quadrupole effects. taken from [Kelly et al., J. Phys. Chem. B 107 (2003) p. 668].

Secondly, the relationship between the geometrical shape of an individual NP and its SPE band has been experimentally investigated by Mock et al. [91]. Their results clearly demonstrate that the NP shape changes: sphere -> pentagon -> triangle are reflected in the red-shift of SPE band - Fig. 6.

Thirdly, the influence of the surrounding medium is usually related to its refractive index [89], since Mie theory predicts the resonance excitation (of a dipole) to occur when

$$\varepsilon_1(\lambda) = -2\varepsilon_m$$

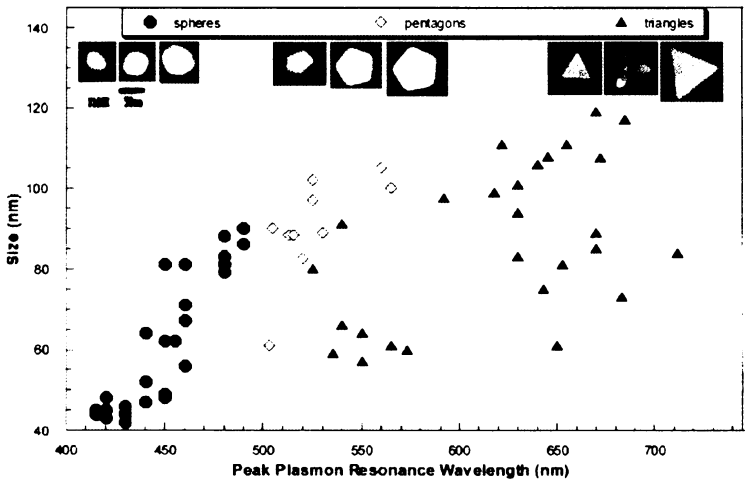

Fig. 6: The plot illustrating the relationship between the size (as determined from TEM image measurement) and the spectral peak wavelength for a diverse collection of individual silver NPs. The characteristic dimension for a spherical NP (full circles) is the diameter, for a pentagon (open diamonds) it is the length between opposite corners and for a triangle it is the length of a side. Taken from [Mock et al., J. Phys. Chem. 116 (2002) p. 6755].

($\varepsilon_1(\lambda)$ being the real component of the metal dielectric function at a given λ and ε_m the medium dielectric constant) as shown above, but this is only valid for dilute NP dispersions in nonabsorbing media. However, when concentrated systems are considered, the NPs become closer to each other, and interactions between neighboring NPs can arise, so that the models for isolated NPs do not hold any longer. The theoretical modeling of concentrated systems requires the use of effective medium theories, such as those derived in the early twentieth century by Maxwell-Garnett [94, 95] and Bruggemann [96], which allow the calculation of the average dielectric function for composite media with varying concentration of an infiltrated material.

An overview of the relative magnitudes of effects that different parameters (particle size, deviation from spherical shape, and interparticle interactions) have on the SPR frequency has been published very recently in article [92] where both calculated and experimental data have been successfully compared for Au NPs. The comparisons (in [92]) have proved that the deviations from spherical geometry are much more relevant than NP size for affecting the position of the SPE band. Furthermore, they have shown that interparticle interactions also play a significant role in the optical absorption of colloids: as soon as the NP volume fraction increases, the SPE band of isolated spheres starts to red-shift and broaden (i.e. the FWHM value increases), as a result of dipole-dipole interactions, toward the response expected for a continuous metal film, with high absorption in the IR (free carrier absorption) and the UV (interband transitions) but a small dip in the visible region of spectrum. Similar interparticle interactions have been shown to be responsible for huge field enhancements at silver NP junctions, with very important implications on surface enhanced Raman scattering (SERS) [97] and will be discussed in [Introduction, Section (4)].

In ref. 93 the changes in the optical absorption of silver NPs upon accumulation of excess electrons and positive holes were measured using the method of pulse radiolysis. The blue shift of the SPE band occurred upon electron donation to the NPs; while the injection of positive holes resulted in the red shift of SPE band.

Furthermore, as a result of the chemisorption of some ions intentionally added to a hydrosol, the SPR of silver NPs can be damped (e.g. by I^-, SH^-, and $C_6H_5S^-$ ions [89, 93, 98, 99]) and/or activated (e.g. by Cl^- [93, 100-104]). In addition, the interaction with a chemical species can change the surface of NPs, their mutual interactions, and consequently, their aggregation state. If the NPs aggregates, the SPE band red-shifts and broadens.

However, the same observation, a red-shifted and broad SPE band, can be induced by a larger mean NP size and/or by NP shape changes (as mentioned above). Hence, it is obvious that the SPE band changes in UV-vis spectrum of a particular hydrosol are quite complicated. Other methodologies, such as transmission electron microscopy (TEM), are thus required to provide a more accurate information about NP shapes and sizes in a particular system. Moreover, through systematic combined TEM and SPE spectral investigations, a useful correlation between the morphological characteristics of plasmonic metal NPs systems and their SPE spectral parameters have been established.

(3.4) Morphologies of NPs:

For the visualization of NPs immobilized (by simple deposition of a small amount of a particular hydrosol) on coated TEM grids, the TEM and/or HR-TEM (high-resolution TEM) can be employed. As a result of these measurements, the NP sizes, shapes and PSD can be determined. Moreover, by using HR-TEM, the differences between the touching (Fig. 7A) and the interpenetrating (Fig. 7B) NPs can be determined.

From the morphological point of view, the following types of space arrangements are recognized:

I. noninteracting NPs – isolated single NPs;
II. interacting NPs (closely spaced) (Fig. 7A) – can be further differentiated into:

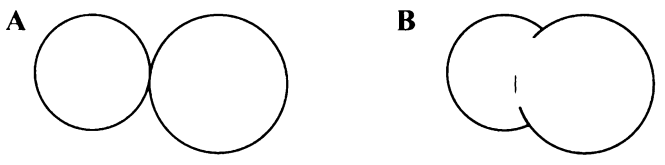

Fig. 7: Schematic depiction of (A) touching and (B) interpenetrating silver NPs.

a) NP systems in 1-D space – an example is a chain of NPs [105],
b) NP systems in 2-D space, an example can be highly ordered hexagonally packed assemblies in monolayered NP films [106],
c) NP systems in 3-D space – an example are large NP aggregates.

For all three types of interacting NPs, there are enforced dipole-dipole interactions because the incident radiation induces dipole in each NP and the neighbouring NP resonances mutually interact (further details in reference [1,7]). In the case of the interacting, approximately spherical NPs [107], average interparticle distances and their distribution are the most important factors which govern the λ_{max} of the SPE band.

III. Interpenetrating (intergrowing and/or sintered) NPs (Fig. 7B) – according to the calculations [108, 109] of the optical fields in the cavities between two interpenetrating NPs, the magnitude of excited electromagnetic field critically depends on the ratio of the interpenetrated NP diameters. Silver NP sintering, induced growth and interpenetrating induced by adsorption of small ions and its implications for the formation of surface-adsorbate complexes as well as for large SERRS enhancement of biologically important chromophoric molecules has been reported [110-112].

(4) SERS/SERRS spectroscopy

Before the beginning of the SERS (surface-enhanced Raman scattering) spectroscopy principle explanation, it should be reminded that Raman scattering (RS), an inelastic scattering of photons by molecules, discovered by the Indian physicist, C.V. Raman in 1928, is a method of vibrational spectroscopy which complements IR spectroscopy. Since the RS is not very efficient (comprises a very small fraction, about 1 in 10^7, of the incident photons, thus continuous lasers need to be used for its measurement), its enhancement by nm-scale rough surfaces of plasmonic metals has become the basis of a quite elegant and sophisticated method of SERS spectroscopy development of which started about 25 years ago.

SERS is one of the few phenomena that can be truly described as nanoscience due to the fact that the metal particles or metal features responsible for its operation must be small with respect to the wavelength of the exciting light. Indeed, the SERS-active systems must ideally possess a structure in the 5-100 nm range [2]. The upper dimension boundary is related to wavelength of the exciting light; the lower one is induced by the fact that when the metal particle becomes small enough, it needs to be treated as a fully quantum object, a metal cluster, whose electronic properties show so-called quantum size effects.

(4.1) Principle of SERS:

RS arises from the induced dipole $\boldsymbol{P}$ (the bolt letter means a vector) produced by the interaction of the electromagnetic field of the intensity $\boldsymbol{E}$ with a molecule characterized by the molecular polarizability $\ddot{\alpha}$ (a tensor):

$$\vec{P} = \ddot{\alpha} * \vec{E}$$

The intensity of RS is proportional to the square of induced dipole $\boldsymbol{P}$:

$$I_{RS} \approx \left|\vec{P}\right|^2 .$$

Therefore, we are able to consider that the origin of the enhancement of RS observed in SERS is due to an increase of either $\boldsymbol{E}$, or $\ddot{\alpha}$, or both of them. Thus, SERS-enhancement is explained by contributions of two mechanisms, the electromagnetic (EM) and the molecular resonance mechanism.

(4.1.a) Electromagnetic (EM) mechanism of SERS

The principal component of SERS is due to the enhancement of the EM fields close to the surface of a nanostructured plasmonic metal. This occurs when the wavelengths of incident and/or Raman scattered light obey the LSPR condition dubbed the EM resonance for the particular nanostructured or NP systems. Hence, SERS effect has been almost entirely confined to those metals, namely Ag, Au and Cu, whose nanostructures or NPs show distinct extinction bands (the SPE band) in the visible range (as discussed in the previous section), and thus accessible lasers can be used to excite resonantly the SPRs. According to Aravind et al. [107] who have emphasized that Ag is a rather special material for which the electromagnetic resonances have very small damping; while Au and Cu are similar, but have larger damping and consequently their ability to generate large resonant local fields is smaller.

In this Thesis, silver NPs prepared by LA/NF were employed as light amplifiers in SERS-active systems. The principle of light amplification via resonance Mie scattering of light by a silver NP (as the most simple model system) has been explained in [Introduction, Section (3.1)].

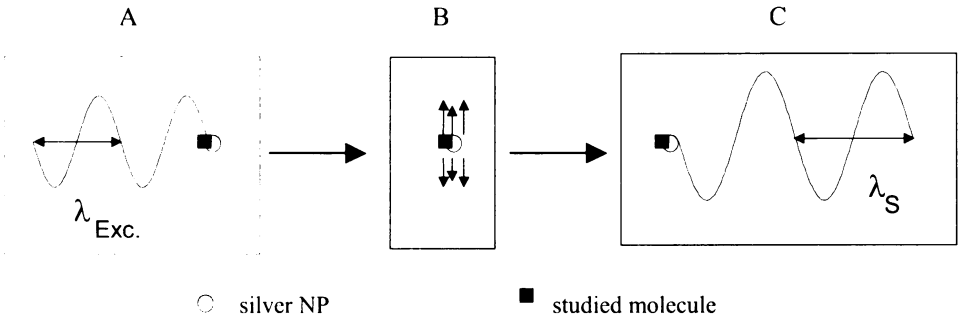

Fig. 8: Schematic depiction of (A) the interaction between exciting laser light of wavelength λ_{exc} and a silver NP with a studied molecule in the vicinity and/or on its surface, (B) the oscilating dipole system, and (C) the emission dipole system (λ_S is the scattered light).

In the EM mechanism of SERS, a silver NP acts as an amplifier for the exciting electromagnetic radiation and, simultaneously, for the Raman scattered radiation from a molecule (which is located in the vicinity and/or is adsorbed on the NP surface) at frequency ν_s (or wavelength λ_s), Raman shifted frequency. The dipole moment of the entire system, the so-called emission dipole of the molecule plus silver NP system, includes the effect of both the enhanced electromagnetic field and the antenna effect – Fig. 8.

A detailed description of EM mechanism is provided in refs 2 and 113.

(4.1.b). Molecular resonance mechanisms of SERS

In RS process molecular resonance is achieved whenever the energy of the exciting radiation matches the energy of an allowed electronic transition in a molecule. This gives rise to resonance Raman scattering (RRS).

In SERS/SERRS, the molecular resonance mechanism operates in conjunction with the EM mechanism of SERS. Therefore, a molecular resonance contribution to the EM mechanism of SERS requires that the molecular resonance condition is fulfilled simultaneously with the SPR condition, i.e. at approximately the same wavelength of the exciting radiation.

Furthermore, while in the case of RRS the electronic absorption spectrum of a molecule is a safe guideline for determining the molecular resonance condition, in SERS/SERRS, the determination of the molecular resonance contribution is complicated by interaction of the molecule with the metal surface which, in general, leads to a perturbation of the electronic energy levels of the molecule. Moreover, the extend of this perturbation and the consequent magnitude of the shifts of the electronic energy levels are difficult to be determined experimentally, since the weak absorption of an adsorbate molecular monolayer (or submonolayer) is overlapped by a SPE band of the NP assembly. Therefore, measurement of the SERS/SERRS spectra as a function of the excitation wavelength and calculations of excitation profiles of the SERS spectral bands are required for a reliable determination of the molecular resonance contribution to SERS/SERRS [104].

Concerning the terminology, two types of molecular resonance contributions in SERS/SERRS are generally considered in literature. The criterion on which the categorization is based, is the chromophoric (absorbing) or non-chromophoric (non-absorbing) character of a free (non-adsorbed) molecule at the selected excitation wavelength (which, apriori, has to match the SPR condition):

(a) Chemical mechanism contribution to the overall SERS enhancement: A non-chromophoric molecule is chemisorbed and a surface-adsorbate complex is formed. The exciting radiation is in resonance with a charge-transfer transition of the newly formed surface-adsorbate complex.

(b) SERRS: A chromophoric molecule is adsorbed on the surface and only weak or no perturbations of its electronic energy levels are assumed. The molecular resonance condition is thus roughly estimated from the electronic absorption spectrum of a free (non-adsorbed) molecule.

Obviously, this categorization does not involve the case of a chromophoric molecule strongly interacting with the metal surface. This case is extensively discussed in connection with explanation of the ~10^{14} SERS enhancement factors in published single molecule SERS experiments [78, 103, 114].

(4.2) SERS-active systems:

So far only one NP (an amplifier) inducing SERS enhancement (of ~10^4 magnitude) has been considered in order to simplify the basis of its explanation. However, most SERS-active systems consist of assemblies of interacting NPs [2]. Examples are NP aggregates, rough metal surfaces and island films. The simplest systems where SERS is highly enhanced are dimers, i.e. two closely-spaced NPs.

(4.2.a) Two or three NP assemblies and SERS enhancement

In the early 1980s [107, 115-117], a model calculations have shown that the SERS intensity can be greatly enhanced when two (or more) NPs are brought closely together. This work was extended in about 2000 by Xu et al. [108, 109] in order to model and, thus, explain the reported single molecule sensitivity in SERS and SERRS spectral probing [78, 103, 114]. Xu et al. [9, 108, 109, 118] have calculated that when two NPs are brought close together,

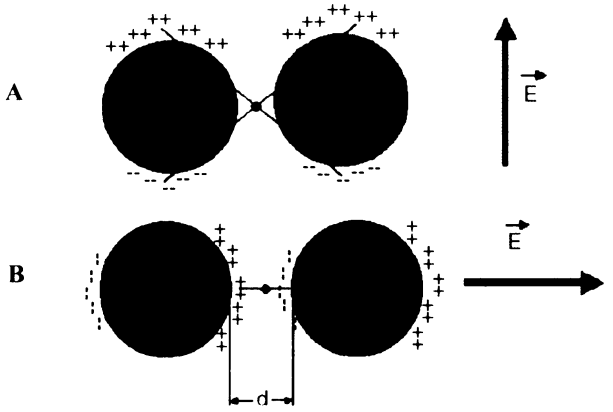

Fig. 9: Simple graphical illustration of the reason why light polarized with the ***E*** vector along the inter-particle axis (B) can result in huge enhancements in the gap between the two NPs whereas the orthogonal polarization (A) cannot. Explanation: For light polarized along the inter-particle axis (B) the proximity of the charges (induced by the optical fields) to the molecule can be made arbitrarily small and hence the field sensed by the molecule is commensurately large as the NPs are brought closer together. This capability is not available for light polarized orthogonally to the inter-particle axis (A). Taken from [Moskovits, J.Raman Spectrosc. 36 (2005) p. 458].

the optical field strength in the interstice between the two NPs can be increased so greatly that SERS enhancements of $\sim 10^{11}$ can be obtained for molecules located at that spot provided that (i) the two NPs are brought close enough together (i.e. <1 nm), (ii) light of the appropriate wavelength is used, and (iii) the exciting electric field vector is polarized along the interparticle axis (Fig. 9B). For each point only very short discussion follows: ad (i) - The giant enhancement, which exceeds that at isolated metal NPs by about six orders of magnitude, falls off rapidly as the interparticle gap increases. Ad (ii) - Bringing two NPs together also brings about other effects that should be taken into account, for example, the SPR splits into two polarization-sensitive components [105, 107-109, 115] one of which has a resonance that depends strongly on the distance between the two NPs. Thus the choice of appropriate excitation wavelength is crucial. Ad (iii) - For light polarized across the interparticle axis (Fig. 9A), the enhancement is almost negligibly different from its value at a single, isolated NP.

Very recently, the same group has also reported a theoretical analysis of the field enhancement and molecular response in SERS and fluorescence spectroscopy for a chromophoric molecule located between two [9, 118] and three [119] NPs.

(4.2.b) Larger NP assemblies and SERS enhancement

As it has been revealed experimentally [120, 121], a further aggregation into larger aggregates will create opportunities for other 'hot' interstitials, each of which will have its own characteristics of polarization and field strength. The precise structure of the NP aggregates is an important aspect in this case. For highly (geometrically) symmetric aggregates, the degeneracies of the normal modes describing SPR will be characterized generally by relatively narrow excitation spectra (=a narrow SPE band), whereas aggregates with lower geometrical symmetries will have much broader excitation spectra (ensuring resonance over a very broad range of wavelengths) [2].

A special mention needs the SERS enhancement in an important class of large aggregates – fractals. NP aggregates grown by self-assembly from monomers in solution often show scaling symmetry either as self-similar or self-affine systems [122-124]. The origin of the electromagnetic hot spots formation in such systems comes from the symmetry breaking because the exciting field does not possess scaling symmetry while the aggregate does. Therefore, a form of EM field localization arises that can lead to the formation of electromagnetic hot spots with high field [2].

The list of possible NP assemblies important for a higher SERS enhancement achievement would not be finished if ellipsoids and nanowires with regions of very large curvature [125, 126] were not mentioned.

To sum up this section, with dimers and larger NP aggregates capable of producing enhancements five or six orders of magnitude larger than those of single isolated NPs, even a very small fraction of particle dimers or small clusters will overwhelm the SERS signal from many thousands of isolated NPs. As a result, all reports of SERS spectra claiming to originate from single, isolated particles may arise some doubts, even if rather compelling TEM images are reproduced showing the presence of virtually only monomers. One cannot be certain that in the optical experiment the laser did not excite some of the very few aggregates present in the sample [2]. Nevertheless, in almost every instance the average SERS enhancement of $\sim 10^6$ is, in fact, an average over a very broad distribution of enhancements present within the portion of the SERS-active sample probed by the laser, which can range from values of near unity to values exceeding 10^{11} [2].

(4.3) Analytical application of SERS-active systems:

The facts, such as the sensitivity resulting from an enhancement in scattering by an average factor of approximately 10^5-10^6, the detailed structural information, and the selectivity resulting from the inherent selectivity of a vibrational spectroscopic method enable the characterization of molecules adsorbed at submonolayer coverage onto roughened plasmonic metal surfaces. Furthermore, the selective enhancement associated with SERRS spectroscopy gives good molecular specificity, free from interference from non-SERRS-active contaminants. Fluorescence may be quenched and good signals recorded over a greater range and at much lower concentrations. Thus, SERRS can be used for sensitive qualitative and semiquantitative analysis. However, before SERRS can fully develop its potential as an analytical method, a well characterized SERS substrate and a reliable procedures are required which will yield fully reproducible results.

(5) Molecules and biomolecules used as testing adsorbates

(5.1) Simple model adsorbate: 2,2'-bipyridine and its SERS spectral forms

The compound 2,2'-bipyridine (bpy), depicted in Scheme I, belongs to N-bases and is well known as a ligand in coordination chemistry. Surface complexes formed by N-bases on nanostructured and/or nanoparticulate Ag surfaces have been the subject of numerous SERS spectral studies [127, 128]. These studies were focused on probing of the surface species structure in relation to the conditions of their formation (such as the applied potential in experiments with roughened Ag electrodes) as well as on elucidation of the relative contributions of the EM and chemical mechanism to the overall SERS signal. In the particular case of bpy, 4 SERS spectral forms of Ag-bpy surface species (f1-f4) were identified on Ag electrodes.

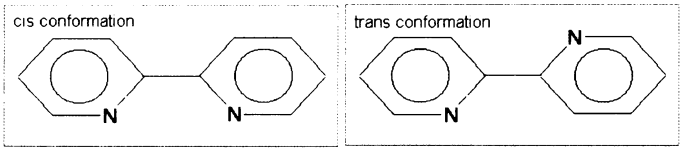

Scheme I: Two conformations of the 2,2'-bipyridine structure.

Two spectrally different forms of Ag-bpy surface complex on silver colloidal particles, f1 and f3, were described in ref. [129]. In this and the subsequent studies [104, 111, 112, 129-132], the following characteristics of f1 and f3 were determined:

Ag-bpy f1 surface species (Fig. 10):

- SERS excitation profiles 458-600 nm: no photoinduced CT (charge transfer) [104]
- spectral analogue of $[Ag(bpy)_2]^+$ [104, 111, 112, 129-132]
- detected in the absence of chlorides (or other adsorbing ions), i.e. in Ag hydrosol/bpy systems [104, 111, 129-132]
- detected as the only SERS spectral component in Ag hydrosol/HCl/bpy with HCl concentrations lower than $5x10^{-4}$ M which is the threshold concentration for changes of Ag nanoparticle morphology [104, 111, 130].

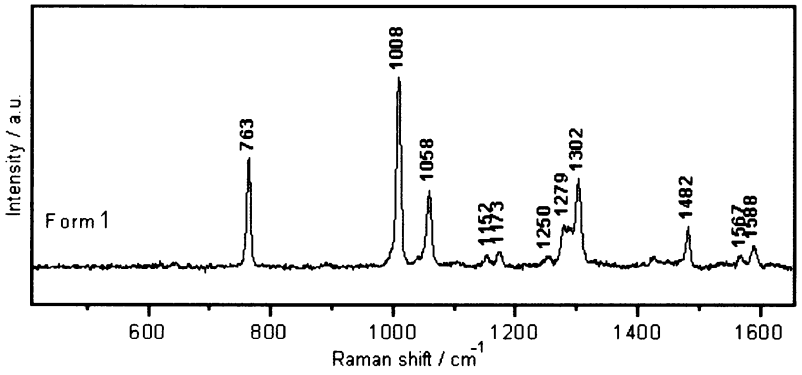

Fig. 10: SERS spectrum of pure f1 Ag-bpy surface species obtained from factor analysis (FA), taken from [Šloufová, I. PhD Thesis, Charles University, Prague, 2000].

Ag-bpy f3 surface complex (Fig. 11) :SERS excitation profiles 458-600 nm: photoinduced CT at ca 540 nm [104]

- spectral analogue of $[Ru(bpy)_3]^{2+}$ (both in resonance and off-resonance spectral patterns) and a variety of bpy complexes possessing a photoinduced CT [104]

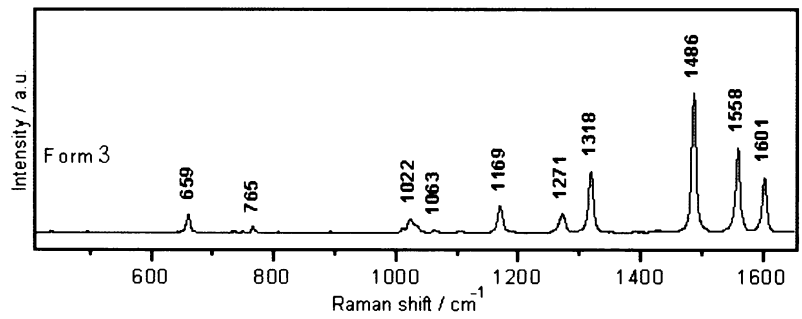

Fig. 11: SERS spectrum of pure f3 of Ag-bpy surface species obtained from factor analysis (FA); taken from [Šloufová, I. PhD Thesis, Charles University, Prague, 2000].

- formation is induced by addition of chlorides to silver NP hydrosols both in the neutral and acidic ambient, but above a certain threshold chloride concentration [111, 112, 130]
- generated in Ag colloid/HCl/bpy systems with HCl concentrations higher than 5×10^{-4} M, which is the threshold concentration above which changes of Ag nanoparticle morphology described as sintering and additional growth were observed [111, 112, 130]
- detected under the strongly reducing conditions of reduction of silver nitrate by sodium borohydride in the presence of bpy [112, 132].

In references [111, 112, 130], f1 and f3 of Ag-bpy surface complex were identified as independent spectral components by factor analysis (FA) of the set of SERS spectra of Ag colloid/HCl/bpy system measured as a function of HCl concentration. SERS spectra of pure f1 (Fig. 10) and f3 (Fig. 11) were thus obtained. While f1 was identified as Ag^+-bpy surface species, f3 was attributed to Ag(0)-bpy surface complex [112, 132]. For the

interpretation of the vibrational spectra of Ag-bpy surface species the normal coordinate analysis (NCA) of bpy [133] and of $[Ru(bpy)_3]^{2+}$ [134] were used.

(5.2) Biologically important adsorbates: selected porphyrins and their SERS spectral forms

SERS and SERRS spectroscopy has been shown to be a promising tool for investigation of the structural and conformational properties of biomolecules [135]. There are several characteristics of SERRS that are highly favourable for this application: fingerprint quality of the vibrational spectral information, the large enhancement factor of SERRS, in combination with quenching of fluorescence. The last two factors help to overcome a common problem in Raman scattering of biologically interesting chromophoric molecules that is the interference of the strong fluorescence signal with the weak Raman signal. Furthermore, due to high sensitivity of SERRS, the spectra of species present in solutions at rather low, physiological concentrations can be measured. This aspect is very important for bioanalytical as well as biomedical applications. An especially useful task appears to be the development of SERRS spectral probes for porphyrins which are employed in photodynamic therapy of cancer and/or cancer diagnostics.

On the other hand, there are also some disadvantages related to SERS/SERRS spectroscopy applied for biomolecule study. First of all, the molecule directly adsorbed on Ag surface does not retain its native structure. Hence, in the case of porphyrins, their free base forms are changed due to a kind of metallation by Ag surface. One can prevent such a reaction by the modification of Ag surfaces using the spacers, i.e. the molecules adsorbed on the Ag surfaces and possessing suitable functional groups which attract porphyrin molecules to Ag surface while hindering a direct porphyrin-Ag surface interaction. The native structure of porphyrins thus remains unperturbed [136-139]. Another problem to be solved in employment of SERS/SERRS as a method in bioanalytical and biomedical applications is a reliable quantification of signal and its reproducibility.

In this Thesis, the selected porphyrins (Fig. 12) have been employed as it follows:

(a) 5,10,15,20-tetrakis(1-methyl-4-pyridyl)-21H,23H-porphine, tetra-p-tosylate salt (TMPyP)
(b) 5,10,15,20-Tetra(4-pyridyl)-21H,23H-porphine (TPyP)
(c) 5,10,15,20-Tetrakis(4-aminophenyl)-21H,23H-porphine (TAPP)
(d) 5-(4-Aminophenyl)-10,15,20-triphenyl-21H,23H-porphine (APTPP)
(e) 5,10,15,20-Tetra(4-methoxy-phenyl)-21H,23H-porphine (TMPP)

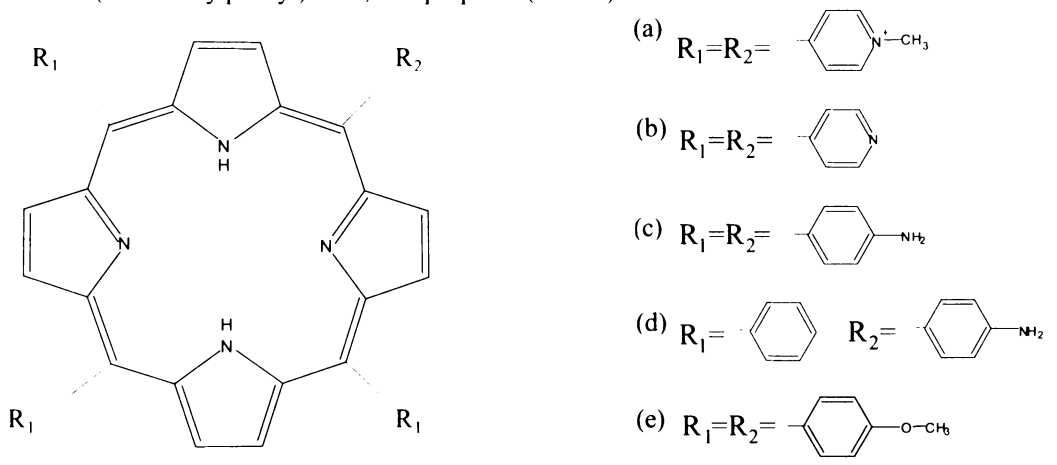

Fig. 12: Schematic structures of selected porphyrines: (a) TMPyP, (b) TPyP, (c) TAPP, (d) APTPP, and (e) TMPP.

TMPyP is currently tested as a new, prospective photosensitizer in the photodynamic therapy of cancer. The specificity of this cationic porphyrin is the ability to intercalate into DNA [140]. TPyP is its non-charged (and without methyl group) analog, thus, the interest of its using is to investigate probable changes in the interaction rate with Ag NP surfaces. The next two non-charged porphyrins with at least one amino-group ending in their substituents, TAPP and APTPP, are employed to look closer into the orientation of a porphyrin molecule on the Ag NP surface. The last porphyrin, TMPP, with its methoxy group endings of substituents is selected for making a comparison of its possible interaction with Ag NP surface to the employed aminoporphyrins.

Since no spacer molecule is used, four different SERRS spectral forms of surface complex Ag-porphyrin [132, 137, 141, 142] could be observed in systems containing silver NPs: (i) free base porphyrin, (ii) porphyrin metallated by Ag^+, (iii) porphyrin metallated by Ag^0, and finally, (iv) aggregates consisted of many porphyrin molecules. Even for the cationic TMPyP all four SERRS spectral forms have been distinguished by FA [132, 141, 142] and are shown in Figs 13, 14. Nevertheless, J-type aggregates formed by ion pair associates constituted by cationic $[TMPyP]^{4+}$ and 4 BH_4^- anions [141] requires at least $1x10^{-6}$ M TMPyP concentration in final system and a strongly reducing ambient generated by $NaBH_4$ [132].

The assignment of bands in RRS spectra of free base and metallated porphyrin were accomplished on the basis of NCA - in [143] for TMPyP and TPyP and/or in [144] for the others.

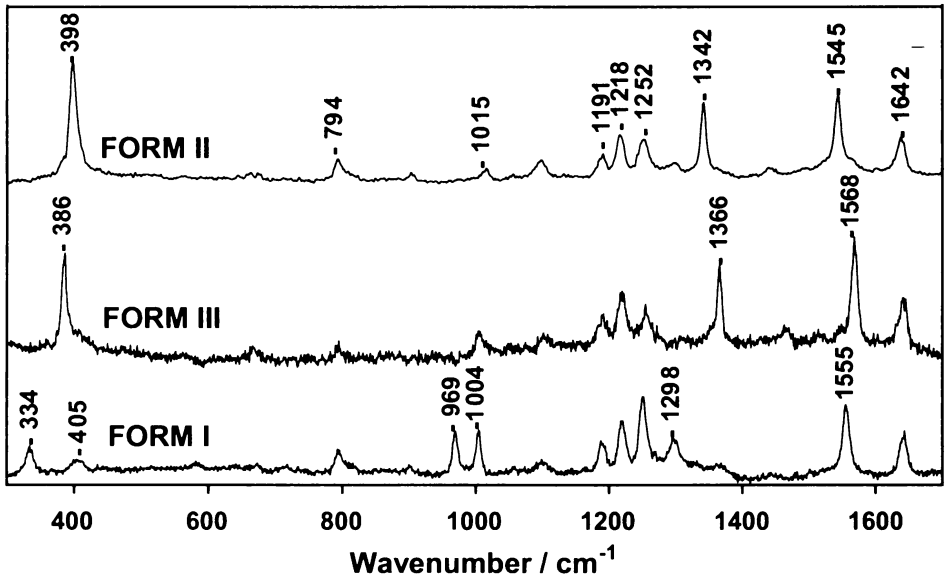

Fig. 13: The SERRS spectral pure components of TMPyP interaction with Ag NPs obtained by factor analysis (FA): Form I – free base, Form II – metallated by Ag^{+}, Form III – metallated by Ag^{0} - taken from [Procházka, M. et al. J.Raman Spectrosc. 33 (2002) p. 758].

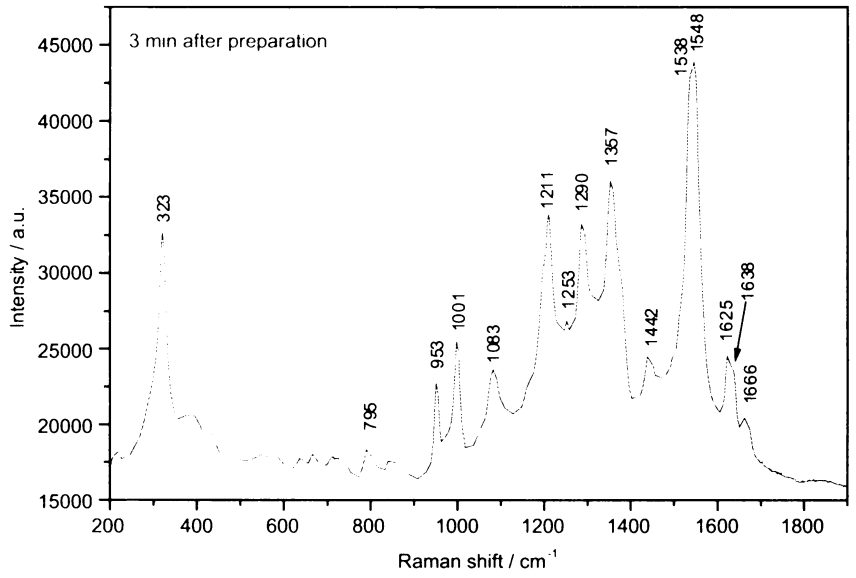

Fig. 14: Fourth SERRS spectral form of TMPyP generated in the TMPyP($NaBH_4$)-Ag hydrosol system with $1x10^{-6}$ M H_2TMPyP concentration - taken from [Šišková, K. Diploma Thesis, Charles University, Prague 2003].

Objectives

The goal of the Thesis is to provide a substantial contribution to the evaluation of the possibilities and limitations of functionalised (purposefully chemically modified) silver NP preparations by the LA/NF of Ag target in liquid media and of the applicability of these functionalised NPs in Ag NP plasmonics, namely in SERS spectroscopy.

Towards this goal the following steps are proposed:

1. Selection of parameters for the evaluation of the efficiency of the LA/NF of Ag target in aqueous medium and for the characterization of Ag NP hydrosols as the target products of a LA/NF process.
2. Design and realization of testing experiments for the optimisation of experimental setup and physical parameters employed in LA/NF process for the exploration of a particular effect of ionic or molecular species on the efficiency, progress and final outcome of LA/NF.
3. Exploration of a particular effect of selected molecular and ionic species on the efficiency, progress and outcome of LA/NF of Ag target in liquid ambient. Testing the resulting Ag nanoparticle / ionic or molecular species systems, either as substrates, or final systems for SERS spectroscopy by evaluating the SERS-spectral sensitivity of the adsorbate (analyte) detection.
4. Development of LA/NF procedures targeted on a controlled functionalisation of Ag NPs by selected molecular / ionic species (with purposefully varied concentrations) in the course of the LA/NF of Ag target in aqueous solutions. A proposal of the LA/NF mechanism in the electrolyte presence.
5. SERS/SERRS spectral probing of systems constituted by the functionalised NPs and selected porphyrin species with different peripheral substituents. This is targeted on the elucidation of the pophyrin-funcionalised NP surface interaction and/or on the pinpointing of the systems providing SERRS signal at very low porphyrin concentrations.

Experimental

Materials: Analytical grade chemicals and deionized or redistilled deionized water were used for all sample preparations: silver foil (99,99%, app. 1 mm thickness); NaOH (Prolabo), NaCl (Lachema), HCl (Prolabo), $Na_2S_2O_3$ (THS, Prolabo), $AgNO_3$ (Merck), $NaBH_4$ (BH, Aldrich), $Na_3C_6H_5O_7.2H_2O$ (Na_3Citr, Aldrich), H_3C_6 H_5O_7 (H_3Citr, Lachema); 2,2'-bipyridine (bpy, Merck), 5,10,15,20-tetrakis(1-methyl-4-pyridyl)-21H,23H-porphine, tetra-p-tosylate salt (TMPyP, Aldrich), 5,10,15,20-tetra(4-pyridyl)porphine (TPyP, Porphyrins systems), 5,10,15,20-tetrakis(4-aminophenyl)porphine (TAPP, Porphyrins Systems), 5-(4-Aminophenyl)-10,15,20-triphenyl-porphine (APTPP, Porphyrins Systems), 5,10,15,20-Tetrakis(4-methoxy-phenyl)porphine (TMPP, Aldrich) ; spectrally pure ethanol (Uvasol Merck).

The glassware was cleaned by diluted nitric acid (1:1), extensively rinsed with deionized water. Alternatively, the mixture of sulphuric acid and hydrogen peroxide dubbed „piranha" solution (4 parts of concentrated H_2SO_4 and 1 part of concentrated H_2O_2, to remove organics) for 20 minutes and aqua regia (3 parts of concentrated HCl and 1 part of concentrated HNO_3, for removal of metals) for 10 minutes.

The same experimental setup of LA/NF (Schema II) has been employed for all silver NP hydrosols preparations described in this Thesis. Only focused laser pulses of 20 ns pulse duration produced by a NdYAG laser (Quantel YG58110) with 10 Hz repetition rate have been used. The stirring by a magnetic bar placed on the bottom of the cylinder quartz cell was applied during all LA/NF and NF steps. The other experimental conditions such as: laser pulse wavelength, energy per pulse, the kind of solution in which the LA/NF process has been performed, and the presence (or absence) of breaks (pauses) in the course of the LA/NF process, will be specified for a particular part of experiments – i.e. separately for each chapter.

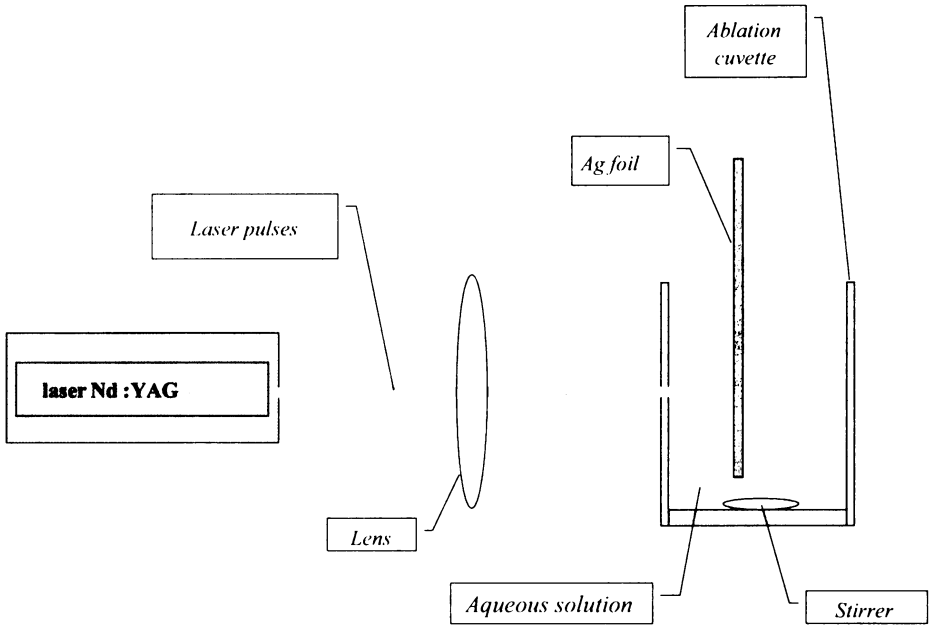

Schema II: Employed experimental setup for LA/NF.

Ad. Chapter 2 :

Ag NP hydrosols preparations: The Ag foil was immersed in the 30 mL of deionised water. The Ag foil placed in the centre of the cylinder quartz cell (4 cm in diameter, 5.5 cm high) was irradiated by focused (focusing lens with 5 cm focal length) laser pulses at 1064 nm line (about 187 or 90 mJ/pulse) and/or at 532 nm line (60 mJ/pulse) for 2+3+3+5+7 minutes (it means that after each number of minutes there was a break in the LA/NF process which was performed to control the process of NPs formation by using SPE spectroscopy) and/or for 20 minutes without any interruption.

Preparation of SERS / SERRS - active systems : The following aqueous stock solutions of agents were prepared and used: $1x10^{-2}$ M, $5x10^{-3}$ M and $1x10^{-3}$ M bpy, $1x10^{-1}$ M HCl, 1 M NaCl, $1x10^{-3}$ M and $1x10^{-1}$ M THS ($Na_2S_2O_3$), $1x10^{-3}$ M BH ($NaBH_4$), $2x10^{-1}$ M $AgNO_3$, $1x10^{-4}$ M TMPyP. Appropriate amounts of stock solution of a particular agent and/or adsorbate were introduced into 1 mL of hydrosol prepared by LA/NF process to obtain required concentration of agent and/or adsorbate in final systems.

SPE and SERS / SERRS spectral measurements: All spectra were measured at room temperature in a quartz cell (optical path length of 1 cm) and are presented without any smoothing. The SERS and/or SERRS spectra of Ag hydrosol/adsorbate systems have been recorded on a Jobin Yvon CCD Raman spectrometer with 514.5 nm excitation line (in the case of bpy) and/or 488.0 nm (in the case of TMPyP) of an Ar^+ laser, using a 90° scattering geometry and 1 min accumulation time. SPE spectra of colloidal systems have been recorded with a UVIKON XL spectrophotometer and are presented without any smoothing.

TEM samples were prepared by depositing a small amount (4 μL) of a hydrosol onto a C-coated copper grid for TEM and were allowed to dry in the air at room temperature. Another technique of TEM samples preparation was based on the reassembling of a 2D-film on the interface formed between water and organic phase. The details of the procedure are described in [106, 130]. The TEM samples were measured after several days by using a Philips

EM201 (in Paris) and/or a JEOL-JEM 200 CX (in Prague) electron microscope at 70,000x, 100,000x and 200,000x magnifications.
The procedures of PSDs determination are described in detail in [Chapter 1].

Ad. Chapter 3 :
Ag NP hydrosols preparations : The Ag foil was immersed in the 30 mL aqueous solution of a particular selected agent of the concentrations as follows: $1x10^{-5}$ M and $1x10^{-4}$ M NaOH; $1x10^{-4}$ M, $1x10^{-3}$ M and $5x10^{-2}$ M NaCl; $1x10^{-4}$ M and $1x10^{-3}$ M HCl; $1x10^{-5}$ M and $1x10^{-4}$ M $AgNO_3$; $1x10^{-7}$ M and $1x10^{-6}$ M THS; $1x10^{-6}$ M and $1x10^{-5}$ M bpy; $1x10^{-7}$ M TMPyP. The other conditions were the same as in [Chapter 2], nevertheless, only the laser pulses at 1064 nm (about 200 mJ/pulse) were employed for 2+3+3+5+7 minutes.
The SPE spectra were recorded on a UVIKON XL spectrophotometer in 1 cm cuvette.
SERS spectral measurements: The SERS spectra of Ag hydrosol/adsorbate systems have been recorded on a Jobin Yvon CCD Raman spectrometer with 514.5 nm excitation line (in the case of bpy) and/or 488.0 nm (in the case of TMPyP) of an Ar^+ laser, using a 90° scattering geometry and 1.5 min accumulation time.

Ad. Chapter 4 :
Ag NP hydrosols preparations: Silver foil was immersed in the 30 mL of deionised water or of a particular solution of NaCl, HCl, Na_3Citr and/or H_3Citr of various concentrations values: $1x10^{-5}$ M, $1x10^{-4}$ M, $1x10^{-3}$ M, $1x10^{-2}$ M. The used energies of laser pulses at 1064 nm were the following: ~200, ~300 and ~400 mJ/pulse. The LA/NF process was carried out for 5+5+10 minutes or 20 minutes without any break.
The SPE spectra have been recorded on a Cary |1E| UV-visible spectrophotometer in 4 mm cuvette.
The SERS spectra were recorded on a Jobin Yvon CCD Raman spectrometer with 514.5 nm excitation line of an Ar^+ laser, using a 90° scattering geometry and 1.5 min accumulation time.
The TEM samples were measured after several days by using a Tecnai F 20 ST (in Evry) and/or a JEOL-JEM 200 CX (in Prague) electron microscope at various magnifications.
The AAS measurements have been done by the Service central d'analyse of CNRS (Centre National de la Recherche Scientifique) in Lyon.

Ad. Chapter 5 :
The porphyrins were dissolved in spectrally pure EtOH to yield the stock solutions of $2x10^{-5}$ M concentration. Porphyrin concentrations in final SERRS-active system were about $2x10^{-8}$ M and/or smaller.
The SPE spectra were recorded on a Cary |1E| UV-visible spectrophotometer in 4 mm cuvette.
The SERRS spectra were recorded on a Jobin Yvon CCD Raman spectrometer with 457.9 nm excitation line of an Ar^+ laser, using a 90° scattering geometry and 3 min accumulation time.

Results and discussion

Chapter 1

Approaches to data treatment and interpretation – evaluation and proposed solution

In this chapter various possible approaches to data treatment and interpretation are evaluated and the particular ones adopted in this Thesis are explained and argued for. The evaluation is based on the previously published papers on LA/NF and SERS (overviewed in the Introduction), on the experimental material obtained in this Thesis and, in some cases, on preliminary experiments performed specifically for assessment of the particular issue.

A seminal question is, what does it mean the LA/NF efficiency and how it can be evaluated? Furthermore, how is the stability of Ag hydrosols assessed? Another important issue is reactivity of Ag NPs, and the ways how it can be evaluated with respect to the SERS-active system formation and performance.

Finally, there are at least two another important points to be established concerning the PSD determination. First, can the technique of the TEM sample preparation influence the resulting PSD obtained by TEM image analysis? Second, which of the possible approaches to PSD determination, i.e. the employment of a computer image analysis program or "manually" performed measurements, provides more realistic results?

1.1. Selection of parameters for evaluation of LA/NF efficiency of a Ag target in liquid ambient

There are two parameters which could be selected for LA/NF efficiency evaluation:

1. *Amount of ablated Ag* = a basic parameter; the simple methods of its determination are AAS (atomic absorption spectroscopy) and AES (atomic emission spectroscopy), both detect all forms of ablated Ag.
2. *Structures formed* by the ablated material in the liquid ambient:
    a. Atoms, ions, molecular structures (complexes)
    b. Clusters of atoms and ions smaller than 4 nm
    c. NPs: size, shape, aggregation state: (i) isolated, (ii) interacting – see below
    d. Larger size (e.g. μm) objects

The major product of LA/NF of a metal target in aqueous ambient are NPs in the form of a sol: either (i) hydrosol – in pure water and aqueous solutions of electrolytes and molecular species; or (ii) organosol – in organic solvents.

Ag hydrosols are the products of LA/NF in our case. Hence, the second criterion of the LA/NF "efficiency" evaluation, i.e. the evaluation of the characteristics of the product, is much more complex than the "total amount of ablated Ag" criterion. The characteristics of the product, i.e. a Ag hydrosol, are as follows:

1) morphological – TEM is adopted as methodology and statistical approaches have to be used for the evaluation:
    a) particle sizes – evaluated in terms of PSD
    b) particle shapes – e.g. the deviation of real shapes from sphere model, e.g. to an ellipsoid model
    c) the presence (in NP aggregates which can be closely spaced, touching, interpenetrating = crystal twins) or absence (for isolated NPs) of interparticle interactions.

2) optical – SPE spectra in the UV-vis spectral region (200-800 nm):
- optical density of the Ag NP sol – not a suitable criterion (will not be used)
- selected parameters to be determined from the SPE spectra:
    (i) λ_{max} – the wavelength of the SPE band maximum
    (ii) A_{max} – the absorbance value in the SPE band maximum
    (iii) FWHM – the width of the SPE band evaluated at $A_{max}/2$
    (iv) I_{SPE} – the integral area of the SPE band
    (v) A_{250} – the absorbance value in the maximum of the interband transition of Ag [36, 93].

The interpretation of the parameters of SPE spectra with respect to the criteria of LA/NF process evaluation is as follows:

λ_{max} : (i) If its values are in the 390-396 nm range then it indicates the presence of "small" particles with sizes 5-30 nm in diameter. These particles have approximately a uniform optical response per particle.

(ii) If it is higher than 396 nm it indicates the presence of larger particles (in addition to "small" ones).

A_{max} : For SPE spectra with a single symmetric SPE band and its λ_{max} 390-396 nm, A_{max} changes are almost proportional to the changes in the amount of small non-interacting particles.

FWHM: The increases of FWHM indicates broadening, usually connected with an asymmetry of the SPE band. This indicates the presence of large particles with diameter higher than 30 nm, or the formation of aggregates (either a small fraction of them, or their small size, or both). The formation of a large amount of larger aggregates results

into the evolution of a tail (or a shoulder), or of a distinct second spectral band (usually broader than the main SPE band) at longer wavelengths (at 390-420 nm) than the main SPE band.

I_{SPE} : For the systems of a type I, i.e. with only small particles 5-30 nm (i.e. λ_{max} in the 390-396 nm range, nearly symmetric SPE band, low FWHM), $I_{SPE} \simeq$ to the number of NPs. Thus, an increase of I_{SPE} indicates that more particles were produced; while a decrease of I_{SPE} means that less NPs were produced.
For the systems of a type II, i.e. systems with a substantial fraction of large particles or aggregates, the changes in I_{SPE} can only be used for a rough estimation of the amount of particles and of aggregates present in the sol. However, the changes in I_{SPE} cannot be mutually compared for systems of type I and II!

A_{250} : It reflects the intensity of the interband transition of Ag (4d →5sp) [36, 93]. It is proportional to the amount of Ag present in the form which supports interband transitions, i.e. in the form of NPs, as opposed to e.g. complexed single Ag^+ ions.

Finally, the following approach is proposed: The outputs of LA/NF processes performed under varying conditions will be mutually compared on the basis of the properly selected parameters of SPE curves which in turn will allow for estimation of the morphological characteristics of the resulting Ag NP hydrosols, namely the presence of small (5-30 nm) and/or large (>30 nm) NPs, and aggregation state (in terms of fractions of isolated particles, small aggregates and large aggregates).

Variations of conditions of LA/NF will be performed in such a way that only one of the parameters expected to affect the outcome of LA/NF will be varied and its real impact on the outcome of LA/NF will be followed and evaluated. Parameters to be varied are: (a) pulse wavelength, (b) laser pulse energy, (c) presence of molecular or ionic species in the liquid – in our case aqueous ambient, (d) continuous or step-wise performed LA/NF.

1.2. Evaluation of stability of Ag NP hydrosols

The main hint for the stability of a Ag NP hydrosol will be a comparison of its SPE spectrum measured immediately after the hydrosol preparation and of that measured again after a certain period of time (usually after several days or weeks). Provided that an irreversible aggregation [145, 146] occurs during the time evolution, i.e. the following changes in the SPE spectrum are observed: the λ_{max} value red-shifts, FWHM increases and the A_{max} value decreases.

Moreover, the TEM images and PSD determined from them can also be used for a preliminary estimation of the stability of a NP hydrosol. A higher portion of larger NPs and/or aggregates leads to higher instability of the hydrosol due to the fact that these larger NPs sediment more easily than the smaller ones.

From the NP point of view, the stability of a hydrosol against aggregation is determined by the height of the electric bilayer repulsive barrier, caused by Coulombic potential of the charges on the NP surface. If this is substantially greater than kT, where k is the Boltzmann factor and T is the temperature, a hydrosol will be stable against aggregation. This barrier will be reduced whenever the extent of the diffuse bilayer surrounding the NPs is decreased. This can be accomplished either by the ionic salts addition (to decrease a screening length in solution) or by the molecular adsorbates addition which reduce the surface charge on NPs [93]. Once the repulsive forces are diminished, NPs can approach one another to distances where attractive van der Waals interactions cause them to stick together irreversibly. Of course, this is in the case of the agent addition to a pre-prepared Ag hydrosol. Another situation could become since the same agent is present during the Ag NPs formation process. Obviously, the investigation of such a situation is one of the interests of this Thesis.

In the case of borohydride-reduced Ag hydrosols, the important role of borohydride, its hydrolytic and oxidation products in the stabilization of the isolated NPs against a spontaneous aggregation into macroscopic Ag particles was demonstrated in [147]. Borohydride and borate anions form the anionic part of the electric bilayer enveloping each of the Ag NPs in which they compensate the positively charged Ag active sites [148- 150].

An interesting question is how are Ag hydrosols prepared by LA/NF stabilized? According to Pfleger et al. [46], the outer charged shell of a NP is created by OH^- (dominantly; originating from water autoprotolysis), HCO_3^- and/or HSO_3^- ions (occasionally; coming from the absorption of gases from the air) so that this NP is stable in the aqueous solution. The experimental evidence of this hypothesis has been given in [62] for Au NPs.

1.3. Reactivity of Ag NPs

By the reactivity of Ag NPs, it is meant in this Thesis the interaction of Ag NP surfaces with various chemical species which are exposed to the NP surfaces (e.g. added as solutions into Ag NP hydrosol) as the prospective adsorbates. The interaction depends mainly on the chemical nature of the adsorbate and the type of the chemical bond which it could form with Ag surface. Nevertheless, it is quite difficult to predict these interactions, since the reactivity of Ag NP surfaces in NP hydrosols (or organosols) differs substantially from that of bulk Ag in vaccuo. On the other hand, during the nearly 30 years of exploration of SERS of a variety of adsorbates in systems with Ag NPs, a vast amount of information about Ag NP-adsorbate interactions has been accumulated for various classes of adsorbates. Therefore, the rough preliminary estimations of the reactivity of Ag NPs towards a particular adsorbate are mostly based on literature data concerning structurally similar adsorbates. Furthermore, as it has been

stressed in the previous [section (1.2.)], a possible charge of an adsorbate molecule plays also an important role. The Ag NP surface-adsorbate interaction ultimately manifests itself in the aggregation state of the system (= Ag hydrosol/adsorbate) and, consequently, in its SPE spectrum and TEM images. Nevertheless, the results of these two methodologies provide only very rough information. If it is desired to gain an more subtle insight into the nature of the interaction between an adsorbate and Ag NP surface, a SERS/SERRS spectral measurement is employed. For this purpose a SPE spectrum of the Ag hydrosol/adsorbate system can, at least, help to decide which one of the excitation lines of a continuous laser should be used for an appropriate system to obtain a maximal enhancement.

In the Thesis, the reactivity of NPs will be mostly related to the results of the SERS/SERRS spectral measurements, i.e. a system is SERS/SERRS-active or -inactive. For the systems displaying the largest SERS/SERRS-activity, the concentration values of SERS or SERRS spectral detection limits for an adsorbate (=the adsorbate concentration value at which at least three specific spectral bands can be clearly distinguished) are determined.

1.4. PSD determination

Two different techniques of TEM samples preparation (introduced in the Experimental) can be used: (i) the simple deposition of a small amount of Ag hydrosol on a carbon-coated Cu grid and allowed to dry at room temperature (=technique (i)), (ii) an interfacial film preparation and its re-assembling (=technique (ii)). However, is the PSD determined by using the TEM imaging of samples prepared by these two techniques really the same for a particular hydrosol? Hence, the resulting PSDs for the same Ag hydrosol (whose SPE band spectrum is shown in Fig. 15) obtained from the samples prepared by (i) and (ii) techniques are mutually compared in Fig. 16 and Table III.

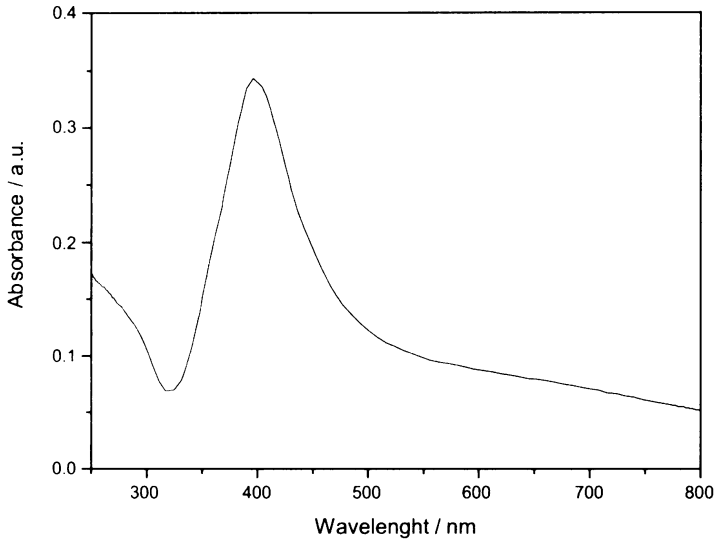

Fig. 15 : The SPE spectrum of a Ag hydrosol from which the samples for TEM imaging and PSD determination were prepared by using two different TEM sample preparation techniques.

Fig. 16 shows that the PSDs are roughly similar but there are some minor differences most probably introduced by the specificity of each of the two TEM samples preparation techniques: a higher fraction of larger NPs, and, simultaneously, a lower fraction of smaller NPs (of ~5-10 nm in diameter) is encountered in the drop-drying technique. On the other hand, the interfacial film re-assembling technique seems to overestimate, a little bit, the smaller NPs content. What is the exact PSD?

To answer this question, it should be reminded that in the interfacial film re-assembling technique, a 2D-film is formed from Ag NPs connected with bpy molecules in an organic-aqueous solution interface. In general, it is assumed that all NP sizes are involved in these geometrically irregular arrangements which can be evidenced by Fig. 17.

On the contrary, the TEM imaging results (the TEM measurement is always performed in more places of the same grid) from the drop-drying technique can be highly influenced by the process of drying, i.e. NPs are arranged randomly in more layers. Such an arrangement can cause the discrepancy between the PSDs. This

Table III: Relative abundances of Ag NPs in a particular Ag hydrosol - the comparison of two different techniques of samples preparation for TEM imaging and PSD determination

NP size [nm]	NPs counts in TEM images obtained from samples prepared by		Relative number of NP sizes in TEM images obtained from samples prepared by	
	technique (i)	technique (ii)	technique (i)	technique (ii)
5	83	149	28,2	28,9
10	119	217	40,5	42,1
15	53	89	18,0	17,3
20	17	31	5,8	6,0
25	9	14	3,1	2,7
30	6	11	2,0	2,1
35	2	2	0,7	0,4
40	1	1	0,3	0,2
45	2	0	0,7	0,0
50	1	1	0,3	0,2
>55	1	0	0,3	0,0

Note: Technique (i) - the drop drying; Technique (ii) - the 2D-interfacial film re-assembling.

argument can be further explained as follows. Considering that the smaller NPs remain in the liquid part of a drop for a longer period while the larger NPs gravitationally sediment, then, during the further drying, the smaller NPs are placed on the layer of settled larger NPs and, consequently, they are located into the unoccupied places in the first layer (= on the C-coated Cu grid). Nevertheless, there can be some very occupied spots, aggregates, where it is impossible for smaller NPs 'to fall' into the first layer. Thus, this fraction of smaller NPs remains on the top of aggregates and is invisible in the 2D-imaging.

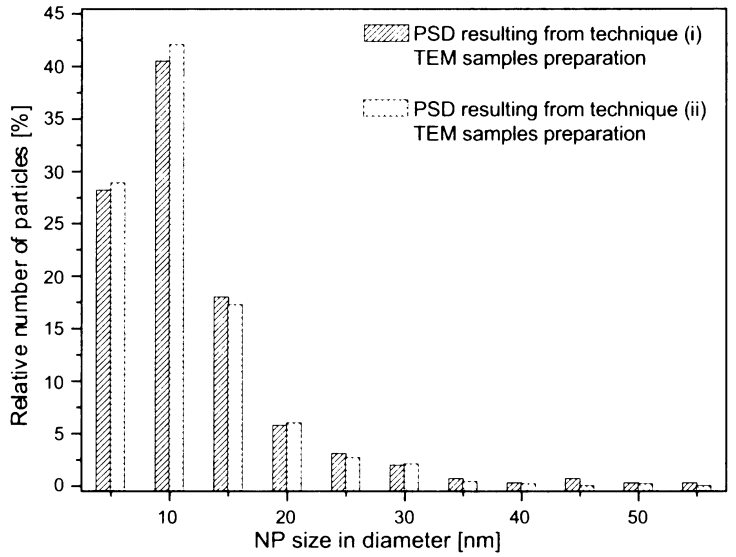

Fig. 16: A comparison of PSDs obtained from the same Ag hydrosol by using two different TEM samples preparation techniques: (i) – the drop drying technique, (ii) – the interfacial film re-assembling technique.

Furthermore, obviously, the number of NPs encountered in a TEM image, Fig. 17 and Table III, is higher for the film preparation technique than that for the drop-drying technique.

Therefore, one can rather prefer the film technique instead of the drop-drying technique of TEM samples preparation for PSD determination. Nevertheless, the reality is never so simple and, thus, not all Ag hydrosols and particularly the systems composed of hydrosols with adsorbate are able to form an interfacial film. Moreover, there is another threat that for some systems (= a hydrosol with an agent intentionally added) the interaction with bpy (to form the interfacial monolayer 2D-film) could change the morphology of the native system. Hence, it should be carefully considered for each system and hydrosol which is the best way of samples preparation for TEM imaging and, consequently, for the PSD determination.

In the Thesis: for the morphology observation, the drop-drying technique has been used; and for the PSD determination, the film technique has been preferentially employed. Provided that the film technique could not be employed, more TEM images of the drop-dried samples have been taken into account for the PSD determination to analyze a statistically meaningful assembly of NPs.

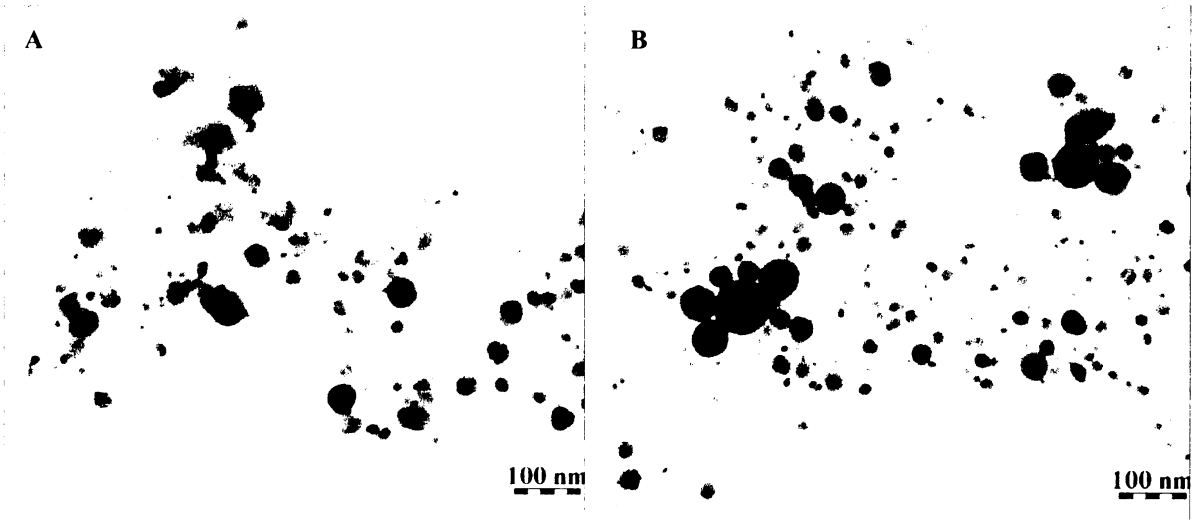

Fig. 17: A comparison of two TEM images obtained from the same Ag hydrosol. The TEM imaging samples were prepared by using two different techniques: (A) by the drop drying (=technique (i)) or (B) by the interfacial film re-assembling (=technique (ii)).

Last, but not least, attention is given to the computer TEM image treatment. Even if there are many programs which allow to count NPs and to evaluate PSDs, their results are not always relevant. In particular, in the case of larger aggregates, where the boundaries of NPs are distinguishable by eye-sight, the computer program divides such a NP incorrectly which leads, consequently, to a different PSD. As a result, in the Thesis, the TEM image treatment for the PSD determination has been preferentially done manually despite the fact that this process is largely time-consuming.

Chapter 2

Optimization of LA/NF process for silver NPs preparations

LA/NF of a Ag target in ultrapure water by ns laser pulses (using the setup depicted in Schema II) was performed and the effect of changes of one of the physical or physico-chemical parameters on the outcome of the process was explored. The parameters which were subjected to changes were laser pulse wavelength (1064 and 532 nm), energy per pulse (for pulses of 1064 nm wavelength), and the continuous or step-wise performing of LA/NF at each of the 1064 and 532 nm wavelengths. Furthermore, the effects of consecutive LA/NF with 1064 nm and 532 nm (and vice-versa) laser pulses, and of the effect of a consecutive LA/NF + NF at each of the two wavelengths were explored.

For evaluation and mutual comparison of various outcomes of the LA/NF process, TEM imaging and PSD determination as well as SPE spectra of the resulting Ag NP hydrosols were employed.

2.1. Reproducibility of LA/NF process at selected conditions

First, it was necessary to verify if the LA/NF process is fully reproducible in our experimental set-up. The step-wise LA/NF procedures have been performed with laser pulses of 1064 nm and of 532 nm wavelength.

At both selected wavelengths, 1064 nm and 532 nm, a good reproducibility of LA/NF was confirmed by a comparison of SPE spectra of three independent measurements. At each selected wavelength, approximately the same SPE-curve shapes were observed and A_{max} values varied only about 4-8 % in each step of LA/NF process, Table IV and Table V.

Table IV: Parameters of SPE bands of three Ag hydrosols prepared by LA/NF in water at 1064 nm (~187 mJ/pulse)

No. of hydrosol	λ_{max}	A_{max}	FWHM [nm]
1	396	0.718	95
2	394	0.756	92
3	393	0.779	89

Table V: Parameters of SPE bands of three Ag hydrosols prepared by LA/NF in water at 532 nm (~60 mJ/pulse)

No. of hydrosol	λ_{max}	A_{max}	FWHM [nm]
1	393	0.495	74
2	392	0.515	72
3	393	0.522	71

2.2. Influence of laser pulse wavelength on LA/NF

The outcomes of LA/NF performed in the previous section with laser pulses of 1064 nm (~187 mJ/pulse) and 532 nm (~60 mJ/pulse) have been mutually compared.

A characteristic morphology of Ag NP hydrosol prepared at 1064 nm laser pulses is shown in Fig. 18A and its appropriate PSD is depicted in Fig. 18B. The PSD in Fig. 18B indicates that more than 40 % of NPs are in the range of sizes of about 10 - 15 nm in diameter, and more than 15 % of NPs are larger than 35 nm.

On the other hand, NPs prepared at 532 nm laser pulses, the characteristic morphology of which is shown in Fig. 18C, are by more than 50 % of 10 - 15 nm in diameter and only about 5 % of them are larger than 35 nm in diameter – Fig. 18D.

The comparison of the above presented systems prepared by using 1064 nm and/or 532 nm laser pulses indicates that a greater portion of smaller NPs is formed at 532 nm pulses, most probably due to a more efficient NF at this wavelength than at 1064 nm [32, 49, 151]. The results of TEM imaging are corroborated by the results of SPE measurements which will be discussed in detail in [Chapter 2.4.].

2.3. Influence of energy per pulse on LA/NF with 1064 nm pulses

For LA/NF performed with laser pulses of a particular wavelength, energy per pulse has emerged as an important parameter affecting the outcome of the LA/NF process. Therefore, Ag hydrosols were prepared with: (i) the energy of ~90 mJ/pulse and (ii) the energy of ~187 mJ/pulse at the same excitation wavelength of 1064 nm, using the step-wise LA/NF procedure. In Fig. 19, the SPE curves obtained after each step of LA/NF processes are compared. The results show that the about twofold increase of the energy per pulse induces roughly twofold increase of LA/NF efficiency, as witnessed by an approximately twofold increase of A_{max} in the SPE of the resulting Ag NP hydrosol.

Fig. 18A and Fig. 20A show the TEM images of the NPs in the two hydrosols prepared by pulses of the same wavelength of 1064 nm but of two different energies per pulse. Their mutual comparison indicates that at the higher energy per pulse (Fig. 20A), larger NPs and/or aggregates of NPs are formed than at lower energies (Fig. 18A). This is confirmed also by the PSD shown in Fig. 20B (in comparison to that in Fig. 18B), because only

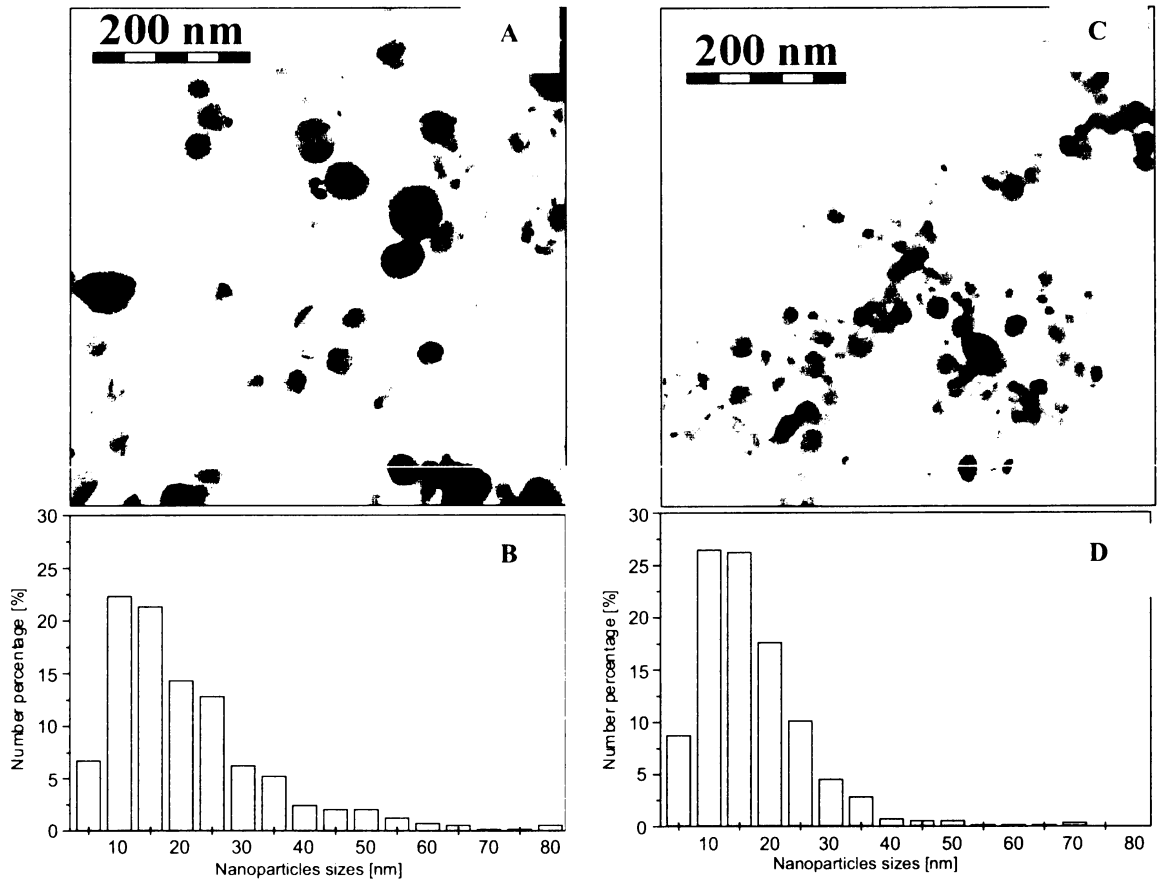

Fig. 18: (A) TEM image of Ag NPs in the hydrosol prepared by{2+3+3+5+7 min} LA/NF at 1064 nm (90 mJ/pulse); (B) PSD of (A); (C) TEM image of Ag NPs in the hydrosol prepared by {2+3+3+5+7 min} LA/NF at 532 nm (60 mJ/pulse); (D) PSD of (C).

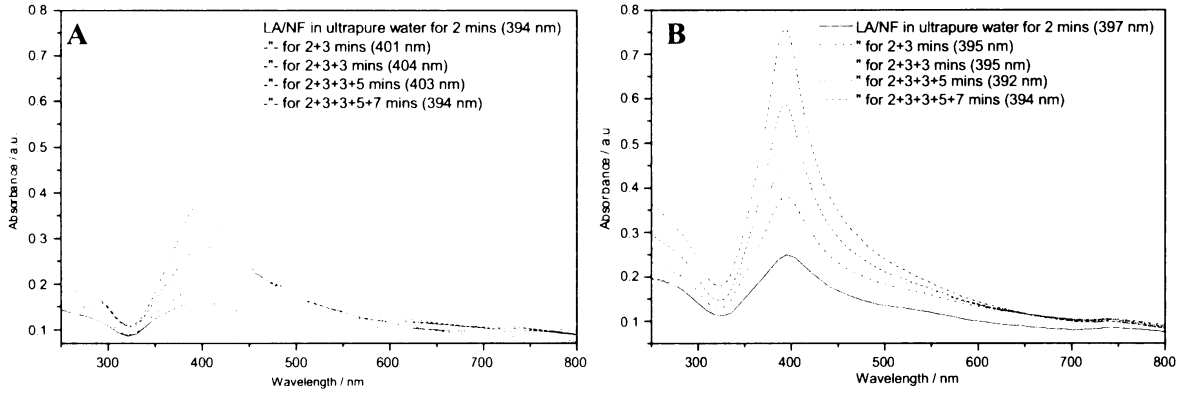

Fig. 19: The SPE spectra of Ag NP hydrosols prepared by step-wise LA/NF at 1064 nm with (A) ~90 mJ/pulse or (B) ~187 mJ/pulse. The positions of the SPE band maxima are given in parenthesis.

about 30 % of NPs is of the 10 - 15 nm sizes in diameter and more than 40 % of NPs is larger than 35 nm in diameter.

2.4. Influence of pauses during 20 minutes of LA/NF

To investigate how much the resulting hydrosol can be influenced by interruptions (of a duration ~2-3 min) during LA/NF, the following experiments were performed: (a) LA/NF without interruption for 20 min (continuous) and (b) LA/NF with four breaks during these 20 min (after 2, 5, 8 and 13 min from the start of LA/NF process: step-wise; the appropriate systems are labeled as 2 min, 2+3 min, 2+3+3 min etc.). The experiments were performed with 1064 nm as well as 532 nm laser pulses.

From the comparison of TEM images in Fig. 20A and Fig. 21 (depicting Ag NPs in hydrosols prepared at 1064 nm) one can conclude that in the case of interruptions during LA/NF with 1064 nm laser pulses a larger amount of smaller NPs is formed. This result can be caused by the fact that during each pause, there is sufficient

time for a dispersion of NPs into the bulk solution due to the stirring. Moreover, the dark period allows for an efficient build-up of the electric bilayer around each small NP and, consequently, the NPs do not aggregate into larger ones.

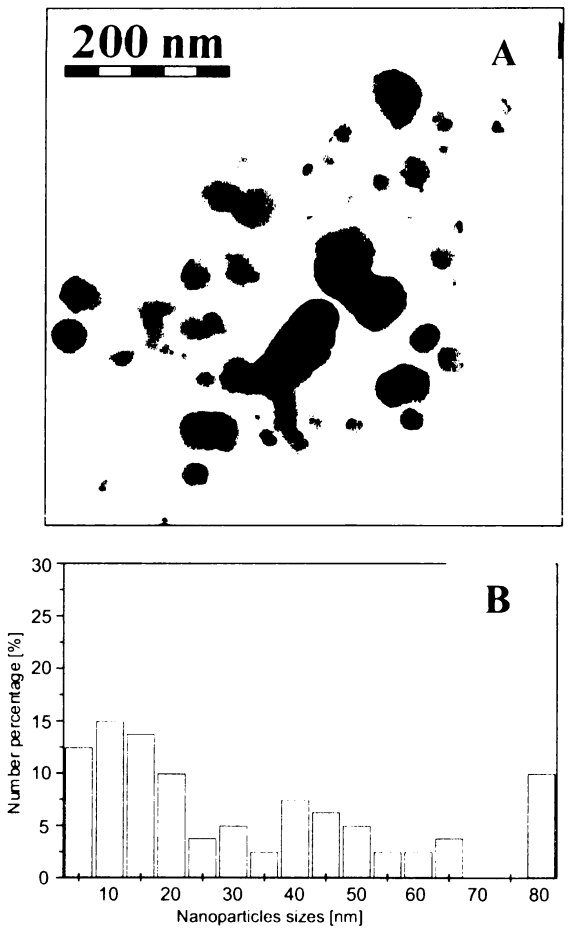

Fig. 20: (A) TEM image of Ag NPs in the hydrosol prepared by {2+3+3+5+7 min} LA/NF at 1064 nm (~187 mJ/pulse); (B) PSD of (A).

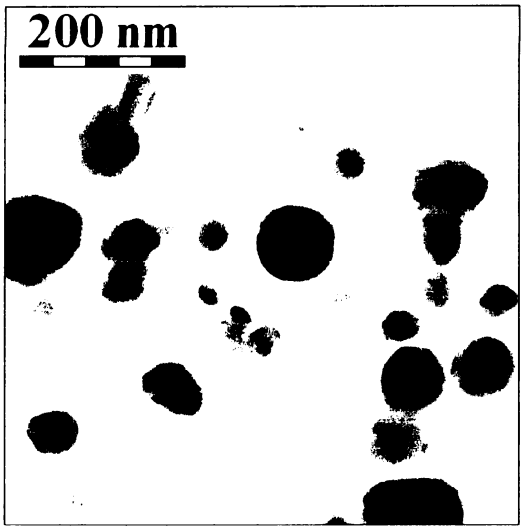

Fig. 21: TEM image of Ag NPs in the hydrosol prepared by 20 min LA/NF at 1064 nm (~187 mJ/pulse).

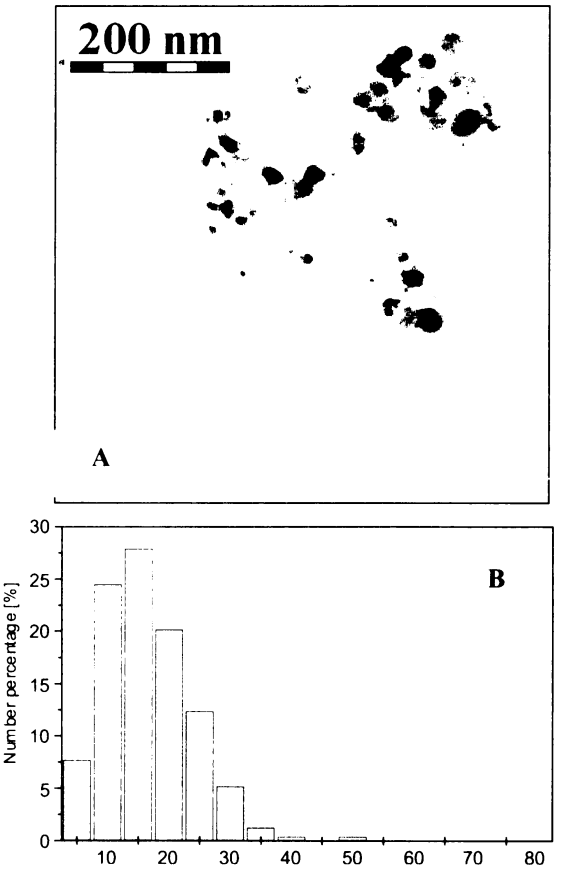

Fig. 22: (A) TEM image of Ag NPs in the hydrosol prepared by 20 min LA/NF at 532 nm (60 mJ/pulse); (B) PSD of (A).

The comparisons of TEM images depicting Ag NPs in hydrosols prepared at 532 nm (Fig. 18C and Fig. 22A) as well as of their PSDs (Fig. 18D and Fig. 22B) reveal that the sizes of NPs do not significantly differ if using continuous or step-wise preparation procedure.

In Fig. 23, SPE spectra of Ag NP hydrosols prepared by the continuous and the step-wise LA/NF procedure are compared. Fig. 23A provides this comparison for LA/NF with 1064 nm pulses, Fig. 23B for that with 532 nm pulses. The comparison of the SPE spectra in Fig. 23A corroborated the conclusions drawn from the comparison of the TEM images of the same hydrosols (Fig. 18A and Fig. 21) that the step-wise LA/NF provides the hydrosol containing a larger fraction of small NPs, while formation of large NPs and/or aggregates is suppressed as opposed to that prepared by the continuous procedure in which a fraction of large NPs and/or aggregates is witnessed by increased extinction in the 450-800 nm region, as well as by the shift of the A_{max} of the main extinction band from 394 nm to 405 nm.

In the case of 532 nm laser pulses (Fig. 23B), there is an increase of A_{max} while prevailing the symmetric SPE band. The possible explanation, supported by the above mentioned comparisons of TEM images and of the appropriate PSDs, i.e. no significant difference between sizes of NPs prepared by step-wise or continuous

procedure, is that the dark periods in the step-wise LA/NF procedure with 532 nm laser pulses provide sufficient time for the formation of a more concentrated Ag NP hydrosol.

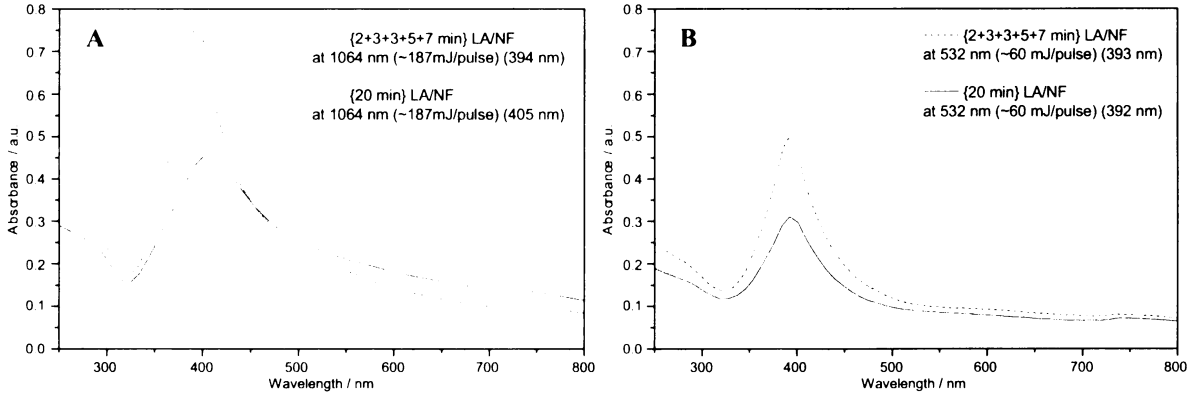

Fig. 23: The SPE spectra of Ag NP hydrosols prepared by step-wise and/or continuous LA/NF (A) at 1064 nm (187 mJ/pulse) or (B) at 532 nm (60 mJ/pulse).

The comparison of part A and B of Fig. 23 allows for evaluation of the effect of a different wavelength of laser pulses on both the continuous, and the step-wise LA/NF. For both processes, the SPE spectra indicate a preferential formation of small NPs with 532 nm laser pulses. For the step-wise process, an analogous conclusion has been already drawn from comparison of the TEM images of Ag hydrosols prepared with 532 nm and 1064 nm laser pulses [Chapter 2.2.]. The effect of the change of the laser pulse wavelength is more pronounced in the case of the continuous process.

2.5. Consecutive LA/NF with laser pulses of two wavelengths

2.5.1. Sequence of 1064 nm / 532 nm pulses

This wavelengths sequence has been selected on the basis of the results reported in [49, 73], which indicate that the NF process is more efficient at 532 nm laser pulses, and supported also by those presented in [Section 2.2.].

Fig. 24A demonstrates how the SPE of the hydrosol prepared at 1064 nm (90mJ/pulse) changes after further irradiation by 532 nm laser pulses with the energy of only 12 mJ/pulse. In particular, the long-wavelength tail (450-750 nm) which is characteristic for Ag NP hydrosols prepared at 1064 nm clearly disappears and the SPE curve is sharper in the 390-400 nm region. This observation indicates that larger particles (>35 nm) and/or aggregates are not present in the hydrosol prepared by LA/NF with 1064 and 532 nm pulses.

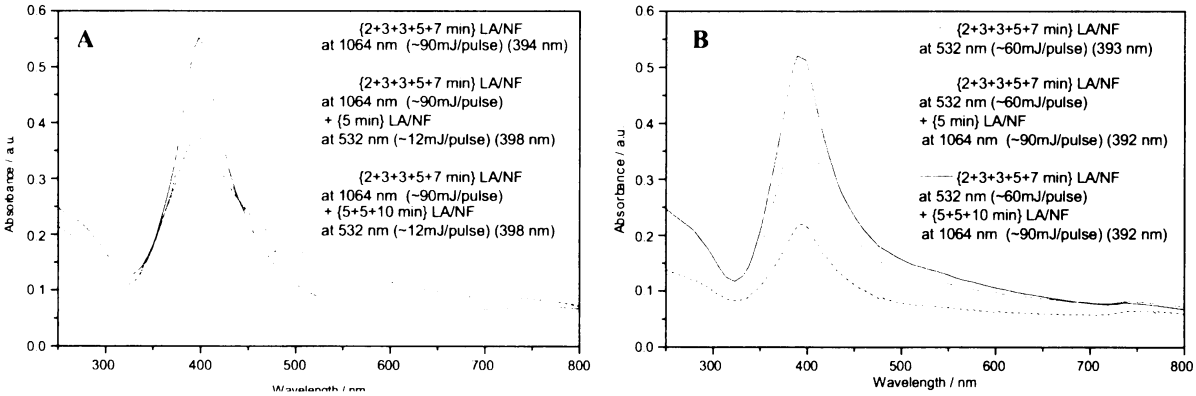

Fig. 24: The SPE spectra of the Ag NP hydrosols prepared by sequential, step-wise performed LA/NF: (A) with 1064 and 532 nm pulses, (B) with 532 and 1064 nm pulses.

Analogous conclusions are drawn from a comparison of the TEM images and PSDs of the hydrosol prepared by 1064 nm before (Fig. 18A, PSD in Fig. 18B) and after further LA/NF with 532 nm pulses (Fig. 25A, PSD in Fig. 25B). In particular, it can be concluded that larger NPs present in a Ag hydrosol prepared by 1064 nm pulses (Fig. 18A) are fragmented into smaller ones by 532 nm pulses.

2.5.2. Sequence of 532 nm / 1064 nm pulses

This sequence of used wavelengths for LA/NF was tested for the sake of a comparison with the former sequence.

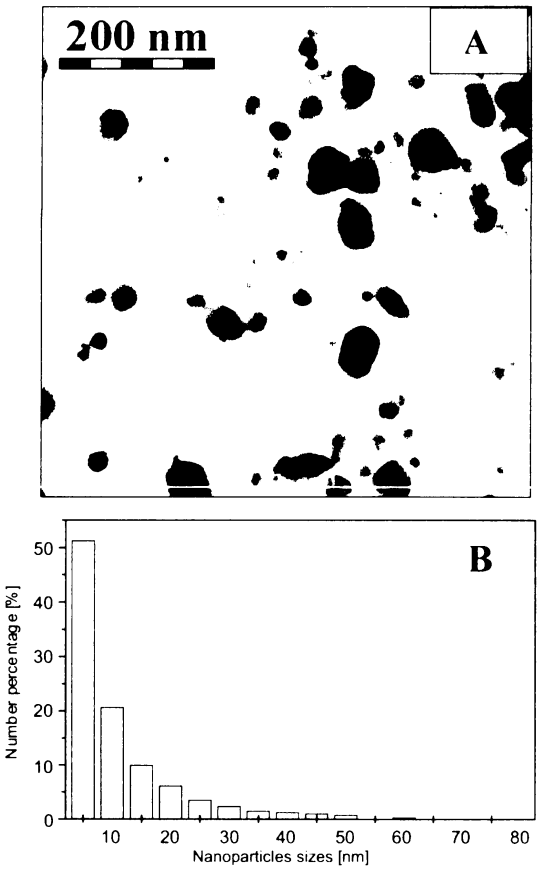

Fig. 25: (A) TEM image of Ag NPs in the hydrosol prepared by sequential, step-wise performed LA/NF at 1064 nm (90 mJ/pulse) and 532 nm (12 mJ/pulse); (B) PSD of (A).

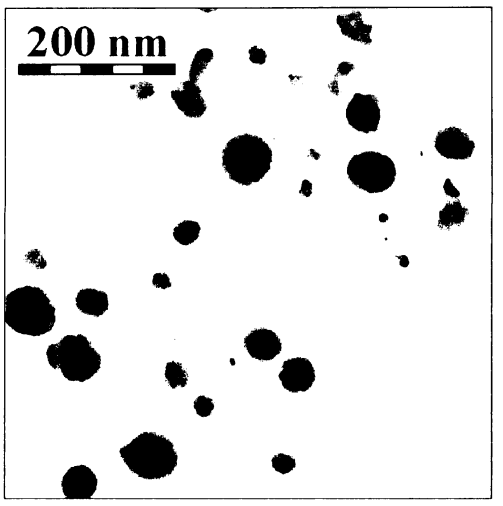

Fig. 26: TEM image of Ag NPs in the hydrosol prepared by sequential, step-wise performed LA/NF at 532 nm (60 mJ/pulse) and 1064 nm (90 mJ/pulse).

The SPE curve of the Ag hydrosol possesses the long-wavelength tail (450-750 nm) – Fig. 24B. Furthermore, the NPs of such a hydrosol, in comparison to those present in the sol before the additional LA/NF with 1064 nm pulses (i.e. after LA/NF with 532 nm pulses only), were observably larger – compare Fig. 18C with Fig. 26. The larger NPs observable in Fig. 26 have probably been formed by LA/NF at 1064 nm, i.e. in the second part of this LA/NF sequence.

2.6. Consecutive LA/NF + NF processes

2.6.1. LA/NF + NF with 532 nm pulses

For the processes performed with laser pulses of this wavelength, the additional NF, i.e. irradiation of the sol in the absence of the Ag target, which followed the LA/NF process has not produced any effect on the SPE of the resulting hydrosol (Fig. 27A). A possible reason for this observation is that the NPs in the sol have been efficiently fragmented during the first LA/NF step of the process.

2.6.2. LA/NF + NF with 1064 nm pulses

For the LA/NF + NF with 1064 nm laser pulses, the comparison of the SPE spectra of the Ag NP hydrosols obtained prior and after the second NF only step (Fig. 27B) indicates some increase of the absorbance >650 nm and a small decrease of A_{max} after the NF step. These spectral changes indicate that some aggregation of the sol occurred during NF. A similar effect was observed in [55], while an efficient size-reduction of NPs without any aggregation was reported in [11]. A possible reason for the difference between the results presented in [this Thesis] and in [11] is a substantial difference in the energies per pulse employed: 30 mJ/pulse [11] and 187 mJ/pulse [this Thesis]. Another contribution to the instability of the sol [this Thesis] can stem from interruptions of the NF process.

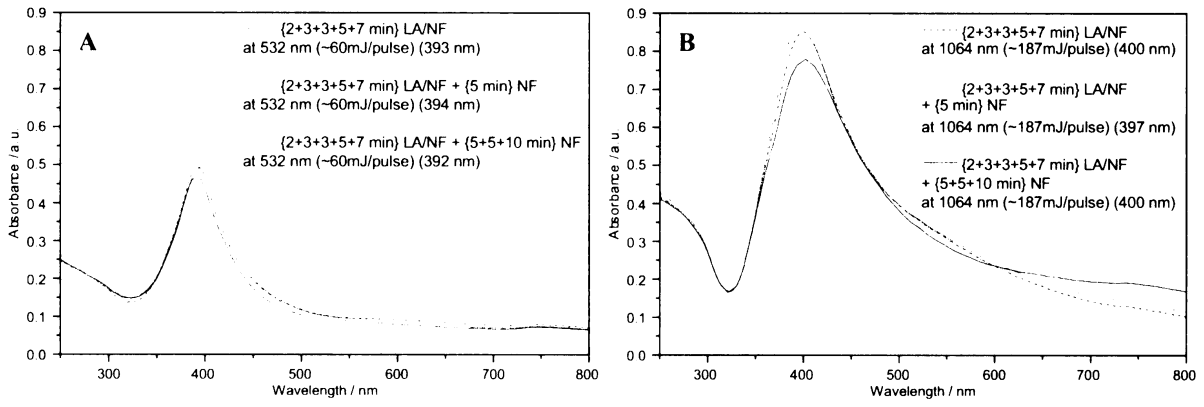

Fig. 27: The SPE spectra of the Ag NP hydrosols prepared by consecutive, step-wise performed LA/NF and NF: (A) with 532 nm and (B) with 1064 nm pulses.

2.7. Stability of Ag NP hydrosols (2.1.-2.6.) during aging

All hydrosols prepared only by the 532 nm laser pulses were more stable than those prepared by the 1064 nm whose were precipitated in 1-3 days after their preparation. This fact can be caused by the presence of a larger portion of smaller NPs in 532nm-LA/NF prepared hydrosols. Nevertheless, the λ_{max} positions even of these hydrosols were red-shifted in 8 days of a value about 11 nm and their A_{250} values and integrated areas of the SPE bands decreased by about 20 % - Fig. 28A and Table VI.

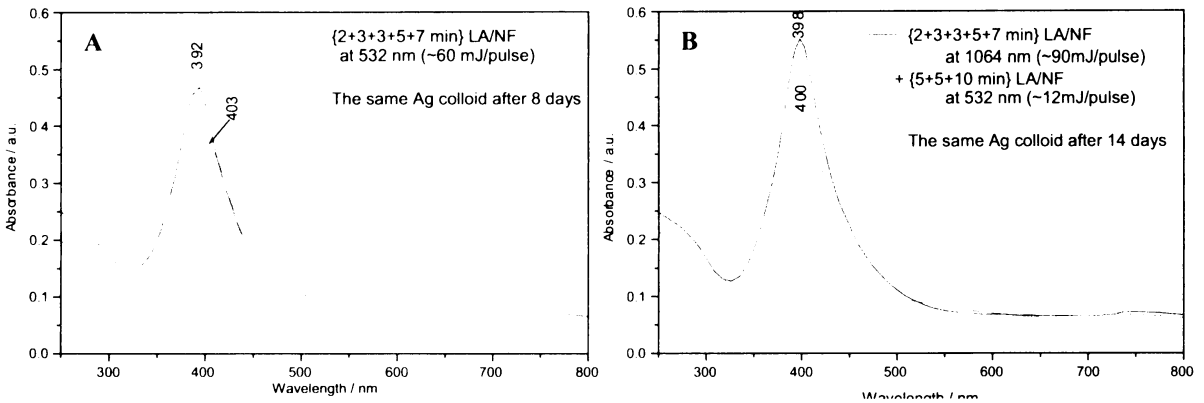

Fig. 28: The SPE spectral changes of Ag NP hydrosols prepared by step-wise performed LA/NF (A) with 532 nm pulses and (B) with 1064 and 532 nm pulses.

Table VI: Parameters of SPE bands of Ag hydrosols prepared by LA/NF - aging

Ag hydrosol prepared by LA/NF with	Time after LA/NF [day]	A_{250}	A_{max}	Integrated area	FWHM [nm]	SPE spectra depicted in
532 nm laser pulses	0	0.250	0.473	67	75	Fig. 28A
	8	0.198	0.364	55	81	
1064nm + 532 nm laser pulses	0	0.248	0.552	70	72	Fig. 28B
	14	0.213	0.424	60	71	

On the contrary, the hydrosols prepared by the consecutive two wavelengths LA/NF with the sequence of 1064 and 532 nm laser pulses, were stable enough during 14 days: their λ_{max} positions red-shifted only about 2 nm and their A_{250} values and integrated areas of the SPE bands (in the 320-800nm interval) they both decreased of ~14 % (during 14 days) – Fig. 28B and Table VI.

These most prospective hydrosols (the sequence of 1064 and 532 nm LA/NF) were used for further investigations of their reactivity with bpy and TMPyP by using SERS and SERRS spectroscopy.

2.8. Results of optimization of LA/NF for Ag NP hydrosol preparation

1) A step-wise or continuous performing of LA/NF is an important parameter which affects the outcome of LA/NF with both 532 nm and 1064 nm pulses. This result indicates that the 2-3 min dark periods between each of the irradiation steps play a role in the process of Ag NPs formation. Several factors contributing to this role can be envisaged. In particular, the dark periods can be considered to provide a surplus time for (i) NPs growth, (ii) efficient build-up of the electric bilayer enveloping (and stabilizing) the NPs, (iii) a homogenous distribution of NPs within the sol (by stirring) prior to further irradiation.

2) Both for the step-wise and continuously performed LA/NF, the employment of 532 nm pulses produces Ag NP hydrosols constituted predominantly by small Ag NPs of sizes <35 nm. By contrast, the same procedure performed by 1064 nm pulses yields a rather wide distribution of small as well as large particles. This result can be explained by a more efficient NF with 532 nm pulses than with the 1064 nm ones, in accord with refs 32, 151. On the other hand, the efficiency of LA (i.e. of the transport of Ag from the target to water) appears to be more efficient for 1064 nm pulses than for 532 nm pulses, as demonstrated in ref. 32, 151 and indicated also by the results presented in [Chapter 2.4.] and [Chapter 2.6.]. The differences in the LA and the NF processes efficiencies at 1064 nm and 532 nm probably originate from (i) a more efficient light absorption by Ag NPs at 532 nm than at 1064 nm; (ii) substantially larger absorption index k (directly related to the absorption coefficient) of bulk Ag at 1064 nm than at 532 nm [32, 151].

3) The differences between the efficiencies of the LA process and NF process outlined in 2) can possibly be responsible for some wavelength specificity of the difference between the outcome of the step-wise and the continuous LA/NF [Chapter 2.4.]. When these two processes performed with 1064 nm pulses are compared, the

substantial increase of small nanoparticle fraction in Ag NP hydrosol prepared by the step-wise process stems most probably from a sufficient stabilization of the NPs during the dark periods which, in turn, prevents their further aggregation and/or growth. This stabilization is of a particular importance in this case, since NF is less efficient, hence larger particles tend to be present in the sol. For LA/NF performed with 532 nm pulses, the Ag NP sol produced by the step-wise process appears to be more "concentrated" than that obtained by a continuous process, while the PSDs of both sols are comparable. A possible explanation can be found in a combination of a large efficiency of NF at this wavelength with the existence of dark periods in the step-wise performed process. During these dark periods, sufficient time for NP growth (from Ag clusters or very small particles efficiently produced during the irradiation periods) is provided, and hence the concentration of the NPs increases in comparison to the continuously performed process.

4) Ag NP hydrosol prepared by the step-wise performed consecutive LA/NF with 1064 nm and 532 nm laser pulses proved itself to be the most stable during aging of all the hydrosols reported in this Chapter. The sol is constituted predominantly by small (<35 nm) NPs (with 50% of NPs being of 5 nm size) and shows a narrow and symmetric SPE band. This hydrosol has been selected for SERS/SERRS spectral testing.

2.9. SERS/SERRS spectral probing of reactivity of the „optimized" Ag NP hydrosol

SERS spectral testing of Ag NPs prepared (in the form of a hydrosol) by the optimized LA/NF procedure has been focused on:

(i) probing of the ability of the Ag NPs to act as efficient Raman scattering amplifiers in Ag hydrosol/model adsorbate systems (both in the presence and in the absence of additional selected ions, such as Cl^-, THS, BH_4^-, Ag^+),

(ii) probing the Ag NPs' surface – model adsorbate interaction on the basis of the assignment of the SERS or SERRS spectra of model adsorbates obtained from each SER(R)S-active system. The particular goal is to detect the presence of Ag^0 and/or Ag^+ adsorption sites on the surfaces of Ag NPs, both bare and modified by action of the selected ions (Cl^-, THS, BH_4^-, Ag^+) via identification of (a) an unperturbed form of the model adsorbate, (b) Ag^+-model adsorbate species and/or (c) Ag(0)-model adsorbate species. For the selected model adsorbate, bpy and TMPyP, SERS or SERRS spectra (mostly as) pure component spectra obtained by factor analysis (FA) of such species are (for the sake of comparison and assignment) available in the previously published papers [130, 132, 142] and presented in [Introduction] (Figs 10, 11, 13 and 14).

(iii) the investigation of a relationship between the surface structure changes (manifesting themselves by a change in the presence of Ag^+ and Ag^0 adsorption sites) and changes in the morphology of Ag NPs. Such relationship (in particular a simultaneous formation of new Ag^0 adsorption sites and of compact aggregates of touching and/or interpenetrating NPs induced by Cl^- adsorption) has been recently revealed for Ag NPs prepared chemically by reduction of $AgNO_3$ by $NaBH_4$ and modified by adsorbed chlorides [104, 112, 130, 132]. In these systems, however, the surface-adsorbate interactions can be affected by the presence of residual borate (or even polyborate) anions. In contrast to those, surfaces of Ag NPs prepared by LA/NF are considered to be more chemically "clean". This aspect has been the driving force for inventing Ag NPs prepared by LA as SERS-active substrates [11, 153]. More recent studies have shown that Ag NPs prepared by LA/NF are probably mostly stabilized by adsorbed OH^- anions [46]. Nevertheless, comparative studies of surface-adsorbate interactions on both types of Ag NP hydrosols can provide important information for further applications of laser ablated Ag NPs as substrates for SERS/SERRS spectroscopy.

2.9.1. Effect of HCl on Ag hydrosol/bpy systems

In [152, this Thesis – Chapter 3], it is demonstrated that chlorides induce intergrowth of silver NPs prepared by LA/NF of a Ag foil in the presence of chloride solution. To investigate how the addition of chlorides, intentionally added into the system containing bpy and Ag NPs, influences the morphology of the system and the SERS signal obtained from it, the following systems were prepared: (i) Ag hydrosol/bpy/HCl (= post-treating by HCl) and/or (ii) Ag hydrosol/HCl/bpy (= pre-treating by HCl).

In Figs 29A and 29B, the TEM images of the Ag hydrosol and of the system prepared from this parent hydrosol by addition of bpy and, subsequently, HCl, are compared. While the parent hydrosol contains almost entirely the small, isolated NPs (Fig. 29A); the system post-treated by HCl consists of large (>80 nm) interpenetrating NPs (Fig. 29B). Such morphologies were found to be typical for systems where SERS spectral form of Ag(0)-bpy surface complex dominates [112, 130, 132] (in systems with BH_4^--reduced Ag hydrosols). The SERS spectrum of this system is shown in Fig. 29C where the framed peaks belong to the Ag(0)-bpy surface species and are its characteristic markers (pure component SERS spectrum of Ag(0)-bpy is shown in Introduction - Fig. 11; that of Ag^+-bpy in Fig. 10). Thus, SERS spectrum in Fig. 29C is formed by combination of marker bands of both forms, Ag^+-bpy and Ag(0)-bpy surface complexes. The final concentration of HCl necessary for Ag(0)-bpy formation was established between $5x10^{-4}$ M and $1x10^{-3}$ M HCl in the final Ag hydrosol/bpy/HCl systems; which is the same value as for systems of BH_4^--reduced Ag-hydrosols [112, 130]. However, as demonstrated in Fig. 30, the bpy:HCl ratio plays a key role in Ag(0)-bpy SERS signal observation. Nevertheless, it is not possible to quantify the content of Ag^+-bpy versus Ag(0)-bpy and to relate it to the bpy:HCl ratio because no internal standard was introduced to the

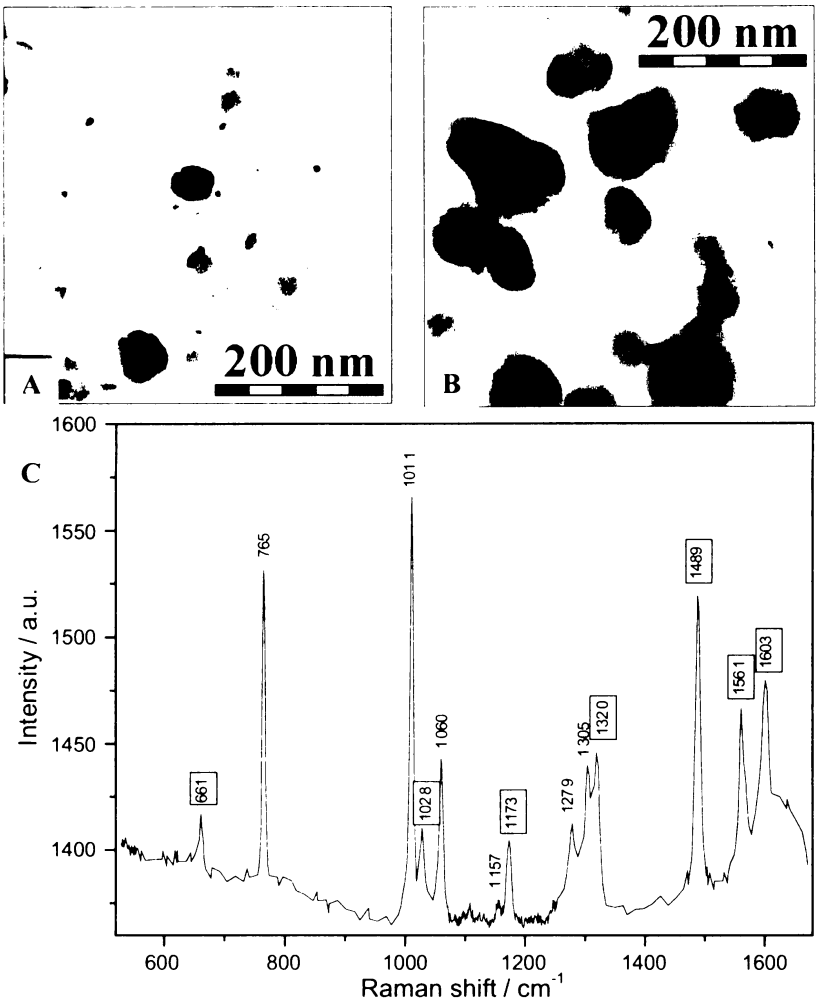

Fig. 29: TEM images of (A) the parent Ag NP hydrosol and (B) of a system prepared from this hydrosol: Ag hydrosol/bpy($5x10^{-5}$ M)/HCl($1x10^{-3}$ M). (C) SERS spectrum measured from the system depicted in (B). The characteristic markers of Ag(0)-bpy surface complex are framed.

systems and the Raman spectral bands of water were not sufficiently intense at 514.5 nm excitation wavelength to serve as such a standard. The ratio of integral intensities of two selected bands (e.g. the 1305 and 1320 cm^{-1} bands) also cannot be used for the Ag^{+}-bpy vs. Ag(0)-bpy content determination because in some spectra, these bands are not well separated. The same applies also in the case of the other characteristic markers of each form. Therefore, in Fig. 30 SERS spectra of appropriate systems are compared without any smoothing and other software treatment. Nevertheless, as it was mentioned above, the concentration threshold of HCl for Ag(0)-bpy formation lies in the range between $5x10^{-4}$ M and $1x10^{-3}$ M HCl concentration in the final system in the case of the post-treating by HCl for all studied concentrations of bpy, i.e. $5x10^{-4}$ - $5x10^{-6}$ M bpy concentrations in the final systems.

In contrast to that, in the case of the pre-treating by HCl, the threshold HCl concentration value for Ag(0)-bpy formation has been determined as low as $1x10^{-4}$ M HCl in the final Ag hydrosol/HCl/bpy system for the range of $1x10^{-5}$-$1x10^{-7}$ M bpy concentrations. In Fig. 31, three SERS spectra of systems with different HCl:bpy ratios are compared (without any normalization). A trend of the Ag(0)-bpy SERS signal dominance appears clearly with an increase of HCl:bpy ratio, from spectrum a to spectrum c in Fig. 31: an increase of the 1321 cm^{-1} band and a decrease of the 1305 cm^{-1} band; the appearance of the 1024 cm^{-1} and 660 cm^{-1} bands; and, last but not least, the 1488 cm^{-1} band becomes the most intensive band in spectrum which is typical for Ag(0)-bpy [112, 130, 132, Introduction – Fig. 11].

2.9.2. Effect of NaCl on Ag hydrosol/bpy systems

In the previous studies performed on BH_4^--reduced hydrosols [112, 130, 132], the effect of NaCl to the formation of Ag(0)-bpy surface complex was observed at the threshold concentration as high as $1.5x10^{-2}$ M NaCl in the final system. We have found out that in hydrosols prepared by LA/NF, the threshold concentration value of NaCl for Ag(0)-bpy formation is shifted to a lower value in the case of pre-treating by NaCl ($1x10^{-2}$ M NaCl in the final system), and

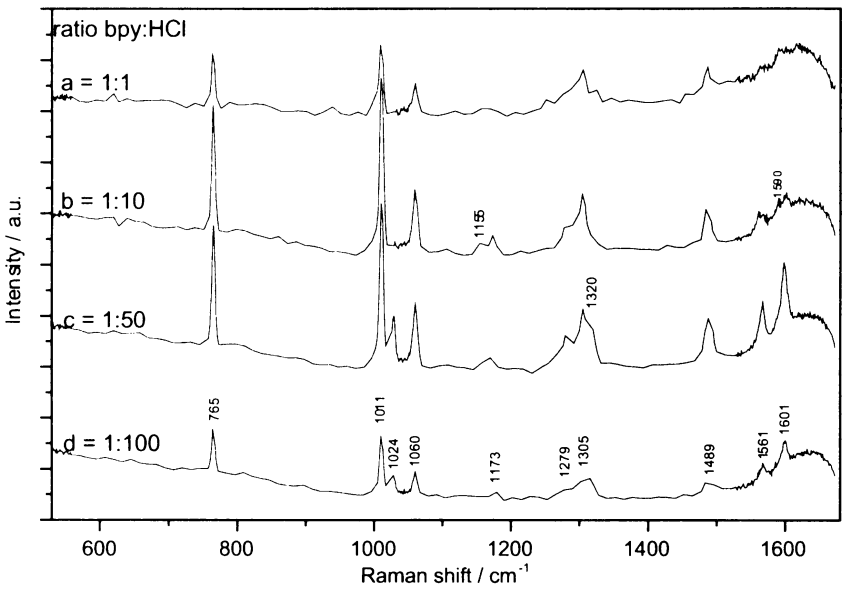

Fig. 30: The effect of bpy:HCl ratio in Ag hydrosol/bpy/HCl systems. The SERS spectra of the Ag hydrosol/bpy(c_x)/HCl($5x10^{-4}$ M) systems where c_x equals to: a = $5x10^{-4}$ M, b = $5x10^{-5}$ M, c = $1x10^{-5}$ M and d = $5x10^{-6}$ M.

remains of the same value for systems post-treated by NaCl.

Thus, it means that, as in the case of HCl, the pre-treating by chlorides leads to an decrease of the threshold concentration value of chlorides which is necessary for Ag(0)-bpy surface complex formation.

The TEM images (not shown here) of typical morphologies of systems treated by NaCl (pre- and/or post-) at and above the threshold NaCl concentration value for Ag(0)-bpy formation have confirmed the intergrowth of NPs (interpenetrating NPs) – similarly to the systems with HCl at and above the threshold HCl concentration value for Ag(0)-bpy formation. It could be thus concluded that addition of chlorides causes NPs intergrowth independently on the way how they were introduced into the system, i.e. by (a) LA/NF in chlorides solution [152, this Thesis – Chapter 3], (b) the addition of chlorides to the hydrosol after its preparation (the pre-treating by chlorides), (c) the addition of chlorides to the hydrosol after its preparation and after addition of the probing adsorbate bpy (the post-treating by chlorides). In all these cases chlorides have induced NPs intergrowth.

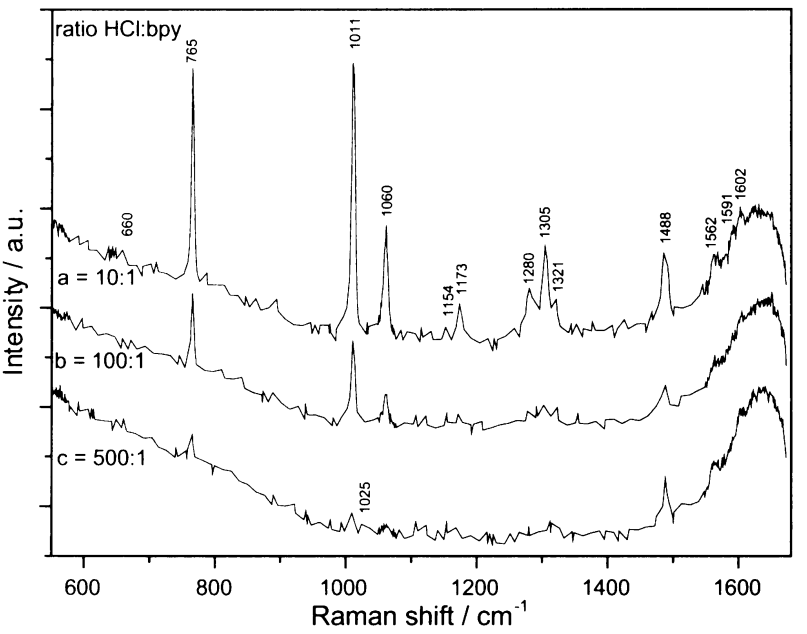

Fig. 31: The effect of HCl:bpy ratio on Ag hydrosol/HCl/bpy systems. The SERS spectra of the Ag hydrosol/HCl($1x10^{-4}$ M)/bpy(c_x) systems where c_x equals to: a = $1x10^{-5}$ M, b = $1x10^{-6}$ M and c = $2x10^{-7}$ M.

2.9.3. Effect of THS on Ag hydrosol/bpy systems

The previous studies of THS influence on the SERS spectral signal of bpy in systems with BH_4^--reduced Ag hydrosol [132] have reported observation of Ag(0)-bpy surface complex SERS signal if the concentration of THS in the final system achieved $2x10^{-3}$ M. In the present study, the effect of THS addition was tested in the concentration range $1x10^{-3}$-$1x10^{-5}$ M THS in the final system.

In Fig. 32, SERS spectra of Ag hydrosol/bpy/THS systems with various THS concentrations are presented. The THS threshold concentration value for Ag(0)-bpy surface complex formation appears to be about $5x10^{-5}$ M THS in the final system, which is a lower THS concentration value than for systems of BH_4^--reduced Ag hydrosols with bpy [132]. Moreover, it could be pointed out that a higher concentration of THS in the systems leads to observation of a higher signal of Ag(0)-bpy (Fig. 32 – spectrum a). This observation is quite interesting, since THS has been reported as a SERS-deactivating agent [93, 103, 142]. An increase of SERS signal thus probably stems from an efficient generation of Ag(0)-bpy species which exhibits the CT-resonance contribution to the overall SERS enhancement at 514.5 nm excitation.

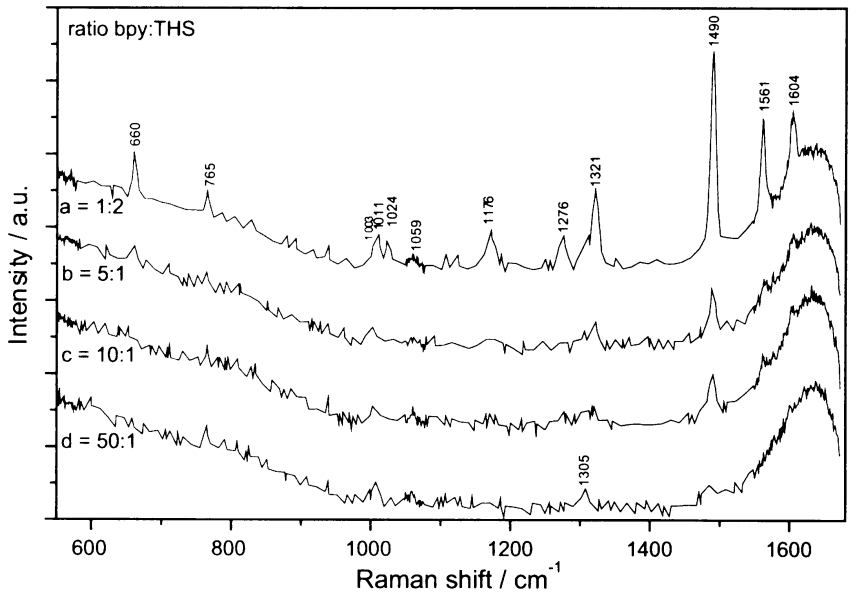

Fig. 32: The effect of ratio bpy:THS on Ag hydrosol/bpy/THS systems. The SERS spectra of Ag hydrosol/bpy($5x10^{-4}$ M)/THS(c_y) systems where c_y equals to: a = $1x10^{-3}$ M, b = $1x10^{-4}$ M, c = $5x10^{-5}$ M, and d = $1x10^{-5}$ M.

2.9.4. Effect of BH_4^- on Ag hydrosol/bpy systems

The investigation of the effect of BH_4^- on Ag(0)-bpy surface complex formation on LA-Ag NP surfaces has been motivated by the results of the earlier experiments [132] which showed that a reducing ambient is necessary for Ag(0) adsorption sites generation on NP surfaces.

Sodium borohydride is a well known reducing agent, frequently used for Ag hydrosols preparation. In the previous studies [132], bpy was introduced in a $AgNO_3$ solution which was followed by addition of $NaBH_4$ solution. Bpy molecules were thus present during the process of Ag NP growth driven by the chemical reduction. When this process was accomplished, Ag(0)-bpy species was detected.

The present study tries to investigate the influence of the post-treating and/or pre-treating of Ag hydrosol/bpy system by BH_4^-.

In Fig. 33A, SERS spectra of Ag hydrosol/bpy/BH_4^- systems with various BH_4^- concentration are presented. Spectrum a shows the characteristic marker bands of Ag^+-bpy surface species detected in Ag hydrosol/bpy system in the absence of BH_4^- ions. Spectrum b shows that even a very small amount of BH_4^- ($5x10^{-6}$ M in the final system) increases the SERS signal. Spectrum c obtained for the system where bpy: BH_4^- ratio reaches the 1:1 value indicates that Ag(0)-bpy is generated. Finally, in spectrum d, the characteristic bands of this surface species are clearly distinguishable.

In the case of Ag hydrosol/BH_4^-/bpy system (Fig. 33B), the BH_4^- threshold concentration value for Ag(0)-bpy formation appears to be a somewhat lower than the $1x10^{-5}$ M BH_4^- concentration value in the final systems because at this concentration value (spectrum b in Fig. 33B) the characteristic markers of Ag(0)-bpy are already clearly developed. The threshold concentration value for Ag(0)-bpy formation probably lies between $1x10^{-5}$ M and $5x10^{-6}$ M, because in spectrum a in Fig. 33B, SERS signal of Ag^+-bpy still dominates. Hence, analogously to systems modified by addition of chlorides, a somewhat lower BH_4^- concentration in the final system is necessary for the formation of Ag(0)-bpy surface species in the case of the pre-treating by BH_4^- in comparison to the post-treating by BH_4^-.

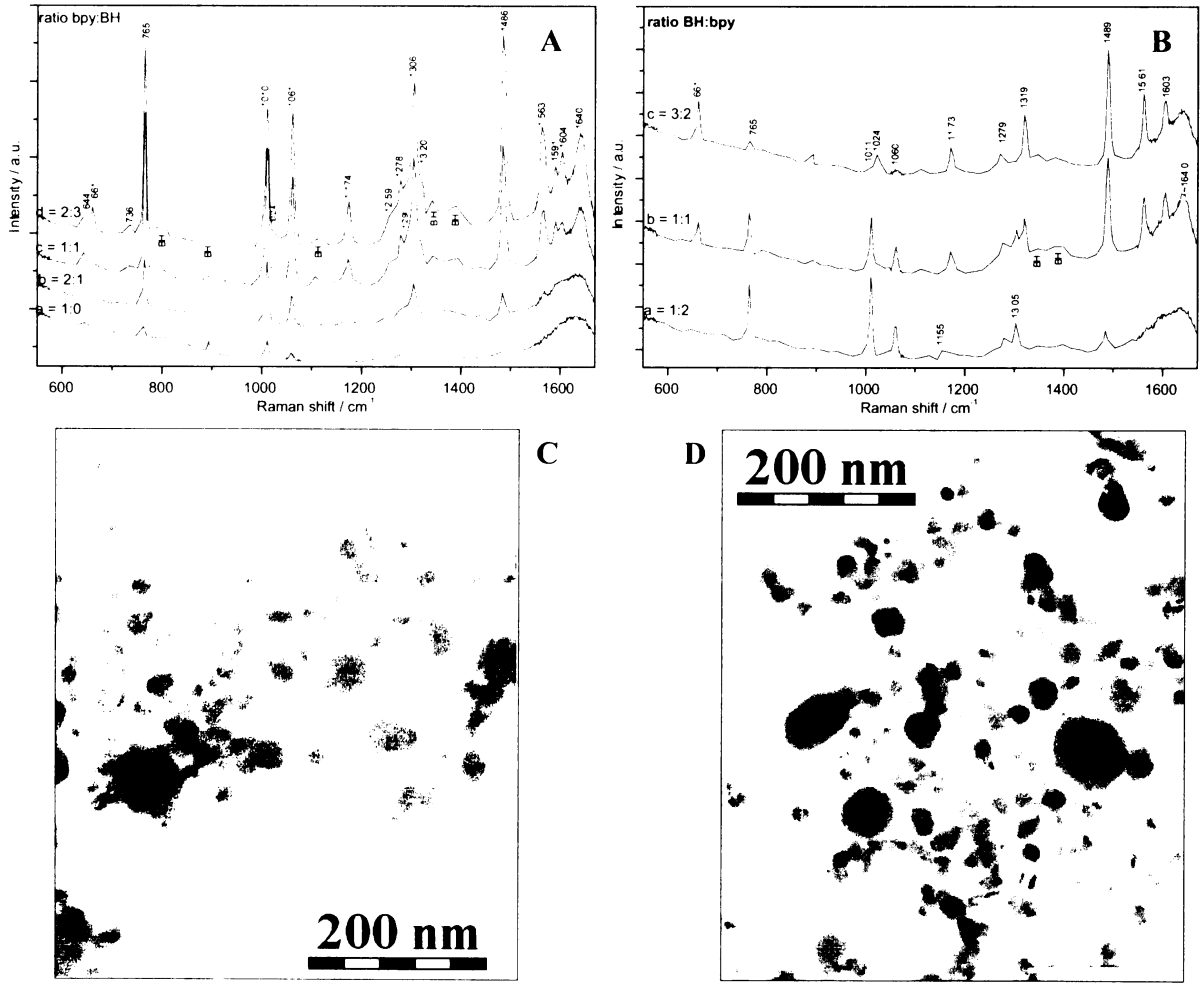

Fig. 33: (A) SERS spectra of the Ag hydrosol/bpy($1x10^{-5}$ M)/BH_4^-(c_y) systems where c_y equals to: a = 0M, b = $5x10^{-6}$M, c = $1x10^{-5}$ M and d = $1.5x10^{-5}$ M; (B) SERS spectra of the Ag hydrosol/BH_4^-(c_y)/bpy($1x10^{-5}$ M) systems where c_y equals to: a = $5x10^{-6}$ M, b = $1x10^{-5}$ M and c = $1.5x10^{-5}$ M; (C) TEM image of the Ag hydrosol/bpy($1x10^{-5}$ M)/BH_4^-($1.5x10^{-5}$ M) system (corresponding SERS signal = spectrum d in A); and (D) TEM image of the Ag hydrosol/BH_4^-($1.5x10^{-5}$ M)/bpy($1x10^{-5}$ M) system (corresponding SERS signal = spectrum c in B).

The morphologies of systems treated by BH_4^- were also investigated and two examples of TEM images are shown in Figs 33C and 33D. The former one originates from the Ag hydrosol/bpy/BH_4^- system (whose SERS spectrum is presented as spectrum d in Fig. 33A) and the later one from the Ag hydrosol/BH_4^-/bpy (whose SERS spectrum is shown in Fig. 33B, spectrum c). Both systems contain the same ratio of bpy:BH_4^-, i.e. 2:3. Similarly to the systems treated by chlorides, Ag NPs in systems treated by BH_4^- slightly interpenetrate each other, nevertheless, they are not so large in diameter as those in Fig. 29B (Ag hydrosol/bpy/HCl).

2.9.5. Effect of Ag^+ and BH_4^- on Ag hydrosol/bpy system

The following experiments were performed to find out if Ag(0) adsorption sites formation on the surfaces of LA-Ag NPs treated by BH_4^- can be hindered or prevented by the excess of Ag^+ ions (introduced to the system by using $AgNO_3$ solution). For the sake of better comparison to systems presented in [Chapter 2.9.4.] (influence of BH_4^- only) the same concentration of bpy in the final system was used. Two concentration values of Ag^+ ions were selected: $2x10^{-5}$ M and $4x10^{-4}$ M Ag^+ in the final systems. In the former case of Ag hydrosol/$AgNO_3$($2x10^{-5}$M)/bpy/BH_4^- system depicted in Fig. 34, the BH_4^- threshold concentration for Ag(0)-bpy formation was slightly higher than $1x10^{-5}$ M (i.e. higher than in systems treated only by BH_4^- itself); while in the other system (i.e. Ag hydrosol/$AgNO_3$($4x10^{-4}$ M)/bpy($1x10^{-5}$ M)/BH_4^-), the Ag(0)-bpy surface complex formation was not achieved even at ~$2x10^{-4}$ M BH_4^- concentration value, and only Ag^+-bpy signal dominated in the SERS spectrum (not shown here). These results indicate that formation of Ag(0)-bpy is hindered by the presence of Ag^+ ions.

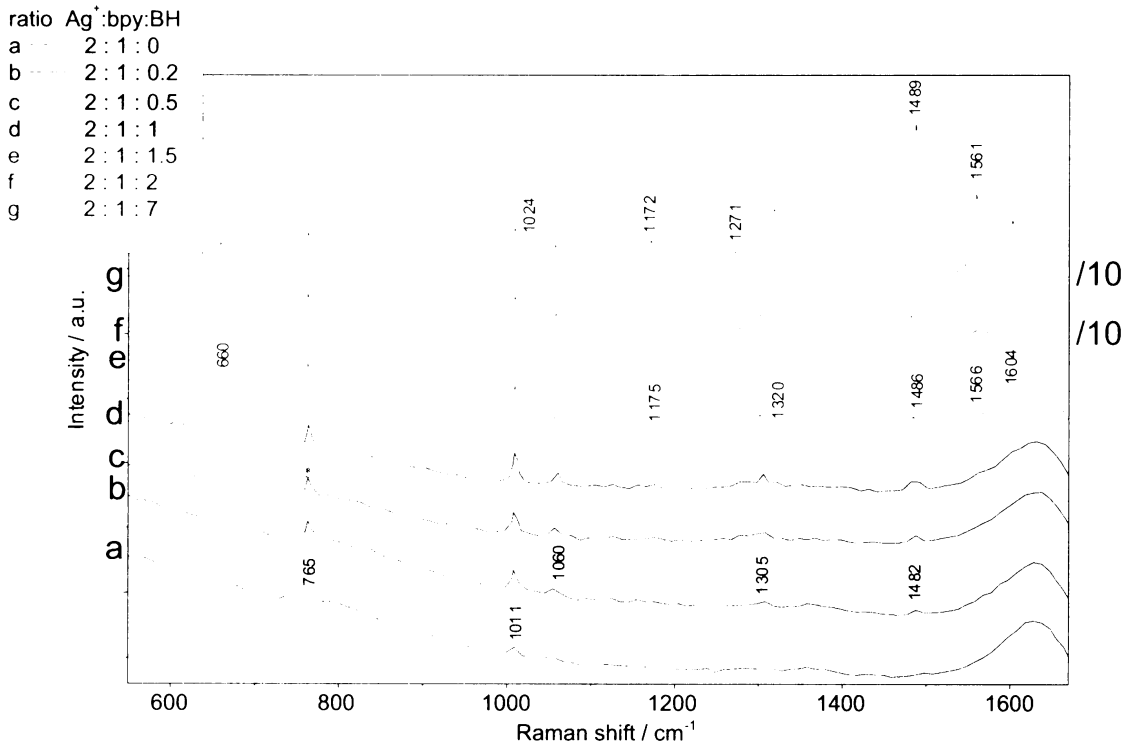

Fig. 34: SERS spectra of Ag hydrosol/$AgNO_3$ ($2x10^{-5}$ M)/bpy ($1x10^{-5}$M)/BH_4^-(c_y) system where c_y is: a = 0 M, b = $2x10^{-6}$ M, c – $5x10^{-6}$ M, d – $1x10^{-5}$ M, e – $1.5x10^{-5}$ M, f – $2x10^{-5}$ M, g – $7x10^{-5}$ M.
Spectra f and g had to be divided by 10 in order to be comparable with spectra a-e. The red color of spectra e-g signifies that at these systems the SERS spectrum of not only Ag^+-bpy, but also Ag(0)-bpy surface complex is observed.

Furthermore, to explore the influence of Ag^+ ions excess onto a Ag(0)-bpy surface complex formed in systems where simultaneously Ag^+ ions and BH_4^- anions were present, an even more complicated system was prepared: Ag hydrosol/$AgNO_3$($2x10^{-5}$ M)/bpy($1x10^{-5}$ M)/BH_4^-($9x10^{-5}$ M)/$AgNO_3$. SERS spectra of these systems are shown in Fig. 35. The sequence of the SERS spectra in Fig. 35 (spectra a-c) has been obtained in the following manner: to the Ag hydrosol/$AgNO_3$($2x10^{-5}$ M)/bpy($1x10^{-5}$ M)/BH_4^-($9x10^{-5}$ M) system (where the SERS signal of Ag(0)-bpy has dominated - Fig. 35A, spectrum a), $AgNO_3$ solution has been added yielding $2.2x10^{-4}$ M Ag^+ in the final system and hence the bpy: BH_4^-:Ag^+ ratio was 1:9:22. The SERS spectrum has been measured and is shown as b in Fig. 35A. The SERS signal of Ag(0)-bpy remained preserved, nevertheless, the overall intensity of SERS signal has decreased. This decrease could be caused by either a partial aggregation of the system due to the change of ionic strength in the system (added $AgNO_3$ is fully dissociated into ions); or by the decrease in the Ag(0)-bpy:Ag^+-bpy species signal ratio. The latter factor would stem from the fact that the SERS signal of Ag(0)-bpy is at least 10x stronger [104, 130] (due to the CT resonance contribution to the overall SERS signal) than that of Ag^+-bpy (possessing no CT resonance contribution). To distinguish between these two factors, the addition of $AgNO_3$

solution has been continued up to ~$2x10^{-3}$ M $AgNO_3$ in the final system (the bpy:BH_4^-:Ag^+ ratio ~1:9:202 – spectrum c in Fig. 35A). The main reason for doing so was that if the Ag(0)-bpy:Ag^+-bpy ratio changes are responsible for the changes in SERS signal intensity, the mutual intensities of following bands: 660/765, 1024/1011 and 1320/1305 cm^{-1}, should change due to the very large excess of Ag^+, i.e. the mutual intensities of these bands in spectrum c in Fig. 35A (the bpy:BH_4^-:Ag^+ ratio equal to 1:9:202) change in comparison to that observed in spectrum b in Fig. 35A (with the bpy:BH_4^-:Ag^+ ratio equal to 1:9:22).

Therefore, the areas of the 660, 765, 1011, 1024, 1305 and 1320 cm^{-1} bands were determined (some of these bands were carefully separated prior to integration) and their ratios (representing the Ag(0)-bpy/Ag^+-bpy signal ratios) are depicted in Fig. 35B. The mutual ratios of all three bands decrease with the increasing Ag^+ concentration in the system, which indicates that the Ag^+-bpy surface concentration increases on the expenses of that of Ag(0)-bpy.

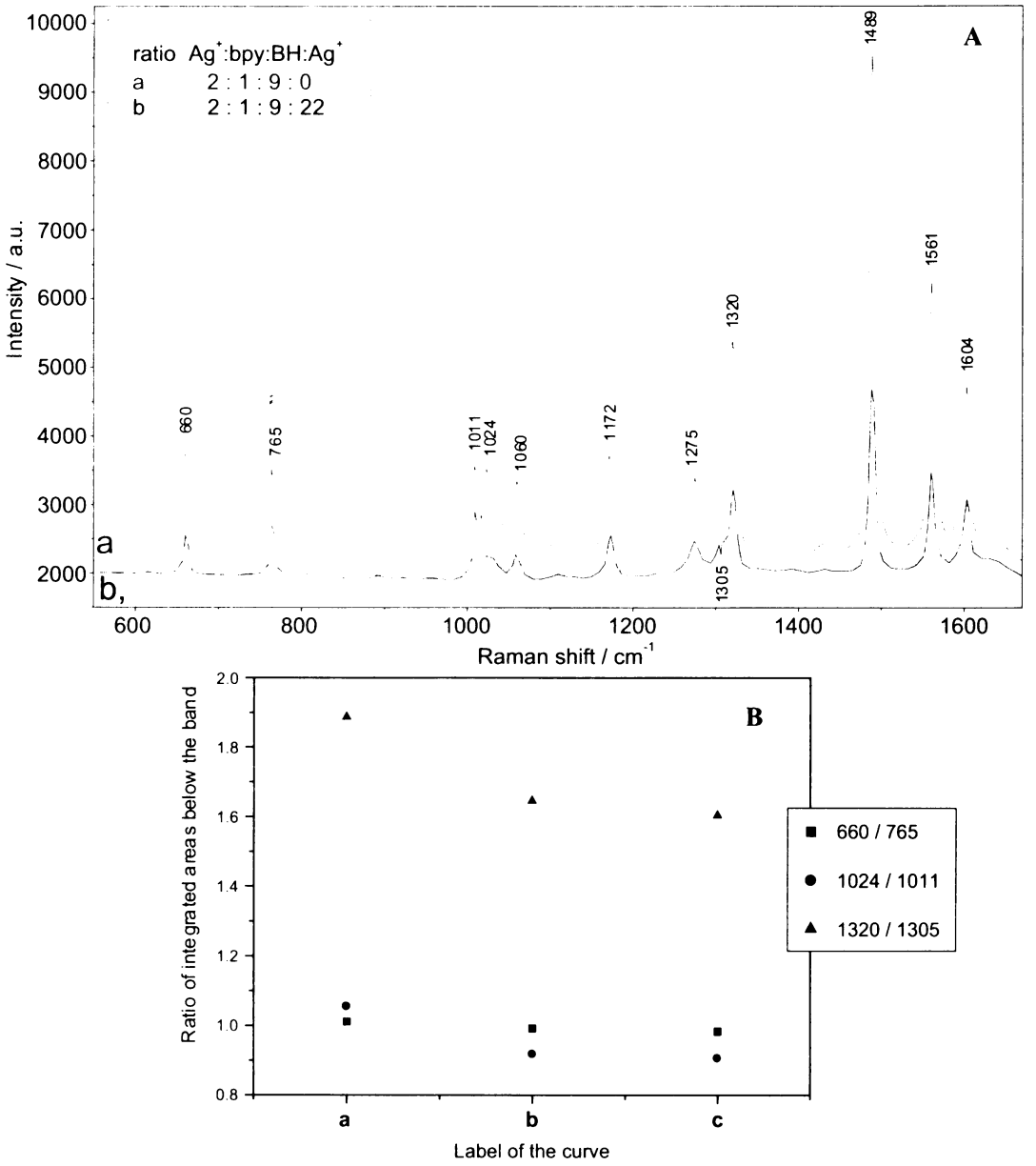

Fig. 35: (A) SERS spectra of the Ag hydrosol/$AgNO_3$($2x10^{-5}$ M)/bpy($1x10^{-5}$ M)/BH_4^-($9x10^{-5}$ M)/$AgNO_3$(c_y) systems where c_y is: a – 0 M, b – $2.2x10^{-4}$ M, c – $2.02x10^{-3}$ M.
(B) The ratios of integrated areas of the bands in SERS spectra in (A) attributed to Ag(0)-bpy (660, 1024 and 1320 cm^{-1}) or Ag'-bpy (765, 1011 and 1305 cm^{-1}) surface species.

2.9.6. Effect of BH_4^- on Ag hydrosol/TMPyP systems

In our previous experiments carried out in systems with BH_4^--reduced Ag hydrosols [132], four different SERRS spectral forms of the tetracationic porphyrin TMPyP have been identified (Fig. 13 and Fig. 14): free-base porphyrin (fI), Ag^+ metallated porphyrin (fII) [154], Ag^0 metallated porphyrin (fIII) [142] and J-aggregates of porphyrin adsorbed on Ag^0 (fIV) [132, 141].

SERS spectra of Ag hydrosol/BH_4^-/TMPyP/BH_4^- system are shown in Fig. 36. It demonstrates that a small amount of BH_4^- (i.e. ratio TMPyP:BH_4^- equal to 1:1, spectrum a in Fig. 36) does not induce any changes in SERRS spectrum of fI surface species; however with the increase of BH_4^- content, the SERRS spectrum changes its character and the markers of fIV begin to dominate in the SERRS spectrum (i.e. the 325, 673, 953, 1085, 1212, 1290, 1360 cm^{-1} bands) – from spectrum b to e in Fig. 36. It should be emphasized that the TMPyP concentration has been chosen to exceed that required for a mono-layer coverage (estimated in [155]) so that the J-aggregates could be generated. Such a system can be directly compared with the similar one in which borohydride-reduced Ag hydrosol was used [132].

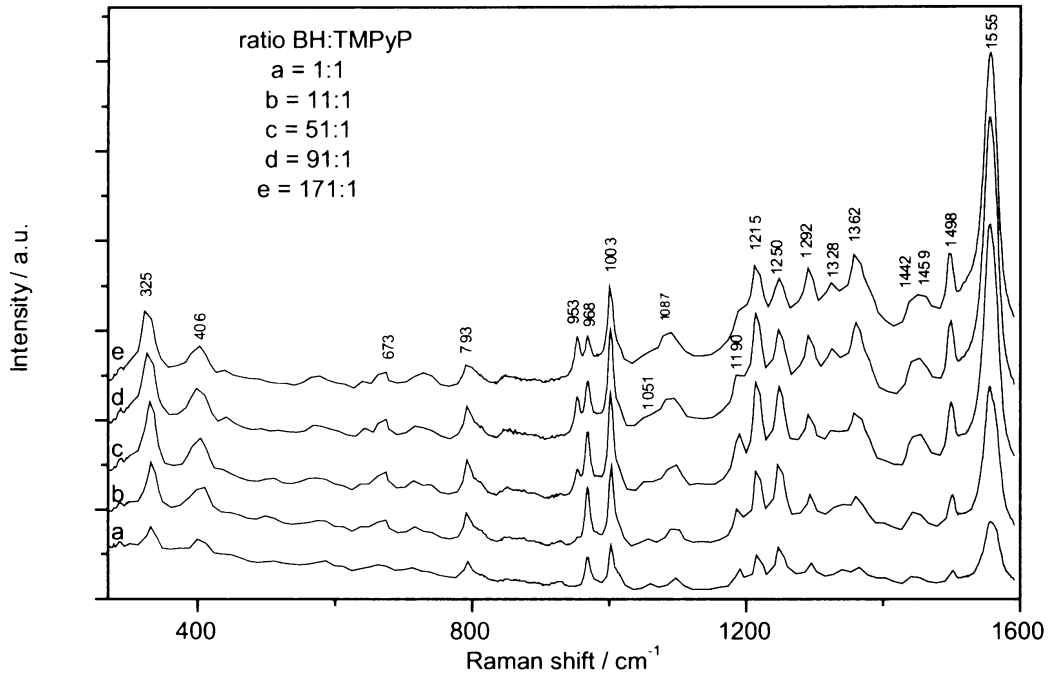

Fig. 36: SERRS spectra of Ag hydrosol/BH_4^-($1x10^{-5}$ M)/TMPyP($1x10^{-6}$ M)/BH_4^-(c_y) systems where c_y equals to: a = 0M, b = $1x10^{-5}$ M, c = $5x10^{-5}$ M, d = $9x10^{-5}$ M and e = $1.7x10^{-4}$ M.

It has been shown previously [132, 141] that the fIV SERRS signal observation is related to the formation of J-aggregates constituted of the tetracationic porphyrin TMPyP in ion pairs with BH_4^- anions, and the adsorption of these aggregates to Ag^0 surfaces. The presented results of the experiments confirm the key role of BH_4^- anions in the formation of J-aggregates of the tetracationic TMPyP porphyrin.

2.9.7. Effect of Ag^+ and BH_4^- on Ag hydrosol/TMPyP systems

The influence of BH_4^- was investigated also under the conditions where an abundance of Ag^+ ions was present before addition of BH_4^-, i.e. the BH_4^- solution was added into the Ag hydrosol/$AgNO_3$/BH_4^-/TMPyP system. Therefore, the Ag^+:BH_4^-:TMPyP ratio was changed from 200:1:1 to 200:201:1 and SERRS spectra were recorded (Fig. 37).

All presented spectra show SERRS signal of fI and fII, while the SERRS signal of fIV is absent. This result indicates that the excess Ag^+ ions prevented either the formation of TMPyP.$4BH_4^-$ J-aggregates, or of Ag(0) adsorption sites, or both.

2.9.8. Results of SERS spectral probing of the reactivity of Ag NPs prepared by LA/NF

(1) The hydrosols prepared by LA/NF and treated by chlorides consist of large (>80 nm) interpenetrating NPs. In these systems, SERS spectral form of Ag(0)-bpy surface complex has been detected.

(2) The threshold concentrations of selected agents (HCl, NaCl, THS, BH_4^-) for Ag(0)-bpy surface species generation on NP surfaces of Ag hydrosols prepared by LA/NF were established to be of a lower or the same value as those on chemically prepared Ag NPs (borohydride-reduced Ag hydrosols).

(3) In the case of the pre-treating of Ag hydrosols by the selected agent, a lower threshold concentration value of agent in the final solution has been required for Ag(0)-bpy surface complex formation in comparison to the post-treating by the same agent.

(4) The bpy:agent ratio seems to be very important in Ag(0)-bpy surface complex generation on Ag NPs prepared by LA/NF.

(5) The excessive Ag^+ ions present simultaneously in the solution interact preferably with added reducing agent (BH_4^-), therefore, the threshold concentration values of used reducing agent for a Ag(0)-adsorbate complex formation are shifted to the higher values in such systems.

(6) The key role of BH_4^- anions in the J-aggregates of tetracationic TMPyP porphyrin formation was confirmed in systems with Ag hydrosols prepared by LA/NF.

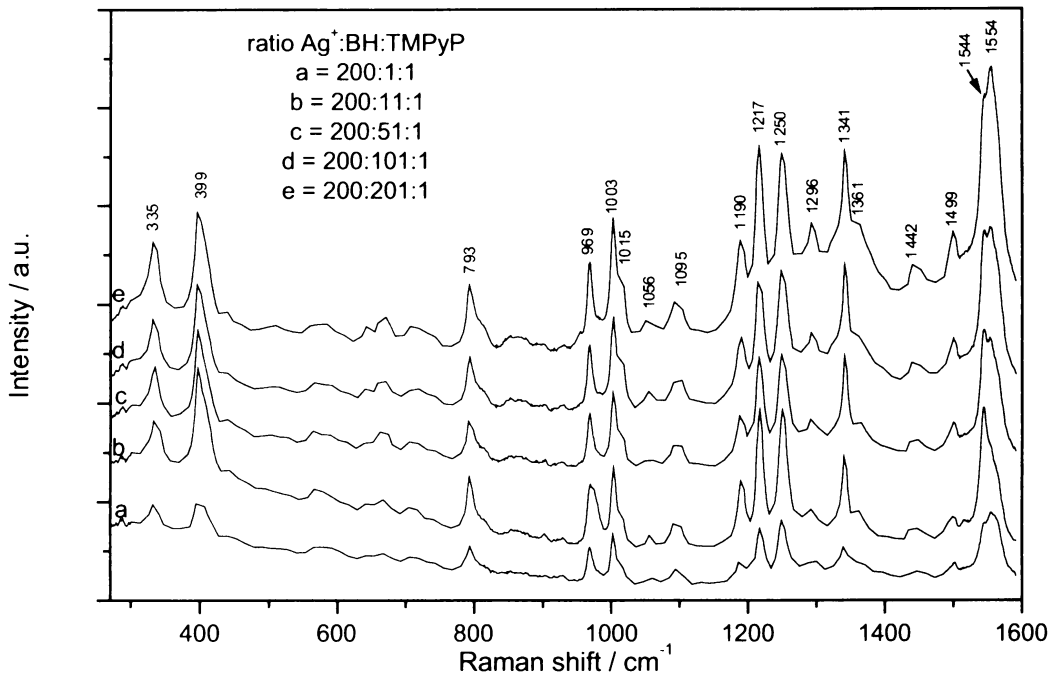

Fig. 37: SERRS spectra of the Ag hydrosol/$AgNO_3$($2x10^{-4}$ M)/BH_4^-($1x10^{-6}$ M)/TMPyP($1x10^{-6}$ M)/BH_4^-(c_y) systems where c_y equals to: a = 0 M, b = $1x10^{-5}$ M, c = $5x10^{-5}$ M, d = $1x10^{-4}$ M and e = $2x10^{-4}$ M.

2.9.9. Conclusions: applicability of Ag NPs prepared by LA/NF in ultrapure water as substrates for SE(R)RS

Ag NPs in hydrosols prepared by the optimised LA/NF procedure proved themselves to be suitable substrates for SERS and SERRS spectral studies of model adsorbates.

The systematic measurements and interpretations of SERS spectra of bpy and SERRS spectra of TMPyP have shown that the same types of adsorption sites, i.e. oxidized (Ag^+) and reduced (Ag^0), can exist on laser-ablated Ag NPs as on those prepared chemically by reduction driven by $NaBH_4$.

Importantly, the oxidation state of the available adsorption sites can be changed by addition of a reducing (e.g. BH_4^-) or oxidizing (e.g. Ag^+) agent.

The oxidation state of available adsorption sites can possibly be changed also by another mechanism. In particular by complexation (extraction) of Ag^+ from Ag NP surface by a strongly complexing agent (e.g. THS), exposing thus Ag(0) adsorption sites. Nevertheless, at higher THS concentration and in the presence of OH^- ions (which are expected to stabilize Ag NPs prepared by LA/NF), THS can also act as a reducing agent.

The changes in the oxidation state of adsorption sites prevailing on Ag NPs surface appear to allow for the formation of a desired Ag(0)-adsorbate or Ag^+-adsorbate surface species for the model adsorbates, bpy and TMPyP. The extension of this possibility to other types of adsorbates, although quite probable, is the subject of further investigation.

Chapter 3

LA/NF in selected ionic and molecular species

3.1. LA/NF in electrolytes solutions

In this section, the effect of selected ions addition to the aqueous ablation medium on the progress as well as the output of LA/NF of Ag target (performed with the selected physical parameters given in [Experimental] and with the setup depicted in Schema II) will be explored and compared with LA/NF carried out in pure water (under the same conditions). The step-wise LA/NF process performed with 1064 nm ns laser pulses has been followed by SPE measurements after each of the individual steps. The resulting hydrosols have been characterized by TEM, SPE measurements and SERS spectral probing by bpy. The overview of parameters used for SPE spectra evaluation is provided in [Chapter 1].

The selected ions were OH^-, Cl^-, $S_2O_3^{2-}$ (THS) anions and Ag^+ cations. Their specific effects will be discussed in more details in each section of this chapter, however, in the beginning, it should be explained why particularly these ions have been employed.

The selection of hydroxide ions was motivated by their proposed (for Ag [46]) and proved (for Au [62]) stabilizing effect on hydrosols prepared by LA/NF.

Chlorides were found to increase the efficiency of LA/NF of Ag in neutral ambient [11, 12], while their effect in acidic medium has not been previously explored. Moreover, as it was discussed for chemically prepared Ag hydrosols in [104, 112, 130] and found out in the previous chapter for LA/NF-prepared Ag hydrosols, the modifications of NP surfaces by adsorption of chlorides in both neutral and acidic ambient induce specific morphological changes which are accompanied by changes in the oxidation state of adsorption sites. Therefore, for the exploration of the effect of chlorides, LA/NF of Ag foil has been performed in NaCl or HCl solutions of various concentrations, and, in the latter case, at various pHs.

The selection of THS has been motivated by the recently published report in which a strongly concentration dependent effect of THS treatment on morphology and surface reactivity of Ag NPs pre-prepared by LA/NF in pure water [156] has been probed. In ref. 156, THS was shown to act as an efficient complexation agent (which removes Ag^+ ions and/or Ag_n^+ clusters from the surface of Ag NPs) even at its very low concentrations. Therefore, it is anticipated that the strong complexation effect of THS, in combination with the expected presence of Ag^+ ions and/or Ag_n^+ clusters as the primary products of LA/NF, can principally affect the outcome of LA/NF process.

By performing LA/NF in the presence of an excess of Ag^+ ions, it is intended to test further the above mentioned hypothesis concerning the stabilization of Ag NPs. In particular, provided that NPs are stabilized by OH^- ions, the addition of Ag^+ ions may lead to the destabilization of NPs through a mutual interaction between Ag^+ (intentionally added to create an excess of them) and OH^- (formed in the solution by the dissociation of water).

Finally, for the sake of brevity, the particular Ag NP hydrosols are labeled as a prefix by the formula or an abbreviation of the agent present in aqueous medium during their preparation (e.g. NaOH-Ag hydrosol, NaCl-Ag hydrosol, HCl-Ag hydrosol, THS-Ag hydrosol, $AgNO_3$-Ag hydrosol). Sols prepared in pure water are labeled w-Ag hydrosol.

3.1.1. LA/NF in NaOH solutions

For a better recognition of OH^- ions effect, the NaOH concentrations (in final system) have been selected to be of two or three orders higher than those originating from the dissociation of water (i.e. $1x10^{-5}$ M and $1x10^{-4}$ M).

In Table VII, the characteristics of SPE bands measured after each step of LA/NF in the presence of NaOH and in pure water are compared. The A_{250}, A_{max} values increase in the course of LA/NF and with NaOH concentration increase. On the contrary, FWHM decreases in the course of LA/NF, both in pure water and in NaOH solution, and is of a slightly smaller value in water than in NaOH-Ag hydrosols at the end of LA/NF. The λ_{max} values blue-shift in the course of LA/NF. In the final sols, λ_{max} values of the NaOH-Ag hydrosols are red shifted with respect to those of the w-Ag hydrosol.

These results indicate that the process of NPs formation is more efficient in the presence of NaOH in comparison to the LA/NF performed in the absence of any agent at the same physical conditions.

Unfortunatelly, the NaOH-Ag hydrosols are not stable enough, especially those prepared at the higher concentration of NaOH. This is clearly seen precisely 4 days after the preparation, because the A_{max} value decreases drastically, the FWHM increases enormously and the λ_{max} shifts to 403 nm – in Table VIII.

3.1.2. LA/NF in chlorides solutions

The concentration values of NaCl and HCl solutions in which LA/NF was performed were selected with respect to their threshold concentration values in systems with LA/NF pre-prepared Ag NPs and bpy reported in [Chapter 2]. For HCl and NaCl concentrations below the threshold value, Ag^+-bpy surface species was present on Ag NPs surface; while at and above this threshold, Ag(0)-bpy was detected and the morphology changes, namely the formation of compact aggregates of interpenetrating NPs, were observed [Chapter 2].

Table VII: Parameters of SPE bands of Ag hydrosols prepared by step-wise LA/NF process in water and in NaOH solutions

LA/NF performed		λ_{max}	A_{max}	FWHM	A_{250}
in	for [min]	[nm]	[arb.units]	[nm]	[arb.units]
pure water	2	397	0.251	194	0.199
	2+3	395	0.380	143	0.235
	2+3+3	395	0.471	116	0.267
	2+3+3+5	392	0.586	93	0.297
	2+3+3+5+7	**394**	**0.756**	**79**	**0.367**
$1x10^{-5}$ M NaOH	2	405	0.409	203	0.281
	2+3	401	0.605	173	0.372
	2+3+3	399	0.750	138	0.424
	2+3+3+5	398	0.890	107	0.449
	2+3+3+5+7	**398**	**1.031**	**90**	**0.479**
$1x10^{-4}$ M NaOH	2	402	0.437	143	0.285
	2+3	402	0.678	114	0.378
	2+3+3	399	0.803	106	0.415
	2+3+3+5	399	0.957	95	0.470
	2+3+3+5+7	**397**	**1.085**	**84**	**0.504**

Table VIII: Parameters of SPE bands of Ag hydrosols prepared by step-wise LA/NF process in water and in NaOH solutions - aging

System	SPE measured	λ_{max} [nm]	A_{max} [arb.units]	FWHM [nm]	A_{250} [arb.units]
pure water	immediately	394	0.756	79	0.367
	after 3 days	402	0.650	69	0.303
$1x10^{-5}$ M NaOH	immediately	398	1.031	90	0.479
	after 4 days	403	0.750	116	0.387
$1x10^{-4}$ M NaOH	immediately	397	1.085	84	0.504
	after 4 days	403	0.301	181	0.301

The concentration values of NaCl solution present in the course of LA/NF were thus selected to be: $5x10^{-2}$ M, $1x10^{-3}$ M and $1x10^{-4}$ M; the HCl concentrations $1x10^{-3}$ M and $1x10^{-4}$ M (Table IX).

The comparison of the SPE spectra of w-Ag hydrosol, NaCl-Ag hydrosols and HCl-Ag hydrosols (Table IX) indicates that the presence of both, NaCl and HCl solutions in concentrations $1x10^{-4}$ M and $1x10^{-3}$ M, has caused an increase of A_{max} and A_{250} values and a reduction of FWHM in each step, while maintaining almost the same λ_{max} positions as in Ag hydrosol. In contrast to that, the results obtained for the highest NaCl concentration differ: the NaCl($5x10^{-2}$ M)-Ag hydrosol has shown smaller A_{max} values than w-Ag hydrosol (in each step), broader SPE curves (i.e. higher FWHMs) at the end of LA/NF. Moreover, this NaCl-Ag hydrosol has been very unstable (it has precipitated within 1 hour after preparation) - Table X. In contrast to that, sols prepared at the lowest chloride concentrations employed ($1x10^{-4}$ M HCl and/or NaCl) were more stable than w-Ag hydrosol (by considering the maintaining of nearly the same λ_{max} positions and a small decrease in A_{max} values as the appropriate stability criteria).

The characteristic morphologies of HCl-Ag hydrosol deposited immediately after their preparation, prepared at two different HCl concentration values are shown in Fig. 38. It is obvious that HCl at both concentration values in the final hydrosols (Figs 38A,B) influences Ag NPs formation: at the lower HCl concentration, smaller NPs with respect to those prepared by LA/NF in the absence of any agent (Fig. 38C) are formed; while the presence of the higher HCl concentration leads to the formation of interpenetrating NPs. This observation of NPs intergrowth (interpenetrating) induced by chlorides is in a good agreement with the results obtained for systems with LA/NF-prepared Ag NPs modified by chlorides reported in [Chapter 2], as well as, with those reported earlier [104, 130, 132]. On the basis of this agreement, it can thus be concluded that the presence of BH_4^- or borates and simultaneously chlorides is not the necessary condition for NPs interpenetrating. NPs intergrowth is the intrinsic effect of modification of Ag NPs by chloride.

3.1.3. LA/NF in THS solutions

The very low THS concentration values have been selected ($1x10^{-7}$ M and $1x10^{-6}$ M in final systems) because in ref. 137, 138, 142 a pronounced effect on the morphologies of NPs was determined even for such small amounts of THS anions present in a solution.

Table IX: Parameters of SPE bands of Ag hydrosols prepared by step-wise LA/NF process in water and in chloride solutions

LA/NF performed in	for [min]	λ_{max} [nm]	A_{max} [arb.units]	FWHM [nm]	A_{250} [arb.units]
pure water	2	397	0.251	194	0.199
	2+3	395	0.380	143	0.235
	2+3+3	395	0.471	116	0.267
	2+3+3+5	392	0.586	93	0.297
	2+3+3+5+7	**394**	**0.756**	**79**	**0.367**
$1x10^{-4}$ M HCl	2	395	0.503	80	0.278
	2+3	395	0.741	67	0.341
	2+3+3	395	0.933	65	0.395
	2+3+3+5	395	1.230	58	0.476
	2+3+3+5+7	**394**	**1.462**	**52**	**0.499**
$1x10^{-3}$ M HCl	2	397	0.488	95	0.296
	2+3	396	0.617	84	0.344
	2+3+3	395	0.839	72	0.400
	2+3+3+5	395	1.074	61	0.438
	2+3+3+5+7	**395**	**1.225**	**58**	**0.462**
$1x10^{-4}$ NaCl	2	394	0.486	78	0.277
	2+3	394	0.714	64	0.333
	2+3+3	394	0.944	58	0.388
	2+3+3+5	393	1.219	53	0.441
	2+3+3+5+7	**394**	**1.541**	**52**	**0.515**
$1x10^{-3}$ NaCl	2	397	0.383	81	0.207
	2+3	396	0.667	67	0.317
	2+3+3	399	0.816	66	0.366
	2+3+3+5	395	1.015	60	0.396
	2+3+3+5+7	**395**	**1.155**	**52**	**0.416**
$5x10^{-2}$ NaCl	2	402	0.214	158	0.238
	2+3	399	0.259	133	0.249
	2+3+3	400	0.277	109	0.251
	2+3+3+5	399	0.331	95	0.258
	2+3+3+5+7	**399**	**0.388**	**87**	**0.293**

Table X: Parameters of SPE bands of Ag hydrosols prepared by step-wise LA/NF process in water and in chloride solutions - aging

System	SPE measured	λ_{max} [nm]	A_{max} [arb.units]	FWHM [nm]	A_{250} [arb.units]
pure water	immediately	394	0.756	79	0.367
	after 3 days	402	0.650	69	0.303
$1x10^{-4}$M HCl	immediately	394	1.462	52	0.499
	after 2 days	393	1.300	42	0.362
$1x10^{-3}$M HCl	immediately	395	1.225	58	0.462
	after 2 days	397	0.800	52	0.285
$1x10^{-4}$ NaCl	immediately	394	1.541	52	0.515
	after 2 days	395	1.300	52	0.394
$1x10^{-3}$ NaCl	immediately	395	1.155	52	0.416
	after 3 days	400	0.900	68	0.379
$5x10^{-2}$ NaCl	immediately	399	0.388	87	0.293
	after 2 days	-	-	-	0.134

As it is shown in Table XI, the A_{max} values in the THS-Ag hydrosols are lower than those of a w-Ag hydrosol, particularly, at the end of LA/NF. FWHM are specially enlarged in each step and the λ_{max} positions of the THS-Ag hydrosols change in the course of LA/NF to be finally red-shifted with respect to the λ_{ma} position of a w-

Ag hydrosol. The red-shift increases during aging (within days), i.e. the aggregation of Ag NPs and, consequently, the destabilization of these systems significantly proceeds (Table XII).

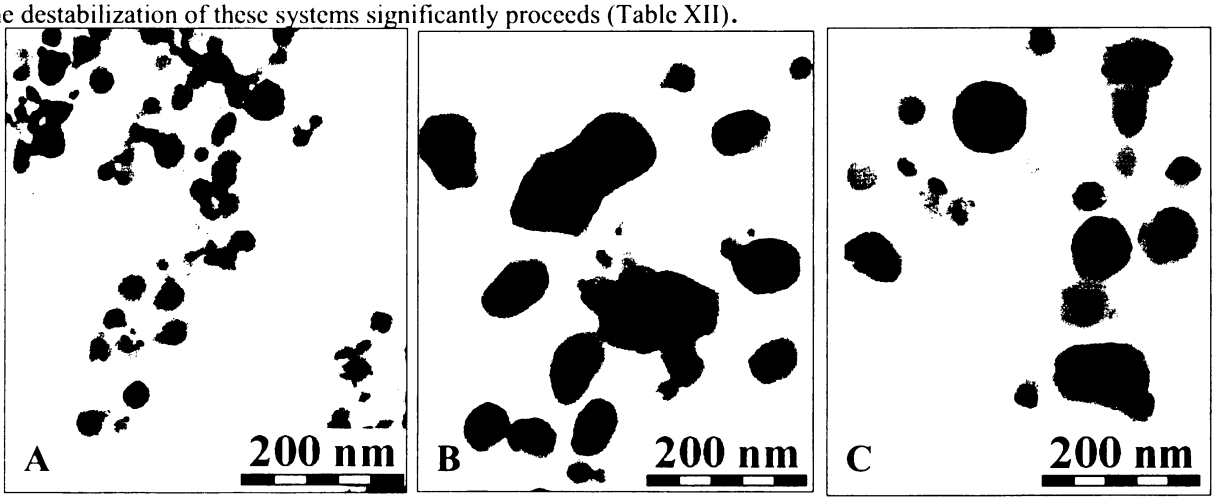

Fig. 38: TEM images of HCl-Ag hydrosol systems with HCl concentrations: A) $1x10^{-4}$ M and B) $1x10^{-3}$ M; C) TEM image of a w-Ag hydrosol (without HCl presence).

Table XI: Parameters of SPE bands of Ag hydrosols prepared by step-wise LA/NF process in water and in THS solutions

LA/NF performed in	for [min]	λ_{max} [nm]	A_{max} [arb.units]	FWHM [nm]	A_{250} [arb.units]
pure water	2	397	0.251	194	0.199
	2+3	395	0.380	143	0.235
	2+3+3	395	0.471	116	0.267
	2+3+3+5	392	0.586	93	0.297
	2+3+3+5+7	**394**	**0.756**	**79**	**0.367**
$1x10^{-7}$ M THS	2	387	0.294	249	0.276
	2+3	387	0.308	284	0.291
	2+3+3	395	0.273	271	0.275
	2+3+3+5	398	0.251	279	0.256
	2+3+3+5+7	**398**	**0.261**	**259**	**0.267**
$1x10^{-6}$ M THS	2	383	0.213	480	0.244
	2+3	393	0.300	263	0.268
	2+3+3	387	0.304	432	0.296
	2+3+3+5	391	0.439	246	0.367
	2+3+3+5+7	**397**	**0.512**	**216**	**0.459**

Table XII: Parameters of SPE bands of Ag hydrosols prepared by step-wise LA/NF process in water and in THS solutions - aging

System	SPE measured	λ_{max} [nm]	A_{max} [arb.units]	FWHM [nm]	A_{250} [arb.units]
pure water	immediately	394	0.756	79	0.367
	after 3 days	402	0.650	69	0.303
$1x10^{-7}$ M THS	immediately	398	0.261	259	0.267
	after 2 days	407	0.229	335	0.185
$1x10^{-6}$ M THS	immediately	397	0.512	216	0.459
	after 2 days	405	0.273	186	0.215

3.1.4. LA/NF in $AgNO_3$ solutions

The $AgNO_3$ concentrations were selected to be of the same values as those of NaOH, i.e. $1x10^{-5}$ M and $1x10^{-4}$ M in final system, so that it is possible to compare the resulting SPE characteristics measured in both hydrosols.

$AgNO_3$-Ag hydrosols have been very unstable and from the very beginning, their λ_{max} positions have been red-shifted with very low A_{max} values and their FWHM have been enormously enlarged (Table XIII) in comparison to those of a w- and/or NaOH-Ag hydrosols (Table VII). Therefore, it seems that $AgNO_3$ presence substantially decreases the stability of NPs (Table XIV).

Table XIII: Parameters of SPE bands of Ag hydrosols prepared by step-wise LA/NF process in water and in $AgNO_3$ solutions

LA/NF performed in	for [min]	λ_{max} [nm]	A_{max} [arb.units]	FWHM [nm]	A_{250} [arb.units]
pure water	2	397	0.251	194	0.199
	2+3	395	0.380	143	0.235
	2+3+3	395	0.471	116	0.267
	2+3+3+5	392	0.586	93	0.297
	2+3+3+5+7	**394**	**0.756**	**79**	**0.367**
$1x10^{-5}$ M $AgNO_3$	2	386	0.247	268	0.235
	2+3	396	0.325	309	0.262
	2+3+3	403	0.283	313	0.248
	2+3+3+5	410	0.262	319	0.243
	2+3+3+5+7	**410**	**0.237**	**329**	**0.230**
$1x10^{-4}$ M $AgNO_3$	2	390	0.237	314	0.231
	2+3	398	0.261	321	0.249
	2+3+3	404	0.265	337	0.251
	2+3+3+5	397	0.271	346	0.259
	2+3+3+5+7	**398**	**0.269**	**365**	**0.262**

Table XIV: Parameters of SPE bands of Ag hydrosols prepared by step-wise LA/NF process in water and in $AgNO_3$ solutions - aging

System	SPE measured	λ_{max} [nm]	A_{max} [arb.units]	FWHM [nm]	A_{250} [arb.units]
pure water	immediately	394	0.756	79	0.367
	after 3 days	402	0.650	69	0.303
$1x10^{-5}$ M $AgNO_3$	immediately	410	0.237	329	0.230
	after 2 days	414	0.221	276	0.180
$1x10^{-4}$ M $AgNO_3$	immediately	398	0.269	365	0.262
	after 2 days	408	0.182	500	0.172

3.1.5. SERS/SERRS spectral probing of reactivity of hydrosols described in 3.1.1.-3.1.4. by selected adsorbates

To probe the reactivity and the available adsorption sites on surfaces of Ag NPs in the hydrosols prepared by LA/NF in selected agents solutions, the same two model adsorbates, which were used for probing of sols prepared by LA/NF and treated by the selected agents in [Chapter 2], have been selected: bpy and TMPyP.

NaOH-Ag hydrosols have been only probed by addition of TMPyP. Immediately, the free base form started to be metallated by Ag^+ ions. The higher the NaOH concentration was, the faster has the metallation proceeded – Table XV.

In SERS spectral testing of NaCl-Ag hydrosols by bpy, the Ag(0)-bpy surface complex was detected in the NaCl($5x10^{-2}$ M)-Ag hydrosol/bpy and NaCl($1x10^{-3}$ M)-Ag hydrosol/bpy systems (Fig. 39). Hence, the threshold concentration value of NaCl for Ag(0) adsorption sites formation in hydrosols prepared by LA/NF in the presence of NaCl is lower than in systems with Ag NPs prepared by LA/NF and treated by NaCl [Chapter 2.9.2.], as well as, in systems with Ag NPs prepared by chemical reduction (BH_4^--reduced) [112, 130, 132].

SERS spectral probing of HCl($1x10^{-3}$ M)-Ag hydrosol/bpy systems has also demonstrated the Ag(0)-bpy surface complex formation (Table XV). For Ag hydrosols prepared in NaCl and HCl solutions of $1x10^{-4}$ M concentration value, the Ag^+-bpy surface complex has dominated the SERS spectra (spectrum b in Fig. 39).

The interaction of chloride-Ag hydrosols with porphyrin results in free base porphyrin SERRS spectrum observation, nevertheless, the HCl-Ag hydrosols also include the diacidic form (not shown here).

The THS-Ag hydrosols were tested by addition of both selected model adsorbates. Only the SERS signal of Ag^+-bpy surface complex has dominated in spectra of THS-Ag hydrosol/bpy systems and the concentration value of

Table XV: SERS and SERRS spectral probing of Ag hydrosols prepared by step-wise LA/NF process in electrolytes solutions

Concentration and type of ions in which Ag NPs were prepared	Surface species of bpy observed in SERS spectral measurements	Concentration values of the detection limit of bpy [mol.dm^{-3}]	Surface species of TMPyP observed in SERRS spectral measurements	Concentration values of the detection limit of TMPyP [mol.dm^{-3}]
1x10^{-5} M NaOH	-	-	free base, Ag^{+}-TMPyP	<1x10^{-8}
1x10^{-4} M NaOH	-	-	Ag^{+}-TMPyP	<1x10^{-8}
1x10^{-4} M NaCl	Ag^{+}-bpy	<1x10^{-6}	free base	<5x10^{-9}
1x10^{-3} M NaCl	Ag(0)-bpy	5x10^{-8}	free base	<1x10^{-8}
5x10^{-2} M NaCl	Ag(0)-bpy	<5x10^{-7}	-	-
1x10^{-4} M HCl	Ag^{+}-bpy	1x10^{-6}	free base + diacidic form	<1x10^{-10}
1x10^{-3} M HCl	Ag(0)-bpy	<1x10^{-6}	free base + diacidic form	1x10^{-9}
1x10^{-7} M THS	(Ag^{+}-bpy)	1x10^{-5}	(free base,? Ag^{+}-TMPyP)	<1x10^{-9}
1x10^{-6} M THS	(Ag^{+}-bpy)	1x10^{-5}	(free base, Ag^{+}-TMPyP, Ag(0)-TMPyP)	<1x10^{-7}
1x10^{-5} M $AgNO_3$	Ag^{+}-bpy	<1x10^{-5}	free base, Ag^{+}-TMPyP	<1x10^{-7}
1x10^{-4} M $AgNO_3$	Ag^{+}-bpy	1x10^{-6}	free base, Ag^{+}-TMPyP	<1x10^{-7}

Note: forms in parenthesis provided very weak SERS/SERRS signal

the detection limit was very high – Table XV. All SERS spectral signals were weak; hence, these systems are not particularly suitable as substrates for SERS spectral measurements. In SERRS of THS-Ag hydrosol/TMPyP systems, the appropriate SERRS spectral forms were distinguishable with problems (marked by parenthesis in Table XV).

SERS spectral testing of $AgNO_3$-Ag hydrosols by using bpy has resulted in observation of Ag^{+}-bpy surface complex (which is not surprising) and the SERRS spectral testing revealed the metallation by Ag^{+}– Table XV.

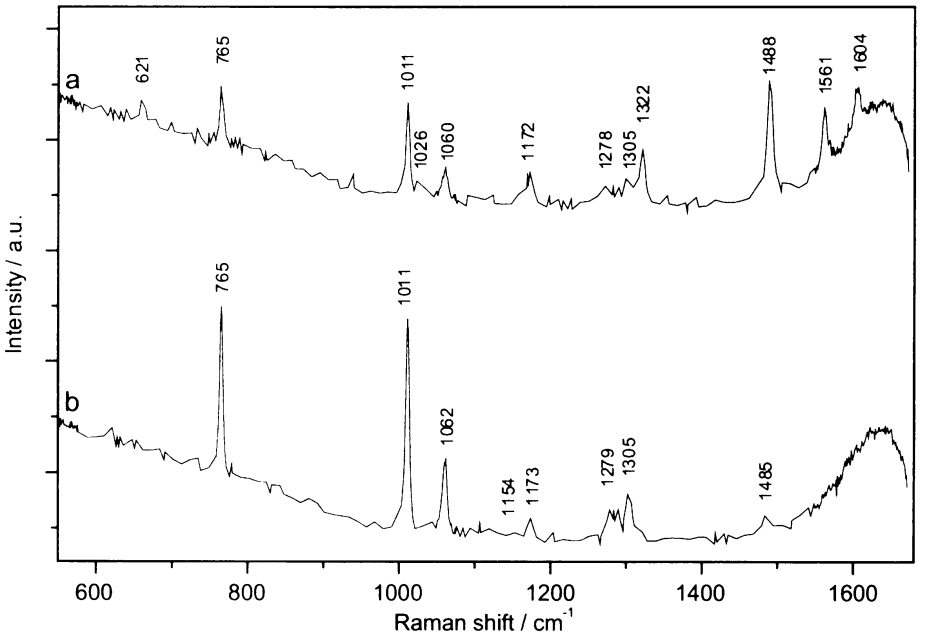

Fig. 39: SERS spectra of NaCl-Ag hydrosol/bpy(1x10^{-6} M) systems: a = 1x10^{-3} M NaCl and b = 1x10^{-4} M NaCl in the final solution.

3.1.6. Mutual comparison of selected agents effects

SPE spectral characteristics of Ag hydrosols prepared in NaOH, NaCl, HCl, and $AgNO_3$ solutions of 1x10^{-4} M concentration, in 1x10^{-6} M THS solution and in ultrapure water are compared in Fig. 40. From this comparison and from the above mentioned observations [sections 3.1.1-3.1.4], a sequence of the employed agents from the point of view of the preferentially small NPs formation and stabilization efficiency (from the most efficient which stabilize Ag NPs in solution to the destabilizing one) was determined: NaCl>HCl>NaOH>>pure water>THS>>$AgNO_3$. The analogous ordering of the employed agents results when the stability is inspected after several days of aging: NaCl>HCl>>pure water>NaOH>>THS>$AgNO_3$ (as follows from the comparison of the SPE characteristics in Tables VIII, X, XII, XIV).

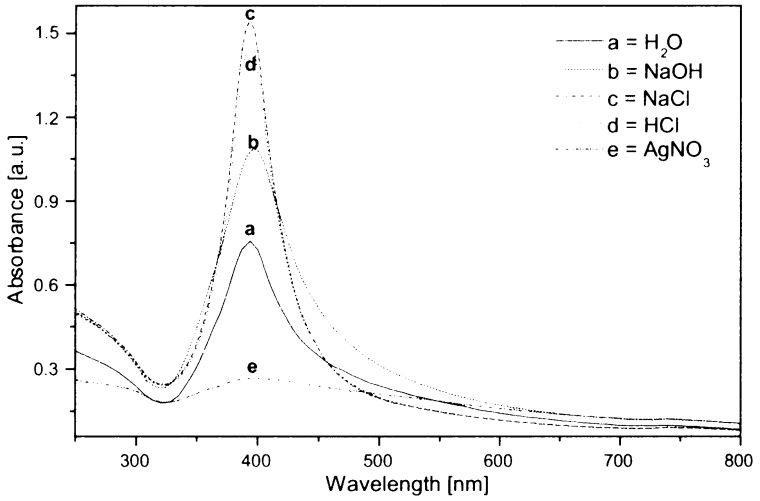

Fig. 40: SPE spectra of resulting hydrosols prepared by LA/NF performed in the presence of (a) pure water, (b) $1x10^{-4}$ M NaOH, (c) $1x10^{-4}$ M NaCl, (d) $1x10^{-4}$ M HCl, (e) $1x10^{-4}$ M $AgNO_3$ and (f) $1x10^{-6}$ M THS.

TEM images of NaCl-, HCl- and $AgNO_3$-Ag hydrosols are compared in Fig. 41. For a w-Ag hydrosol (Fig. 41A), larger NPs and aggregates are characteristic; while for the NaCl-Ag hydrosols (Fig. 41B) and/or HCl-Ag hydrosol (Fig. 41C), the smaller, round shaped NPs and/or asymmetric interpenetrating NPs are observed. In HCl-Ag hydrosols, the interpenetration of NPs is encountered more frequently than in NaCl-Ag hydrosols. On the TEM images of $AgNO_3$-Ag hydrosol (Fig. 41D), NPs in the vicinity of micro-crystals are observed. Thus, the morphologies give evidence that larger NPs are formed in $AgNO_3$-hydrosols. Simultaneously, the broader SPE curve with lower A_{max} values is obtained and, consequently, the hydrosol is less stable. Therefore, information obtained from TEM images and SPE curves correlates very well.

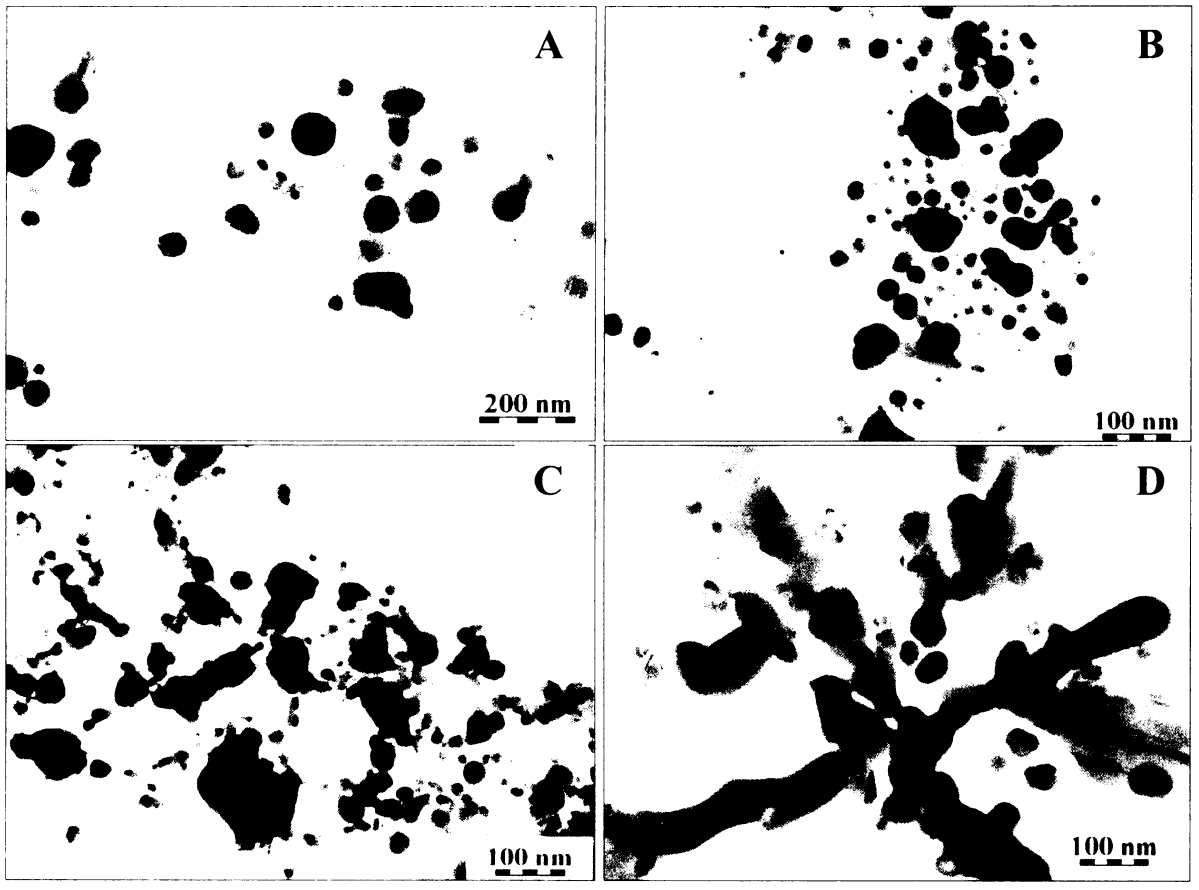

Fig. 41: TEM images of: (A) w-Ag hydrosol, (B) NaCl($1x10^{-4}$ M)-Ag hydrosol, (C) HCl($1x10^{-4}$ M) -Ag hydrosol, (D) $AgNO_3$($1x10^{-4}$ M)-Ag hydrosol.

3.1.7. Summary of simple ions effect on LA/NF

A comparison of the SPE characteristics, TEM images and SERS/SERRS reactivity of NPs prepared in the presence of the selected ions has shown the following facts:

(i) The formation of Ag NPs is faster, more efficient, the number of smaller NPs is higher and the resulting hydrosol is more stable in the long time-scale evolution provided that the LA/NF process was carried out in the presence of NaCl and/or HCl in concentration range between $1x10^{-4}$ M and $1x10^{-3}$ M.

(ii) TEM images give evidence that chlorides are responsible of NPs intergrowth and that this effect is not encountered only in systems of borohydride-reduced Ag hydrosols with chlorides but also for systems of chloride-Ag hydrosols (prepared by LA/NF). These hydrosols are proposed to be the perspective substrates for SERS/SERRS spectral measurements.
(iii) The generation of Ag NPs in the NaOH-Ag hydrosols with $1x10^{-5}$ M and $1x10^{-4}$ M NaOH concentration values is faster and more efficient in comparison to a w-Ag hydrosol, however, such a NaOH-Ag hydrosol is less stable in the long time-scale evolution in comparison to the NaCl- and/or HCl-Ag hydrosols.
(iv) The systems of NPs prepared in the presence of THS and/or $AgNO_3$ are substantially less stable than w-Ag hydrosols.
(v) A good agreement of results obtained by SPE and TEM measurements has been observed.

3.2. LA/NF in bpy or TMPyP

The original idea of LA/NF carried out in the presence of an adsorbate was to detect possible photoproducts (or thermal decomposition products) formed during LA/NF from this adsorbate. In addition to that, provided that the adsorbates prove themselves to be resistant against decomposition (photochemical and/or thermal) during LA/NF, this preparation procedure can lead to a "one pot preparation" of SERS-active systems. For the sake of a better comparison, the physical and physico-chemical (step-wise LA/NF) conditions of LA/NF have been maintained the same as in the case of LA/NF performed in the presence of simple ions [Chapter 3.1.]. SPE spectra were measured in each pause of LA/NF and after several days of systems aging, in each concentration of a particular adsorbate. Two bpy concentrations in resulting hydrosols were selected, $1x10^{-5}$ M and $1x10^{-6}$ M; while only one TMPyP concentration value was employed, $1x10^{-7}$ M.

The resulting SPE characteristics are summarized in Table XVI. A comparison of the w-Ag hydrosol with the bpy-Ag hydrosols and TMPyP-Ag hydrosol shows that the presence of an adsorbate changes the conditions of NP formation: SPE bands are red-shifted, lowered in their A_{max} values and broadened. If SPE spectra are re-measured after several days, the destabilization effect of used adsorbates to NPs manifests itself – Table XVII.

On the basis of the characteristics determined from the SPE spectra (Tables XVI and XVII), the presence of higher bpy concentration in the final system has caused smaller changes of these characteristics than that of lower one in comparison to those of a w-Ag hydrosol. On the other hand, the SPE characteristics of Ag hydrosols prepared in $1x10^{-6}$ M bpy and $1x10^{-7}$ M TMPyP and their evolution show some similarities (Tables XVI, XVII).

Table XVI: Parameters of SPE bands of Ag hydrosols prepared by step-wise LA/NF in water and in adsorbates solutions

LA/NF performed		λ_{max}	A_{max}	FWHM	A_{250}
in	for [min]	[nm]	[arb.units]	[nm]	[arb.units]
pure water	2	397	0.251	194	0.199
	2+3	395	0.380	143	0.235
	2+3+3	395	0.471	116	0.267
	2+3+3+5	392	0.586	93	0.297
	2+3+3+5+7	**394**	**0.756**	**79**	**0.367**
$1x10^{-5}$ M bpy	2	396	0.187	106	0.272
	2+3	397	0.241	113	0.293
	2+3+3	398	0.370	88	0.329
	2+3+3+5	398	0.485	75	0.352
	2+3+3+5+7	**398**	**0.585**	**69**	**0.368**
$1x10^{-6}$ M bpy	2	395	0.268	103	0.249
	2+3	403	0.270	125	0.252
	2+3+3	405	0.206	169	0.219
	2+3+3+5	402	0.204	150	0.235
	2+3+3+5+7	**397**	**0.210**	**125**	**0.245**
$1x10^{-7}$ M TMPyP	2	407	0.225	111	0.220
	2+3	405	0.264	185	0.228
	2+3+3	406	0.283	148	0.246
	2+3+3+5	407	0.262	170	0.238
	2+3+3+5+7	**406**	**0.228**	**176**	**0.220**

Table XVII: Parameters of SPE bands of Ag hydrosols prepared by step-wise LA/NF in water and in adsorbate solutions - aging

System	SPE measured	λ_{max} [nm]	A_{max} [arb.units]	FWHM [nm]	A_{250} [arb.units]
pure water	immediately	394	0.756	79	0.367
	after 3 days	402	0.650	69	0.303
$1x10^{-5}$ M bpy	immediately	398	0.585	69	0.368
	after 2 days	399	0.304	69	0.239
$1x10^{-6}$ M bpy	immediately	397	0.210	125	0.245
	after 2 days	406	0.153	63	0.150
$1x10^{-7}$ M TMPyP	immediately	406	0.228	176	0.220
	after 4 days	426	0.072	-	0.116

The tendency of Ag NPs prepared by LA/NF in adsorbate solution towards aggregation probably originates from a decrease of the electrostatic repulsion barrier between Ag NPs caused by adsorption of a cationic (TMPyP) or a neutral (bpy) adsorbate.

TEM images of NPs in Ag hydrosol prepared by LA/NF in $1x10^{-5}$M and $1x10^{-6}$M bpy are compared to those in w-Ag hydrosols in Fig. 42. Aggregation and interpenetration of NPs disable the determination of PSD. Therefore, the PSD was determined for system with $1x10^{-6}$M bpy (Fig. 42E) and can be compared with the PSD of a w-Ag hydrosol (Fig. 42B). As it is seen, the presence of bpy leads, on one hand, to a decrease of the average NP size; since 5 nm NPs are mostly encountered in the bpy-Ag hydrosol. On the other hand, very large NPs (>80 nm) are present too and, especially, these probably induce the precipitation of hydrosols – Table XVII.

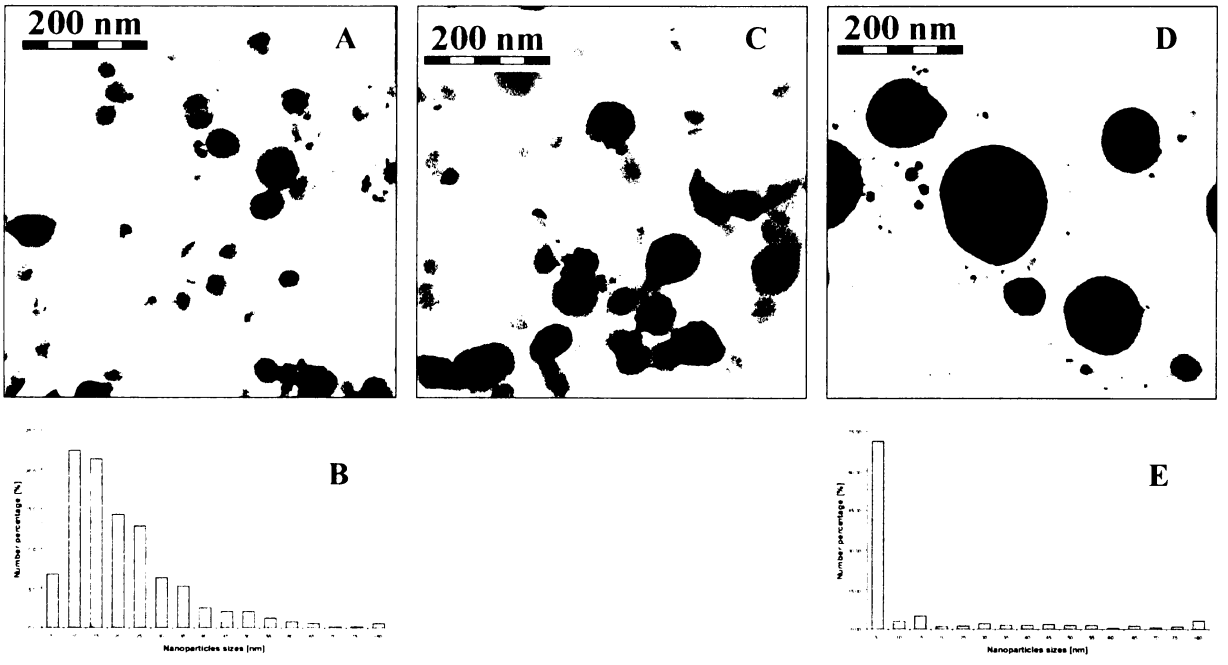

Fig. 42: (A) TEM image of a w-Ag hydrosol after 2+3+3+5+7 min of LA/NF; (B) PSD of the w-Ag hydrosol in (A); (C) TEM image of bpy($1x10^{-5}$ M)-Ag hydrosol after 2 min of LA/NF; (D) TEM image of bpy($1x10^{-6}$ M)-Ag hydrosol after 2 min of LA/NF; (E) PSD of the bpy-Ag hydrosol in (D).

SERS spectra of bpy-Ag hydrosol and TMPyP-Ag hydrosol were measured and assigned. For both adsorbates, the surface species detected earlier in systems, in which those adsorbates were added to pre-prepared Ag hydrosols [Chapter 2] were identified, which indicates that neither bpy, nor TMPyP have decomposed during LA/NF.

In SERS spectra of Ag hydrosols prepared by LA/NF in the presence of $1x10^{-5}$ M bpy, Ag^{+}-bpy surface complex, as well as, Ag(0)-bpy surface complex (Fig. 43, spectra a,b) were detected. In the first five minutes of LA/NF process, Ag^{0} adsorption sites were available; while in further steps (8, 13, 20 min – Fig. 43, spectra c,d,e, respectively) only Ag^{+}-bpy surface complex has dominated in SERS spectra. All our experiments have been carried out in the air and under vigorous stirring of solution, hence, the oxidation could proceed easily. This fact may, in

turn, explain why Ag(0)-bpy surface complex was observed only in the early times of LA/NF. The samples measured immediately after their formation (in each step) were stored for half an hour in dark without stirring in closed tubes so that the further oxidation is extinguished. After half an hour, they were re-measured. The results of such an experiment are summarized in Table XVIII. Obviously, Ag^0 adsorption sites have remained preserved in the systems where they were observed before.

In the SERRS spectra of TMPyP-Ag hydrosol (Table XVIII and Fig. 44), all three expected SERRS spectral forms were observed. Nevertheless, only some characteristic bands of Ag^0-TMPyP surface species were detected as shoulders (386 and 1567 cm^{-1}) and/or very weak bands (e.g. 1366cm^{-1}) in the early times of LA/NF (spectrum a in Fig. 44). In the further steps of LA/NF, the oxidation of NP surfaces probably proceeded and, consequently, Ag^+-TMPyP surface species became dominant in SERRS spectra which indicates that the metallation of porphyrin by its interaction with Ag^+ adsorption sites takes place during the time-evolution of TMPyP-Ag hydrosol [157].

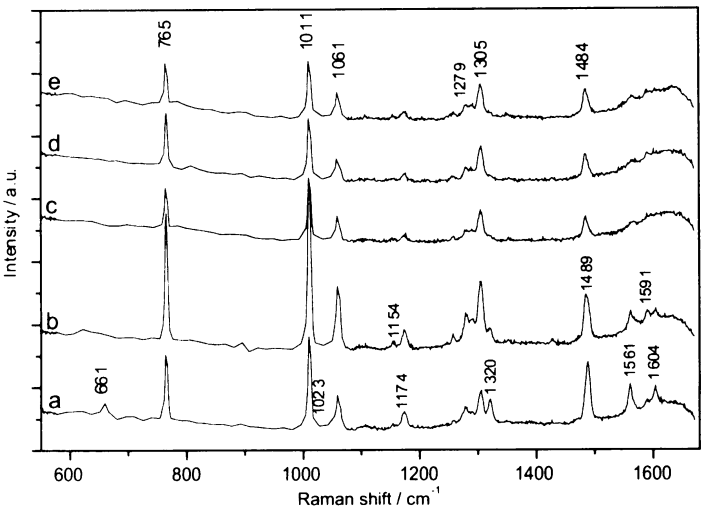

Fig. 43: The SERS spectra of bpy($1x10^{-5}$ M)-Ag hydrosol after: (a) 2 min, (b) 2+3 min, (c) 2+3+3 min, (d) 2+3+3+5 min and (e) 2+3+3+5+7 min of LA/NF.

Table XVIII: Summation of observation of SERS/SERRS spectral forms of Ag hydrosol systems prepared by step-wise LA/NF in adsorbate solutions

Time of LA/NF	LA/NF in $1x10^{-5}$ M bpy		LA/NF in $1x10^{-6}$ M bpy		LA/NF in $1x10^{-7}$ M TMPyP
[min]	immediatelly	after 1/2 hour*	immediatelly	after 1/2 hour*	
2	Ag^+-bpy, Ag(0)-bpy	Ag^+-bpy, Ag(0)-bpy	Ag^+-bpy, Ag(0)-bpy	Ag^+-bpy, Ag(0)-bpy	free base, (? Ag(0)-TMPyP)
2+3	Ag^+-bpy, Ag(0)-bpy	Ag^+-bpy, (Ag(0)-bpy)	Ag^+-bpy	Ag^+-bpy	free base, Ag^+-TMPyP
2+3+3	Ag^+-bpy	Ag^+-bpy	Ag^+-bpy	Ag^+-bpy	free base, Ag^+-TMPyP
2+3+3+5	Ag^+-bpy	Ag^+-bpy	Ag^+-bpy	Ag^+-bpy	free base, Ag^+-TMPyP
2+3+3+5+7	Ag^+-bpy	Ag^+-bpy	(Ag^+-bpy)	Ag^+-bpy	free base, Ag^+-TMPyP

Notes: underlined form dominates in a particular spectrum; ? means that only some characteristic bands are observable; parenthesis mean very weak signal of the SERS/SERRS spectral form; * the same sample was used as in the immediate measurement.

To sum up this section, the characteristics obtained by SPE measurements show that the presence of a particular adsorbate changes the conditions of NPs formation and that these hydrosols are unstable (they are precipitating within days after their preparation).

The morphologies observable by TEM measurements are influenced by the final concentration of a particular adsorbate.

By the SERS and SERRS spectral measurements of interactions between selected adsorbate and freshly formed silver surface, Ag^0 adsorption sites were identified upto 5 minutes after the beginning of LA/NF. Both bpy and TMPyP were found to be resistant against a possible photochemical and/or thermal decomposition during LA/NF.

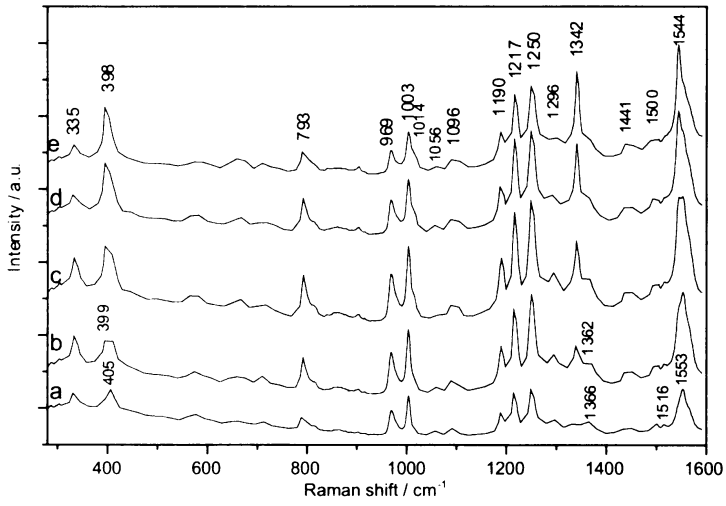

Fig. 44: The SERRS spectra of TMPyP($1x10^{-7}$ M)-Ag hydrosol after (a) 2 min, (b) 2+3 min, (c) 2+3+3 min, (d) 2+3+3+5 min and (e) 2+3+3+5+7 min of LA/NF.

Chapter 4

In this Chapter the possibilities to prepare Ag NPs modified by various surface coverages of adsorbed citrates by LA/NF of Ag target in aqueous solutions of sodium citrate (Na_3Citr) and/or citric acid (H_3Citr) of various concentrations are probed. The hydrosols of citrate-modified Ag NPs prepared by LA/NF are tested as prospective substrates for SERS using bpy as the testing adsorbate. A detailed SERRS spectral testing of citrate-modified Ag NPs with various citrate coverages is provided in [Chapter 5].

Prior to this study, some of the most important new observations and results obtained in [Chapter 2] and [Chapter 3] were verified, or studied in more detail, using the physical and physico-chemical parameters employed further for LA/NF in citrate solutions. These parameters are given in detail in Experimental related to [Chapter 4], and somewhat differ from those used in [Chapter 2] and [Chapter 3]. In particular, a different sequence of light and dark periods in the process of LA/NF has been employed and tested. In this case, the sequence has been 5 min of irradiation, followed by 2 min of dark period, then 5 min of irradiation, followed again by 2 min of dark period, and finally, 10 min of irradiation.

4.1. Step-wise performed LA/NF in pure water – effects of energy in pulse changes

As it was mentioned in [Introduction], many authors have investigated the effect of the changes of energy per pulse on the outcome of LA/NF carried out with ns laser pulses in pure water. However, those experiments have very mostly been done for a continuous LA/NF process. In [Chapter 2], the effect of the energy per pulse (changed from ~90 mJ/pulse to ~187 mJ/pulse) for the step-wise performed LA/NF has been demonstrated.

In this section, the effect of energy-per-pulse changes on the outcome of step-wise LA/NF performed in pure water is investigated for higher values of energies per pulse, and for a different sequence of light and dark periods during LA/NF. The LA/NF was carried out at three different energies per pulse (~200, ~300, and ~400 mJ/pulse) under otherwise the same experimental conditions.

Table XIX shows the parameters of the SPE spectra of Ag hydrosols prepared by LA/NF carried out at ~200, ~300, and ~400 mJ/pulse. During the step-wise LA/NF, the λ_{max} positions have red-shifted and the A_{max} and A_{250} value have increased with the increasing energy per pulse. Therefore, it may appear advantageous to perform LA/NF at higher energies per pulse due to the higher NP formation efficiency. Nevertheless, a comparison of the FWHM values in the SPE spectra of the Ag hydrosol prepared at the highest energy per pulse (~400 mJ/pulse) with those prepared at lower energies (~200 and ~300 mJ/pulse), which shows a substantial broadening of the SPE band in the former case, indicates that the ~400 mJ/pulse-hydrosol consists of higher fraction of larger NPs which, consequently, can lead to instability of Ag hydrosol. This has been confirmed by SPE spectral measurements after several days of aging (Table XX). In particular, the A_{max} value of the 400 mJ/pulse-Ag hydrosol decreased four times during only 8 days of aging which indicates precipitation of Ag NP aggregates from the hydrosol.

Table XIX: Parameters of SPE bands of w-Ag hydrosols prepared by step-wise LA/NF performed at various energies per pulse

LA/NF performed at [mJ/pulse]	for [min]	λ_{max} [nm]	A_{max}	FWHM [nm]	A_{250}
~200	5	393	0.189	113	0.096
	5+5	393	0.305	110	0.147
	5+5+10	396	0.343	110	0.173
~300	5	398	0.270	113	0.13
	5+5	398	0.358	110	0.216
	5+5+10	405	0.493	110	0.254
~400	5	401	0.309	130	0.131
	5+5	403	0.435	210	0.299
	5+5+10	406	0.852	175	0.501

Table XX: Parameters of SPE bands of w-Ag hydrosols prepared by LA/NF performed at various energies per pulse – aging

LA/NF performed at [mJ/pulse]	System after x days	λ_{max} [nm]	A_{max}	FWHM [nm]	A_{250}
~300	0	405	0.493	110	0.254
	7	405	0.239	185	0.126
	21	408	0.209	100	0.080
~400	0	406	0.852	175	0.501
	8	406	0.214	105	0.081
	29	411	0.186	115	0.080

4.2. Comparison of step-wise and continuously performed LA/NF in pure water

On the basis of the previous results [section 4.1.], LA/NF has been performed both step-wise and as a continuous process in pure water using laser pulse energies of ~200 and ~300 mJ/pulse. SPE spectra of the resulting hydrosols are compared in Fig. 45 where the important characteristics of SPE spectra are also listed.

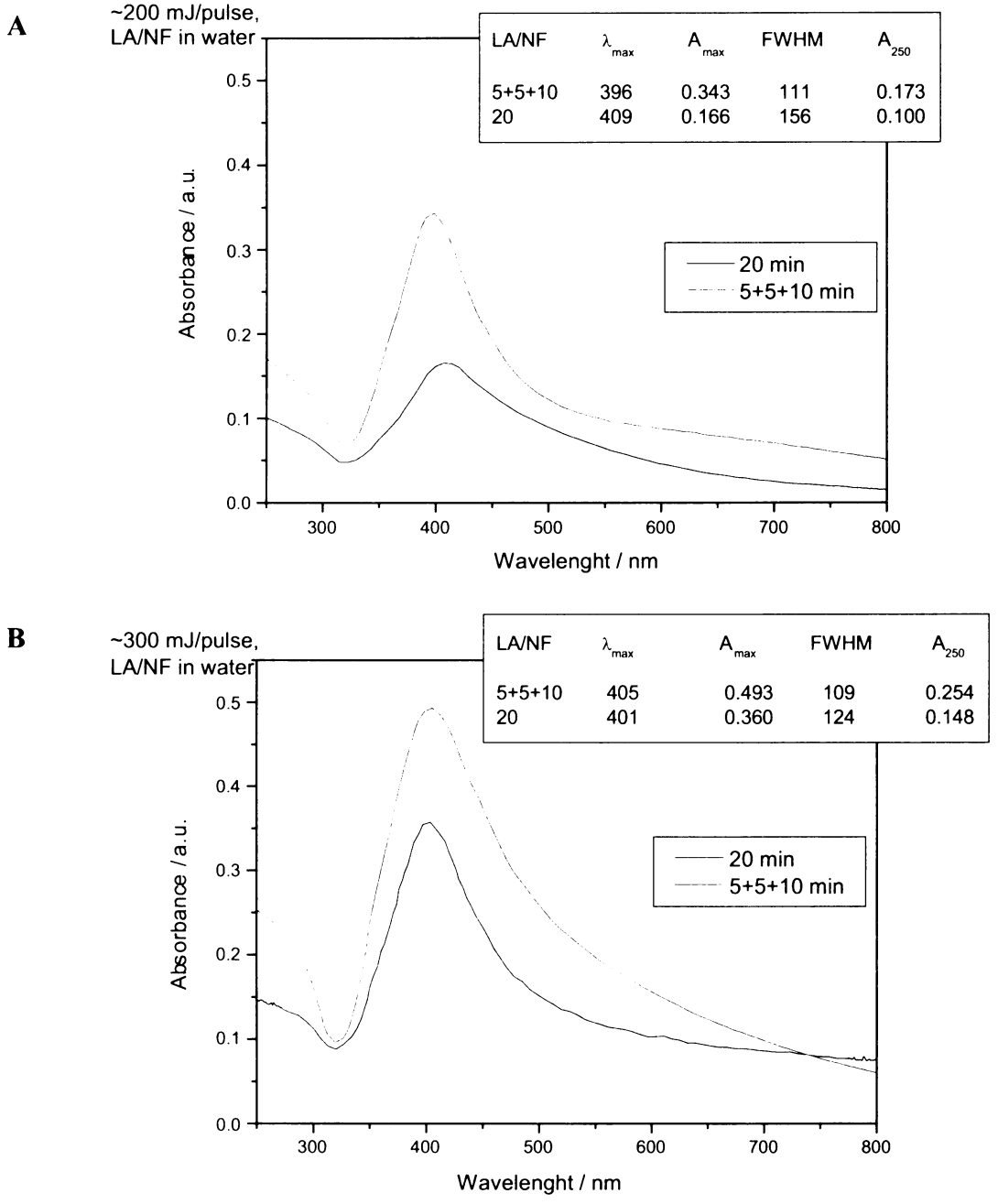

Fig. 45: Comparison of SPE spectra of Ag hydrosols prepared by step-wise and continuous LA/NF in ultrapure water at (A) ~200 and (B) ~300 mJ/pulse.

At both used energies per pulse, the same trend of the SPE characteristics appears: in the case of continuous LA/NF, the A_{max} and A_{250} values decrease, while the FWHM values increase when compared to the step-wisely performed LA/NF. The only exception is the λ_{max} value because in the case of ~300 mJ/pulse-Ag hydrosol, the position of SPE band is blue-shifted for the continuous LA/NF in comparison to the step-wise LA/NF; while in the case of 200 mJ/pulse, an enormous red-shift is observed. Moreover, the mentioned FWHM value increase is higher in SPE spectrum of a hydrosol prepared at ~200 mJ laser pulses than that in a hydrosol prepared at ~300 J/pulse. Therefore, the changes in SPE characteristics due to the interruption of LA/NF seem to be more noticeable in Ag hydrosols prepared at ~200 mJ/pulse than that in hydrosols prepared at higher energy per pulse.

To summarize the obtained results of this section, the step-wise performed LA/NF in pure water appears to be better for a more efficient NPs formation than a continuous LA/NF.

4.3. Detailed study of LA/NF in NaCl and/or HCl solutions

With respect to the results presented in [sections 4.1. and 4.2.], the LA/NF in NaCl and HCl solutions has been performed at 300 mJ/pulse by a step-wise procedure. This systematic study was motivated by the results obtained in [Chapter 3] which have shown that the Ag hydrosols prepared by LA/NF in NaCl and HCl solutions showed a good long term stability (with exception of a highly concentrated solution of $5x10^{-2}$ M NaCl) and excellent SERS-activity.

Four different values of chloride concentrations were selected and used: $1x10^{-5}$ M, $1x10^{-4}$ M, $1x10^{-3}$ M and $1x10^{-2}$ M (Table XXI). Furthermore, LA/NF in the chloride-containing solutions has been carried out with the same physical (e.g. ~300 mJ/pulse) and physico-chemical parameters and with the same setup (Schema II) as in the case of LA/NF performed in ultrapure water (presented in [sections 4.1. and 4.2.]) and, hence, the results can be mutually compared.

Table XXI: Parameters of SPE bands of Ag hydrosols prepared by step-wise LA/NF in water and in chloride solutions

LA/NF performed in	for [min]	λ_{max} [nm]	A_{max} [a.u.]	FWHM [nm]	A_{250} [a.u.]
water	5	398	0.270	113	0.130
	5+5	398	0.358	110	0.216
	5+5+10	405	0.493	110	0.254
$1x10^{-5}$ M NaCl	5	398	0.302	115	0.137
	5+5	398	0.361	105	0.232
	5+5+10	394	0.540	80	0.271
$1x10^{-4}$ M NaCl	5	393	0.320	70	0.150
	5+5	394	0.468	55	0.263
	5+5+10	393	0.628	55	0.295
$1x10^{-3}$ M NaCl	5	394	0.518	65	0.170
	5+5	394	0.772	60	0.268
	5+5+10	394	0.948	60	0.383
$1x10^{-2}$ M NaCl	5	398	0.478	60	0.191
	5+5	395	0.588	55	0.204
	5+5+10	395	0.646	50	0.222
$1x10^{-5}$ M HCl	5	392	0.518	77	0.157
	5+5	392	0.695	81	0.251
	5+5+10	392	0.808	84	0.337
$1x10^{-4}$ M HCl	5	392	0.570	67	0.192
	5+5	393	0.699	73	0.265
	5+5+10	392	0.838	87	0.345
$1x10^{-3}$ M HCl	5	395	0.572	67	0.236
	5+5	395	0.795	73	0.333
	5+5+10	398	0.908	100	0.529
$1x10^{-2}$ M HCl	5	400	0.407	60	0.133
	5+5	401	0.569	80	0.230
	5+5+10	407	0.618	120	0.340

4.3.1. SPE measurements

The main bands in the SPE-curves are nearly symmetric for all NaCl-Ag hydrosols, in contrast to those of w-Ag hydrosols. This symmetry of SPE-curves is also characteristic for HCl-Ag hydrosols with $1x10^{-3}$ M and $1x10^{-4}$ M HCl concentrations. On the contrary, in the case of the HCl-Ag hydrosols with the lowest ($1x10^{-5}$ M) and the highest ($1x10^{-2}$ M) HCl concentrations, the symmetry of the SPE-curve is disturbed by a long-wavelength tail.

The characteristics obtained from SPE-curves are summarized in Table XXI. In comparison to w-Ag hydrosol, the λ_{max} of NaCl-Ag hydrosols (for all four concentrations) are in the region between 393-398 nm and the λ_{max} of HCl-Ag hydrosols (except of that with the highest HCl concentration) are in the region between 392-398 nm (Table XXI).

The FWHM values reveal some differences between NaCl- and HCl-Ag hydrosols observable in the course of the step-wise LA/NF. While FWHM decreases in NaCl-Ag hydrosols during LA/NF and with the NaCl concentration increase; this characteristic increases in HCl-Ag hydrosols during LA/NF and with the HCl concentration increase (Table XXI).

The A_{max} and A_{250} values, which increase in each step during the step-wise LA/NF, also increase with the increasing NaCl and/or HCl concentrations in the region $1x10^{-5}$ - $1x10^{-3}$ M chloride concentration value. The exceptional behaviour thus show only the Ag hydrosols with the highest chloride concentrations ($1x10^{-2}$ M).

Summarizing the results of the SPE spectral probing of Ag NP hydrosols prepared by LA/NF in chloride solutions, we obtain:

For NaCl-Ag hydrosols (i.e. Ag hydrosols prepared in the neutral chloride solutions), the SPE spectral parameters of the hydrosols (Table XXI) indicate that the presence of NaCl in the $1x10^{-5}$ – $1x10^{-3}$ M range promotes formation of small Ag NPs and their stabilization in the hydrosol. In this concentration range, the effect progresses with the increasing chloride concentration, and maximizes at $1x10^{-3}$ M. The promoting effect drops for $1x10^{-2}$ M concentration. The reason for that was expected to be revealed by TEM imaging and image analysis of Ag NPs in samples prepared from these hydrosols [Section 4.3.2.].

For HCl-Ag hydrosols (i.e. Ag hydrosols prepared in the acidic chloride solutions, the pH of which is listed in Table XXII), the SPE spectral parameters indicate that while the presence of HCl probably promotes formation of

Table XXII: Measurements of pH in HCl solutions before and after step-wise LA/NF performed in them

Measured system	pH
$1x10^{-5}$ M HCl	5,07
HCl($1x10^{-5}$ M)-Ag hydrosol	5,60
$1x10^{-4}$ M HCl	4,05
HCl($1x10^{-4}$ M)-Ag hydrosol	4,08
$1x10^{-3}$ M HCl	3,07
HCl($1x10^{-3}$ M)-Ag hydrosol	3,09
$1x10^{-2}$ M HCl	2,10
HCl($1x10^{-2}$ M)-Ag hydrosol	2,10

Ag NPs, another effect occurs and manifests itself by broadening of the main SPE band. The promoting effect increases with the increasing concentration in the $1x10^{-5}$ – $1x10^{-3}$ M range, the SPE band broadening effect appears to progress throughout the overall range of HCl concentrations. The results obtained in [Chapter 3] indicate that the effect causing broadening of the main SPE band can be formation of compact aggregates of intergrown particles. This assumption has been confirmed by TEM imaging [Section 4.3.2.].

Furthermore, the long-term stability of the chloride-hydrosols has been followed by SPE measurements. All chloride-Ag hydrosols and a the w-Ag hydrosol were stored in dark in closed tubes and their SPE spectra have been re-measured after approximately one week. In addition to that, the most stable, NaCl($1x10^{-3}$ M)-Ag hydrosol, and the w-Ag hydrosol (as a reference sample) were stored for a longer time period (3-4 weeks) and their SPE curves were re-measured again after this longer time period. The characteristics of SPE bands are presented in Table XXIII. After 6-8 days of aging, Ag hydrosols prepared in $1x10^{-2}$ M NaCl and HCl have almost completely precipitated. Ag hydrosols prepared in solutions of two intermediate NaCl and HCl concentrations ($1x10^{-3}$ M and $1x10^{-4}$ M) remain preserved, however, even those show the distinct SPE characteristics of slowly precipitating hydrosols, in particular the λ_{max} values red-shift, the FWHM values increase and the A_{max} and A_{250} values decrease. The most stable is the NaCl($1x10^{-3}$ M)-Ag hydrosol, however, even that shows a distinct progress of precipitation after 4 weeks of aging.

To summarize the SPE curve observation, a hydrosol of better stability and most probably of a more monodisperse PSD (which is characteristic by narrower and higher SPE band, i.e. a SPE band positioned at around 393 nm, of a smaller FWHM and a higher A_{max} value) is formed in the presence of even $1x10^{-5}$ M chlorides concentration value. From the above-mentioned facts and in comparison to the results presented in [Chapter 3.1]. (where the best NaCl concentration value seemed to be the $1x10^{-4}$ M value for LA/NF at ~200 mJ/pulse), it can be assumed that the presence of NaCl during LA/NF positively influences the NP properties at each selected energy per pulse, nevertheless, the optimal NaCl concentration will be different : it reveals that with a higher energy value per pulse (~300 mJ/pulse here), a higher NaCl concentration (the $1x10^{-3}$ M NaCl here) is necessary for achieving the best hydrosol from the NaCl- concentrational set. However, there is also an upper limit of NaCl concentration for an optimal hydrosol achievement and above this limit, the hydrosol is no more stable and precipitate easily.

As for HCl-Ag hydrosols, they are even less stable than NaCl-Ag hydrosols presumably due to their acidic pH which has been measured before the beginning and after 5+5+10 min of LA/NF - Table XXII. As a consequence of the chloride presence and, simultaneously, of acidic ambient, it is assumed that NPs interpenetrate and grow as it has been already revealed in [Chapter 3.1]. Therefore, larger NPs might be present in HCl-Ag hydrosols which leads to destabilization and, consequently, to precipitation (this is in agreement with the SPE characteristics observation) – it will be evidenced by TEM imaging in the next section.

Table XXIII: Parameters of SPE bands of Ag hydrosols prepared by step-wise LA/NF in water and in chloride solutions - aging

LA/NF performed in	System after x days	λ_{max} [nm]	A_{max} [a.u.]	FWHM [nm]	A_{250} [a.u.]
water	0	405	0.493	110	0.254
	7	405	0.239	185	0.126
	21	408	0.209	100	0.080
$1x10^{-5}$ M NaCl	0	394	0.540	80	0.271
	7	-	-	-	-
$1x10^{-4}$ M NaCl	0	393	0.628	55	0.295
	8	407	0.120	290	0.031
$1x10^{-3}$ M NaCl	0	394	0.948	60	0.383
	8	402	0.860	75	0.131
	28	407	0.692	93	0.122
$1x10^{-2}$ M NaCl	0	395	0.646	50	0.222
	7	-	-	-	0.006
$1x10^{-5}$ M HCl	0	392	0.808	84	0.337
	6	-	0.001	-	0.040
$1x10^{-4}$ M HCl	0	392	0.838	87	0.345
	6	415	0.420	120	0.117
$1x10^{-3}$ M HCl	0	398	0.908	100	0.529
	6	394	0.617	63	0.161
$1x10^{-2}$ M HCl	0	407	0.618	120	0.340
	6	406	0.004	-	0.061

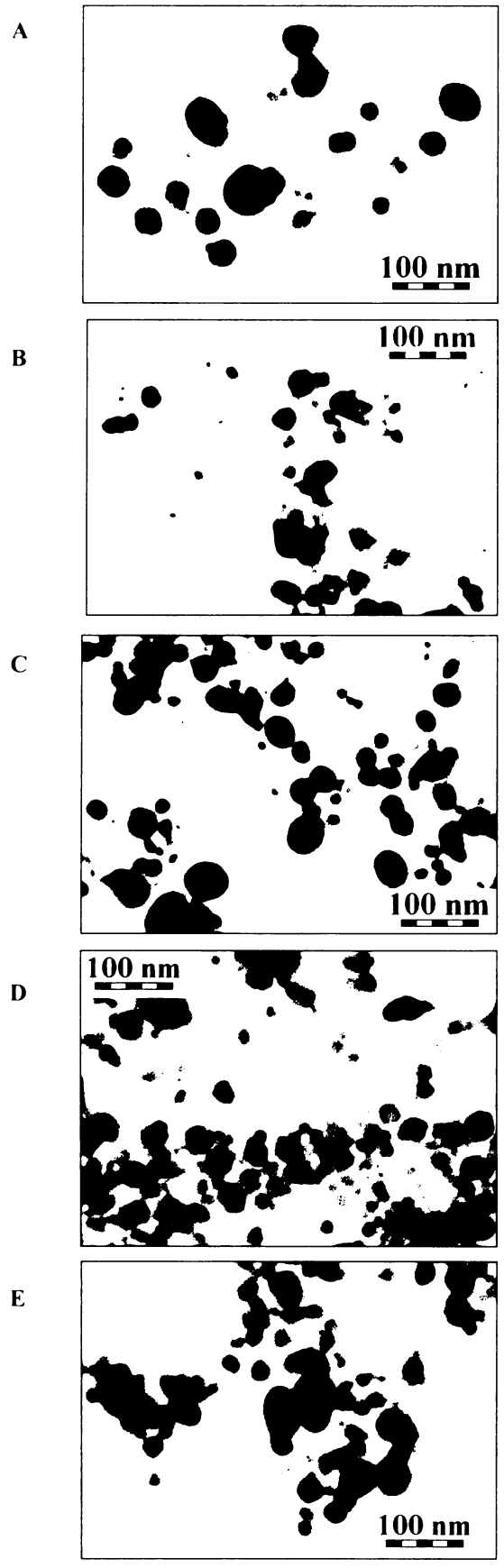

Fig. 46 : TEM images of hydrosols prepared by LA/NF in the presence of: (A) water, (B) $1x10^{-5}$ M NaCl, (C) $1x10^{-4}$ M NaCl, (D) $1x10^{-3}$ M NaCl, and (E) $1x10^{-2}$ M NaCl.

4.3.2. TEM imaging and image analysis

The comparison of the TEM images (Fig. 46) shows that the NaCl concentration increase induces a higher fraction of smaller NPs in resulting hydrosol. In addition to that, in TEM images of NaCl($1x10^{-2}$ M)-Ag hydrosol, the aggregates of small NPs and interpenetrating NPs are encountered (Fig. 46E). To verify this observation, PSDs have been determined for these systems and are presented in Table XXIV and also as histograms in Fig. 47. The NPs smaller than 20 nm in diameter dominate (around 70%) in NaCl-Ag hydrosols for $1x10^{-5}$ and $1x10^{-4}$ M NaCl concentrations and the largest value of ~75% was achieved for $1x10^{-3}$ M NaCl concentration, while the ~64% was achieved for $1x10^{-2}$ M NaCl. The NPs larger than 45 nm in diameter were almost absent in NaCl-Ag hydrosols (~0.6%), while they were of about 6% generated in w-Ag hydrosol.

Furthermore, the TEM images of the w-Ag hydrosol, the NaCl($1x10^{-3}$M)-Ag hydrosol, and the HCl($1x10^{-3}$M)-Ag hydrosol are mutually compared in Fig. 48. The presented TEM images obviously demonstrate the formation of compact aggregates and NP interpenetration in the case of HCl-Ag hydrosols. Hence, in HCl-Ag hydrosols, it was not possible to determine PSDs since large 3D-aggregates and interpenetrated agglomerates were formed and the individual NPs could not be clearly distinguished.

4.3.3. Summary of results of the SPE spectral probing and TEM imaging of Ag hydrosols prepared by LA/NF in NaCl and HCl solutions

1. The presence of NaCl solutions in $1x10^{-5}$-$1x10^{-3}$ M concentrations promotes formation of small Ag NPs, the fraction of which is the highest for the NaCl($1x10^{-3}$ M)-Ag hydrosol. This hydrosol also shows the largest long-term stability. Therefore, for LA/NF carried out by a step-wise procedure with laser pulse energy of 300 mJ/pulse, the presence of $1x10^{-3}$ M NaCl solutions leads to the production of the optimally stabilized Ag NP hydrosols.

2. The comparison of the results of LA/NF in NaCl solutions carried out by a step-wise procedure at laser pulse energy of ~187 mJ/pulse in Chapter 3.1. with those summarized here in paragraph 1 shows that in the former case (i.e. at the lower energy per pulse used for LA/NF) the optimal concentration for resulting Ag NP hydrosol stabilization was $1x10^{-4}$ M, while in the latter case (i.e. at the higher energy per pulse) the optimal NaCl concentration was higher, i.e. $1x10^{-3}$ M. This comparison indicates that the physical parameter of energy per pulse value and the chemical parameter of the stabilizing chloride ions concentration in the neutral ambient (NaCl solutions) are most probably interrelated. A possible explanation of this relationship is provided below. With the increase of the energy per pulse used in the LA/NF process, the total amount of ablated Ag (i.e. of Ag transferred from the target to solution) is higher, as demonstrated particularly in ref. 32. Therefore, it can be anticipated that for higher energy per pulse larger chloride concentrations are required to yield the optimal chloride coverage required for the optimal stabilization of small Ag NPs.

3. The observed drop in small Ag NP stabilization efficiency observed for NaCl($1x10^{-2}$ M)-Ag hydrosol and deduced from its SPE spectral characteristics, most probably originates from formation of compact aggregates of interpenetrating (intergrown) Ag NPs, the presence of which was revealed by TEM imaging. In addition to that, come precipitation of the aggregates induced by high ionic strength of

Table XXIV: Relative abundances of Ag NPs in Ag hydrosols prepared by the step-wise LA/NF in water and in NaCl solutions

NP size [nm]	LA/NF carried out in				
	pure water	$1x10^{-5}$M NaCl	$1x10^{-4}$M NaCl	$1x10^{-3}$M NaCl	$1x10^{-2}$M NaCl
5	18,8	19,2	18,8	18,9	21,7
10	24,4	25,5	23,2	30,7	24,1
15	17,0	27,9	26,9	25,2	19,3
20	11,6	12,5	16,2	16,3	12,1
25	7,5	6,3	7,6	6,5	11,0
30	4,4	4,3	3,4	1,3	5,9
35	4,1	1,4	1,8	0,7	3,4
40	3,1	1,9	1,3	0,4	1,7
45	2,8	0,5	0,3	0,0	0,7
50	3,3	0,5	0,3	0,0	0,0
>55	3,1	0,0	0,3	0,0	0,0

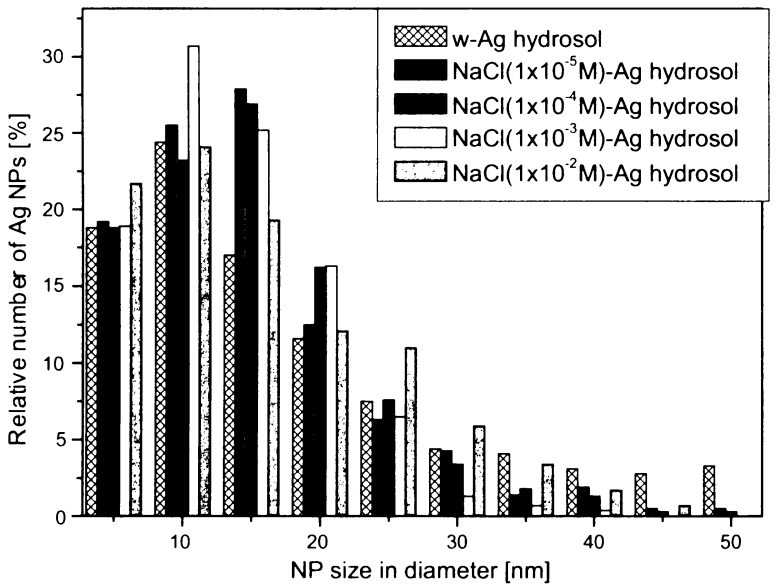

Fig. 47: PSD obtained from TEM images of Ag hydrosols prepared by the step-wise LA/NF in water and in NaCl solutions.

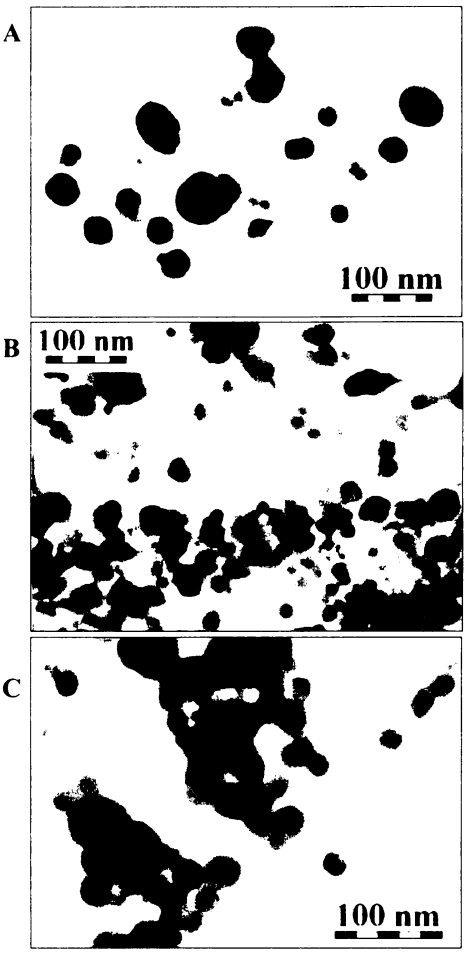

Fig. 48 : TEM images of (A) w-Ag hydrosol, (B) NaCl($1x10^{-3}$ M)-Ag hydrosol, (C) HCl($1x10^{-3}$ M)-Ag hydrosol.

the $1x10^{-2}$ M NaCl solution can also contribute to the observed effect.

4. The presence of HCl in $1x10^{-5}$ M-$1x10^{-3}$ M concentrations possibly also promotes small Ag NPs formation, however, this effect is overpowered by another one, which is formation of compact aggregates of interpenetrating (or touching) Ag NPs. For HCl($1x10^{-2}$ M)-Ag hydrosol, this effect is probably accompanied by the effect of high ionic strength of the HCl solution which causes some precipitation of the aggregates from the hydrosol. Apparently, the change of pH of the chloride-containing ablation medium from neutral to acidic strongly decreases the threshold chloride concentration (which, according to [112], is directly related to the coverage of Ag NPs by adsorbed chlorides) required for the compact aggregate formation and the further Ag NP growth and intergrowth. Analogous pH effects have been observed for both Ag hydrosols prepared by LA/NF in water and chemically prepared (by reduction of $AgNO_3$ by $NaBH_4$) after their treatment by NaCl and/or HCl (laser-ablated Ag hydrosol/Cl^- and borohydride-reduced Ag hydrosol/Cl^-, respectively). A possible explanation of the pH effect can be the promotion of chloride adsorption by low solution pH. Evidence of such promotion (by EDX analysis) has been provided in [112], and has been reported also for chloride-adsorption on Ag electrode surfaces [158]. Borohydride-reduced Ag hydrosol/Cl^-, laser-ablated Ag hydrosol/Cl^-, and HCl-Ag hydrosol, the effect of low pH is most pronounced for the last mentioned system studied in this Chapter 4, i.e. that of Ag hydrosol prepared by LA/NF in HCl solutions, since the Ag NP intergrowth was observed for HCl concentrations as low as $1x10^{-5}$ M.

4.3.4. SERS spectral probing of Ag hydrosols prepared by LA/NF in NaCl and HCl solutions

Analogously to the SERS-activity probing in [Chapter 3.1.], bpy has been used as the probing adsorbate. The $1x10^{-5}$ M bpy concentration value in the final system was selected, NaCl-Ag hydrosol/bpy systems with NaCl concentrations in the $1x10^{-5}$ M-$1x10^{-2}$ M range were prepared. Their SERS spectra are mutually compared in Fig. 49.

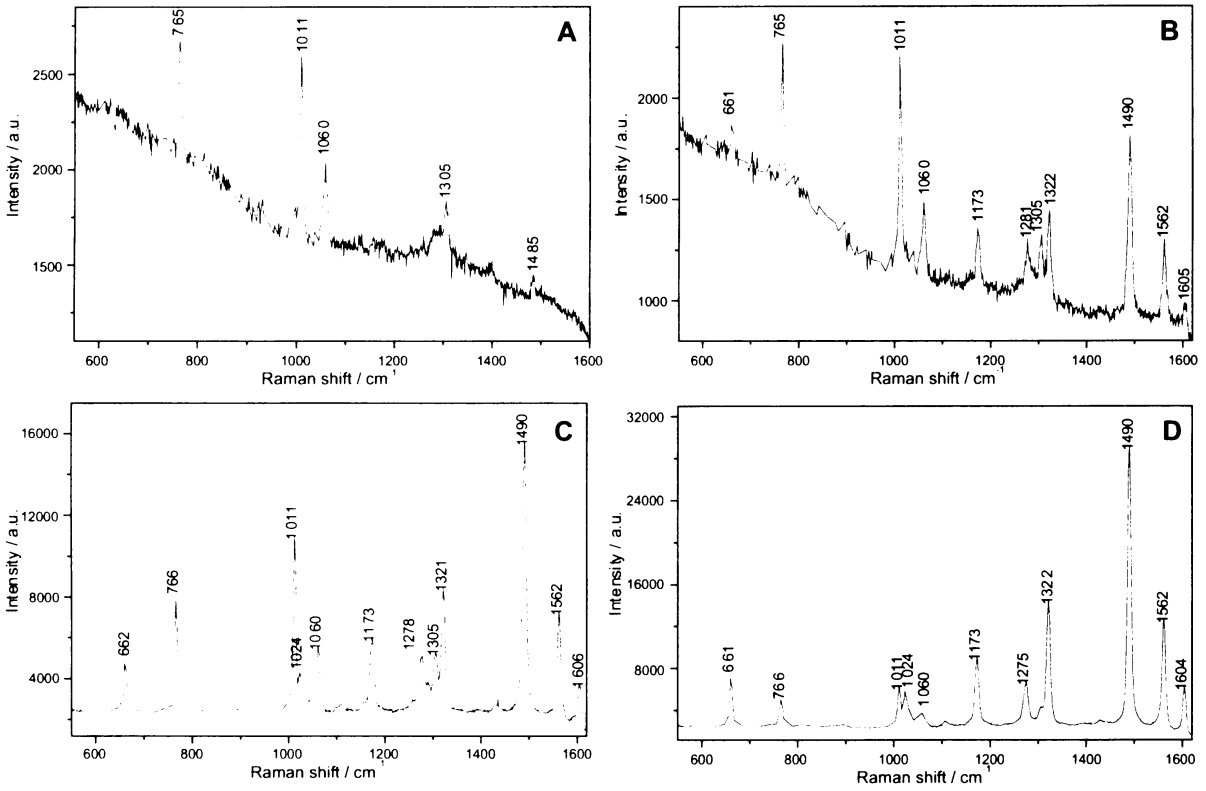

Fig. 49: The SERS spectra of NaCl-Ag hydrosol/bpy(10^{-5} M) systems containing: (A) $1x10^{-5}$M NaCl, (B) $1x10^{-4}$M NaCl, (C) $1x10^{-3}$M NaCl, (D) $1x10^{-2}$M NaCl.

The SERS signal of Ag^{+}-bpy surface species was observed in the system with $1x10^{-5}$ M NaCl concentration, while the Ag^{+}-bpy and Ag(0)-bpy surface species were detected at the higher NaCl concentrations. Obviously, the best SERS signal is observed for the system with the highest ($1x10^{-2}$ M) NaCl concentration. This fact may be caused by two factors: (i) the NaCl($1x10^{-2}$ M)-Ag hydrosol contains compact aggregates and interpenetrating NPs [Sections 4.3.1. - 4.3.3.] in which a strongly enhanced electromagnetic fields (so called "hot spots") are generated in the interstices. The location of bpy molecules into "hot spots" can be responsible for the SERS signal enhancement increase. (ii) molecular resonance (chemical mechanism) contribution to the overall SERS signal enhancement. This contribution is encountered only for Ag(0)-bpy, but not for Ag^{+}-bpy. Since the relative contribution of the Ag(0)-bpy signal increases with the increasing NaCl concentration in the system (as witnessed e.g. by the increase of the mutual ratio of the 1320 cm^{-1}/1305 cm^{-1} band intensities), the chemical mechanism contribution to the overall SERS enhancement increase as well.

The bpy SERS spectral probe was also employed to test the Ag NP surfaces in systems with HCl-Ag-hydrosols. The HCl-Ag hydrosol/bpy systems were prepared for HCl concentrations in Ag hydrosol in the $1x10^{-5}$ M - $1x10^{-2}$ M range. In the SERS spectra of all four systems Ag(0)-bpy surface complex signal dominated. The concentration values of the detection limit of bpy in a HCl-hydrosol/bpy system were determined to be about $1x10^{-7}$ M bpy (or lower) in HCl($1x10^{-5}$ M)-Ag hydrosol and HCl($1x10^{-4}$ M)-Ag hydrosol and they were even lower (around $1x10^{-8}$ M bpy) in systems with HCl-Ag hydrosols of $1x10^{-3}$ M and $1x10^{-2}$ M HCl concentrations.

Finally, the comparison of the results of SPE spectral and TEM imaging of Ag hydrosols prepared by LA/NF in NaCl and HCl solutions with the results of SERS spectral probing of the same systems indicates that the observation of the SERS signal of Ag(0)-bpy surface species is inter-related with the changes in the Ag NP morphology, in particular, the formation of compact aggregates of touching and/or interpenetrating Ag NPs. Both observed effects are thus probably related to a particular surface coverage of Ag NPs by adsorbed chlorides.

4.4. Detailed study of LA/NF in Na_3Citr and/or H_3Citr solutions

The original idea of citrates presence in the course of LA/NF was evoked by the fact that citrate anions are able to stabilize Ag NPs in aqueous solutions as it was published in literature. Mostly, Na_3Citr is used to produce Ag NPs by the chemical reduction of $AgNO_3$. Nevertheless, in this case, the initial Na_3Citr concentration changes due to

the reduction reaction and, therefore, only an unknown part of the initial Na_3Citr concentration value remains in the end of NPs production in the solution. Thus, one cannot be sure of the exact final citrate concentration which stabilizes Ag NPs. On the contrary, one can expect that when LA/NF in a citrate solution is employed to produce Ag NPs, the Na_3Citr concentration value is not only well known, but can be also varied. Therefore, it is expected that by performing LA/NF carried out with citrate solutions of varying concentrations and pH, it will be possible to investigate the effect of varying Ag NP coverages by adsorbed citrate. The final aim of these investigations is the SERS and/or SERRS spectral testing of citrate-modified Ag NPs as the adsorbate–preorienting or adsorbate-protecting substrates for SERS/SERRS.

With respect to the initial Na_3Citr concentrations used in the Lee-Meisel Ag NPs chemical synthesis [159] which is of $7x10^{-4}$ M value, the Na_3Citr concentration range was chosen from $1x10^{-5}$ M to $1x10^{-2}$ M in one-order steps.

Last, but not least, the employment of H_3Citr was inspired by the effect of low pH observed for Ag hydrosols prepared by LA/NF in chloride solutions. Hence, the H_3Citr concentrations were selected to be of the same values as Na_3Citr. The physical conditions of LA/NF were the same as in the previous study of LA/NF in chloride solutions. Briefly: ns laser pulses of ~300 mJ/pulse energy and of 1064 nm wavelength were employed [Experimental for Chapter 4] and the procedure was performed step-wise (in 5, 5+5, 5+5+10 steps). In addition to that, the same parameters of LA/NF process, also the same concentrations of citrate ions ($1x10^{-5}$ –$1x10^{-2}$ M) as those of chlorides were employed.

4.4.1. SPE and TEM measurements

The SPE spectra of Ag hydrosols measured in each step of the LA/NF performed in the presence of Na_3Citr, H_3Citr and in pure water have been analysed, the λ_{max}, FWHM, A_{max} and A_{250} values were determined and are listed in Table XXV. The symmetric SPE bands are observed for Ag hydrosols with Na_3Citr in the overall $1x10^{-5}$ – $1x10^{-2}$ M concentration range, while the H_3Citr-Ag hydrosols do not show such a kind of symmetric SPE bands. As for the course of a step-by-step LA/NF in Na_3Citr solutions, the λ_{max} position lies around 393 nm which is blue-shifted with respect to the λ_{max} value of the w-Ag hydrosol. Moreover, the FWHM of SPE bands in all Na_3Citr-Ag hydrosols is of a smaller value in comparison to the w-Ag hydrosol and this behaviour is maintained in each LA/NF step. In addition to that, the FWHM value slightly decreases with the Na_3Citr concentration increase and with the ablation time so that the final value is around 60 nm. Simultaneously, the A_{max} values in Na_3Citr- hydrosols increase during the LA/NF and also with the Na_3Citr concentration increase.

On the contrary, in H_3Citr-Ag hydrosols, the λ_{max} position significantly changes especially in higher H_3Citr concentration values so that the λ_{max} values are similar to those obtained for a w-Ag hydrosol. The FWHM values of H_3Citr-Ag hydrosols start at smaller values than in a w-Ag hydrosol (however, still at higher values than in Na_3Citr-Ag hydrosols) and they increase during LA/NF. The only exception is the $H_3Citr(10^{-2}M)$-Ag hydrosol where the FWHM value begins at the same value as in a w-Ag hydrosol and it further increases to 160 nm.

Table XXV: Parameters of SPE bands of Ag hydrosols prepared by step-wise LA/NF in water and in citrate solutions

LA/NF performed in	for [min]	λ_{max} [nm]	A_{max} [a.u.]	FWHM [nm]	A_{250} [a.u.]
water	5	398	0.270	113	0.130
	5+5	398	0.358	110	0.216
	5+5+10	**405**	**0.493**	**110**	**0.254**
$1x10^{-5}$ M Na_3Citr	5	392	0.308	70	0.124
	5+5	394	0.503	70	0.188
	5+5+10	**392**	**0.678**	**65**	**0.296**
$1x10^{-4}$ M Na_3Citr	5	392	0.376	65	0.132
	5+5	392	0.573	65	0.192
	5+5+10	**393**	**0.846**	**63**	**0.324**
$1x10^{-3}$ M Na_3Citr	5	393	0.484	65	0.173
	5+5	393	0.623	60	0.215
	5+5+10	**393**	**1.148**	**60**	**0.373**
$1x10^{-2}$ M Na_3Citr	5	392	0.512	65	0.182
	5+5	392	0.755	60	0.238
	5+5+10	**392**	**1.226**	**60**	**0.381**
$1x10^{-5}$ M H_3Citr	5	395	0.276	80	0.112
	5+5	395	0.504	87	0.257
	5+5+10	**393**	**0.937**	**93**	**0.455**
$1x10^{-4}$ M H_3Citr	5	397	0.348	80	0.229
	5+5	397	0.469	87	0.379
	5+5+10	**398**	**0.870**	**93**	**0.432**
$1x10^{-3}$ M H_3Citr	5	399	0.372	77	0.258
	5+5	404	0.436	90	0.299
	5+5+10	**407**	**0.798**	**100**	**0.354**
$1x10^{-2}$ M H_3Citr	5	397	0.398	113	0.230
	5+5	399	0.418	133	0.255
	5+5+10	**403**	**0.396**	**160**	**0.304**

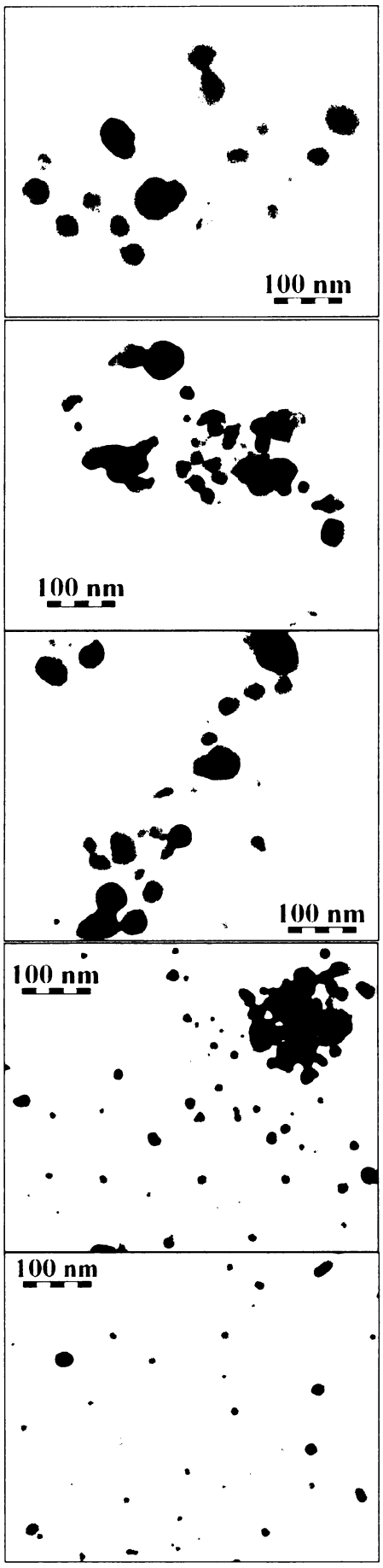

Fig. 50: The TEM images of w-Ag hydrosol (A) and Na_3Citr-Ag hydrosols with Na_3Citr concentrations : (B) $1x10^{-5}$ M, (C) $1x10^{-4}$ M, (D) $1x10^{-3}$ M, and (E) $1x10^{-2}$ M.

Concerning the A_{max} values, they increase in the course of LA/NF, however, they decrease with the H_3Citr concentration increase. In the $H_3Citr(1x10^{-2}$ M)-Ag hydrosol, the final A_{max} value even decreases below the one observed for the w-Ag hydrosol although it has been higher in two first LA/NF steps in H_3Citr-Ag hydrosol than in the w-Ag hydrosol.

In Fig. 50, TEM images of a w-Ag hydrosol and Na_3Citr-Ag hydrosols with varying Na_3Citr concentrations are presented. With the increasing Na_3Citr concentration in the hydrosol, smaller NPs are more frequently encountered and, moreover, they are well separated even in the system with highest Na_3Citr concentration, as evidenced by Fig. 50E.

On the contrary, the H_3Citr concentration increase induces NPs agglomeration, their aggregation and interpenetration (Fig. 51). In Table XXVI, pH values of H_3Citr measured before

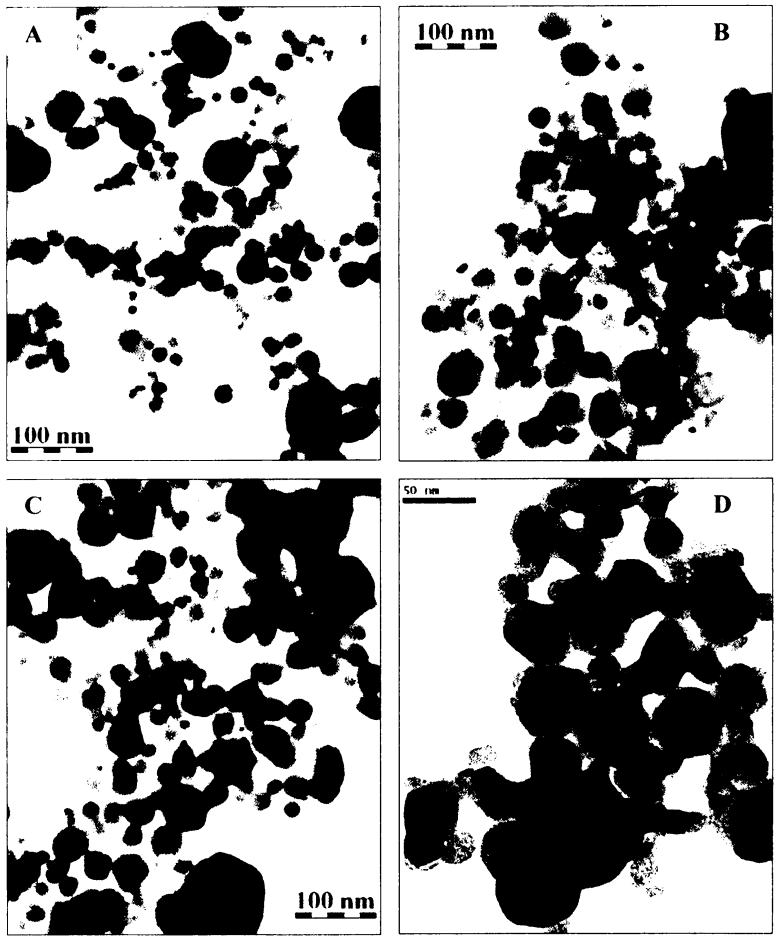

Fig. 51: TEM images of H_3Citr-Ag hydrosols with varying H_3Citr concentrations: (A) $1x10^{-5}$ M, (B) $1x10^{-4}$ M, (C) $1x10^{-3}$ M, and (D) $1x10^{-2}$ M.

Table XXVI: Measurement and calculation [159] of pH values in citric acid solutions and measurement of pH values in H_3Citr-Ag

Measured system	measured pH	Calculated pH
$1x10^{-5}$ M H_3Citr	5,19	5,21
$H_3Citr(1x10^{-5}$ M)-Ag hydrosol	5,61	
$1x10^{-4}$ M H_3Citr	4,02	4,08
$H_3Citr(1x10^{-4}$ M)-Ag hydrosol	4,09	
$1x10^{-3}$ M H_3Citr	3,09	3,25
$H_3Citr(1x10^{-3}$ M)-Ag hydrosol	3,33	
$1x10^{-2}$ M H_3Citr	2,70	2,62
$H_3Citr(1x10^{-2}$ M)-Ag hydrosol	2,74	

LA/NF and those of H_3Citr-hydrosols (i.e. pH measured after LA/NF) are compared with calculated ones. The pH values calculation is described in more details in [160]. Briefly, a numerical calculation of the equation of 5th order for $[H_3O^+]$ has been done by using MatLab program and by considering the three pK_a values of the citric acid published in literature [161, 162].

In summation, LA/NF performed in Na_3Citr solutions produces small and well stabilized Ag NPs for all concentrations of Na_3Citr solutions in the $1x10^{-5}$ – $1x10^{-2}$ M range. In contrast to that, by LA/NF performed in H_3Citr solutions, Ag hydrosols containing compact aggregates of interpenetrating Ag NPs are prepared. The effect of low pH of the ablation medium is thus similar for LA/NF performed in citrate and in chloride solutions.

4.4.2. PSDs in Ag NP hydrosols obtained at individual steps of LA/NF performed in Na_3Citr solutions

This section is focused on the detailed study of NPs sizes formed in each step of the LA/NF performed in the presence of the $1x10^{-5}$ M Na_3Citr solution and the results will be compared with those obtained for LA/NF performed in the presence of $1x10^{-3}$ M Na_3Citr. After each step of a LA/NF in one of the Na_3Citr solutions, a 2D-interfacial film was formed from the Ag NPs present in the hydrosol, transferred onto the C-coated Cu grid and imaged by TEM. TEM images of selected films are shown in Fig. 52 (for $Na_3Citr(1x10^{-5}$ M)-Ag hydrosol) and in Fig. 53 (for $Na_3Citr(1x10^{-3}$ M)-Ag hydrosol). On the basis of these TEM images, PSDs in Ag hydrosols obtained in each step of LA/NF performed in these two selected Na_3Citr solutions were determined. The results are presented in Table XXVII and Table XXVIII, the corresponding histograms are shown in Fig. 54 and Fig. 55, respectively.

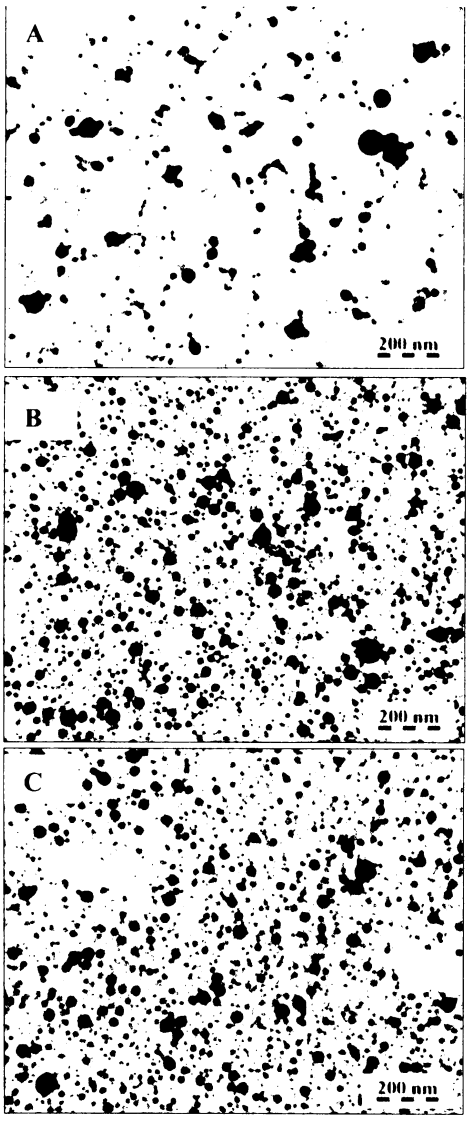

Fig. 52: The TEM images of the reassembled interfacial 2D-films prepared from samples after each step of LA/NF process in the presence of $1x10^{-5}$ M Na_3Citr: (A) 5 min, (B) 5+5 min, and (C) 5+5+10 min.

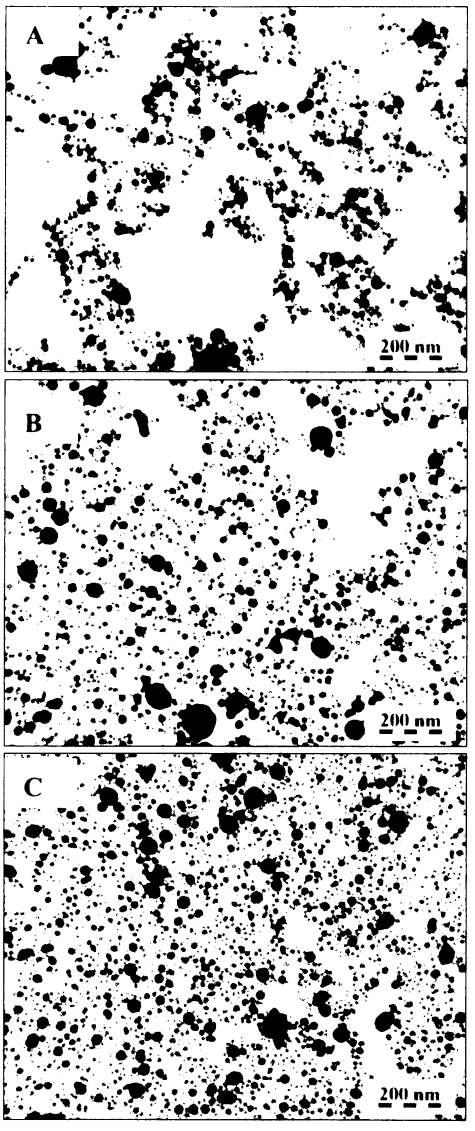

Fig. 53: The TEM images of the reassembled interfacial 2D-films prepared from samples after each step of LA/NF process in the presence of $1x10^{-3}$ M Na_3Citr: (A) 5 min, (B) 5+5 min, and (C) 5+5+10 min.

Table XXVII: Relative abundances of Ag NPs in $Na_3Citr(1x10^{-5}$ M)-Ag hydrosol prepared by the step-wise

NP size [nm]	LA/NF performed for		
	5 min	5+5 min	5+5+10 min
5	8,8	38,8	35,9
10	29,8	39,0	30,7
15	28,2	14,1	20,5
20	10,1	5,0	5,7
25	8,0	2,3	3,4
30	5,5	0,6	2,0
35	4,6	0,0	1,1
40	2,5	0,2	0,5
45	0,8	0,0	0,0
50	0,4	0,0	0,2
>55	1,3	0,0	0,0

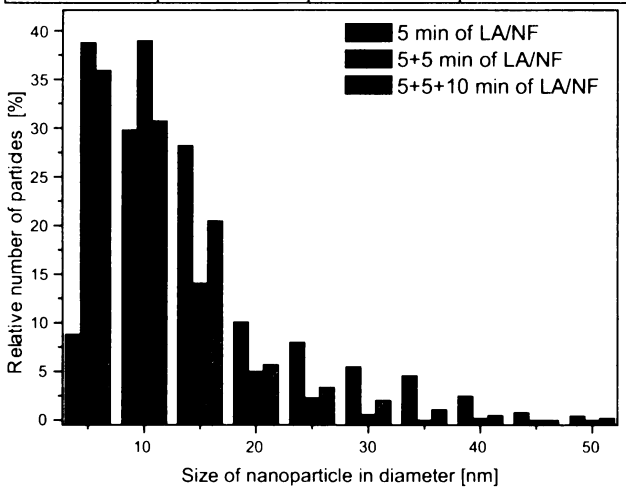

Fig. 54: PSD determined from TEM images of interfacial films prepared in each step of the step-wise LA/NF performed in $1x10^{-5}$ M Na_3Citr.

Table XXVIII: Relative abundances of Ag NPs in $Na_3Citr(1x10^{-3}$ M)-Ag hydrosol prepared by the step-wise

NP size [nm]	LA/NF performed for		
	5 min	5+5 min	5+5+10 min
5	20,8	20,5	20,0
10	35,0	41,3	45,1
15	27,3	21,2	22,7
20	7,1	7,5	5,4
25	5,5	5,4	3,3
30	1,8	2,1	1,6
35	1,2	0,8	1,0
40	0,6	0,3	0,5
45	0,4	0,3	0,5
50	0,2	0,3	0,2
>55	0,0	0,3	0,0

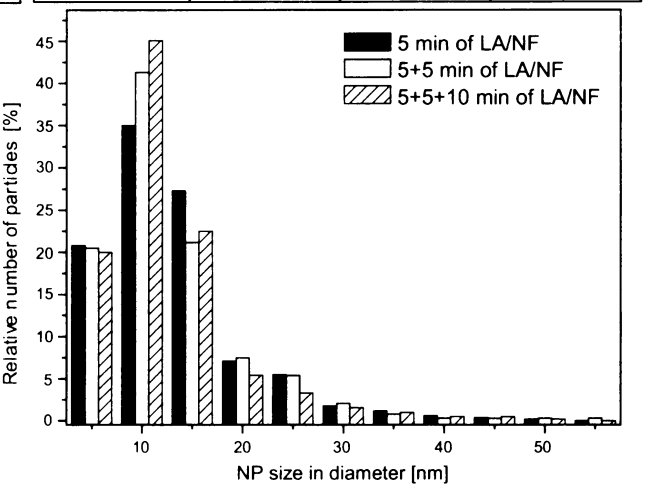

Fig. 55: PSD determined from TEM images of interfacial films prepared in each step of the step-wise LA/NF performed in $1x10^{-3}$ M Na_3Citr.

While in $Na_3Citr(1x10^{-3}$ M)-Ag hydrosol, more than 80% of NPs are smaller than 20 nm already in the first step (after 5 min of LA/NF) and this percentage of smaller NPs content increases very slightly in two next steps; in $Na_3Citr(1x10^{-5}$ M)-Ag hydrosol, the 5 min LA/NF process produces only about 69 % of NPs smaller than 20 nm. This small NPs content increases during two next steps and, at the end, it reaches approximately the same value of smaller NPs content as in the case of $Na_3Citr(1x10^{-3}$ M)-Ag hydrosol. Thus, the first step of LA/NF process is the most citrate concentration-dependent step of LA/NF.

4.4.3. Aging of citrate-Ag hydrosols followed by SPE measurements and TEM imaging

The aging of citrate-Ag hydrosols (and of a w-Ag hydrosol as a reference sample) was investigated for one up to three weeks by using SPE measurements and the resulting SPE spectral characteristics are listed in Table XXIX. Firstly, after the one week aging: a w-Ag hydrosol tends to precipitate because its SPE band is broadened and the A_{max} and A_{250} values decrease. On the contrary, Na_3Citr-Ag hydrosols do not precipitate after one week of aging because their SPE bands do not lose their symmetry, the λ_{max} positions and FWHM remain nearly of the same values, while the A_{max} values even increase! Does this increase indicate the increase of small NPs content of the hydrosol? To answer this question, PSDs were determined for $Na_3Citr(1x10^{-5}M)$-Ag hydrosol and $Na_3Citr(1x10^{-3}M)$-Ag hydrosol from the 2D-interfacial films prepared immediately after LA/NF and prepared after one-week of aging from the same hydrosols samples. As shown in Table XXX and Table XXXI and Fig. 56, PSDs markedly changes during the one-week of aging. In both selected Na_3Citr-Ag hydrosols, 10 nm NPs dominate after one week of aging. Exactly these NP sizes can contribute noticeably to the SPE at ca 394 nm and thus induce the observed A_{max} values increase. From the just presented observation, one can conclude that the Na_3Citr concentration influences hydrosols properties not only during LA/NF process, but also during the hydrosols aging, possibly due to the adsorption-desorption processes undergone by Na_3Citr molecules. In Fig. 57, there are shown the TEM images of interfacial films prepared from w-Ag hydrosol and Na_3Citr-Ag hydrosols after one week of aging. The PSD for all these hydrosols are depicted in Fig. 57F. The exact values of relative numbers of particles are listed in Table XXXII. Obviously, in comparison to the w-Ag hydrosol, Na_3Citr presence in the Na_3Citr-Ag hydrosols strongly promotes formation and stabilization of small NPs: almost ~90% of NPs are of the sizes from 5-15 nm in Na_3Citr-Ag hydrosols, while only ~60% of NPs are of these sizes in the w-Ag hydrosol.

Table XXIX: Parameters of SPE bands of Ag hydrosols prepared by step-wise LA/NF in water and in citrate solutions - aging

LA/NF performed in	System after x days	λ_{max} [nm]	A_{max} [a.u.]	FWHM [nm]	A_{250} [a.u.]
water	0	405	0.493	110	0.254
	7	405	0.239	185	0.126
	21	408	0.209	100	0.080
$1x10^{-5}$ M Na_3Citr	0	392	0.678	65	0.296
	6	394	0.687	60	0.208
	28	399	0.680	63	0.183
$1x10^{-4}$ M Na_3Citr	0	393	0.846	63	0.324
	6	394	0.932	67	0.270
	28	400	0.830	71	0.195
$1x10^{-3}$ M Na_3Citr	0	393	1.148	60	0.373
	7	395	1.182	63	0.322
	28	404	0.585	68	0.301
$1x10^{-2}$ M Na_3Citr	0	392	1.226	60	0.381
	6	395	1.355	60	0.361
	16	397	1.555	58	0.354
$1x10^{-5}$M H_3Citr	0	393	0.937	93	0.455
	7	401	0.744	113	0.326
	13	403	0.620	140	0.292
$1x10^{-4}$M H_3Citr	0	398	0.870	93	0.432
	7	413	0.547	113	0.424
	13	415	0.457	120	0.217
$1x10^{-3}$M H_3Citr	0	407	0.798	100	0.354
	6	414	0.514	123	0.313
	12	417	0.446	133	0.209
$1x10^{-2}$M H_3Citr	0	403	0.396	160	0.304
	6	-	-	-	0.395
	12	-	-	-	0.439

Table XXX: Relative abundances of Ag NPs sizes in $Na_3Citr(1x10^{-5}M)$-Ag hydrosol – influence of aging

NP size [nm]	$Na_3Citr(1x10^{-5}$ M)-Ag hydrosol measured immediately	after 7 days
5	35,9	28,9
10	30,7	42,1
15	20,5	17,3
20	5,7	6,0
25	3,4	2,7
30	2,0	2,1
35	1,1	0,4
40	0,5	0,2
45	0,0	0,0
50	0,2	0,2
>55	0,0	0,0

Table XXXI: Relative abundances of Ag NPs sizes in $Na_3Citr(1x10^{-3}M)$-Ag hydrosol – influence of aging

NP size [nm]	$Na_3Citr(1x10^{-3}$ M)-Ag hydrosol measured immediately	after 7 days
5	20,0	33,9
10	45,1	52,9
15	22,7	8,4
20	5,4	2,5
25	3,3	1,3
30	1,6	0,4
35	1,0	0,2
40	0,5	0,2
45	0,5	0,2
50	0,2	0,0
>55	0,0	0,0

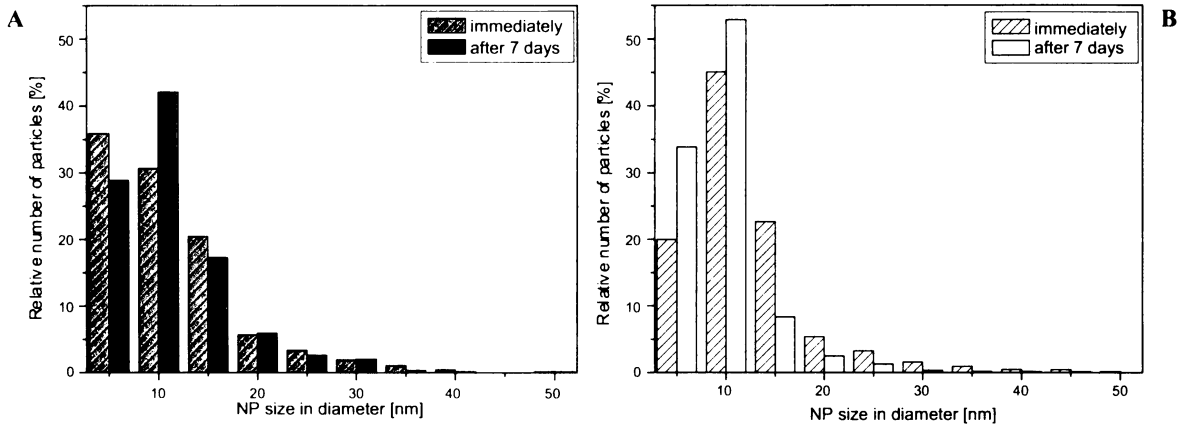

Fig. 56: The PSDs of (A) $Na_3Citr(1x10^{-5}M)$-Ag hydrosol and (B) $Na_3Citr(1x10^{-3}$ M)-Ag hydrosol determined from TEM images of interfacial films formed immediately and 7 days after LA/NF process.

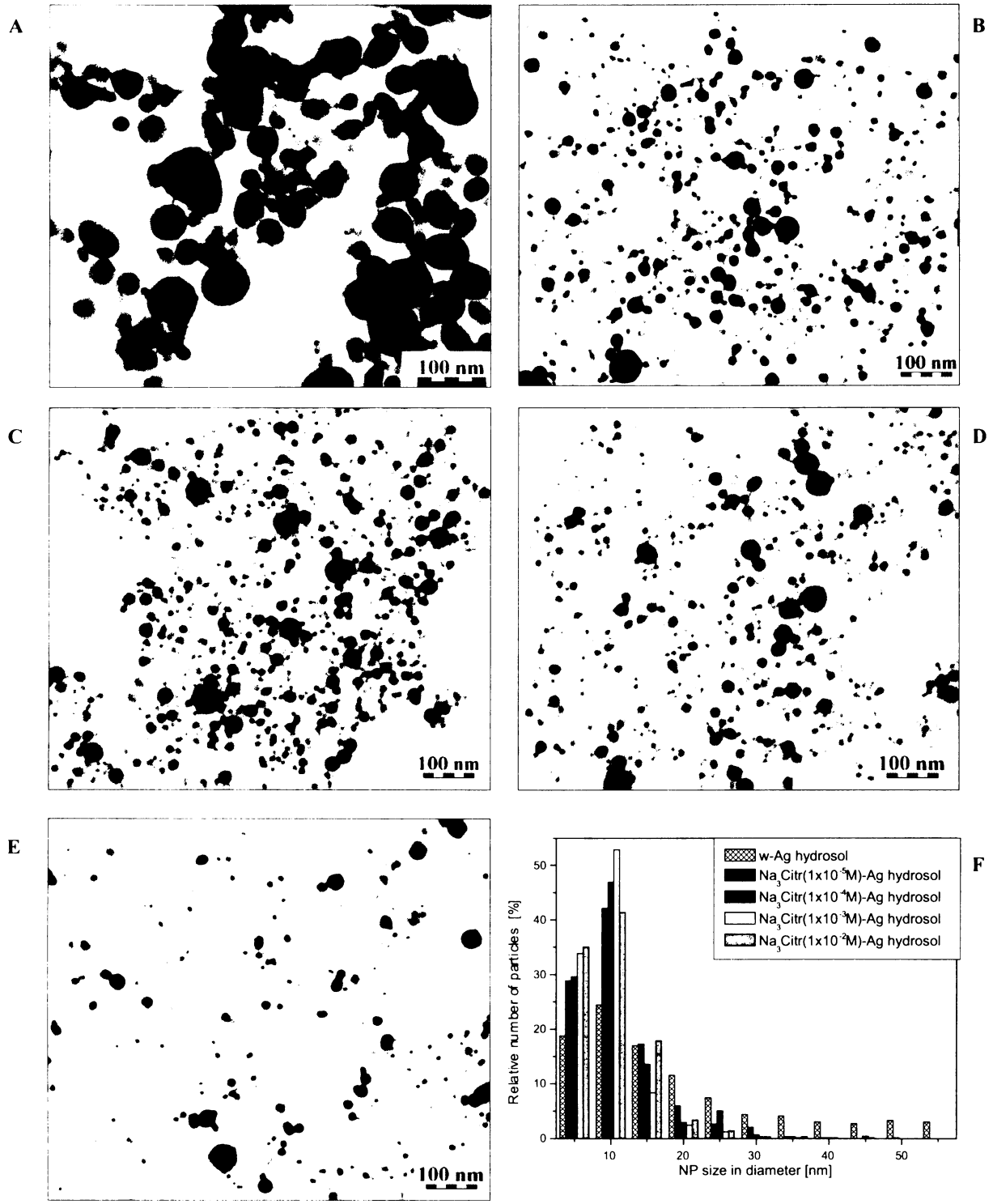

Fig. 57: The TEM images of reassembled interfacial films formed from following systems after 7 days of their preparation: (A) w-Ag hydrosol, (B) $Na_3Citr(1x10^{-5}M)$-Ag hydrosol, (C) $Na_3Citr(1x10^{-4}M)$-Ag hydrosol, (D) $Na_3Citr(1x10^{-3}M)$-Ag hydrosol, (E) $Na_3Citr(1x10^{-2}M)$-Ag hydrosol, and (F) their PSDs.

The SPE spectra of Na_3Citr-Ag hydrosols containing $1x10^{-5}M$, $1x10^{-4}M$ and $1x10^{-3}M$ Na_3Citr were therefore measured again after 3 weeks. The SPE characteristics obtained from them are listed in Table XXIX. The observed changes in the SPE parameters indicate a possible start of precipitation of Na_3Citr-Ag hydrosols with higher Na_3Citr concentrations, while the Na_3Citr-Ag hydrosols containing lower Na_3Citr concentrations show only minor changes in their SPE characteristics after the three weeks of aging.

Concerning H_3Citr-Ag hydrosols aging, the second part of Table XXIX shows SPE characteristics of H_3Citr-Ag hydrosols obtained by SPE measurements one and two weeks after Ag hydrosols preparation. The $H_3Citr(1x10^{-2}M)$-Ag hydrosol precipitates very quickly after its preparation and, thus, no SPE band was observed after one week. Aging of the other H_3Citr-Ag hydrosols induces the following changes in their SPE spectra: the λ_{max} position red-shift, the FWHM value increase and the A_{max}, A_{250} values decrease. However, these changes are not so

Table XXXII: Relative abundances of Ag NPs in Na_3Citr-Ag hydrosols

NP size [nm]	LA/NF performed in the presence of				
	water	$1x10^{-5}$ M Na_3Citr	$1x10^{-4}$ M Na_3Citr	$1x10^{-3}$ M Na_3Citr	$1x10^{-2}$ M Na_3Citr
5	18,8	28,9	29,6	33,9	35,1
10	24,4	42,1	46,9	52,9	41,4
15	17,0	17,3	13,6	8,4	17,9
20	11,6	6,0	3,0	2,5	3,4
25	7,5	2,7	5,1	1,3	1,5
30	4,4	2,1	0,7	0,4	0,4
35	4,1	0,4	0,4	0,2	0,4
40	3,1	0,2	0,2	0,2	0,0
45	2,8	0,0	0,5	0,2	0,0
50	3,3	0,2	0,0	0,0	0,0
>55	3,1	0,0	0,0	0,0	0,0

Table XXXIII: Relative abundances of Ag NPs in Ag hydrosols prepared by the step-wise LA/NF in water and in $1x10^{-5}$ M citrate solutions

NP size [nm]	w-Ag hydrosol	$Na_3Citr(1x10^{-5}M)$-Ag hydrosol	$H_3Citr(1x10^{-5}M)$-Ag hydrosol
5	18,8	28,9	25,5
10	24,4	42,1	27,1
15	17,0	17,3	13,8
20	11,6	6,0	16,3
25	7,5	2,7	5,3
30	4,4	2,1	4,4
35	4,1	0,4	0,7
40	3,1	0,2	0,7
45	2,8	0,0	0,9
50	3,3	0,2	0,9
>55	3,1	0,0	4,4

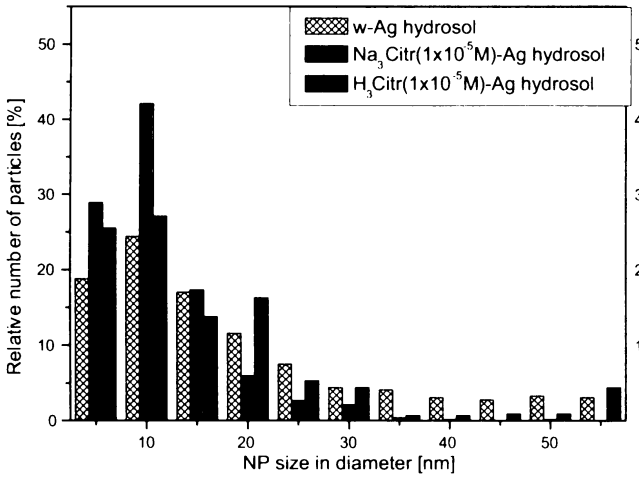

Fig. 58: PSD determined of interfacial films formed from w-Ag hydrosol, $Na_3Citr(1x10^{-5}M)$-Ag hydrosol, and $H_3Citr(1x10^{-5}M)$-Ag hydrosol, 7 days after their preparation by LA/NF process.

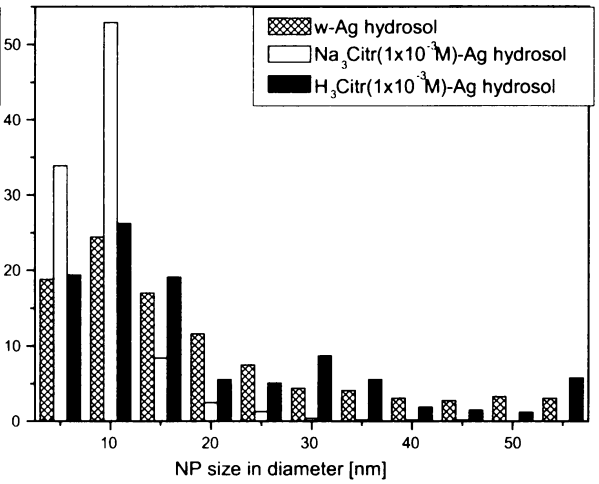

Fig. 59: PSD determined of interfacial films formed from w-Ag hydrosol, $Na_3Citr(1x10^{-3}M)$-Ag hydrosol and $H_3Citr(1x10^{-3}M)$-Ag hydrosol, 7 days after their preparation by LA/NF process.

Table XXXIV: Relative abundances of Ag NPs in Ag hydrosols prepared by the step-wise LA/NF in water and in $1x10^{-3}$ M citrate solutions

NP size [nm]	w-Ag hydrosol	$Na_3Citr(1x10^{-3}M)$-Ag hydrosol	$H_3Citr(1x10^{-3}M)$-Ag hydrosol
5	18,8	33,9	19,4
10	24,4	52,9	26,2
15	17,0	8,4	19,1
20	11,6	2,5	5,6
25	7,5	1,3	5,1
30	4,4	0,4	8,7
35	4,1	0,2	5,6
40	3,1	0,2	1,9
45	2,8	0,2	1,5
50	3,3	0,0	1,2
>55	3,1	0,0	5,8

pronounced as in the w-Ag hydrosol. Furthermore, the changes of SPE characteristics after two weeks of aging are smaller than expected (with respect to the changes observed after 1 week of aging).

For the sake of comparison, the PSDs were determined for $H_3Citr(1x10^{-5}M)$- and $H_3Citr(1x10^{-3}M)$-Ag hydrosols after 7 days of aging. They can thus be compared with those of the w-Ag hydrosol and with the Na_3Citr-Ag hydrosol of the same citrate content and after the same time of aging. For the $1x10^{-5}$ M concentration values, this comparison is depicted in Fig. 58 and the relative numbers of particles are listed in Table XXXIII. The histogram in Fig. 58 shows that larger NPs are formed in H_3Citr than in Na_3Citr presence. For the $1x10^{-3}$ M concentrations, this difference is even more obvious, Fig. 59 and Table XXXIV. Nevertheless, it has to be taken into account that in $H_3Citr(1x10^{-3}M)$-Ag hydrosols the interpenetrated NPs and larger agglomerates of NPs have been already present after the LA/NF process.

4.4.4. SERS probing of citrate-Ag hydrosols by bpy

The SERS activity of citrate-Ag hydrosols has been tested by bpy. Systems with the final bpy concentration of $1x10^{-5}$ M value were prepared. The SERS spectra of the systems with Na_3Citr-Ag hydrosols and bpy (Na_3Citr-Ag hydrosols/bpy) are shown in Fig. 60; those of the H_3Citr-Ag hydrosols/bpy are depicted in Fig. 61.

Interestingly, a SERS signal of bpy was obtained only for the $Na_3Citr(1x10^{-5}M)$-Ag hydrosol/bpy, $H_3Citr(1x10^{-5}M)$-Ag hydrosol/bpy and $H_3Citr(1x10^{-4}M)$-Ag hydrosol/bpy systems, i.e. for systems with low citrate concentrations (Fig. 60A, Fig. 61A, Fig. 61B, respectively). For systems with higher citrate concentrations, the SERS signal of citrate molecules dominates the SERS spectra. Nevertheless, these SERS spectra have their important meaning, since they provide us with a proof that Ag NP surfaces in these Ag hydrosols are functionalised by adsorbed citrate ions. As a result of instability of that $H_3Citr(1x10^{-2}M)$-Ag hydrosol, the only observable SERS signal from the $H_3Citr(1x10^{-2}M)$-hydrosol/bpy system was that of water (Fig. 61D).

SERS spectra of $Na_3Citr(1x10^{-5}M)$-Ag hydrosol/bpy, $H_3Citr(1x10^{-5}M)$-Ag hydrosol/bpy and $H_3Citr(1x10^{-4}M)$-Ag hydrosol/bpy systems (Fig. 60 and Fig. 61) are dominated by the SERS spectral bands of Ag^+-bpy. Nevertheless, weak spectral features of Ag(0)-bpy are observable in SERS of $H_3Citr(1x10^{-4}M)$-Ag hydrosol/bpy system as well as in SERS of $H_3Citr(1x10^{-5}M)$-Ag hydrosol/bpy system in which the spectral bands H_3Citr dominate.

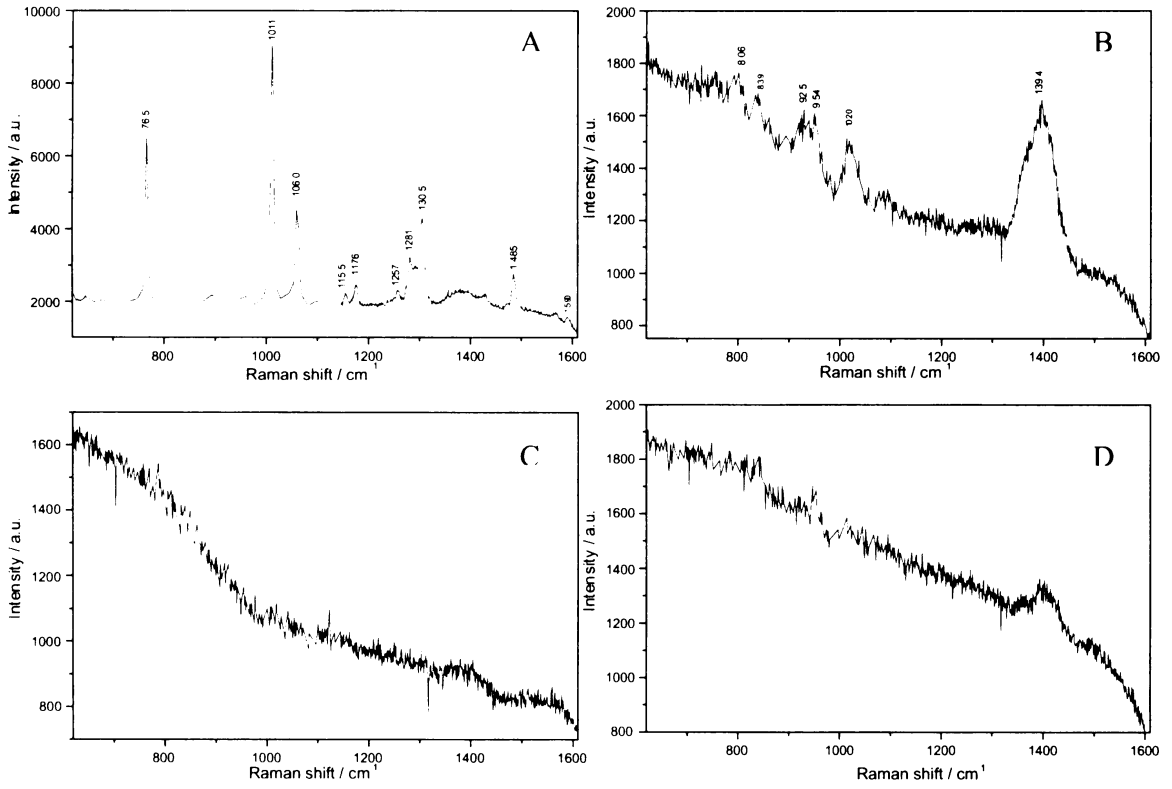

Fig. 60: SERS spectra of the Na_3Citr-Ag hydrosol/bpy($1x10^{-5}$ M) systems with Na_3Citr concentration: (A) $1x10^{-5}$ M, (B) $1x10^{-4}$ M, (C) $1x10^{-3}$ M, and (D) $1x10^{-2}$ M.

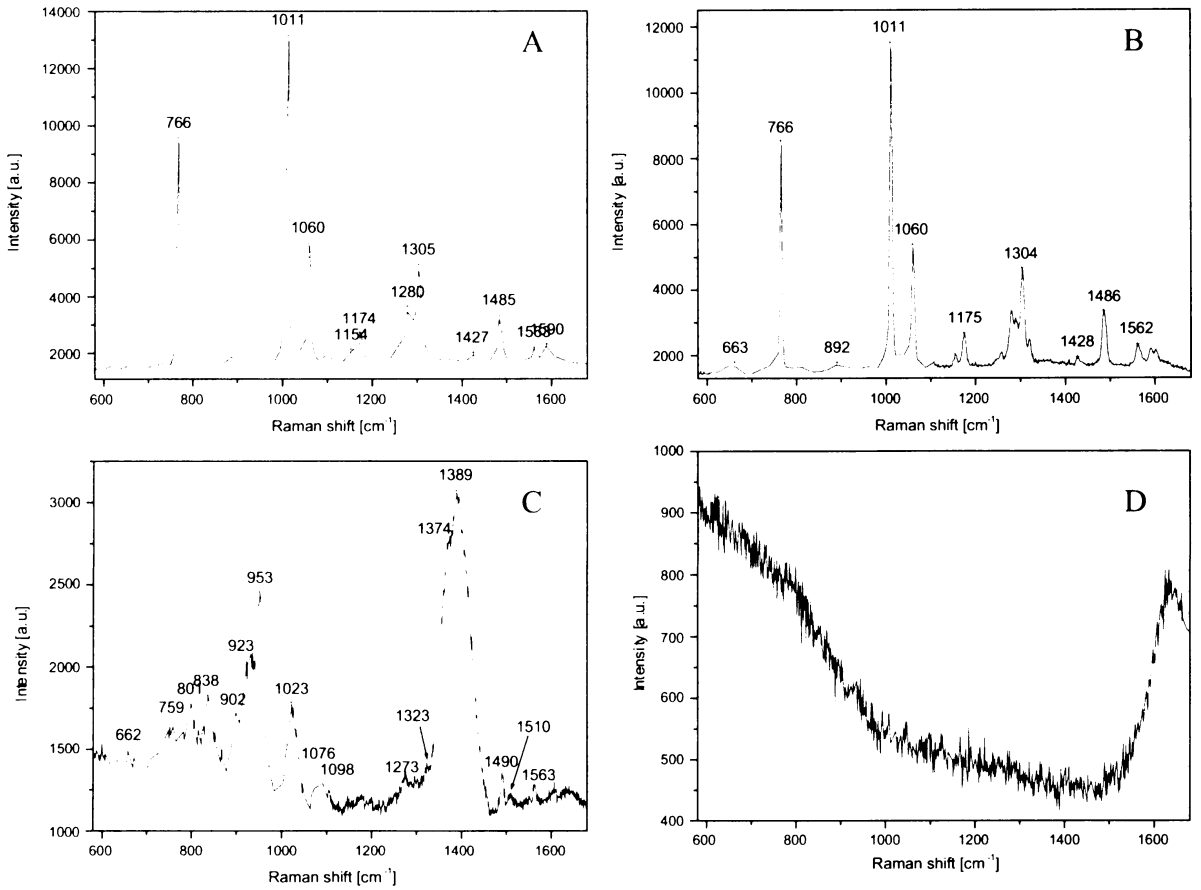

Fig. 61: SERS spectra of the H_3Citr-Ag hydrosol/bpy($1x10^{-5}$ M) systems with H_3Citr concentrations : (A) $1x10^{-5}$ M, (B) $1x10^{-4}$ M, (C) $1x10^{-3}$ M, and (D) $1x10^{-2}$ M.

4.4.5. Determination of Ag content of citrate-Ag hydrosols by AAS

The total amount of ablated Ag can be reliably determined by the atomic absorption spectroscopy (AAS), i.e. the determination of the total amount of Ag present in the aqueous ablation medium after LA/NF. On the other hand, the possibilities to extract such information from SPE spectra are limited. Most importantly, SPE spectra reflect quantitatively only that amount of Ag which is present in the form of the Ag NPs. The amount of Ag possibly present in the form of Ag^+ salts or complexes would thus remain undetected by SPE spectra.

For LA/NF performed in pure water, a very good correlation between total amount of ablated Ag determined by AAS and integral intensity of the SPE band (I_{SPE}) has been obtained [32] which indicates that ablated Ag was present in the form of the Ag NPs. However, in the case of LA/NF in citrate solutions, a possibility of Ag^+ complexes or salts formation cannot be a priori neglected.

The results of experimentally determined total ablated Ag content by AAS and the selected parameters determined from SPE spectra of the w-Ag hydrosol, Na_3Citr-Ag hydrosol, and H_3Citr-Ag hydrosol are compared in Figs 62 and 63, the SPE spectra are also presented. All these hydrosols have been prepared at the same conditions (5+5+10 min of LA/NF at 1064 nm with the ~300 mJ/pulse energy value). The concentrations of citrate ions varied in the $1x10^{-5}$ M - $1x10^{-2}$ M range both in neutral and acidic solutions.

With respect to the fact that the A_{max} values can be considered to reflect the amount of small non-interacting NPs provided that there is only one SPE band with λ_{max} in the range 390-396 nm [Chapter 1], it is quite understandable that this characteristics correlates with the total amount of Ag for the case of Na_3Citr-Ag hydrosols - Fig. 62A and Fig. 62C, while the correlation fails for the case of H_3Citr-Ag hydrosols (almost all their λ_{max} are not in the range 390-396 nm) - Fig. 63A and Fig. 63C.

The A_{250} values which according to [36] are related to the intensity of interband transition of Ag slightly increase in Na_3Citr-Ag hydrosols and thus, except the Na_3Citr($1x10^{-3}$ M)-Ag hydrosol, they can be roughly compared with the experimentally determined Ag content (Fig. 62A and Fig. 62C). Nevertheless, in the case of H_3Citr-Ag hydrosols, Fig 63A and Fig. 63C, A_{250} values and the experimentally determined Ag content do not correspond at all.

The I_{SPE} values (the integrated areas in the region 300-800 nm in this Thesis) correlate very well with Ag content values determined by AAS for all probed hydrosols, with the only exception of the H_3Citr($1x10^{-3}$ M)-Ag hydrosol – Fig. 62D compared with Fig. 62A, and Fig. 63D compared with Fig. 63A. This very good correlation can

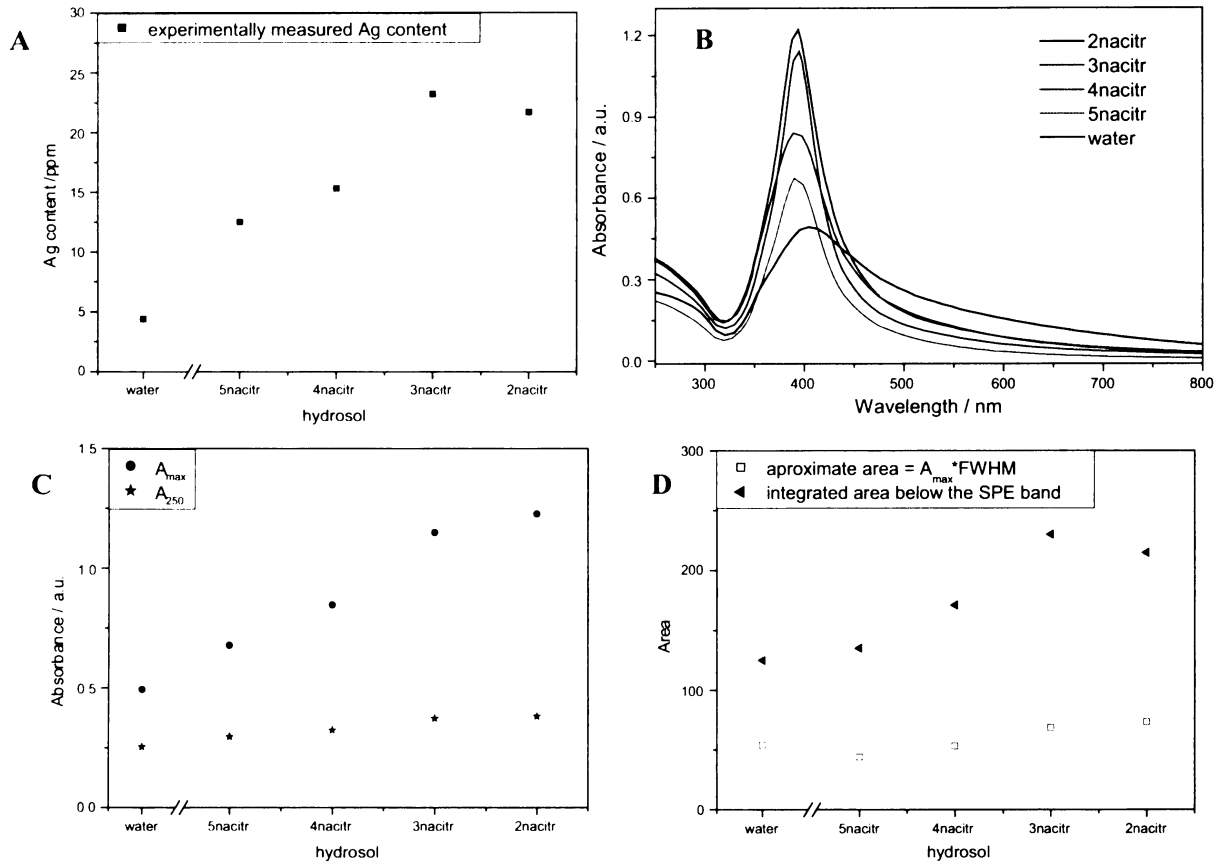

Legend : water = w-Ag hydrosol; 5nacitr = $Na_3Citr(1x10^{-5}$ M)-Ag hydrosol; 4nacitr = $Na_3Citr(1x10^{-4}$ M)-Ag hydrosol; 3nacitr = $Na_3Citr(1x10^{-3}$ M)-Ag hydrosol; 2nacitr = $Na_3Citr(1x10^{-2}$ M)-Ag hydrosol.

Fig. 62: Comparison of (A) AAS results, (B) SPE bands, and (C , D) characteristic parameters of the SPE bands of a w-Ag hydrosol and Na_3Citr-Ag hydrosols.

be explained on the basis of the fact that the studied Na_3Citr-Ag hydrosols posses a symmetric SPE band in the integrated region. Nevertheless, a reasonably good correlation (with exception of one point) has been obtained also for H_3Citr-Ag hydrosols. A similar very good correlation between I_{SPE} band values and total amount of ablated Ag determined by AAS has been reported in [32], however, the comparative study was performed only for Ag hydrosols prepared by LA/NF in pure water. In our case of LA/NF performed in citrate solutions, the existence of this correlation has an additional meaning: Should a severe discrepancy in this correlation occur, it could indicate either a severe error in preparation of samples for AAS, or a pronounced effect of Ag^+ complexes or citrate salts formation. Apparently, more of these problems occurs in this study.

The approximated areas (a FWHM value multiplied by an appropriate A_{max} value) have the same trend as the integrated areas in the case of Na_3Citr-Ag hydrosols (Fig. 62D), and thus, they can be used only for such systems which yield a symmetric SPE band with the FWHM values of nearly the same values. On the contrary, the tendencies for the approximated and the integrated areas are slightly different in H_3Citr-Ag hydrosols (Fig. 63D). Even if the A_{max} values of H_3Citr-Ag hydrosols decrease with the H_3Citr concentration increase, the FWHM values increase (Table XXV). Therefore, the discrepancy between the approximated and the integrated areas can be discussed in terms of the opposite-going trends of the A_{max} and FWHM values (they can cancel as for example for the $H_3Citr(1x10^{-4}$ M)-Ag hydrosol).

The determination of total content of Ag by AAS revealed that the total amount of Ag ablated (i.e. transferred from the Ag target to the aqueous ablation medium) is systematically higher for LA/NF performed in citrate solutions (both neutral and acidic) than in pure water. Furthermore, the results of AAS determination of total amount of Ag correlate very well (for LA/NF in neutral citrate solutions), and reasonably well (for LA/NF in acidic citrate solutions) with the integral intensities of SPE bands (I_{SPE}) of the resulting Ag NP hydrosols. The existence of this correlation indicates that no serious errors occurred during the preparation of samples of AAS. Therefore, it can, indeed, be concluded that the presence of citrates increases the efficiency of LA process.

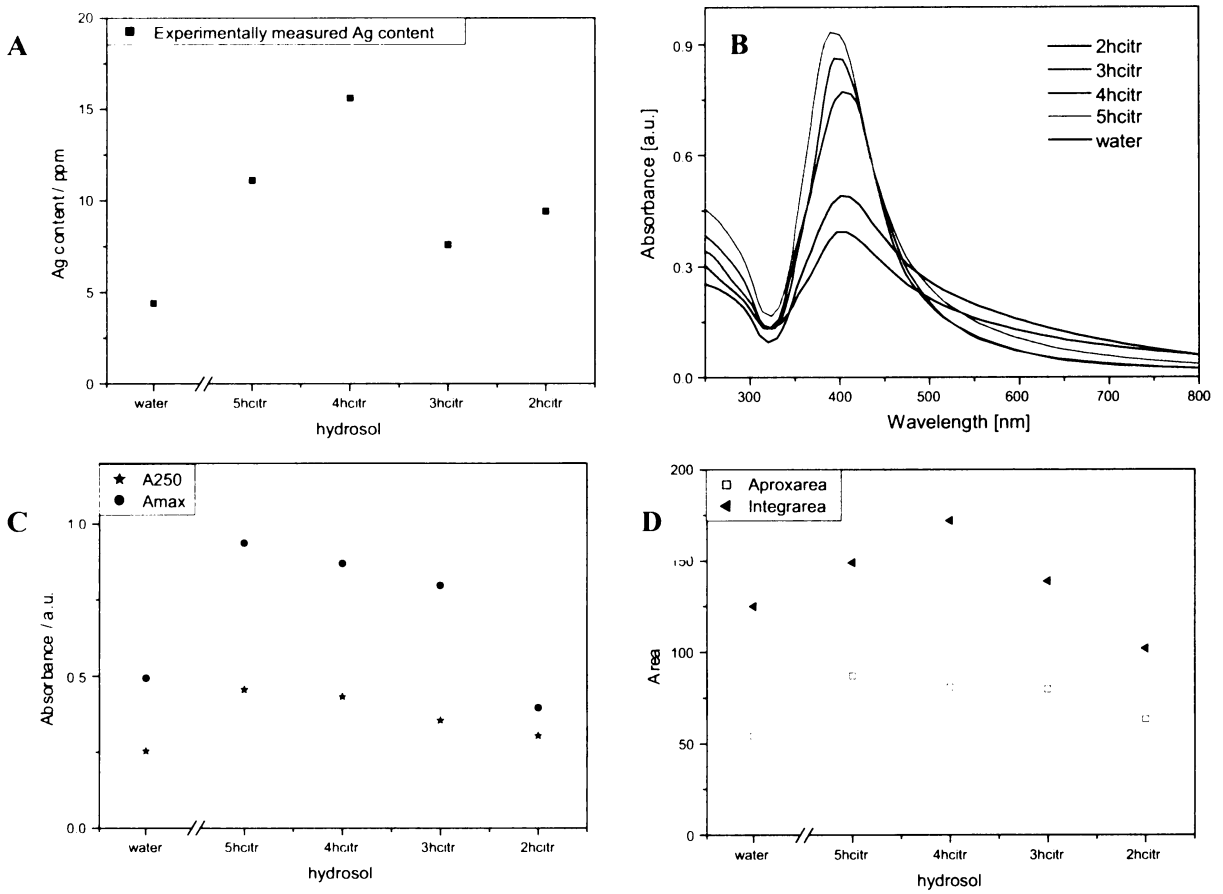

Legend: water = w-Ag hydrosol; 5hcitr = $H_3Citr(1x10^{-5}$ M)-Ag hydrosol; 4hcitr = $H_3Citr(1x10^{-4}$ M)-Ag hydrosol; 3hcitr = $H_3Citr(1x10^{-3}$ M)-Ag hydrosol; 2hcitr = $H_3Citr(1x10^{-2}$ M)-Ag hydrosol.

Fig. 63: Comparison of (A) AAS results, (B) SPE bands, and (C , D) characteristic parameters of the SPE bands of a w-Ag hydrosol and H_3Citr-Ag hydrosols.

4.5. Effects of energy per pulse changes on LA/NF in Na_3Citr solutions

LA/NF in Na_3Citr solution of concentrations in the range $1x10^{-5}$ M – $1x10^{-2}$ M and in pure water has been performed with ns laser pulses (1064 nm wavelength) of three different energies per pulse (~200, ~300, and ~400 mJ/pulse).

The SPE spectra of the resulting Ag hydrosols were measured and the resulting SPE characteristics obtained from them are listed in Table XXXV. The SPE bands of all Na_3Citr-Ag hydrosols are more symmetric, in

Table XXXV: Parameters of SPE bands of Ag hydrosols prepared by step-wise LA/NF in water and in citrate solutions performed with three different energies per pulse

LA/NF performed		at 200 mJ/pulse			at 300 mJ/pulse			at 400 mJ/pulse		
		λ_{max}	A_{max}	FWHM	λ_{max}	A_{max}	FWHM	λ_{max}	A_{max}	FWHM
in	for [min]	[nm]	[a.u.]	[nm]	[nm]	[a.u.]	[nm]	[nm]	[a.u.]	[nm]
water	5	393	0.189	113	398	0.270	113	401	0.309	130
	5+5	393	0.305	110	398	0.358	110	403	0.435	210
	5+5+10	**396**	**0.343**	**110**	**405**	**0.493**	**110**	**406**	**0.852**	**175**
$1x10^{-5}$ M Na_3Citr	5	392	0.288	70	392	0.308	70	393	0.480	89
	5+5	392	0.380	68	394	0.503	70	392	0.655	72
	5+5+10	**392**	**0.438**	**65**	**392**	**0.678**	**65**	**393**	**0.840**	**72**
$1x10^{-4}$ M Na_3Citr	5	392	0.328	70	392	0.376	65	392	0.545	72
	5+5	392	0.421	68	392	0.573	65	392	0.734	72
	5+5+10	**392**	**0.658**	**65**	**393**	**0.846**	**63**	**392**	**0.955**	**64**
$1x10^{-3}$ M Na_3Citr	5	392	0.420	63	393	0.484	65	392	0.655	72
	5+5	392	0.480	60	393	0.623	60	393	0.825	67
	5+5+10	**392**	**0.808**	**60**	**393**	**1.148**	**60**	**393**	**1.170**	**61**
$1x10^{-2}$ M Na_3Citr	5	391	0.465	58	392	0.512	65	392	0.805	64
	5+5	391	0.643	55	392	0.755	60	392	1.160	61
	5+5+10	**392**	**1.070**	**55**	**392**	**1.226**	**60**	**392**	**1.345**	**61**

comparison to that of a w-Ag hydrosol. Secondly, the λ_{max} position remains at around 392 nm for all Na_3Citr concentrations and all used energies per pulse. Thirdly, the FWHM values of the Na_3Citr-Ag hydrosol SPE bands are always markedly lower than those of a w-Ag hydrosol for all values of energies per pulse employed. Furthermore, for hydrosols with a particular Na_3Citr concentration, the FWHM values slightly increase with the energy per pulse increase (rows in Table XXXV). FWHM values for a particular value of energy per pulse decrease with the Na_3Citr concentration increase (columns in Table XXXV).

In Fig. 64, the TEM images of w-Ag hydrosol and $Na_3Citr(1x10^{-5}$ M)-Ag hydrosols prepared at ~200 and/or ~300 mJ/pulse are depicted. The TEM images show that: (i) a higher fraction of smaller NPs is encountered at lower energies per pulse for a hydrosol with the particular Na_3Citr concentrations (compare Fig. 64A with Fig. 64B, Fig. 64C with Fig. 64D); (ii) the presence of increasing Na_3Citr concentration induces the decrease of mean NP diameter at all the energies per pulse compare Fig. 64A with Fig. 64B, Fig. 64C with Fig. 64D).

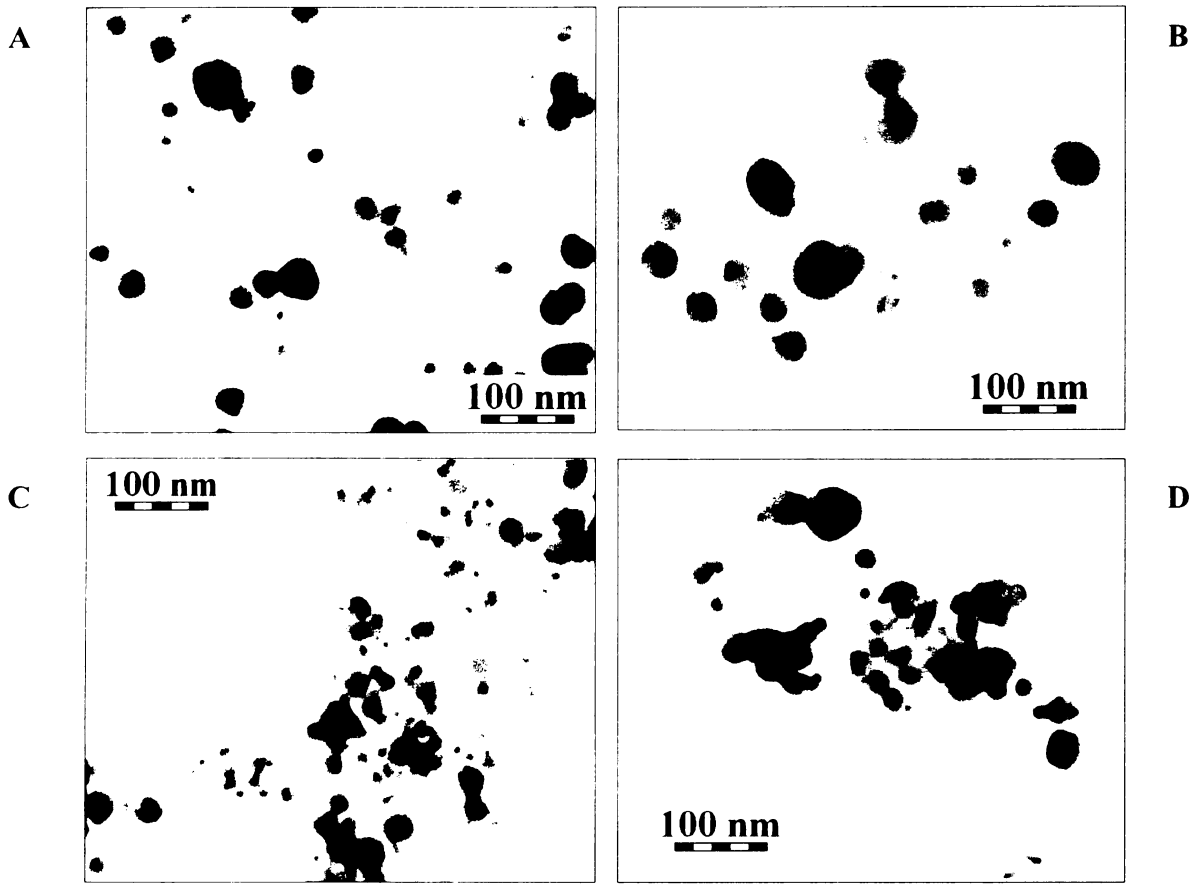

Fig. 64: TEM images of Ag hydrosols prepared at different energies per pulse and in different medium: w-Ag hydrosol at (A) 200 mJ/pulse and (B) at 300 mJ/pulse; $Na_3Citr(1x10^{-5}$ M)-Ag hydrosol (C) at 200 mJ/pulse and (D) at 300 mJ/pulse.

In summation, for LA/NF performed in citrate solutions of various concentrations (by a step-wise procedure, and the 1064 nm laser pulse wavelength), the changes of energy per pulse values, in particular their increase in the 200 mJ – 400 mJ range, have a systematic effect on SPE parameters. Obviously, the efficiency of small NPs formation and stabilization increases with the increasing Na_3Citr concentration for LA/NF performed with all the values of energies per pulse. Moreover, with the increasing energy per pulse, the efficiency of small NPs formation increases for all Na_3Citr-Ag hydrosols. A slightly lower stabilization of the NPs at the highest energy per pulse is observed only for $Na_3Citr(1x10^{-5}$ M)-Ag hydrosol (Table XXXV).

4.6. HR-TEM imaging of Ag NPs for elucidation of LA/NF and Ag NPs growth mechanisms in Na_3Citr solutions and in pure water

Considering the theories published in the literature [25-30] and the fact that our LA/NF has been carried out in aqueous solutions by ns laser pulses, two ablation reactions at the metal target-water interface are thought to be responsible of ablation process: (i) a straight jet of massive Ag clusters and droplets which come from the Ag foil and which can penetrate a cage of solvent more efficiently than light plasma gas, and (ii) a bubble which consists of atoms, molecules and ions of water and Ag. The presence of Ag clusters and droplets smaller than 5 nm in diameter, has been evidenced by HR-TEM measurements and is shown in Fig. 65.

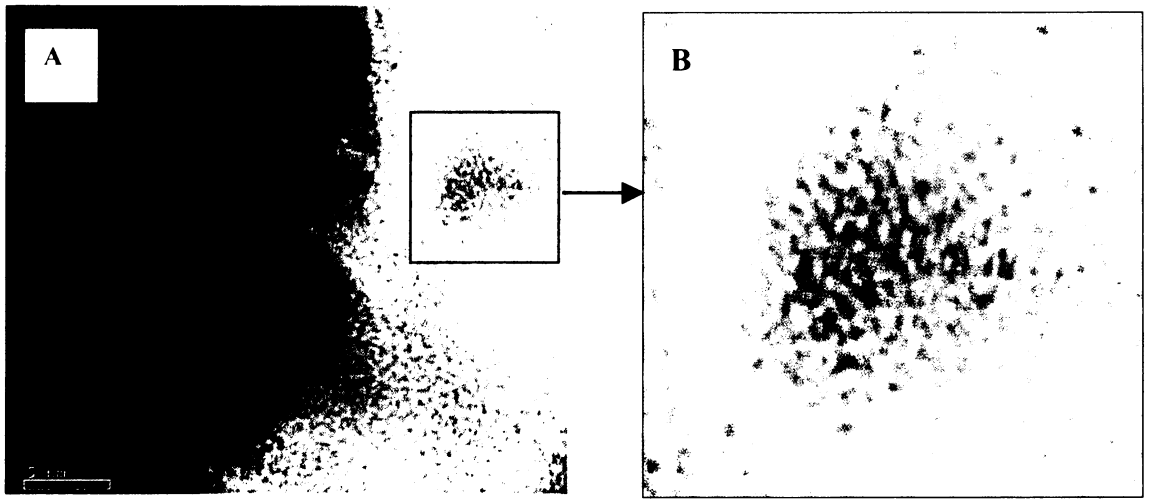

Fig. 65: HR-TEM image of a w-Ag hydrosol (A) and its detail (B) in which the organized structure of a very small Ag nanocluster (smaller than 5 nm in diameter) is shown and can be compared with the amorphous carbon (coming from the C-coated Cu grid).

The Ag clusters and droplets which have left the near vicinity of the Ag target (by the straight jet ablation reaction) can aggregate and grow into NPs. During the next evolution, they can act as the nuclei for a further slow aggregation in which the Ag atoms (stemming from the ablation bubble) add to the NPs and lead to their growth. These two types of aggregation are affected by stirring and by NF.

This theory can be supported by the morphological investigation of a w-Ag hydrosol sampling in the course of LA/NF. In Fig. 66, the TEM and HR-TEM images of a w-Ag hydrosol after 5 min (Fig. 66A), 5+5 min (Fig. 66B), and 5+5+10 min (Fig. 66C) of LA/NF are presented. While in hydrosols after 5 and 5+5 min of LA/NF the large NPs are frequently encountered in the shape of "flowers" and/or "ferns" (Fig. 66A and Fig. 66B); the final hydrosol (Fig. 66C) does not contain such a kind of NP shapes. A possible explanation is that during the last period of LA/NF which lasted 10 min without interruption, these large NPs were efficiently fragmented. A morphological feature that repeats in all steps of sampling is that the very small particles (3-5 nm in diameter) are near the large NPs, "flowers" and/or "ferns".

In electrolyte solutions, the Ag clusters and droplets leaving the vicinity of Ag target are spread through the solution and surrounded quickly by electrolyte. A competition between the aggregation and NP surface coating by the ions of electrolyte occurs and is highly influenced by the electrolyte concentration. The rapid coating of NPs

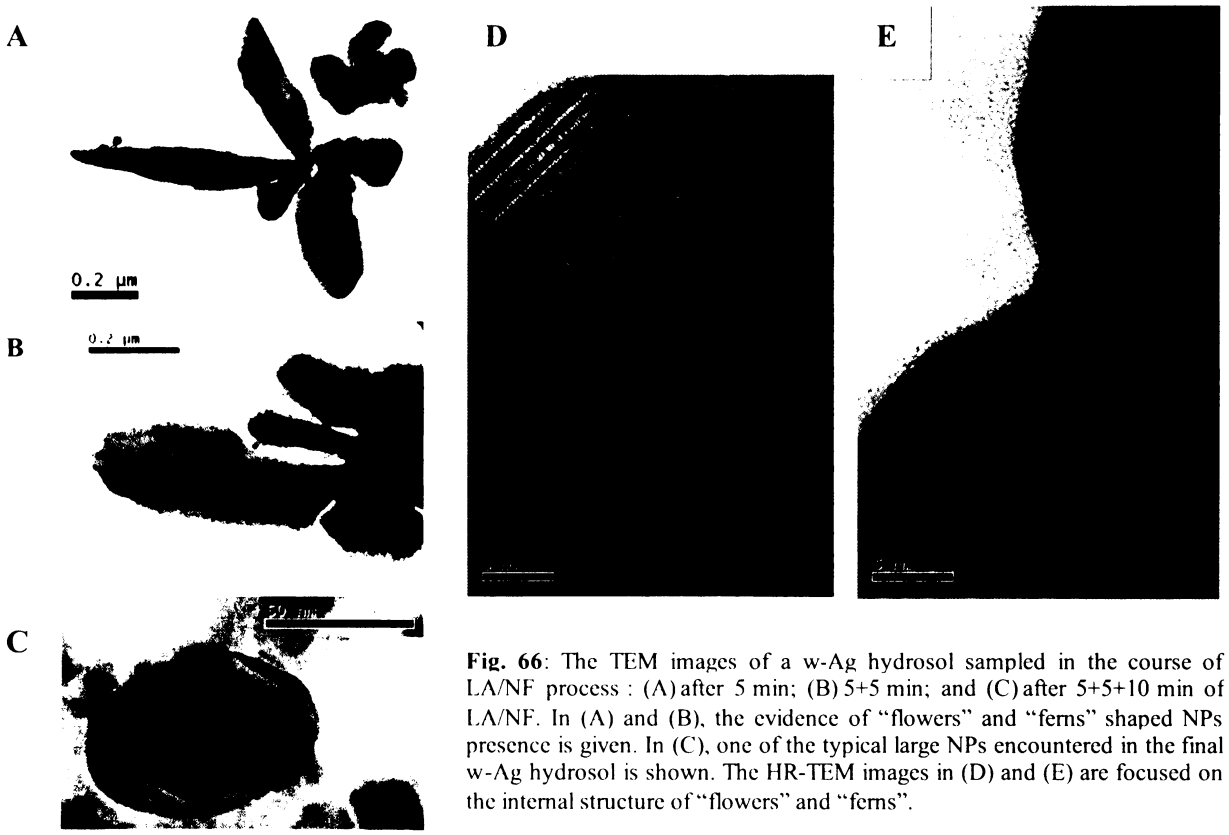

Fig. 66: The TEM images of a w-Ag hydrosol sampled in the course of LA/NF process : (A) after 5 min; (B) 5+5 min; and (C) after 5+5+10 min of LA/NF. In (A) and (B), the evidence of "flowers" and "ferns" shaped NPs presence is given. In (C), one of the typical large NPs encountered in the final w-Ag hydrosol is shown. The HR-TEM images in (D) and (E) are focused on the internal structure of "flowers" and "ferns".

nuclei is a probable reason why no "flowers" and/or "ferns" shaped large NPs have been observed in citrate-Ag hydrosols sampled in the course of LA/NF process (Fig. 52 and Fig. 53) and why the NP sizes are very small (Fig. 54 and Fig. 55).

4.7. Step-wise vs. continuous LA/NF in solutions of stabilizing citrate and destabilizing THS ions

The aim of the study of the interruptions during LA/NF process having an impact on resulting hydrosols has been motivated by the idea of a specific influence of selected electrolytes presence on LA/NF outcomes. Provided that LA/NF is performed in ultrapure water, a more efficient NPs formation and stabilization has been achieved by the step-by-step LA/NF than by the continuous process [Chapter 4.2]. The results have been tentatively explained by a hypothesis that during a dark period of LA/NF (i.e. no laser pulses into Ag foil) in the continuously stirred hydrosol, the build up of the electric bilayer around the NPs can progress efficiency. In this Chapter, the effect of the stabilizing citrate and destabilizing THS on the outcome of LA/NF carried out either with or without dark periods is investigated.

4.7.1. Step-wise vs. continuous LA/NF in Na_3Citr solutions

The step-by-step and the continuous (20 min) LA/NF in water and in the presence of $1x10^{-5}$ M, $1x10^{-4}$ M, $1x10^{-3}$ M, $1x10^{-2}$ M Na_3Citr have been performed. SPE characteristics of the resulting hydrosols are listed in Table XXXVI.

Table XXXVI: Parameters of SPE bands of Ag hydrosols prepared by the step-wise and the continuous LA/NF in water and in citrate solutions, performed with ~214 mJ/pulse

LA/NF performed		λ_{max}	A_{max}	FWHM
in	for [min]	[nm]	[a.u.]	[nm]
pure water	5+5+10	396	0.343	111
	20	409	0.166	156
$1x10^{-5}$ M Na_3Citr	5+5+10	392	0.438	65
	20	392	0.398	70
$1x10^{-4}$ M Na_3Citr	5+5+10	392	0.658	65
	20	392	0.620	65
$1x10^{-3}$ M Na_3Citr	5+5+10	392	0.808	60
	20	393	0.802	60
$1x10^{-2}$ M Na_3Citr	5+5+10	392	1.070	55
	20	392	1.040	58

Note: SPE spectra measured in 4 mm cuvette.

The symmetric shape of the SPE bands of all Na_3Citr-Ag hydrosols remained preserved for both the continuous and the step-wise LA/NF. Moreover, the λ_{max} position remained of the same value for both the continuous and the step-wise LA/NF for all four Na_3Citr concentrations. The FWHM values either slightly increased, or they remained the same with the Na_3Citr concentration increase. The only change reveals itself in the A_{max} value which is lower for a continuous than for the step-wise LA/NF, however, the decrease is very small in comparison to the change observed for the w-Ag hydrosol.

The TEM images in Fig. 67 show that the NP sizes and their aggregates are very similar for the step-wise and continuous LA/NF. Moreover, it appears that the morphological characteristics are much more influenced by Na_3Citr concentration than by the existence of dark periods during LA/NF.

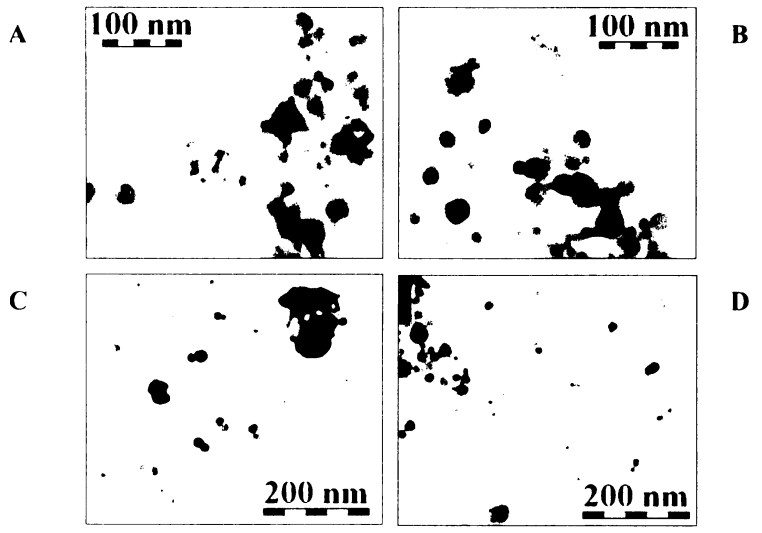

Fig. 67: TEM images of Na_3Citr-Ag hydrosols prepared by step-wise (A, C) and the continuous (B, D) LA/NF at ~200 mJ/pulse in the presence of: $1x10^{-5}$ M Na_3Citr (A, B) and $1x10^{-3}$ M Na_3Citr (C, D).

4.7.2. Step-wise vs. continuous LA/NF in THS solution

In Table XXXVII, the SPE characteristics of Ag hydrosols prepared by the step-wise and the continuous LA/NF in the presence of $1x10^{-7}$ M THS and pure water are compared.

A qualitative comparison (Table XXXVII) reveals that the role of

Table XXXVII: Parameters of SPE bands of Ag hydrosols prepared by the step-wise and the continuous LA/NF in water and in THS solution, performed with ~187 mJ/pulse

LA/NF performed		λ_{max}	A_{max}	FWHM
in	for [min]	[nm]	[a.u.]	[nm]
pure water	2+3+3+5+7	394	0.756	79
	20	405	0.460	180
1x10^{-7} M THS	2+3+3+5+7	398	0.201	274
	20	395	0.326	182

Note: SPE spectra measured in 1cm cuvette.

dark periods in THS-Ag hydrosol formation has opposite effect on LA/NF outcome than in the w-Ag hydrosol formed under the same conditions, i.e. a larger fraction of small, well stabilized Ag NPs is formed by the continuous than by the step-wise procedure.

This observation can be explained in terms of THS complexation activity: during the light period of LA/NF the Ag^+ ions (and Ag_n^+ clusters) are produced. The ions can be partially scavenged (i.e. complexed) by THS anions. In the dark periods, THS probably acts in a similar manner as in the case when a Ag hydrosol prepared by LA/NF in pure water was treated by addition of THS [156, Chapter 2.9.3.]. It has been shown that THS is not adsorbed on Ag NPs surface, however, it most probably penetrates through the elecric bilayer (causing thus its perturbation) and extracts Ag+ ions forming a soluble Ag^+-THS complex. Destabilization of Ag NPs in the hydrosol by THS action thus occurs chiefly in the dark periods (i.e. breaks) in the step-wise performed LA/NF.

4.8. Summary of results of LA/NF performed in citrate solutions and testing of citrate-Ag hydrosols

(1) The effect of various (1x10^{-5} M-1x10^{-2} M) citrate concentrations in the aqueous ablation medium on the progress and outcome of LA/NF performed with ns laser pulses is somewhat different in the neutral and acidic ambient, as witnessed by the differences in both the SPE spectra and the TEM images of the resulting Ag hydrosols. The differences, i.e. the effect of low pH, and their origin are similar to those observed for LA/NF in chlorides solutions [Chapter 4.3.].

(2) For LA/NF performed in Na_3Citr solutions, both the efficiency of small NPs production and their stabilization is remarkably higher than for that performed in pure water, and increases with the increasing Na_3Citr concentration. This trend is preserved at energies of laser pulses in the 200-400 mJ/pulse range.

(3) The outcome of LA/NF is virtually independent on the stepwise or continuous performing of LA/NF.

(4) Furthermore, not only the efficiency of formation and stabilization of Ag NPs during LA/NF, but also the efficiency of LA procedure itself (i.e. of the transfer of Ag from target to solution) is increased by the presence of Na_3Citr in comparison to that in pure water. A full explanation of this effect would require further investigation. A possible, very simple explanation is based on the observed presence of large NPs in w-Ag hydrosols, in contrast to their absence in Na_3Citr-Ag hydrosols. Owing to this situation, the absorption of 1064 nm laser pulses by the w-Ag hydrosol is larger than that of Na_3Citr-Ag hydrosol. Since absorption of laser light by the hydrosol decreases the effective fluence (energy/pulse/target area) impacting the target, the efficiency of LA in Na_3Citr solution can actually be higher than that in pure water.

(5) For LA/NF performed in H_3Citr solutions, the formation of compact aggregates of intergrown Ag NPs has been encountered and found responsible for the differences between SPE spectra and TEM images of Na_3Citr-Ag hydrosols and H_3Citr-Ag hydrosols. These differences can actually stem from protonization of citrate ions in the acidic ambient, and the consequent decrease of the electrostatic repulsion barrier.

(6) The modification of Ag NPs prepared by LA/NF in Na_3Citr and H_3Citr by adsorbed citrate ions was proven by observation of SERS signal of citrate.

(7) An efficient formation of Ag(0) adsorption sites on Ag NPs prepared by LA/NF in the presence of Na_3Citr and H_3Citr solutions has not been detected.

(8) Ag NP surfaces in Na_3Citr (1x10^{-5}M - 1x10^{-2}M) and in H_3Citr (1x10^{-5}M - 1x10^{-2}M) are probably quite densely covered by adsorbed citrate ions (Fig. 68), preventing thus adsorption of the testing adsorbate bpy.

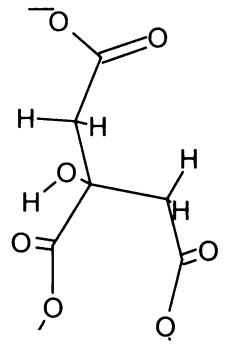

Fig. 68: Schematic depiction of an adsorbed citrate molecule on Ag NP surface. Inspired by [Munro et al. Langmuir 11 (1995) p. 3712].

Chapter 5

SERRS spectral probing of citrate-Ag hydrosols by porphyrins

In our previous experiments [67, Chapter 4.4.], the suitable SERS-active hydrosols prepared by LA/NF in the presence of citrate ions (sodium salt and/or acid) has been identified using bpy as the testing adsorbate. In this Chapter, five different porphyrins [Introduction, section (5) and Fig. 12] have been used for the investigation of their interaction with the Ag NP surfaces of citrate-hydrosols and of a w-Ag hydrosol.

As it was observed for bpy, the Ag NP surfaces are protected by citrates (the higher citrate concentration, the higher protection [Chapter 4.4.4.]). Therefore, there is an idea that these citrates could act as spacers and prevent thus porphyrin molecules from metallation (and from the consequent destruction of their native structure).

With respect to the assumption that citrate-modified Ag NP surfaces are negatively charged and thus they will attract cationic adsorbates by an ionic interaction, a cationic porphyrin – TMPyP - has been selected to probe this assumption. For the sake of comparison, a neutral porphyrin – TPyP - has been selected as well.

The two other porphyrins, TAPP and APTPP, which contain at least one amine terminal group, have been selected in order to investigate the orientation of porphyrin molecules on chemically modified NP surfaces. The main idea is that the amine group(s) will readily bond to Ag surface. Hence, if there is enough space for direct, flat-on porphyrin adsorption, its metallation will be observed in the SERRS spectrum. If there is not enough space, an edge-on adsorption of the porphyrin molecule is anticipated, and consequently, the SERRS spectrum of non-metallated porphyrin is expected to be observed.

The employment of another neutral porphyrin, TMPP, has been motivated by an idea that this porphyrin with its terminal phenyl-methoxy groups as substituents could be almost inert to citrate-modified Ag NPs.

In addition to that, there could be changes in SERRS spectrum of these porphyrins induced by the low pH in H_3Citr-Ag hydrosols.

The porphyrin concentration in the final SERRS-active systems has been selected to be about $2x10^{-8}$ M. This small concentration value has been employed in order to measure the SERRS spectrum (at 457.9 nm excitation laser line) from sub-monolayer coverages of Ag NPs by the porphyrin species. The reason was to avoid the presence of free (non-adsorbed) free base porphyrin molecules in solution. The final porphyrin concentration value has been selected on the basis of the estimation of the porphyrin concentration required for a monolayer coverage of Ag NPs by CuTMPyP [155] which was about $3x10^{-7}$ M. Provided that (i) the NPs concentration is even higher in our w-Ag hydrosol and citrate-Ag hydrosols (compare the A_{max} value of curve a in Fig. 1 in ref. 155 and the A_{max} values in Table XXV multiplied by 2.5 with respect to different cuvette sizes), and (ii) free-base porphyrins (used in this study) occupy, more or less, the same surface as CuTMPyP; then the one order lower porphyrin concentration in the final system should ensure the sub-monolayer coverage.

The aim of the SERRS spectra studies is to investigate the changes in the interaction between a selected porphyrin and Ag NP surface: first, as a function of the citrate ion concentration (in the $1x10^{-5}$ – $1x10^{-2}$ M range) in the citrate-Ag hydrosols and in a w-Ag hydrosol as the reference surface; second, as pH function.; third as a function of time. For the last kind of investigation, SERRS spectra of all systems have been measured after 2 days in order to observe their time-evolution which depicts the evolution of the interaction between a selected porphyrin and the citrate-modified Ag NP surfaces during a two days period.

5.1. Solutions of TMPyP in water and ethanol

The selected porphyrins, except of TMPyP, are not very well soluble in water and thus, their solutions in ethanol have been prepared and used in all experiments. Nevertheless, a question has arisen if the presence of ethanol could influence the porphyrin-Ag surface interaction. One can assume that the concentration of ethanol in the final Ag hydrosol/porphyrin system is so small (~0.1 %) that it does not affect the interaction. To verify this presumption, the same set of reactions of all selected hydrosols has been carried out with TMPyP dissolved in ultrapure water and in ethanol.

First of all, the UV-vis absorption spectra of both TMPyP stock solutions have been recorded for the sake of comparison (Fig. 69). The only difference in UV-vis absorption spectra is that Soret band of TMPyP is slightly higher and narrower in aqueous solution than in ethanolic, while Q bands of TMPyP are slightly higher in the ethanolic solution. This is presumably induced by a different type of interactions between TMPyP, its counter-ion and water and/or TMPyP, its counter-ion and ethanol molecules.

In the next experimental step, a small amount of TMPyP dissolved in water and/or in ethanol has been added to a w-Ag hydrosol and SERRS spectra have been recorded – Fig. 70. The spectra are compared in (Fig. 70A) which demonstrates that the overall SERRS signal is nearly the same. However, in details - Figs 70B, 70C, 70D - the changes in the intensities of the metallation markers reveal (398, 1015, 1342 and 1547 cm^{-1}). It can be concluded from this experiment that the fraction of the metallated TMPyP molecules is slightly higher when the porphyrin is introduced as the aqueous solution than as the ethanolic solution into the w-Ag hydrosol.

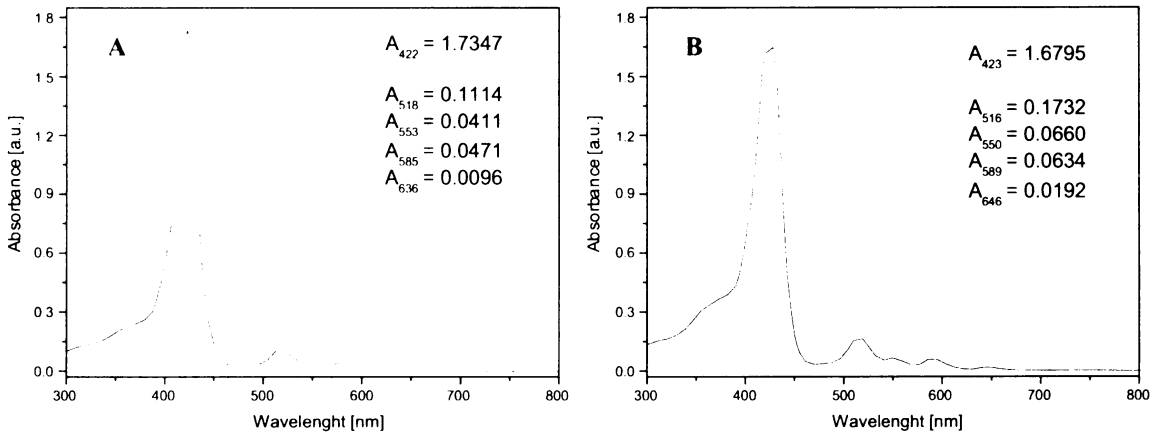

Fig. 69: The UV-vis absorption spectra of ~$2x10^{-5}$ M TMPyP dissolved in (A) ultrapure water and in (B) pure EtOH.

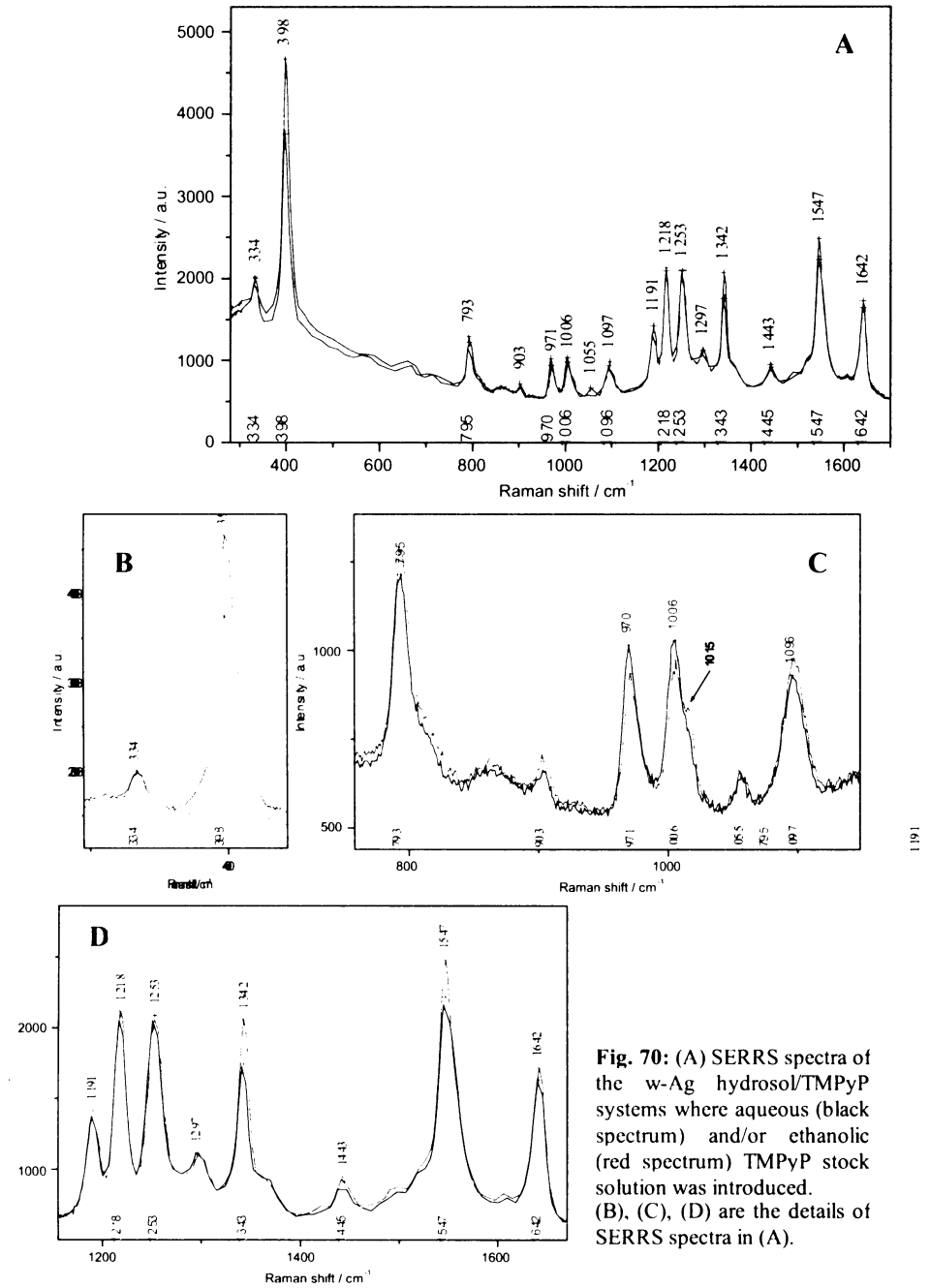

Fig. 70: (A) SERRS spectra of the w-Ag hydrosol/TMPyP systems where aqueous (black spectrum) and/or ethanolic (red spectrum) TMPyP stock solution was introduced. (B), (C), (D) are the details of SERRS spectra in (A).

Subsequently, a small amount of the aqueous and/or ethanolic stock solution of TMPyP has been introduced into each of the Na_3Citr-Ag hydrosols and H_3Citr-Ag hydrosols. The SERRS spectra obtained from these systems are depicted in Fig. 71 and Fig. 72. The overall SERRS spectral intensity is found to be two or three times

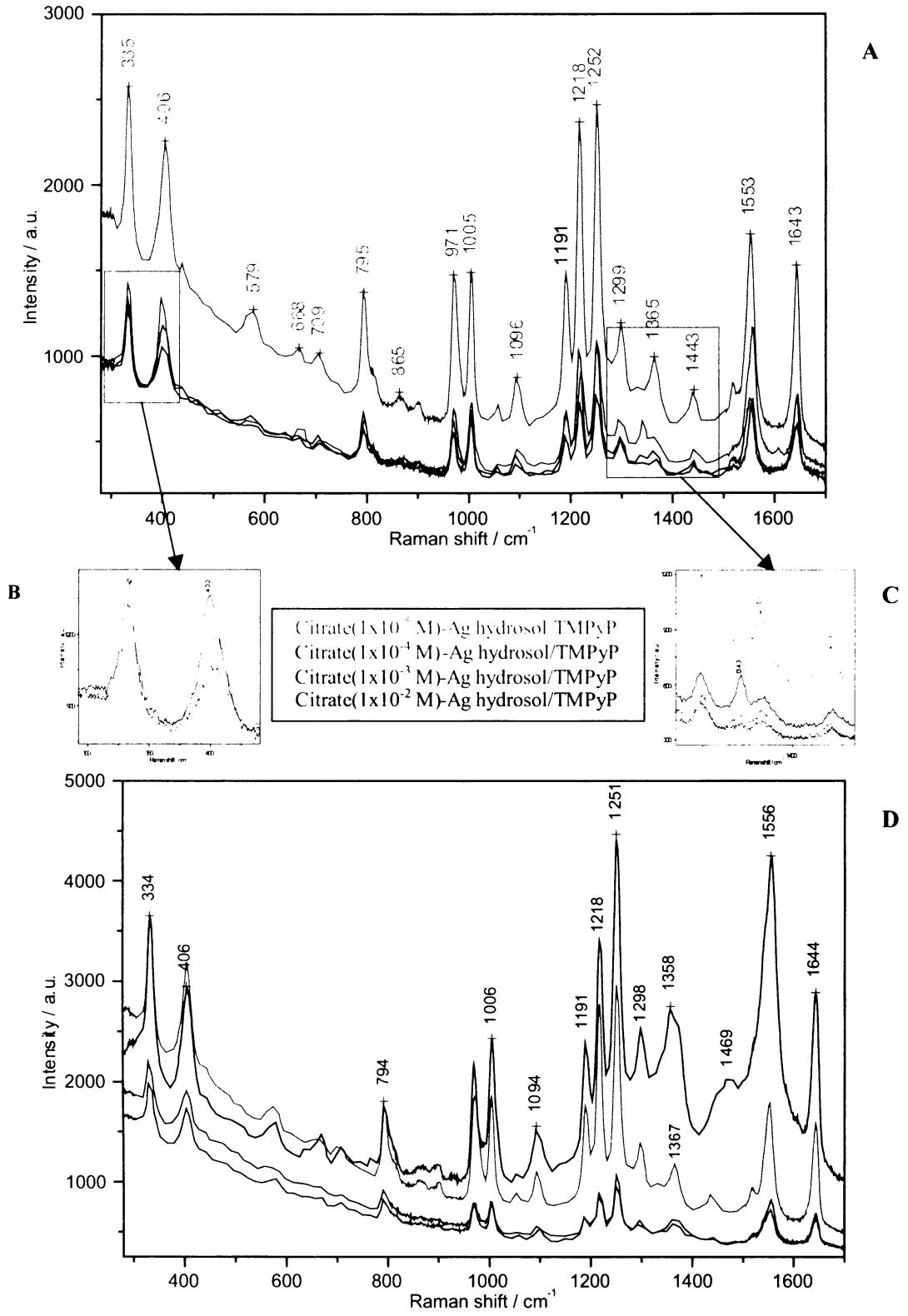

Fig. 71: (A) The SERRS spectra of Na_3Citr-Ag hydrosols/TMPyP(dissolved in water); (B) a detail of SERRS spectra in (A) in the region 300-450 cm^{-1}; (C) a detail of SERRS spectra in (A) in the region 1290-1450 cm^{-1}; (D) the SERRS spectra of H_3Citr-Ag hydrosols/TMPyP(dissolved in water).

higher in citrate-Ag hydrosol/TMPyP systems when TMPyP was introduced in the form of its ethanolic solution. This is quite surprising result with respect to the above mentioned fact that the final TMPyP concentration is nearly the same in both stock solutions (ethanolic and aqueous). However, it should be taken into account that the aggregation of Ag NPs is higher for the system with the ethanolic TMPyP solution and induces a red-shift of the λ_{max} value (initially around 393 nm) closer to the excitation line 457.9 nm – Fig. 73. Therefore, the EM mechanism enhancement is higher in the ethanol-containing system.

Concerning the dependence of the SERRS signal of TMPyP on the Na_3Citr concentration in the Na_3Citr-Ag hydrosol/TMPyP systems – Figs 71A, 71B, 71C and Fig. 72A, there are some similarities and a difference in the

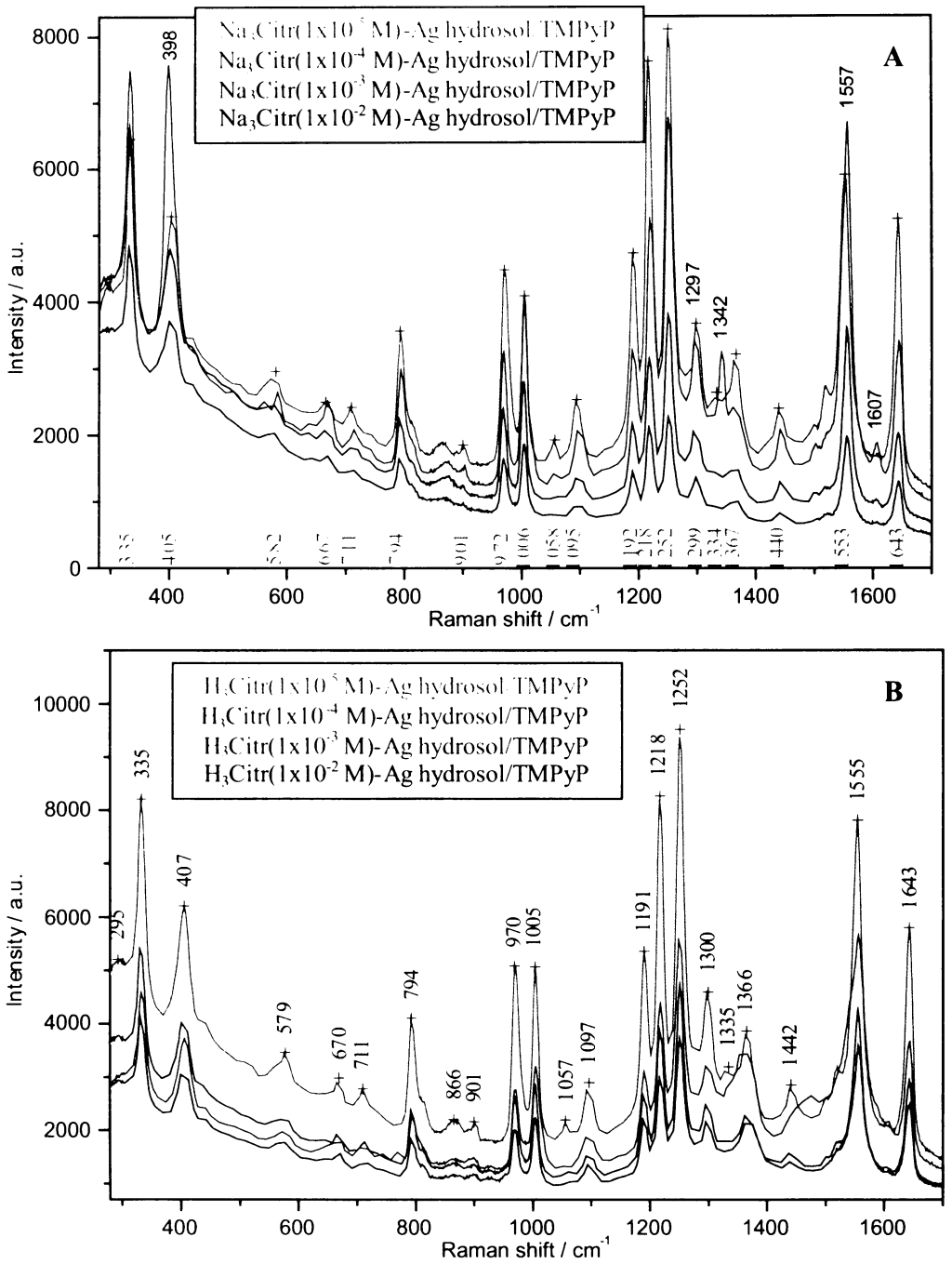

Fig. 72: The SERRS spectra of (A) Na_3Citr-Ag hydrosols/TMPyP(dissolved in ethanol); (B) H_3Citr-Ag hydrosols/TMPyP(dissolved in ethanol).

results obtained for TMPyP dissolved in water and in ethanol. As for the similarities: (i) almost no metallation occurs in systems with the $Na_3Citr(1x10^{-5}\,M - 1x10^{-3}\,M)$-Ag hydrosols; (ii) the SERRS signal intensity decreases with the increasing Na_3Citr concentration in the systems; (iii) two SERRS metallation markers (398 and 1342 cm^{-1}) appear in the $Na_3Citr(1x10^{-2}\,M)$-Ag hydrosol/TMPyP system. The only difference concerns the SERRS signal intensity in the last mentioned system, the $Na_3Citr(1x10^{-2}\,M)$-Ag hydrosol/TMPyP system, with respect to the other systems. Nevertheless, this difference is acceptable in terms of different aggregation states. Another question is why in the system with the highest Na_3Citr concentration, the metallation of TMPyP by Ag^+ occurs (regardless the type of TMPyP stock solution introduced), nevertheless, it will be explained later.

The similar results of SERRS spectral studies of TMPyP in Na_3Citr-Ag hydrosol/TMPyP(dissolved in water) and Na_3Citr-Ag hydrosol/TMPyP(dissolved in ethanol) systems confirm that ethanol does not influence the porphyrin-Ag surface interaction.

As for the TMPyP SERRS signal intensity and character vs. H_3Citr concentration dependence (Fig. 71D and Fig. 72B), it can be said exactly the same as in the case of Na_3Citr for the range of $1x10^{-5}\,M - 1x10^{-3}\,M$ concentration values (see above the points (i) and (ii)). The $1x10^{-2}\,M$ H_3Citr concentration is a little bit exceptional, nevertheless, it can be pointed out that the same characteristic SERRS signal is observed for ethanolic and aqueous TMPyP solutions. The free base porphyrin SERRS spectrum with an enhancement in the regions around 1360 and 1470 cm^{-1} is observed. The possibility of the diacid TMPyP formation which has a strong 1361 cm^{-1} band [143] was

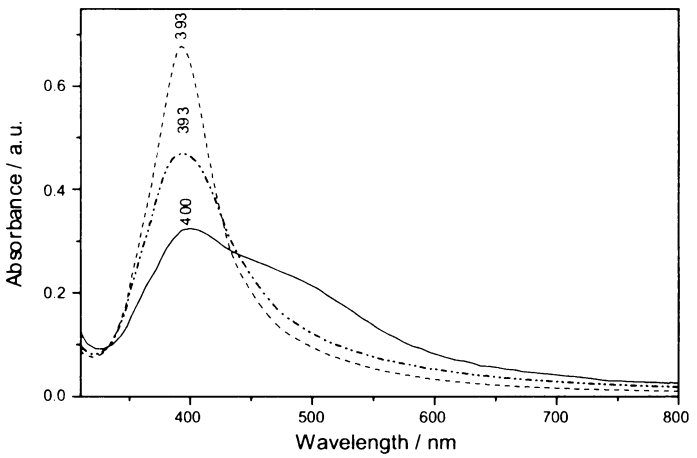

Fig. 73: The UV-vis spectra as an evidence of the aggregation of the parent Na_3Citr-Ag hydrosol (dashed line) induced by the addition of TMPyP stock solutions: aqueous (dash-dot-dot line) and/or ethanolic (solid line).

excluded with respect to a different overall SERRS spectral pattern of diacid TMPyP form [Fig. 55 in ref. 132]) and with respect to the pH value in this system (because the pH = 2.70 in the $1x10^{-2}$ M H_3Citr-hydrosol, and the pH of 2.04 is required for diacid TMPyP form generation, Table XXVI and [132], respectively). Nevertheless, the assignment of the 1360 and 1470 cm^{-1} vibrations [143] indicates changes in symmetric stretching of N-C_α and C_α-C_β bonds of the porphine skeleton. In other words, one can assume an interaction between the porphyrin and citric acid molecules (or citrate ions), or alternatively, some decomposition to graphitic carbon.

Finally, the time evolution of citrate-Ag hydrosol/TMPyP systems will be discussed. As it is depicted in Fig. 74, the bands typical for metallation by Ag^+ appear in the spectra of systems with all Na_3Citr concentrations. This metallation is highest in the $1x10^{-5}$M Na_3Citr concentration and its extent diminishes with increasing Na_3Citr concentration in the systems, as follows from the comparison of the mutual ratios of 398/334 and 1342/1366 bands (Figs 74B, 74C). In the system with the highest Na_3Citr concentration ($1x10^{-2}$ M), the metallation of TMPyP by Ag^+ has remained the same after 2 days of aging as in the

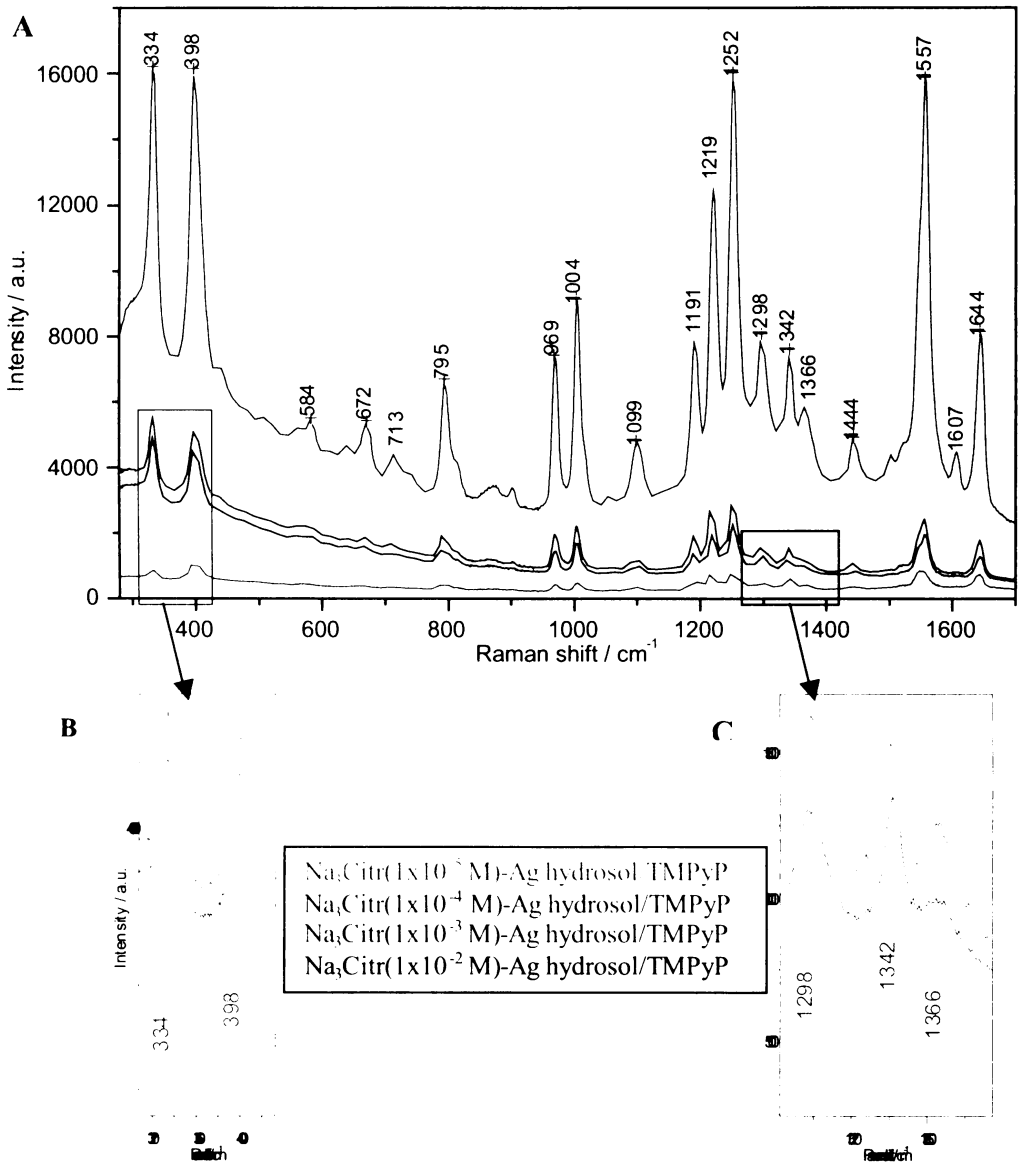

Fig. 74: (A) The SERRS spectra of Na_3Citr-Ag hydrosol/TMPyP systems after 2 days of aging. (B) and (C) the details of (A).

freshly prepared system, and, in addition to that, the intensity of the SERRS signal has increased twice, obviously due to the slow aggregation of $Na_3Citr(1x10^{-2}$ M)-Ag hydrosol/TMPyP system.

These results and those from the immediate measurement of Na_3Citr-Ag hydrosol/TMPyP systems seem to be strange because a priori one could assume that (i) a partial immediate metallation would occur in the smallest Na_3Citr concentration and then it would decrease with Na_3Citr concentration increase; (ii) the metallation would continue during two days with decreasing extent hand in hand with increasing Na_3Citr concentration. A rather unexpected result of this study is that (i) in the system with the highest Na_3Citr concentration ($1x10^{-2}$ M), a partial immediate metallation of TMPyP occurs, while in systems with lower Na_3Citr concentrations, the immediate metallation of the porphyrin has been prevented. (ii) The metallation partially proceeds during 2 days in all Na_3Citr-Ag hydrosol/TMPyP systems except of that with the highest Na_3Citr concentration.

Why are the systems with the highest Na_3Citr concentration so special? It can be found a quite simple explication: in the $1x10^{-5}$ M – $1x10^{-3}$ M Na_3Citr concentration range, the fact is that the higher the Na_3Citr concentration, the higher the Ag NP surface coverage by citrate anions – Schema in Fig. 75A; while the $1x10^{-2}$ M Na_3Citr concentration is so high that a part of it cannot be adsorbed on the NP surfaces any more, and thus, this part remains present in the solution as citrate anions (= solubilized citrate anions). It is also possible that Ag^+ ions and small Ag clusters (which did not form NPs [Chapter 4.6.]) can interact with these solubilized citrate anions and form $\{Ag_n(Citr)_m\}^{n-3m}$ species in the course of LA/NF process (preferentially and most probably: $\{Ag(Citr)\}^{2-}$, $\{Ag_2(Citr)\}^-$ anions and $Ag_3(Citr)$ molecules – Fig. 75B, where *n* index in the formula shall indicate the Ag clusters including more than one Ag atom). When cationic porphyrin TMPyP is introduced into the $Na_3Citr(1x10^{-2}$ M)-Ag hydrosol, the present solubilized anions and/or molecules can quickly interact with this cationic porphyrin and they could induce the metallation of TMPyP by Ag^+ - Schema in Fig. 75C. This cationic Ag^+-TMPyP molecules may easily approach to negatively charged Ag NP surfaces and thus the SERRS signal of Ag^+-TMPyP constant in time is observed.

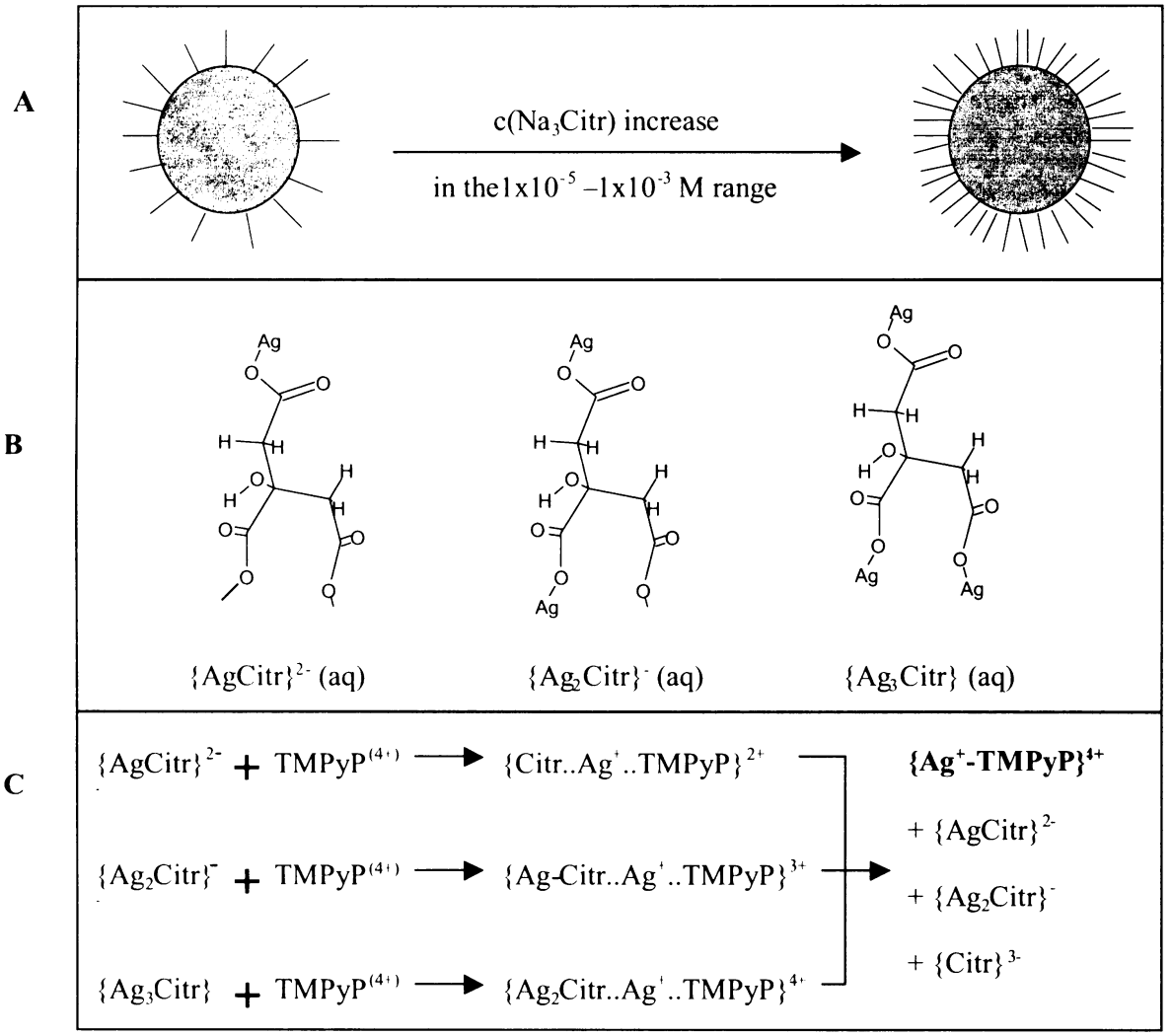

Fig. 75: Schematic depiction of Na_3Citr role in the Na_3Citr-Ag hydrosol/TMPyP systems : (A) chemical modification of Ag NPs (full grey circle) by citrate anions (black lines) in the mentioned concentration range; (B) solubilized citrates (present preferentially in the $Na_3Citr(1x10^{-2}$ M)-Ag hydrosol system) forming species with Ag cations; (C) solubilized silver citrates in the interaction with cationic TMPyP resulting in Ag^+-TMPyP detected in SERRS spectra of $Na_3Citr(1x10^{-2}$M)-Ag hydrosol/TMPyP systems.

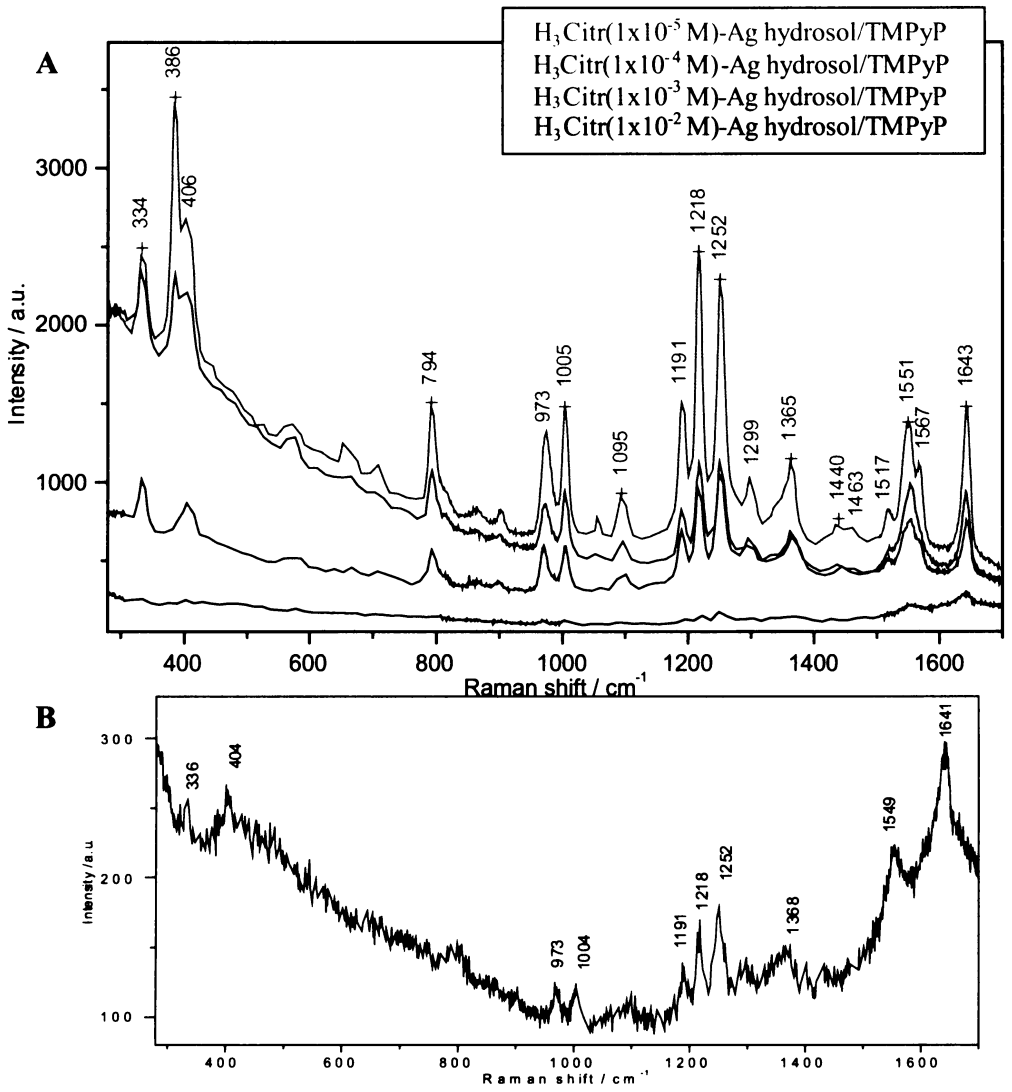

Fig. 76: (A) SERRS spectra of H_3Citr-Ag hydrosol/TMPyP systems after 2 days of aging with H_3Citr concentration values in the $1x10^{-5}$ M - $1x10^{-2}$ M range. (B) A detail of SERRS spectra of $H_3Citr(1x10^{-2}$ M)-Ag hydrosol/TMPyP system after 2 days of aging (= black spectrum in A).

Concerning the time evolution of H_3Citr-Ag hydrosol/TMPyP systems (Fig. 76), the SERRS signal from systems with the higher H_3Citr concentrations ($1x10^{-3}$ M and $1x10^{-2}$ M) decreases (which is not surprising with respect to the instability of H_3Citr-Ag hydrosol due to the large inter-growing NPs presence [Chapters 4.4.1. and 4.4.3.]. Interestingly, characteristic marker bands of Ag(0)-TMPyP complex at the 386, 1365 and 1567 cm^{-1} bands [142] are detected in SERRS spectra. The Ag(0)-TMPyP signal decreases with the overall SERRS signal decrease, i.e. it is maximal in system with $1x10^{-5}$ M H_3Citr and decreases with H_3Citr concentration increase. Therefore, it can be concluded that Ag(0) adsorption sites are present on surfaces of Ag NPs prepared by LA/NF in H_3Citr solutions as it has been already indicated by SERS spectral probing by bpy in [Chapter 4.4.4]. In the case of TMPyP, Ag(0) adsorption sites have not been detected immediately (after systems preparation) but after two days of aging. This might be caused by the facts that cationic porphyrin is (i) so large that it cannot pass the citrates envelope so quickly (thus it needs longer time-periods than bpy) and (ii) attracted by citrate anions which prevent them from direct interaction with Ag surface.

5.2. TPyP

For all the porphyrins, the same approach to SERRS spectral probing of citrate-Ag hydrosols has been adopted. This approach involves: (i) solubility of a particular porphyrin in EtOH, and (ii) determination of the characteristic metallation spectral marker bands will be discussed; (iii) the SERRS signal in the absence and in the presence of citrate molecules will be compared and analyzed; (iv) the effect of citrate concentration changes and (v) pH changes on SERRS spectral signal will be investigated; and last but not least, (vi) the two days evolution of the citrate-Ag hydrosol/porphyrin system will be monitored by SERRS spectral measurements.

The UV-vis absorption spectrum of the TPyP stock solution in EtOH is shown in Fig. 77. The observation of small amount of solid TPyP species in its ethanolic stock solution indicated that not all TPyP

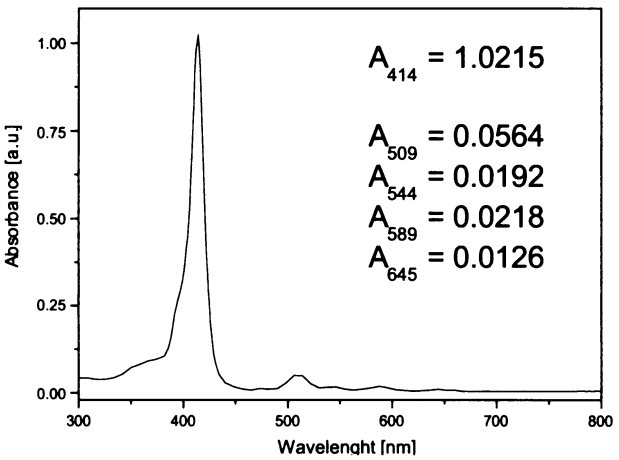

Fig. 77: UV-vis absorption spectrum of TPyP in EtOH.

amount was dissolved and hence a saturated TPyP solution of lower concentration than originally intended has been employed for the final systems preparation. For this reason, the SERRS signal of TPyP cannot be quantitatively compared with the SERRS signals of systems containing TMPyP. However, the results can be discussed qualitatively and/or they can be discussed quantitatively only within the TPyP measurement series.

The interpretation of the SERRS spectra obtained from citrate-Ag hydrosols/TPyP systems is based on the fact that the metallation markers (published for TPyP in [163]) are approximately the same as those of TMPyP, namely: 400, 1015, 1342 and 1542 cm^{-1}.

Moreover, the results of TPyP studies can be qualitatively compared with bpy studies on the same types of citrate-modified hydrosols (presented in [chapter 4.4.4.]) due to the fact that both adsorbates (TPyP and bpy) are not charged (in contrast to TMPyP) and contain pyridyl groups with a free electron pair on their nitrogen atoms.

The SERRS spectrum of the w-Ag hydrosol/TPyP system has been recorded and is depicted in Fig. 78. Apart from the 1342 cm^{-1} band, the metallation marker bands occur, at 400 cm^{-1} band, and the shoulders at 1015 and 1540 cm^{-1}.

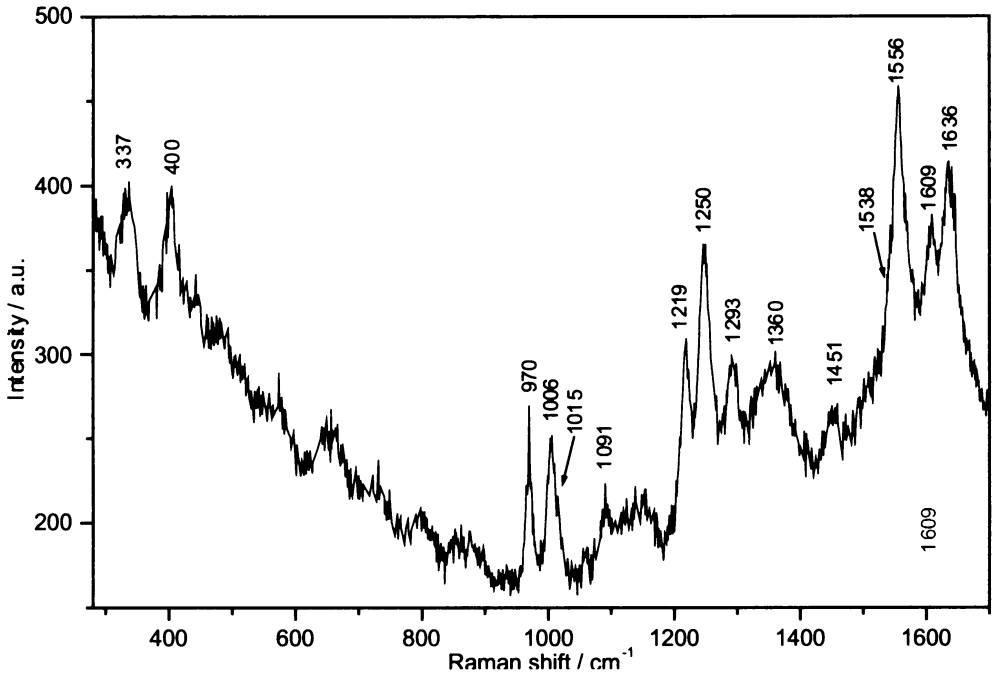

Fig. 78: SERRS spectrum of the w-Ag hydrosol/TPyP system.

In comparison to that, in the Na_3Citr-Ag hydrosol/TPyP systems, almost no metallation (except of the 400 cm^{-1} band) is observed and the overall SERRS signal decreases with Na_3Citr concentration increase (Fig. 79A). This intensity decrease is very similar to the results of the probing of Ag NP surfaces prepared by LA/NF in citrate solutions by bpy [chapter 4.4.4.]. On the other hand, the fact that TPyP signal is observed even in the $Na_3Citr(1x10^{-3}$ M)-Ag hydrosol (while in bpy probing only the $Na_3Citr(1x10^{-5}$ M)-Ag hydrosol/bpy system provided the SERS signal of bpy [Chapter 4.4.4.]) can be attributed to the fact that SERRS signal is detected in TPyP case, while only SERS without a molecular resonance contribution in the bpy case, i.e. the overall enhancement of the Raman scattering is by 2-3 orders of magnitude higher for TPyP than for Ag^+-bpy.

The SERRS spectral intensity in H_3Citr-Ag hydrosol/TPyP systems in the $1x10^{-5}$ M - $1x10^{-3}$ M range of H_3Citr concentration is slightly higher than in Na_3Citr-Ag hydrosol/TPyP systems (Figs 79A and 79B). In addition to that, the intensity of SERRS signal is five times higher in the system with the highest H_3Citr concentration (Fig. 79C), probably due to a larger aggregation of this system. In this place, let us compare the SERRS spectral pattern of TPyP observed in H_3Citr-Ag hydrosols with that in Na_3Citr-Ag hydrosols: there are either some changes in band positions (400→405→409 cm^{-1}, 1004→1009→1012 cm^{-1}, 1218→1209 cm^{-1}, 1555→1543 cm^{-1}); or some new bands appear (988, 1185, 1322, 1372, 1470 cm^{-1}) with H_3Citr concentration increase (Figs 79B and 79C). The changes can be divided in two categories: first, those related to porphine macrocycle, and second, those reflecting the changes of the pyridyl substituents. The 405, 988, 1012, 1372, 1470, and 1543 cm^{-1} bands were attributed to the A_{1g} vibrational modes of the diacid form of TPyP in [143]. On the other hand, the 1185, 1209 and 1322 cm^{-1} bands assigned to vibrational modes of pyridyl substituents [133] (C-H in-plane deformation + ring stretching, ring-H in-plane bend, ring stretching, respectively) become most pronounced in the system with the highest H_3Citr concentration, i.e. with the most intense SERRS signal.

How can be the observations of a higher SERRS spectral intensity of TPyP in acidic hydrosols explained in more details? There are two reasons: first, as it was demonstrated in [Chapter 4.4.1.], the higher the H_3Citr concentration in the system, the greater the portion of interpenetrating NPs encountered and hence the probability of hot spots generation and consequently the larger EM mechanism of enhancement of RRS spectral signal. Second, N-atoms of the pyridyl substituents of TPyP are able to interact with protons and form pyridiniumyl cation - with

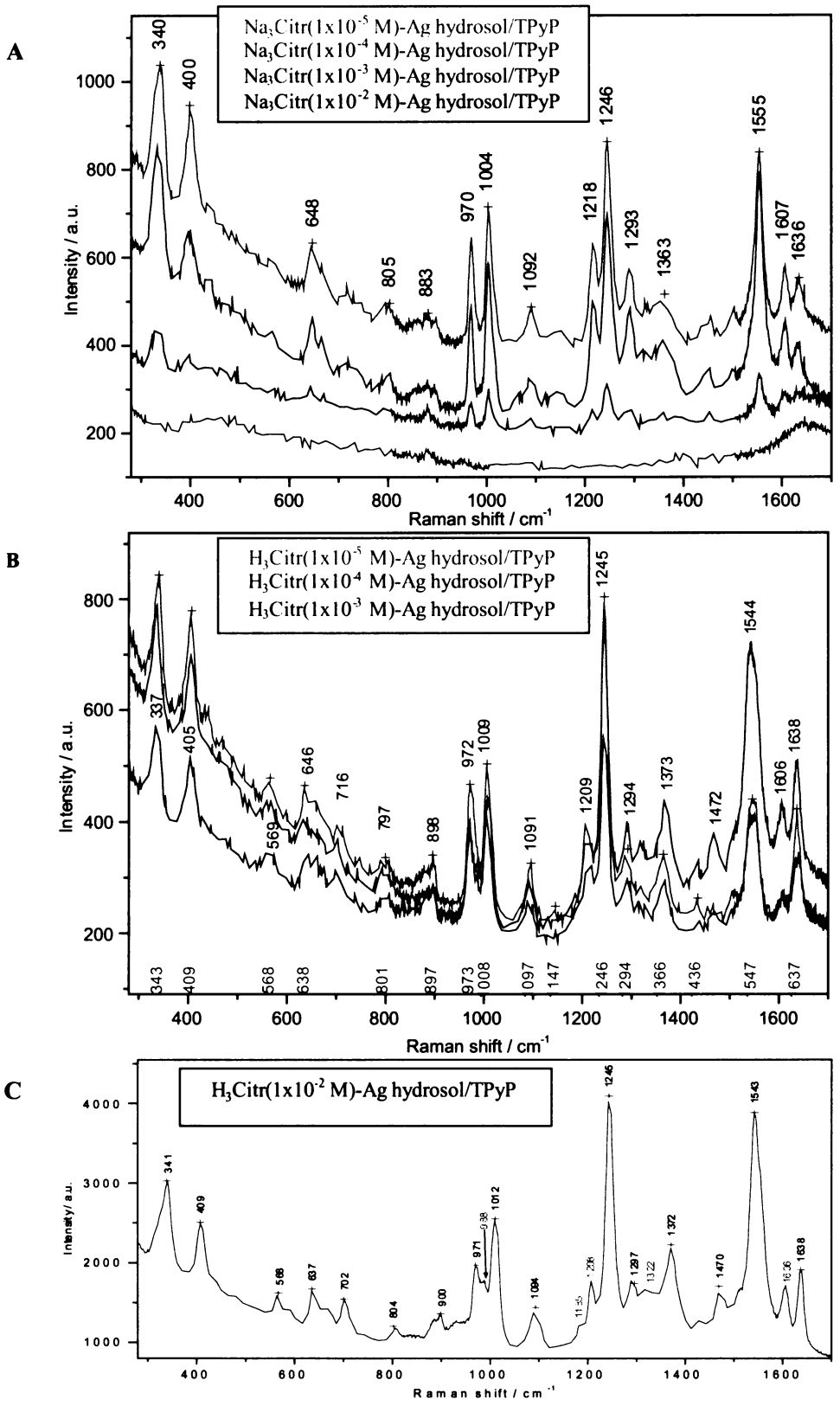

Fig. 79: SERRS spectra of (A) Na_3Citr-Ag hydrosol/TPyP, and (B) H_3Citr-Ag hydrosol/TPyP systems except of the $H_3Citr(1x10^{-2}$ M)-Ag hydrosol/TPyP system which is depicted in (C).

respect to the pK_a value of pyridine being of the 5.18 value [161], almost complete protonation of pyridyl groups (higher than 92 %) can be expected in all H_3Citr-hydrosols except of that with the lowest H_3Citr concentration where maximally 27% of pyridiniumyl cation formation is achieved, as demonstrated in [164]. Formation of the pyridiniumyl cations enables that attraction of TPyP molecules to the citrate anions attached to the Ag NP surfaces.

Finally, the time evolution of citrate-Ag hydrosol/TPyP systems can be discussed. In Fig. 80, the metallation markers are clearly distinguishable (402, 1017, 1344, 1543 cm^{-1}) in a w-Ag hydrosol/TPyP system after 2 days of its evolution, even if the SERRS spectrum is low in intensity and some bands of EtOH appear. In contast

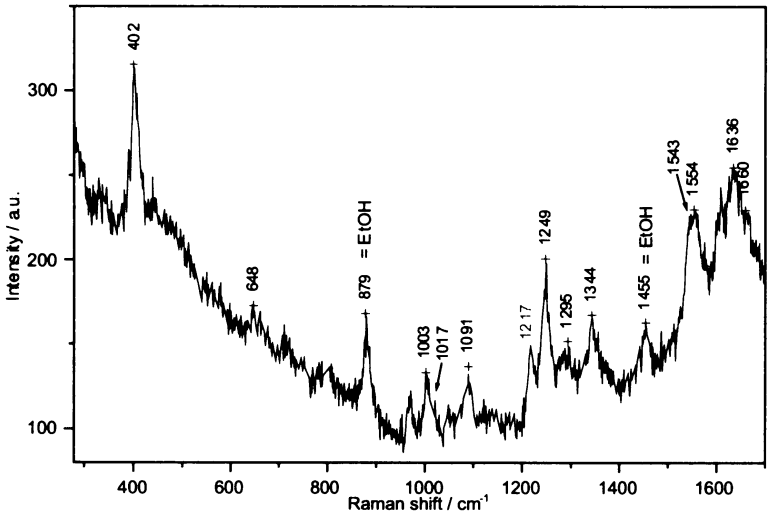

Fig. 80: SERRS spectrum of the w-Ag hydrosol/TPyP system after 2 days of aging.

to that, the free base and the metallated form co-exist in Na_3Citr-Ag hydrosol/TPyP systems after 2 days of their evolution, Fig. 81.

The H_3Citr-Ag hydrosol/TPyP systems after 2 days of their evolution (Fig. 82), are interesting because the above discussed changes in SERRS spectral character of TPyP in acidic ambient continue on proceeding, i.e. the correspondent cation formation from non-charged TPyP and its closer attachment to the NP surface. The $H_3Citr(1x10^{-2}$ M)-Ag hydrosol/TPyP system has precipitated during two days. In contrast to that, the SERRS signal from the systems with $1x10^{-5}$ M - $1x10^{-3}$ M H_3Citr concentrations has increased. This result indicates that the formation of compact aggregates proceeded during aging. Last but not least, the appearance

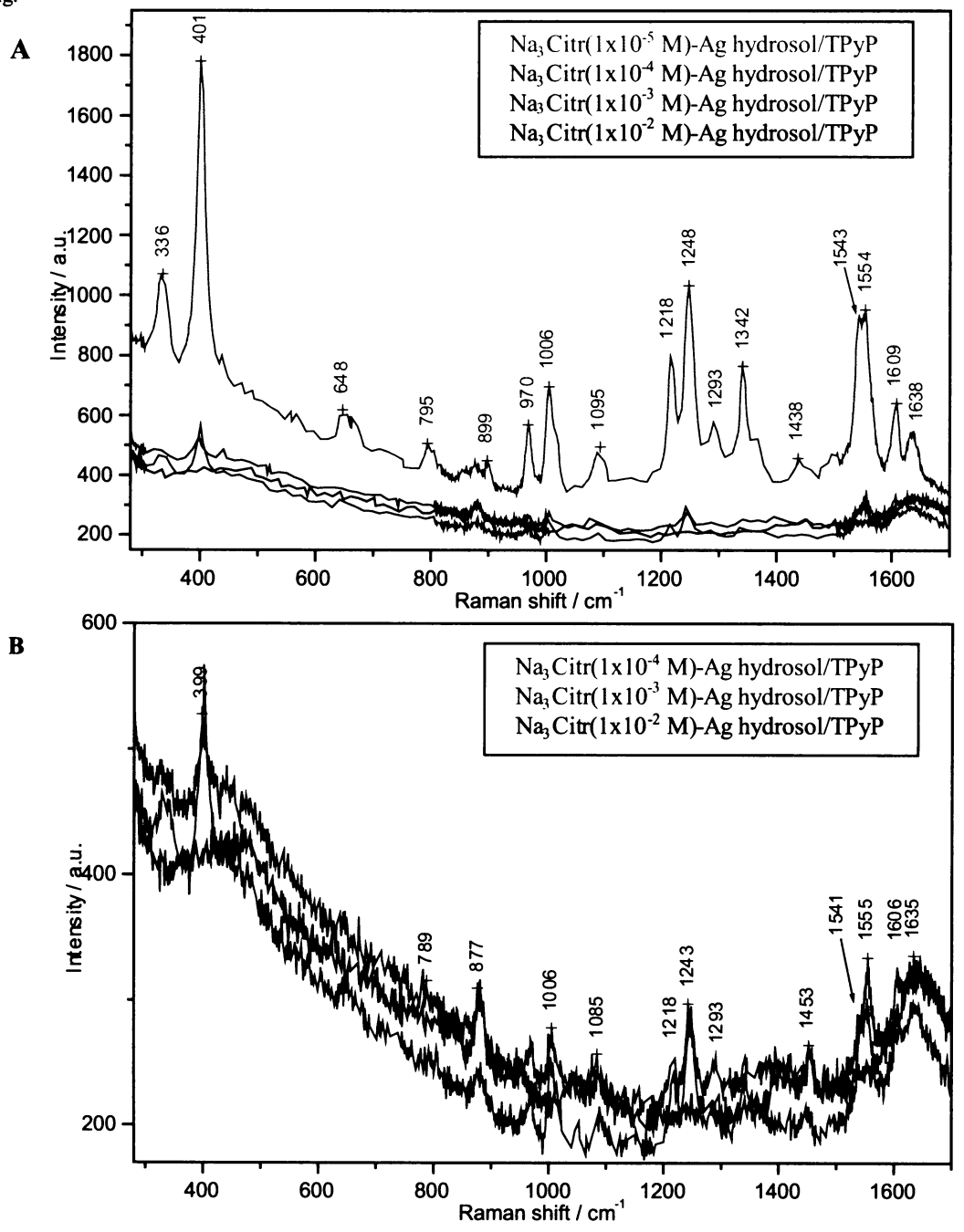

Fig. 81: SERRS spectra of Na_3Citr-Ag hydrosol/TPyP systems after 2 days of aging: (A) all citrate concentrations and (B) a detail of the higher Na_3Citr concentrations.

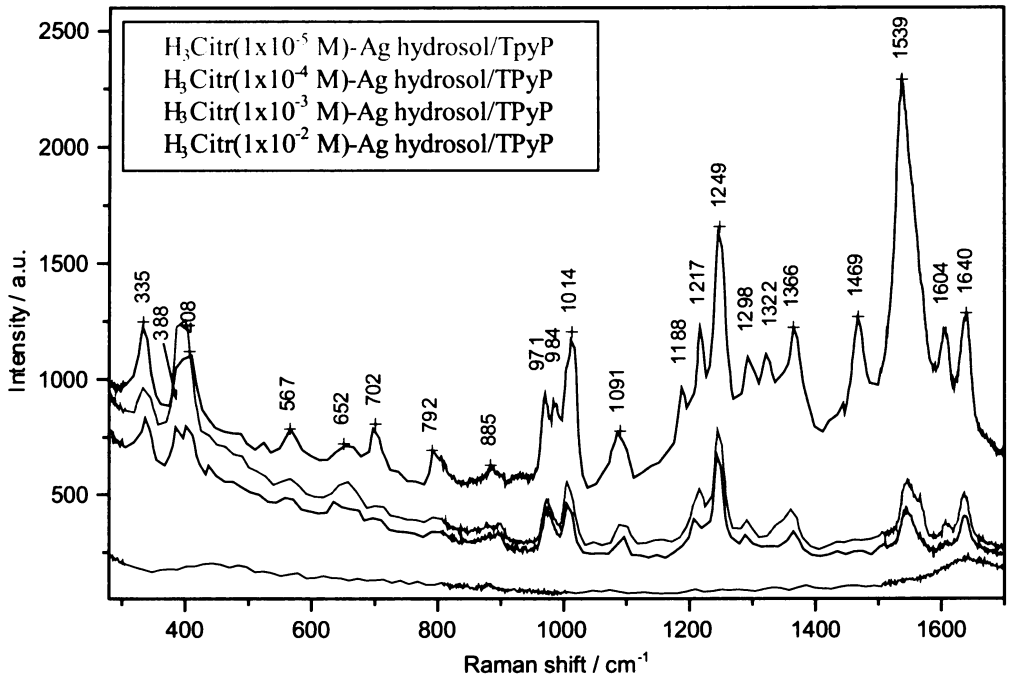

Fig. 82: SERRS spectra of H_3Citr-Ag hydrosol/TPyP systems after 2 days of aging.

of 388, 1366 and 1567 cm^{-1} bands in H_3Citr-Ag hydrosol/TPyP systems presumably indicates the formation of the Ag(0) adsoption sites, analogously with the results obtained for H_3Citr-Ag hydrosol/TMPyP systems (Fig. 82 and Fig. 76). After 2 days of evolution, the SERRS spectra of TPyP in H_3Citr-Ag hydrosol are very similar to the SERRS spectral features of TMPyP in the H_3Citr-hydrosol/TMPyP systems.

5.3. TAPP

Similarly to TPyP, the porphyrin TAPP dissolved in ethanol (Fig. 83) has contained solid residues. Therefore, the final TAPP ethanolic saturated stock solution was not exactly of the $2x10^{-5}$ M concentration and, consequently, the exact TAPP concentration in the final systems has been always lower than the intended value. For this reason, the SERRS signal of TAPP cannot be quantitatively compared with the other porphyrins SERRS signals; nevertheless, it can be compared qualitatively, and quantitatively only within the TAPP series.

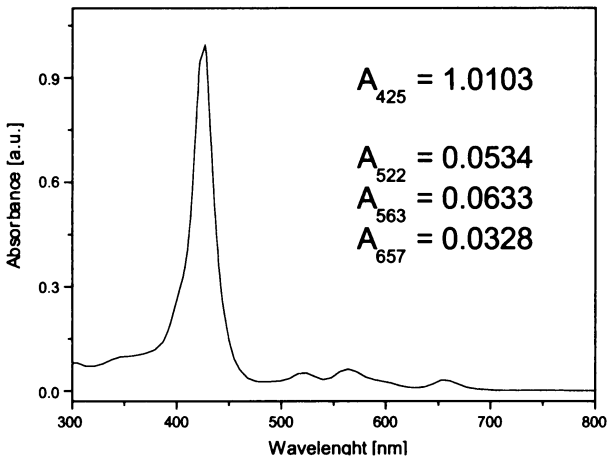

Fig. 83: UV-vis absorption spectrum of TAPP in EtOH.

In order to investigate the metallation markers of this porphyrin, the RRS spectrum of TAPP stock solution in 10% EtOH (Fig. 84) and the SERRS spectrum of the w-Ag hydrosol/TAPP system measured immediately (Fig. 85) and after 2 days of its evolution (Fig. 86) have been recorded at the same conditions and they can be thus compared. From this comparison, one can conclude that the metallation markers are nearly the same as in the cases of TMPyP and TPyP, i.e.: 398, 1020 (as a shoulder near the 1004 cm^{-1} band), 1342, 1536 cm^{-1}. Moreover, from the comparison of RRS and SERRS spectra of TAPP, the 1085, 1279, 1492 cm^{-1} bands appear in SERRS spectrum which were not observable in RRS spectrum due to the interfering EtOH bands. These bands are assigned (according to the NCA for tetraphenylporphine in [144]) to the deformation of C_β-H bond, the C_α-C_β and C_β-C_β stretching vibrations, respectively. Their appearance can be related to the changes of geometry, particularly due to perturbation of D_{4h} symmetry of the porphine skeleton.

For the Na_3Citr-Ag hydrosols/TAPP systems (Fig. 87A), the character of SERRS spectral bands is the same as in the w-Ag hydrosol/TAPP system (Fig. 85): the immediate partial metallation is observed as indicated by detection of the 397 and 1538 cm^{-1} bands, while the relative intensity of two other metallation markers is too small to be distinguished. The extent of metallation (the 397/335 ratio) vs. Na_3Citr concentration dependence is rather unusual: obviously the metallation is smaller in $1x10^{-5}$ M Na_3Citr concentration than in the w-Ag hydrosol/TAPP system, while it is higher in $1x10^{-4}$ M Na_3Citr and then it decreases as the Na_3Citr concentration increases (Fig. 87A). In addition to that, the overall SERRS spectral intensity of TAPP in the Na_3Citr($1x10^{-5}$ M)-Ag

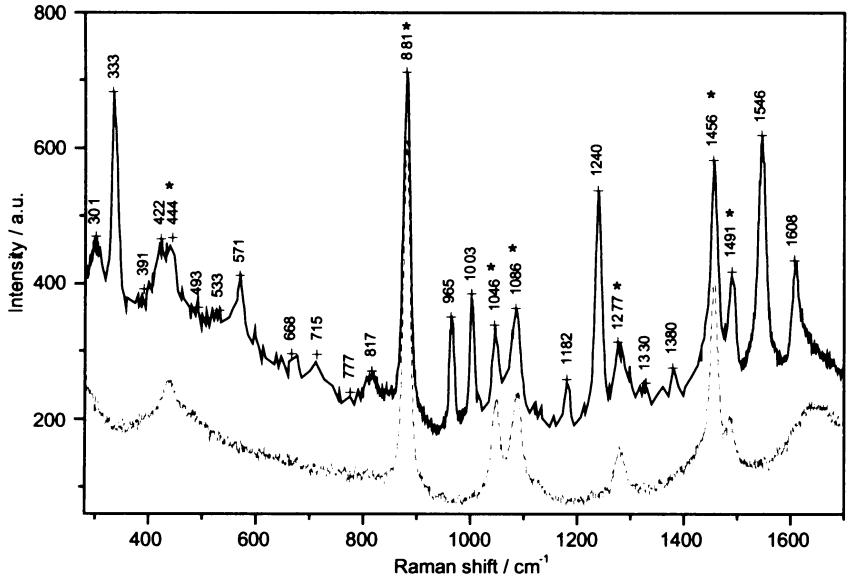

Fig. 84: RRS spectrum of $1x10^{-6}$ M TAPP in 10% EtOH (black spectrum), and RS spectrum of 10% EtOH (grey dash spectrum). Obviously, the peaks with asterix are the bands of EtOH.

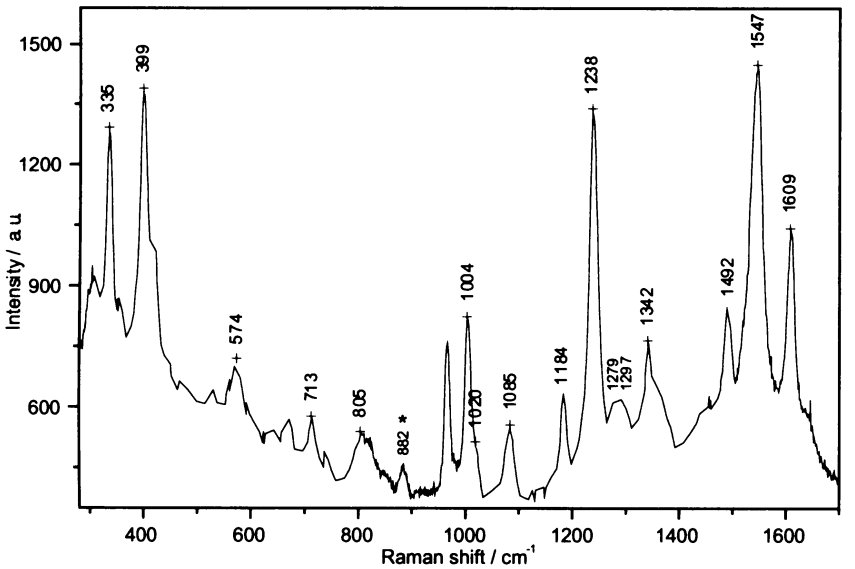

Fig. 85: SERRS spectrum of the w-Ag hydrosol/TAPP system.

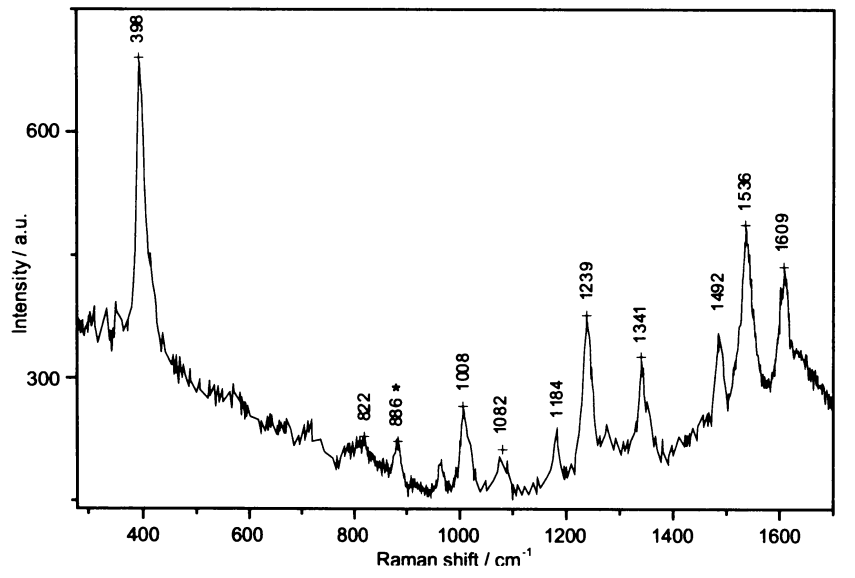

Fig. 86: SERRS spectrum of the w-Ag hydrosol/TAPP system after 2 days.

hydrosol/TAPP and $Na_3Citr(1x10^{-4}$ M)-Ag hydrosol/TAPP systems is higher than that in the w-Ag hydrosol/TAPP system; while, it is similar and/or even lower in intensity in the two higher Na_3Citr concentrations. Thus, for the immediate interaction of TAPP with Ag NPs surfaces, the smaller Na_3Citr concentrations ($1x10^{-5}$ M) in the final system are quite interesting.

In the SERRS spectra of $Na_3Citr(1x10^{-5}$M)-Ag hydrosol/TAPP system (Fig. 87A) the following bands newly appear in comparison to the SERRS spectrum of TAPP in the w-Ag hydrosol/TAPP system (Fig. 85): 417, 986, 1320, 1433, 1470 cm^{-1}. Their appearance will be discussed later.

Furthermore, the SERRS spectra of the $Na_3Citr(1x10^{-5}$ M)-Ag hydrosol/TAPP and $Na_3Citr(1x10^{-4}$ M)-Ag hydrosol/TAPP systems differ by the 356 cm^{-1} band which is assigned to the deformational vibration of porphine macrocycle. Therefore, the differences in these two SERRS spectra are presumably induced by a different kind of TAPP molecules orientation with respect to the NP surfaces.

Regarding the H_3Citr-Ag hydrosol/TAPP and Na_3Citr-Ag hydrosol/TAPP systems comparison, the SERRS spectral signal of TAPP in acidic ambient is markedly different not only by its intensity, but also by its pattern. In contrast to the trends encountered in neutral ambient, the TAPP SERRS spectral signal increases significantly with H_3Citr concentration increase (Fig. 87B). The overall character of the SERRS spectra is the same for all H_3Citr concentrations and may be described (in comparison to TAPP SERRS signal in neutral citrate-Ag hydrosol - Fig. 87A) in more details as: (a) many weak bands in the 300-400 cm^{-1} region and simultaneously no metallation marker occur, (b) the 966 cm^{-1} band (assigned to the symmetric stretching of C_α-C_m bond [144]) disappears, (c) the 987 cm^{-1} appears, (d) the 1006 cm^{-1} shifts to the 1016 cm^{-1} (assigned to the symmetric stretching of C_α-N bond [144]), (e) the 1239 cm^{-1} shifts to the 1243 cm^{-1} with a shoulder and decreases in its intensity (assigned to the symmetric stretching of C_m-Ph bond [144]), (f) the 1322 cm^{-1} increases in its intensity (tentatively assigned to the ring stretching of aniline), (g) the 1433 cm^{-1} shifts to the 1426 cm^{-1} (assigned to the asymmetric stretching of C_α-C_m bond [144]), (h) the

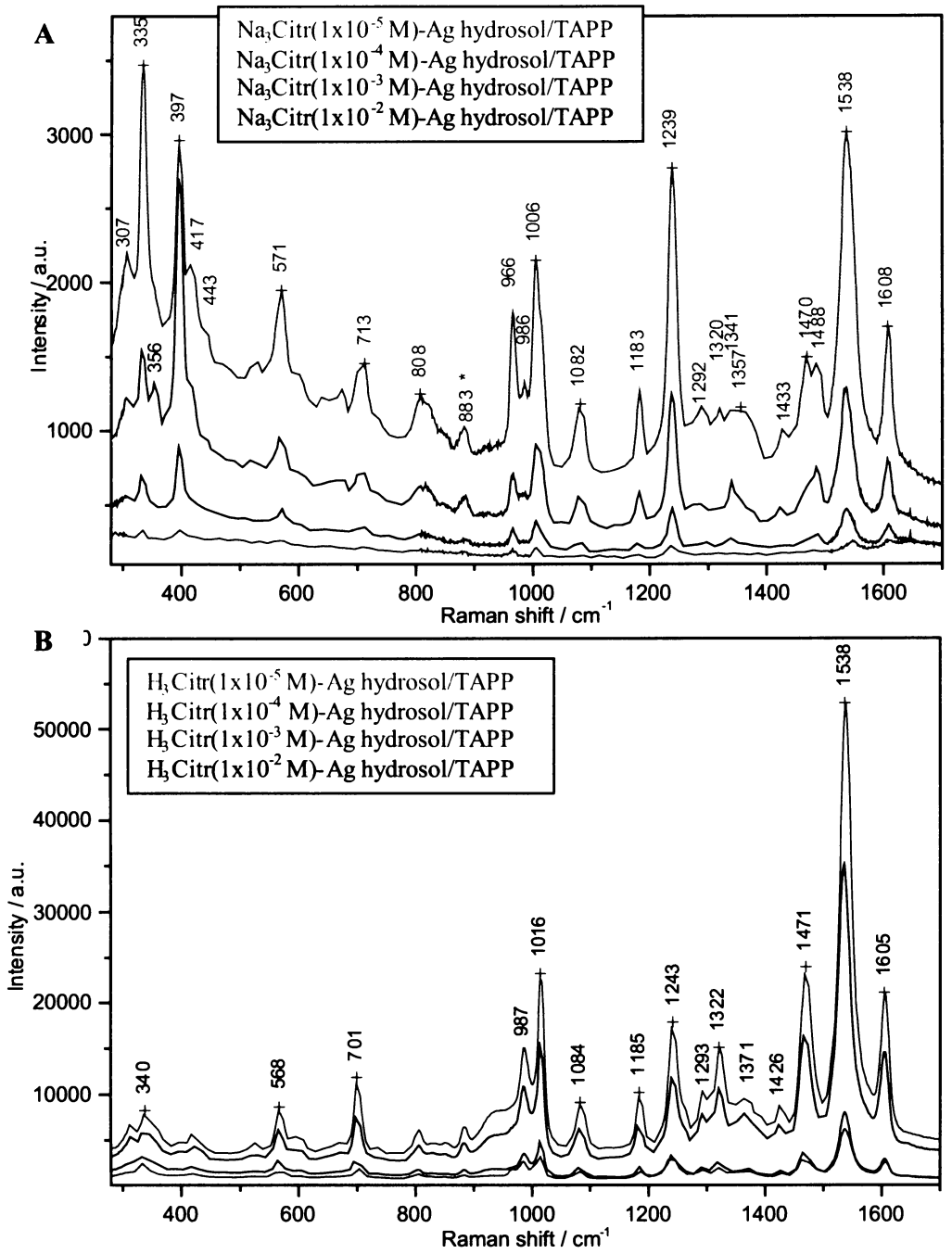

Fig. 87: SERRS spectra of (A) Na_3Citr-Ag hydrosol/TAPP, and (B) H_3Citr-Ag hydrosol/TAPP systems.

1471 cm^{-1} increases in its intensity and simultaneously the 1488 cm^{-1} disappears (assigned to the symmetric stretching of C_β- C_β bond [144]). All these changes probably indicate the diacid form of TAPP formation because an analogous relative intensity increase of vibrational modes lying at higher wavenumbers was published for tetraaryl-substituted porphyrins [165] and was also observed for TMPyP in [132]. Moreover, the 1471 cm^{-1} band has been detected also for TMPyP and TPyP in acidic ambient (i.e. in the H_3Citr-Ag hydrosol/porphyrin systems [Chapter 5.1., Chapter 5.2.]).

Some similarities between SERRS spectra of TAPP in the Na_3Citr(1x10^{-5} M)-Ag hydrosol/TAPP system and in the H_3Citr-Ag hydrosol/TAPP systems can be pointed out, in particular: the 417, 986, 1320, and 1470 cm^{-1} bands. These bands are weak in Na_3Citr(1x10^{-5} M)-Ag hydrosol/TAPP system. Their weak intensity probably indicates that only a small portion of TAPP molecules is oriented similarly on Ag NPs surfaces in the Na_3Citr(1x10^{-5} M)-Ag hydrosol as in H_3Citr-Ag hydrosols, and cannot be metallated immediately. This situation changes after 2 days time-evolution as witnessed by the SERRS spectra of TAPP presented in Fig. 88 which demonstrate that the extent of TAPP metallation depends on Na_3Citr concentration as expected: the higher the Na_3Citr concentration, the lower the 397/334 ratio, and the lower extent of TAPP metallation. In addition to that, the overall SERRS spectral intensity decreases when metallation extent decreases.

Finally, the H_3Citr-Ag hydrosol/TAPP systems time evolution is shown in Fig. 89. While the systems containing the two higher H_3Citr concentrations (1x10^{-2} M and 1x10^{-3} M) have almost precipitated, the two others

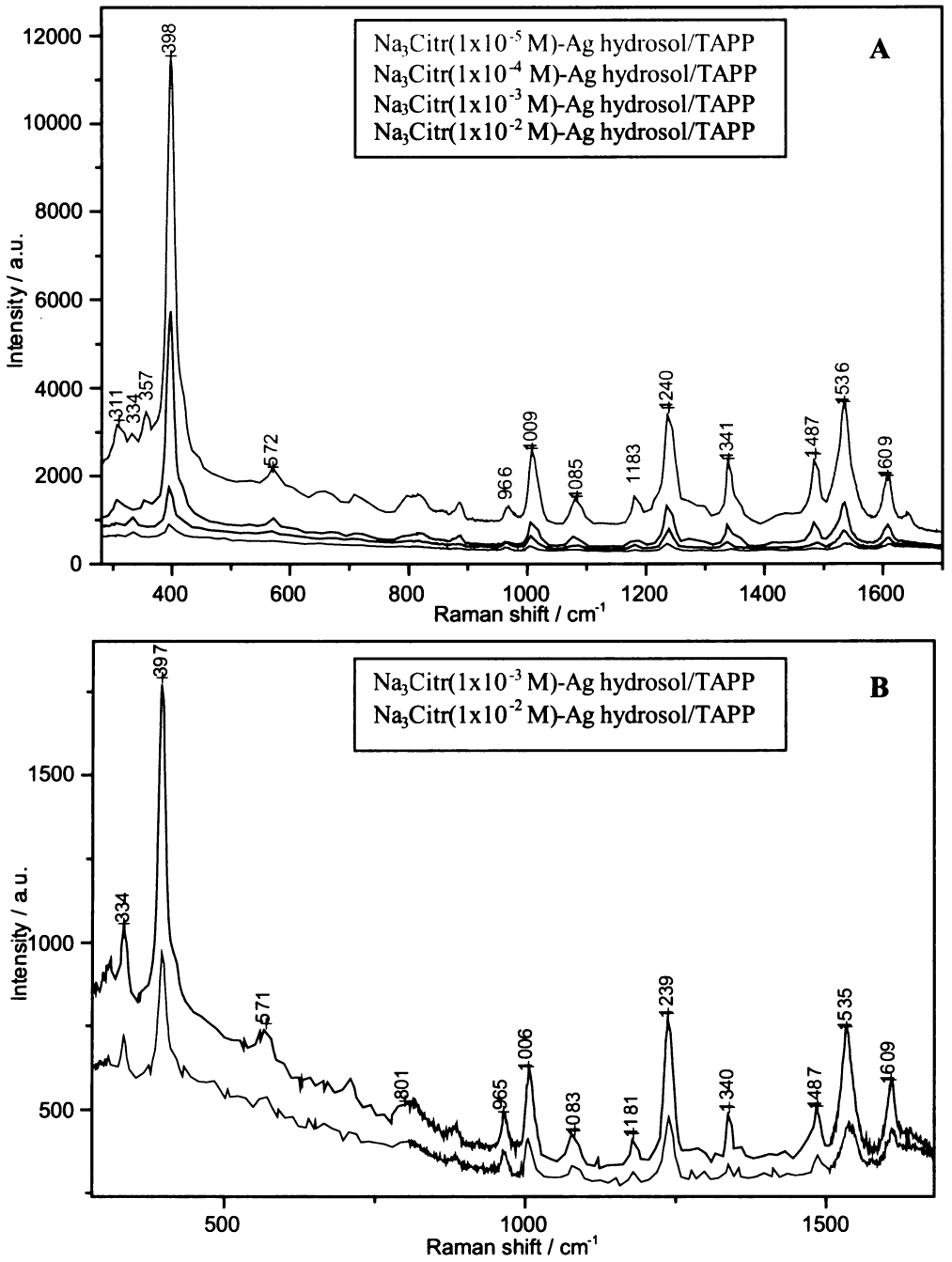

Fig. 88: SERRS spectra of Na_3Citr-Ag hydrosol/TAPP systems after 2 days of aging (A), and the details of two smaller Na_3Citr concentrations (B).

showed a slight increase in the intensities of their SERRS signals. The diacid TAPP form has been detected in systems with all H_3Citr concentrations after this long-time evolution.

Concerning the above mentioned SERRS signal pattern and intensity increase in H_3Citr-Ag hydrosol/TAPP systems (measured immediately after their preparation), an explanation analogous to that proposed in the previous section for TPyP molecules can be adopted. There are two important aspects: first, the presence of compact aggregates of Ag NPs in parent H_3Citr-Ag hydrosols [Chapter 4.4.1]; second, the higher protonation of the $-NH_2$ groups on TAPP substituents with the H_3Citr concentration increase which, in turn, promotes further aggregation of the NPs and previously formed compact aggregates in the H_3Citr-Ag hydrosol/TAPP system. The extent of the porphyrin protonation has been estimated on the basis of simple calculation similar to that made for TPyP in [164], under the assumption that the substituents of TAPP posses nearly the same pK_a value as that of aniline, which is of the 4.62 value [161].

The $H_3Citr(1x10^{-2}\,M)$-Ag hydrosol, which has manifested itself as the best substrate for SERRS of TAPP, has been investigated in more detail in order to elucidate its enormous SERRS activity. The SERRS spectral detection limit of TAPP has been determined to be $1x10^{-10}$ M (Fig. 90), however, the actual concentration value of this detection limit is most probably even lower (due to the fact that a lower actual concentration than the calculated one has to be considered in all systems containing TAPP).

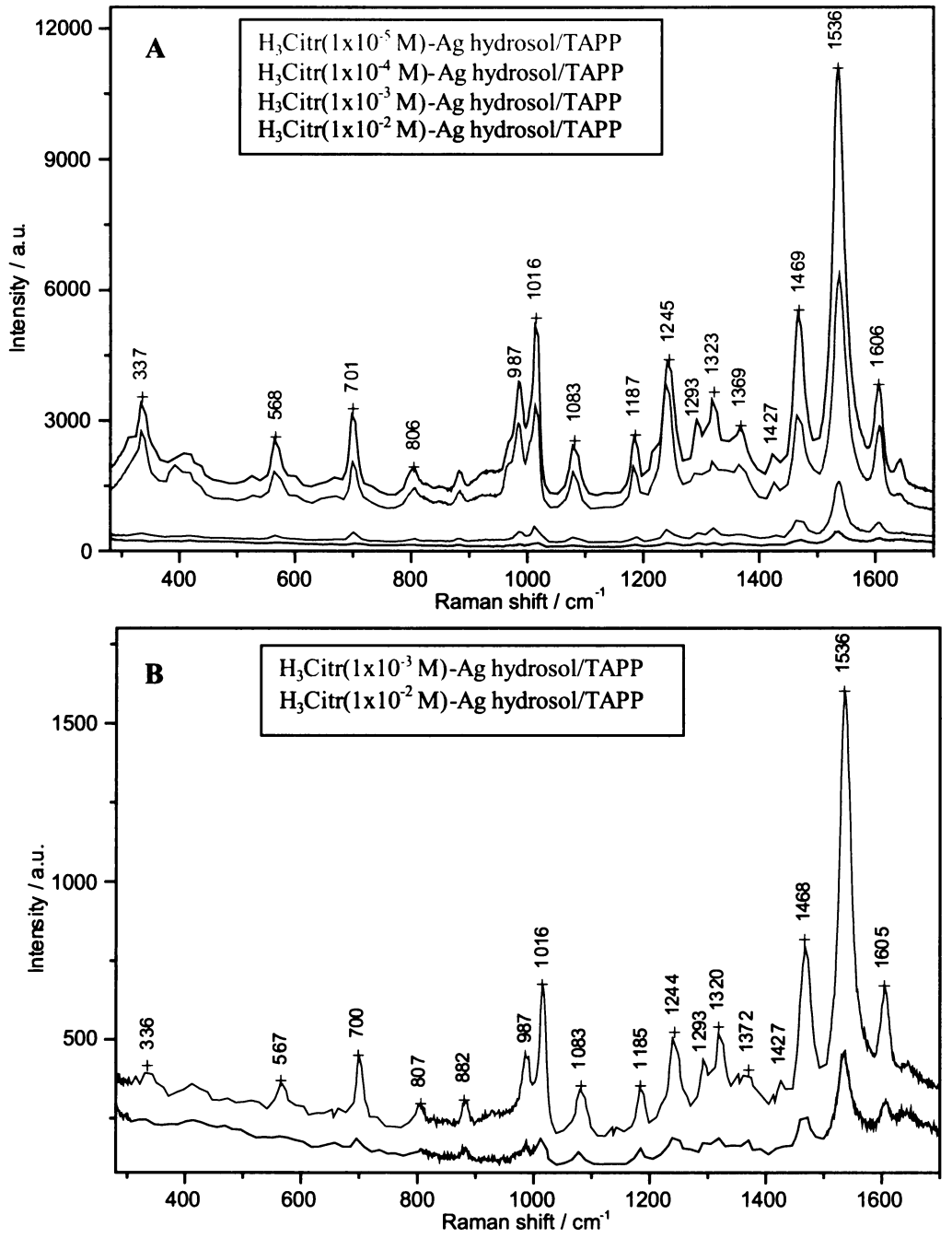

Fig. 89: SERRS spectra of H_3Citr-Ag hydrosol/TAPP systems after 2 days of aging (A), and the details of two smaller H_3Citr concentrations (B).

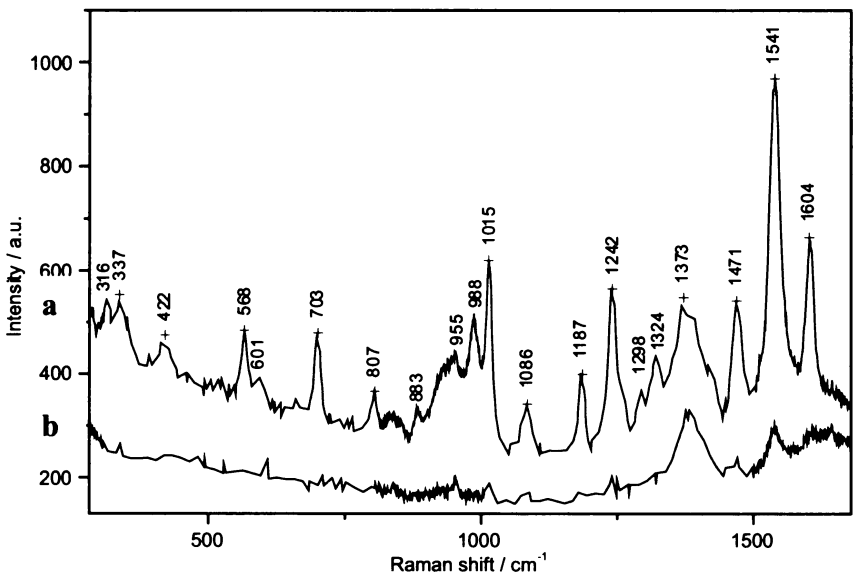

Fig. 90: SERRS spectra of $H_3Citr(1x10^{-2}$ M)-Ag hydrosol/TAPP systems with TAPP concentrations: (a) $1x10^{-10}$ M and (b) $1x10^{-11}$ M

TEM and HR-TEM images of the parent $H_3Citr(1x10^{-2}M)$-Ag hydrosol, of the $H_3Citr(1x10^{-2}M)$-Ag hydrosol/TAPP($2x10^{-8}M$), $H_3Citr(1x10^{-2}M)$-Ag hydrosol/TAPP($1x10^{-10}M$) and $H_3Citr(1x10^{-2}M)$-Ag hydrosol/TAPP($1x10^{-11}M$) systems are shown in Fig. 91. The observed morphological changes can be interpreted as it follows: while in the parent $H_3Citr(1x10^{-2}M)$-Ag hydrosol the single as well as interpenetrating NPs, either isolated, or coalesced into larger aggregates are observed (Figs 91A, 91B, 91C); in the $H_3Citr(1x10^{-2}M)$-Ag hydrosol/TAPP($2x10^{-8}M$) system, the indicies of a further aggregation are detected (Figs 91D, 91E) and NPs in the close touch (e.g. Fig. 91F) are very frequently encountered. This morphology correlates very well with the observed enormous SERRS spectral intensity and also with the instability of this system in the two days evolution. In the $H_3Citr(1x10^{-2}M)$-Ag hydrosol/TAPP($1x10^{-10}M$) system, the dispersed dimers and/or trimers (Fig. 91G) are observed, of course, simultaneously with the interpenetrated NPs coming from the parent hydrosol (Figs 91H, 91I). Finally, in the $H_3Citr(1x10^{-2}M)$-Ag hydrosol/TAPP($1x10^{-11}M$) system, the NPs in a close touch are present only scarcely (Fig. 91J) and, simultaneously, almost no SERRS spectral pattern of porphyrin is detected.

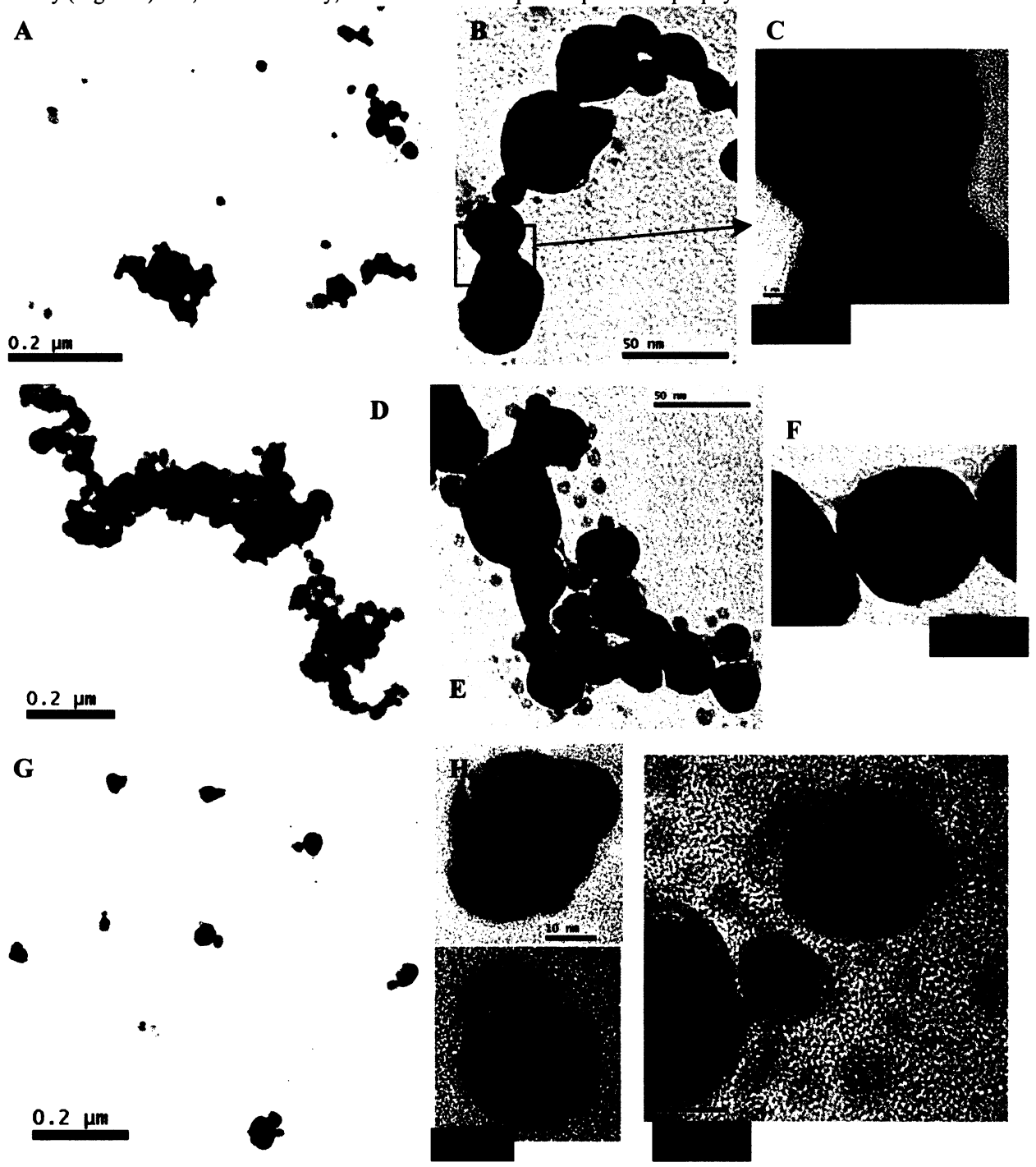

Fig. 91 : TEM and HR-TEM images of the parent $H_3Citr(1x10^{-2}M)$-Ag hydrosol (A, B, C) and of the $H_3Citr(1x10^{-2}M)$-Ag hydrosol/TAPP system with various TAPP concentrations in the final system: $2x10^{-8}M$ (D, E, F), $1x10^{-10}M$ (G, H, I), and $1x10^{-11}M$ (J). The distinction between NPs in touch (F, J) and/or interpenetrating (B, C, H, I) is clearly observable due to HR-TEM measurements.

Specifically, the comparison of the morphologies of Ag NPs and their aggregates encountered in the parent $H_3Citr(1x10^{-2}M)$-Ag hydrosol and in the $H_3Citr(1x10^{-2}M)$-Ag hydrosol/TAPP($1x10^{-10}M$) system (from which a complete SERRS spectrum of TAPP present in the extremely low, $1x10^{-10}M$ concentration, has been obtained) indicates that in addition to the "hot spots" in the compact aggregates present in parent $H_3Citr(1x10^{-2}M)$-Ag hydrosol (which could be occupied by TAPP molecules after their addition into the hydrosol), new "hot spots" are created by the formation of dimers and trimers of closely spaced (nearly touching) Ag NPs after the TAPP addition. It can be well assumed that the TAPP molecules have an important role in the formation of these dimers and trimers, and hence are efficiently incorporated into them, and consequently into "hot spots". Furthermore, since larger enhancements are predicted for molecules localized in "hot spots" in dimers and trimers of the closely spaced Ag NPs than in those of the interpenetrating Ag NPs [108, 119], it is quite probable that the largest contributions to the SERRS signal originate from TAPP molecules incorporated into dimers and trimers. Moreover, it is also highly probable that the protonation of the terminal amine groups of TAPP as well as of the TAPP macrocycle (diacid form formation) plays an important role in assembling of citrate-modified Ag NPs into the dimers and trimers.

5.4. APTPP

The UV-vis absoption spectrum of APTPP dissolved in ethanol is depicted in Fig. 92.

The RRS spectrum of APTPP (Fig. 93) has been also recorded at the same conditions as those of TAPP (Fig. 84). From their mutual qualitative comparison, one can conclude that both porphyrins have very similar RRS spectral patterns, however, some bands of the porphine macrocycle vibrations are slightly shifted to higher wavenumbers in the case of APTPP: 339, 1551, and 1611 cm^{-1} bands. The appearance of the additional bands at 414 and 1178 cm^{-1} can be possibly related to a lower symmetry of APTPP in comparison to TAPP.

The metallation markers have been detected as the band at 1343 cm^{-1} and the shoulders at 397 and 1538 cm^{-1} (Fig. 94). The overall intensity of SERRS spectrum in comparison to the RRS spectrum of APTPP is only slightly increased (approximately by 2 orders of magnitude). The metallation is very slow, and the w-Ag hydrosol/APTPP system is instable because it has precipitated within two days.

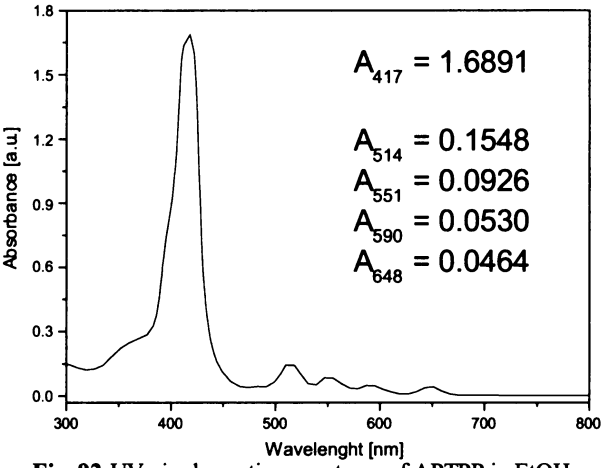

Fig. 92:UV-vis absorption spectrum of APTPP in EtOH.

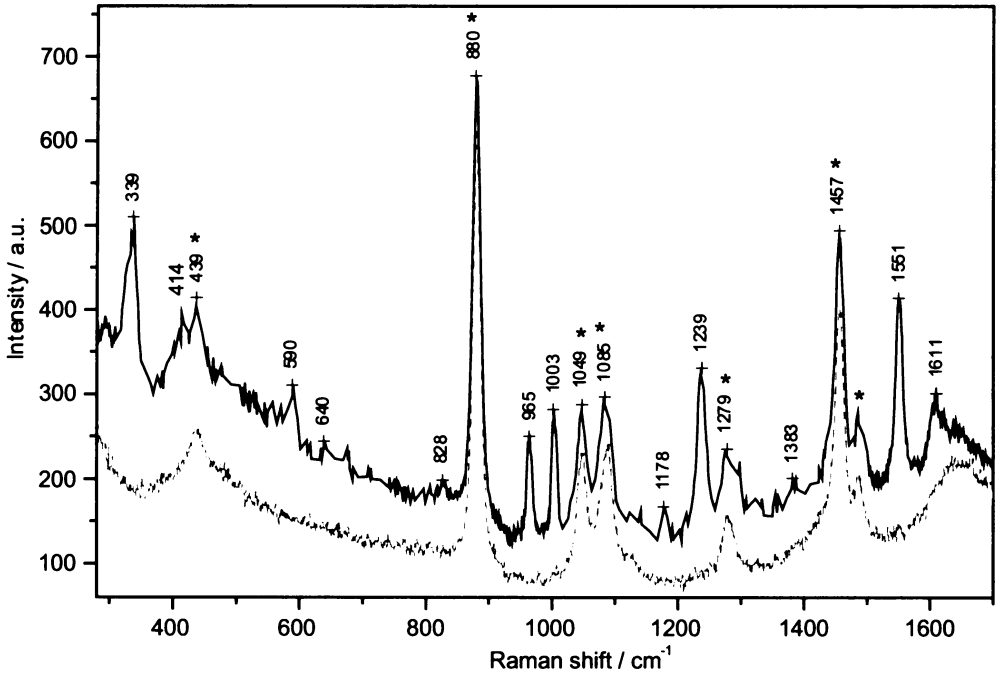

Fig. 93: RRS spectrum of $1x10^{-6}M$ APTPP in 10% EtOH (black spectrum), and RS spectrum of 10% EtOH (grey dash spectrum). Obviously, the peaks with asterix are the bands of EtOH.

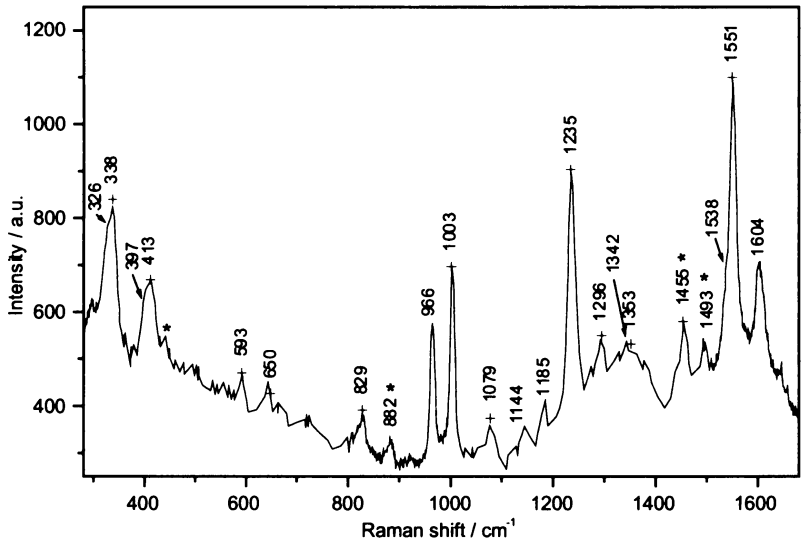

Fig. 94: SERRS spectrum of the w-Ag hydrosol/APTPP system. EtOH bands are labeled with asterix.

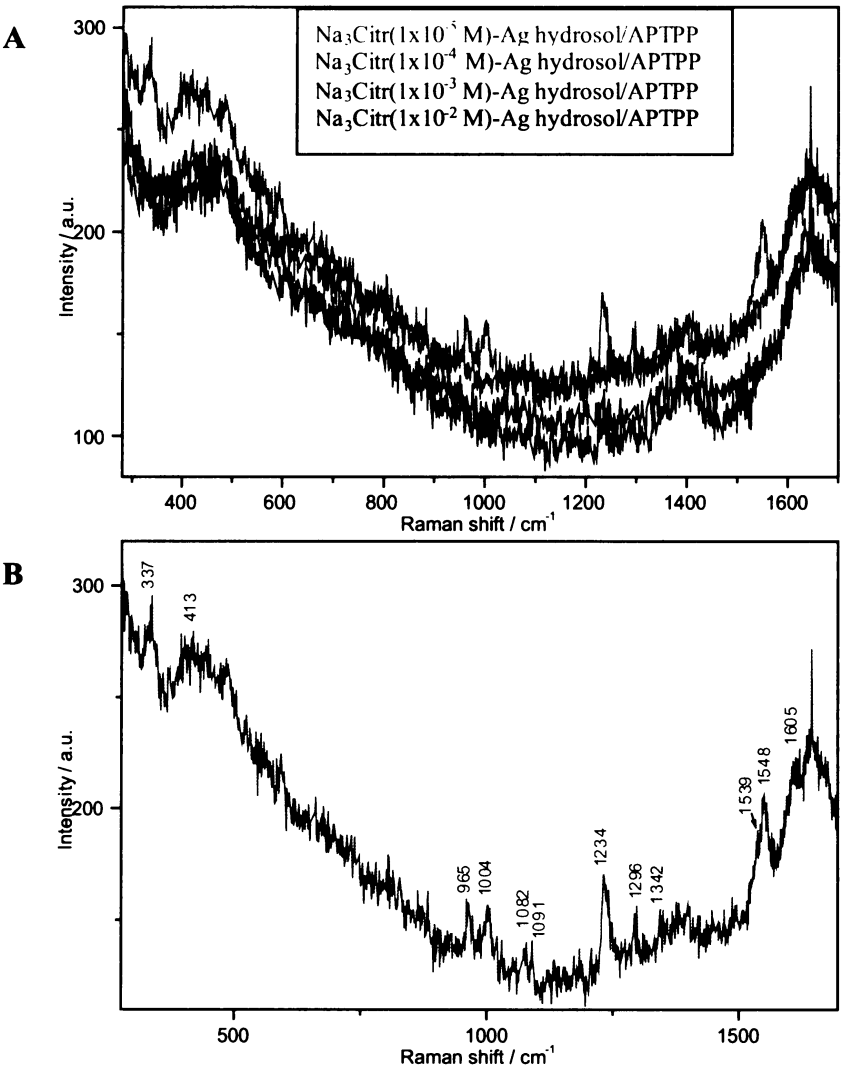

Fig. 95: SERRS spectra of (A) Na_3Citr-Ag hydrosol/APTPP systems with four different Na_3Citr concentration values, and (B) $Na_3Citr(1x10^{-5}$ M)-Ag hydrosol/APTPP system.

As for the Na_3Citr-Ag hydrosol/APTPP systems (Fig. 95) there has been almost no SERRS spectral signal of APTPP obtained from these systems. The exception is the lowest Na_3Citr concentration value (Fig. 95B) in which the metallation markers (the 1342 and 1539 cm^{-1} bands) slightly appear. Their appearance is more evident after two days of the $Na_3Citr(1x10^{-5}$ M)-Ag hydrosol/APTPP system evolution: the 401 cm^{-1}, a shoulder at 1005 cm^{-1}, the 1345 and 1538 cm^{-1} bands (Fig. 96). Moreover, the SERRS spectrum in the $Na_3Citr(1x10^{-4}$ M)-Ag hydrosol/APTPP system is also observed after two days of the system evolution. Therefore, one could conclude that the metallation of APTPP is citrate-concentration dependent (the higher the citrate concentration, the weaker the SERRS spectral signal) and it is more difficult to obtain a fully metallated APTPP than TAPP. The latter result is caused presumably by the presence of only one aminophenyl substituent group present in APTPP structure in comparison to four aminophenyl groups in TAPP.

In Fig. 97, the SERRS spectra of the H_3Citr-Ag hydrosol/APTPP systems are depicted. With the increasing H_3Citr concentration in the system, the intensity of the SERRS spectral signal of porphyrin increases. Comparing the SERRS spectral pattern of APTPP in acidic ambient with that of TAPP (in acidic ambient), it can be concluded that the diacid form of APTPP is generated in systems with the higher H_3Citr concentrations. The overall SERRS spectral pattern of acidified form of tetraphenylporphine published in [165], i.e. the splitting of some bands in the low-frequency region and simultaneously the higher relative intensity in the higher-frequency region, confirms further the APTPP diacid form presence.

In the two systems of lower H_3Citr concentrations ($1x10^{-5}$ M and $1x10^{-4}$ M), the formation of the diacid form has not been accomplished and the SERRS signal of the free base form of APTPP has been detected. The 1371 cm^{-1}

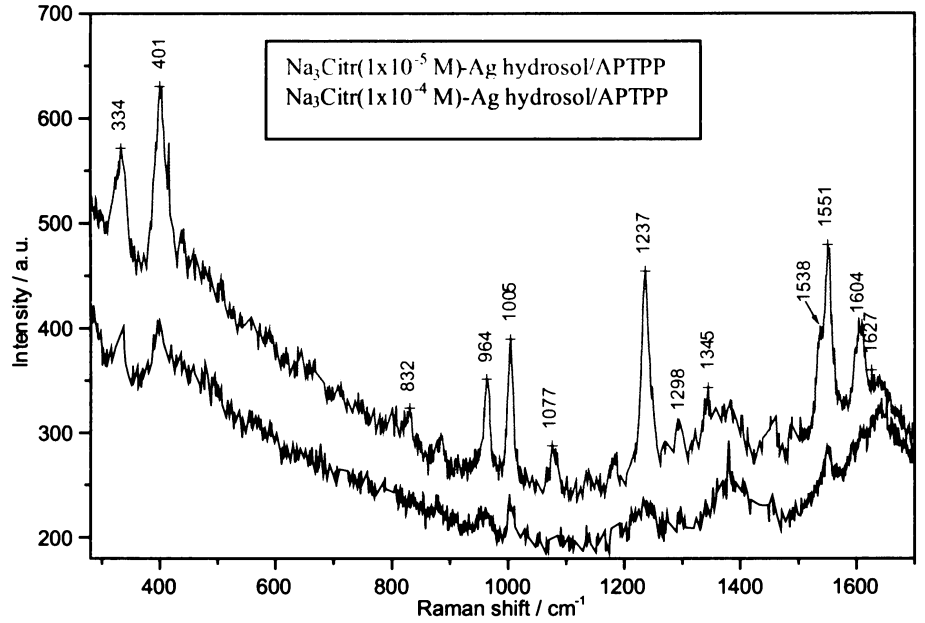

Fig. 96: SERRS spectra of Na_3Citr-Ag hydrosol/APTPP systems after 2 days of aging: two Na_3Citr concentrations: $1x10^{-5}$ M and $1x10^{-4}$ M.

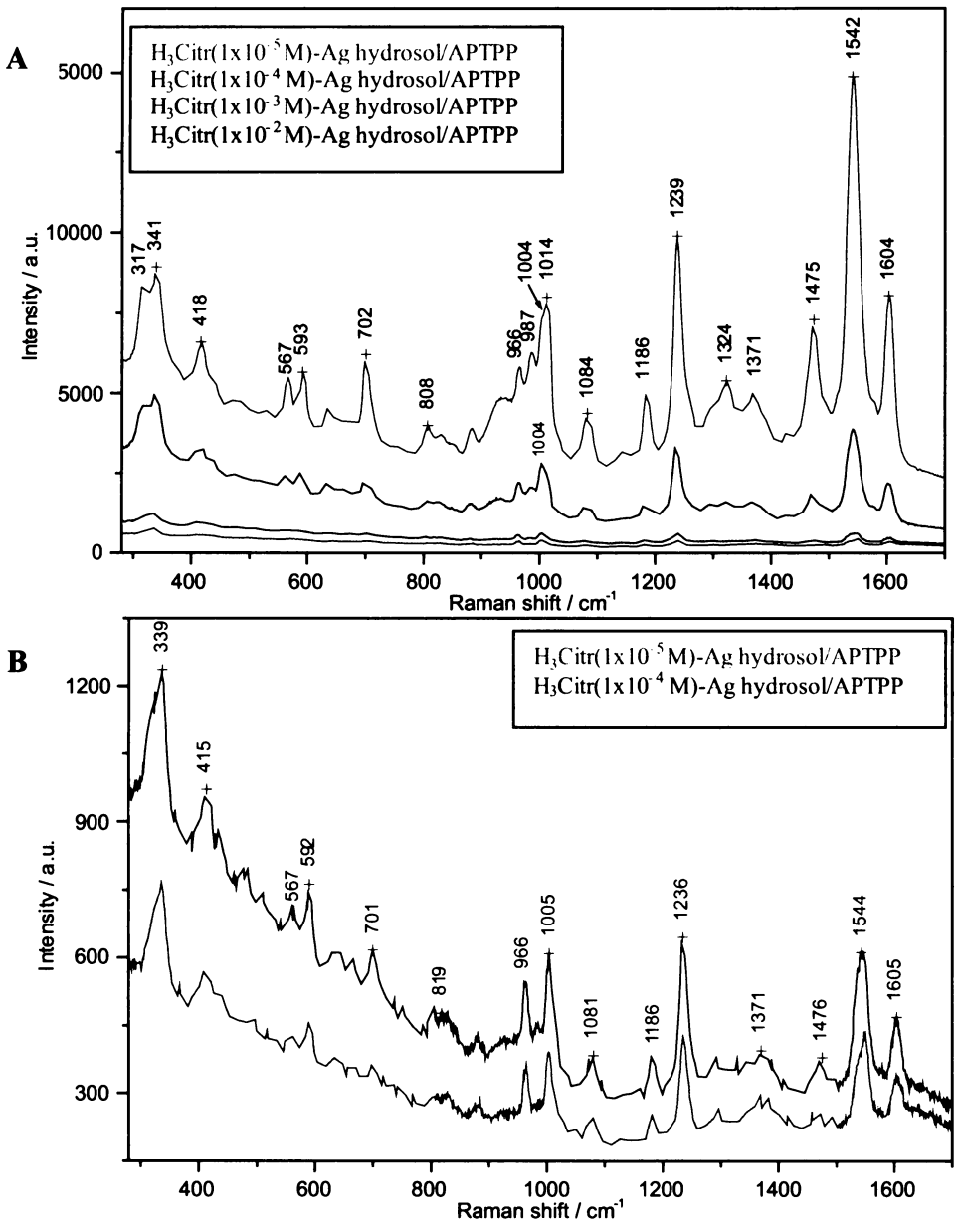

Fig. 97: SERRS spectra of (A) H_3Citr-Ag hydrosol/APTPP systems, and (B) the detail of SERRS spectra of two lower H_3Citr concentrations.

and 1475 cm^{-1} bands (observed already for TMPyP, TPyP, and TAPP porphyrins introduced into acidic ambient), and the 986 cm^{-1} band (detected in H_3Citr-Ag hydrosol/TPyP and/or H_3Citr-Ag hydrosol/TAPP systems) become more dominant with increasing H_3Citr concentration.

After 2 days of evolution, the H_3Citr-Ag hydrosol/APTPP systems with two higher H_3Citr concentrations ($1x10^{-3}$ M and $1x10^{-2}$ M) have already precipitated and therefore only the systems containing two lower H_3Citr concentrations are shown in Fig. 98. There are no substantial differences in SERRS spectral pattern and intensity with respect to the SERRS spectra of the freshly prepared systems (Fig. 97B).

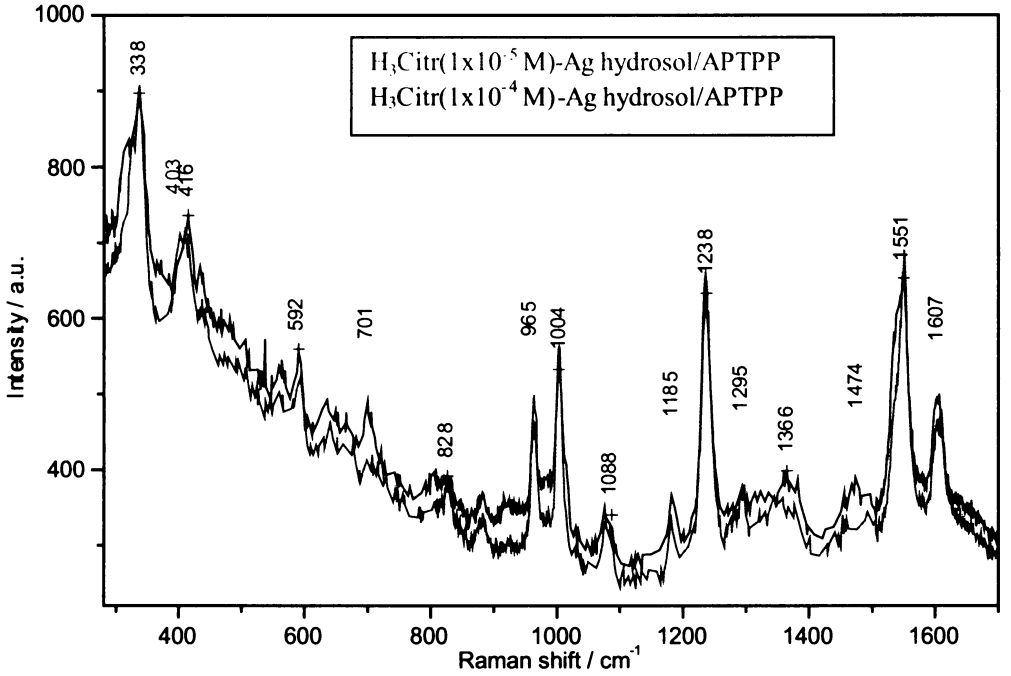

Fig. 98: SERRS spectra of H_3Citr-Ag hydrosol/APTPP systems after 2 days of aging: two H_3Citr concentrations: $1x10^{-5}$ M and $1x10^{-4}$ M.

In summation, the major differences between TAPP and APTPP SERRS spectra in citrate-Ag hydrosol/porphyrin systems originates from the different number of the terminal amine groups (four in comparison to one) which, apparently, governs the interaction of the porphyrin with the citrate-modified Ag NP surfaces.

5.5. TMPP

TMPP has been selected as a kind of referent porphyrin species, since, in neutral ambient, the phenyl-methoxy groups present in TMPP as substituents can hardly interact with carboxyl groups of citrates bound on NP surfaces. Therefore, it can well be expected that no SERRS signal of TMPP will be detected. On the other hand, in acidic ambient, the N-atoms of the porphine macrocycle can be protonized – similarly to TAPP and APTPP. TMPP can form diacid porphyrin (a cation) which is drawn to the Ag NP surfaces enveloped by dissociated citric acid molecules (anions). The results of SERRS spectral probing presented below are in a good agreement with these expectations.

The UV-vis absorption spectrum of TMPP dissolved in ethanol is depicted in Fig. 99.

TMPP has been introduced into the w-Ag hydrosol and into the Na_3Citr-Ag hydrosols with various Na_3Citr concentration values (in the $1x10^{-5}$ – $1x10^{-2}$ M range); however, no SERRS signal has been observed immediately (not shown here). After 2 days of systems evolution, only a negligible SERRS spectral signal of TMPP has been detected in the Na_3Citr($1x10^{-5}$ M)-Ag hydrosol/TMPP system (Fig. 100).

On the contrary, when TMPP has been introduced into the H_3Citr-Ag hydrosols (Fig. 101), the SERRS spectral pattern of porphyrin has been detected immediately after the system preparation. The intensity of the SERRS spectrum depends on H_3Citr concentration: while almost no SERRS spectral signal of TMPP has been distinguishable in the H_3Citr($1x10^{-5}$ M)-

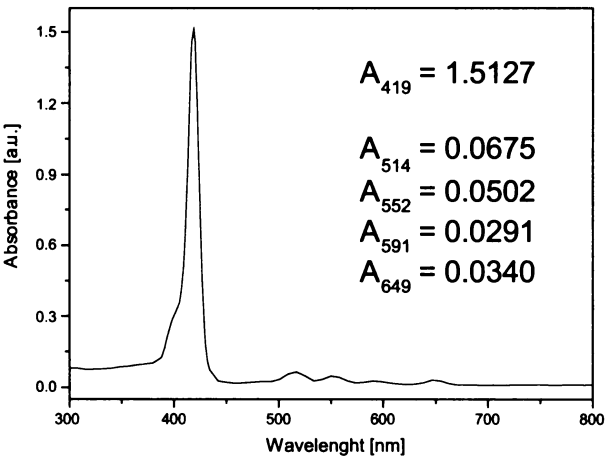

Fig. 99:UV-vis absorption spectrum of TMPP in EtOH.

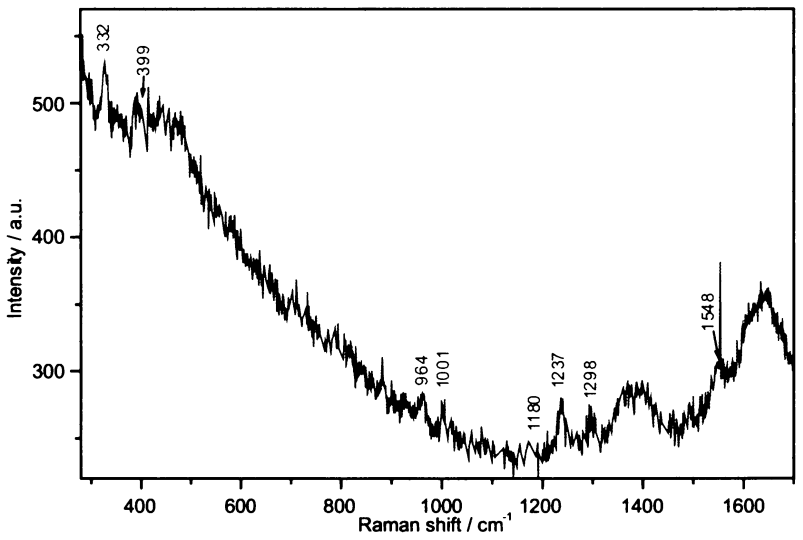

Fig. 100: SERRS spectra of the $Na_3Citr(1x10^{-5}$ M)-Ag hydrosol/TMPP system after 2 days of the system evolution.

Ag hydrosol/TMPP system (Fig. 101B); with increasing H_3Citr concentration, the SERRS spectral signal of TMPP occurs (Fig. 101B) and reaches its maximal intensity in the system with the highest H_3Citr concentration value (the black spectrum in Fig. 101A). An analogous observation has been made for all the other neutral (non-charged) porphyrins investigated (TPyP, TAPP, APTPP) and thus exactly the same explanation involving the two reasons (a specific morphology of the parent $H_3Citr(1x10^{-2}$ M)-Ag hydrosol and the protonation) as in their cases can be adopted.

The formation of the diacid form of TMPP in strongly acidic

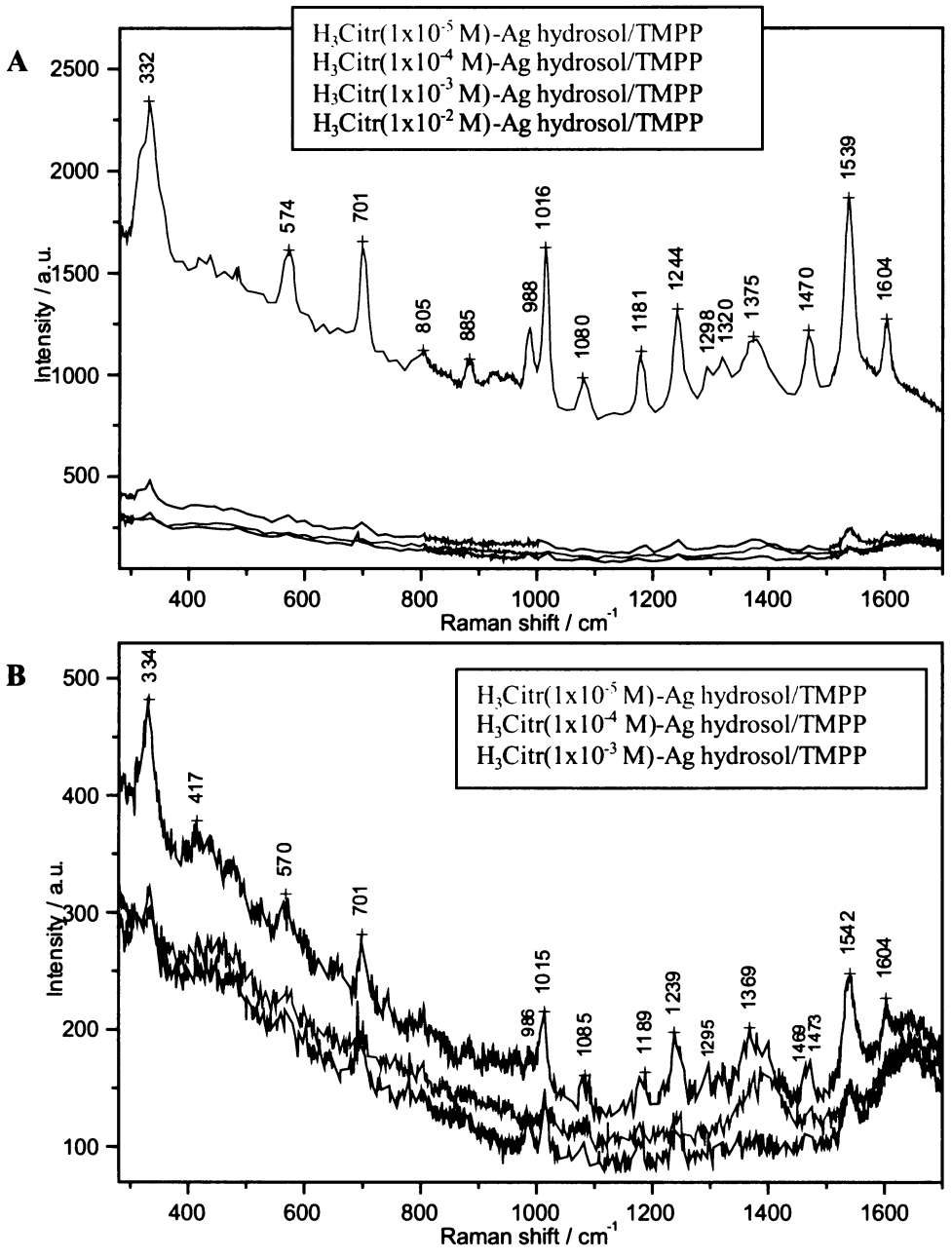

Fig. 101: SERRS spectra of (A) H_3Citr-Ag hydrosol/TMPP systems, and (B) the detail of SERRS spectra without that of the system containing the highest H_3Citr concentration.

ambient is evidenced by a splitting of the low-frequency region bands and by the 987, 1014, 1324 and 1475 cm^{-1} bands appearance. These bands are similar to those of TAPP and APTPP observed in their SERRS spectra in acidic ambient. However, the overall SERRS spectral pattern of relative band intensities even in the highest H_3Citr concentration ($1x10^{-2}$ M) does not correspond to those of diacid forms of TAPP and/or APTPP; hence, TMPP can be characterized as an acidified form.

As for the time evolution of H_3Citr-Ag hydrosol/TMPP systems (Fig. 102); these containing the two higher H_3Citr concentrations have precipitated within 2 days, while that with the $1x10^{-5}$ M H_3Citr concentration has

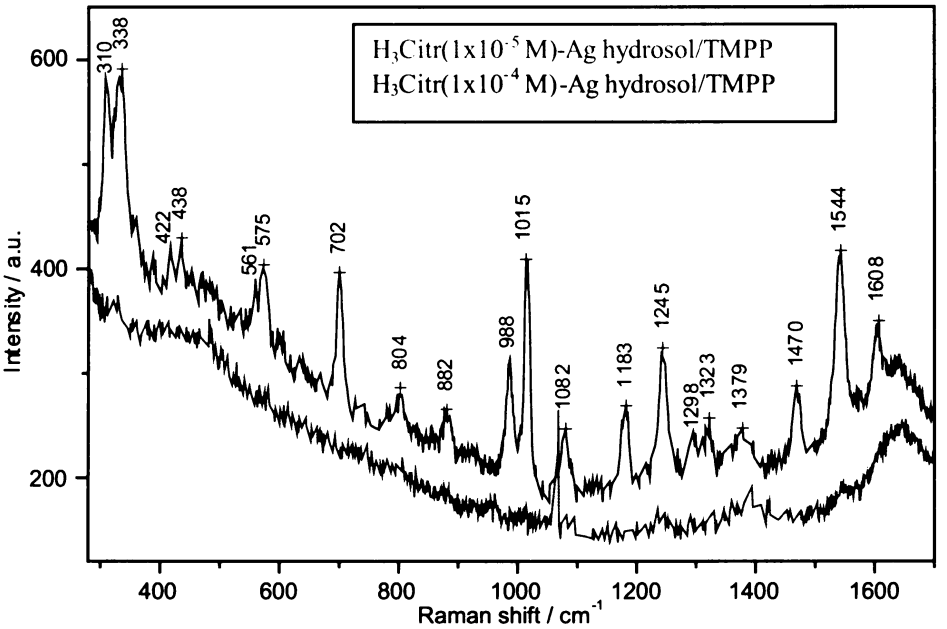

Fig. 102: SERRS spectra of $H_3Citr(1x10^{-5}M)$-Ag hydrosol/TMPP and $H_3Citr(1x10^{-4}$ M)-Ag hydrosol/TMPP systems after 2 days of aging.

remained practically unchanged (the comparison of the green spectrum shown in Fig. 101B with that in Fig. 102). The $H_3Citr(1x10^{-4}M)$-Ag hydrosol/TMPP system has just increased intensity of its SERRS spectrum while its SERRS spectral pattern remained the same.

5.6. Summary of results of SERRS spectral probing

In order to clearly sum up this chapter: (1) a schematic depiction of processes in citrate-hydrosol/porphyrin systems in both neutral and acidic ambient is presented in Fig. 103 and (2) the following results can be pinpointed:

- Ethanol (employed as a solvent for the preparation of porphyrin stock solutions) does not influence the porphyrin-Ag NP surfaces interaction.
- In Na_3Citr-Ag hydrosol/porphyrin systems:
  - The porphyrin-adsorbed citrate interaction is principally different for a positively charged and a neutral (non-charged) pophyrin
  - The presence of citrate ions on Ag NP surfaces prevents porphyrin metallation in short times after the introduction of porphyrin into Na_3Citr-Ag hydrosols, except of TAPP for which the metallation immediately proceeds probably due to a closer attachment of this porphyrin to the Ag surface enabled by four aminophenyl groups (which are both strongly argentophilic) – Table XXXVIII, Fig. 103A.
  - During the time evolution (of 2 days duration), citrate molecules can be replaced by porphyrin molecules, i.e. the formation of four Ag-N bonds in the Ag-metallated porphyrin species (the Ag-N bond between a suitable porphyrin and Ag NP surface is thermodynamically more preferable than the Ag-O bond between a citrate molecule and the Ag NPs surface) – Table XXXVIII, Fig. 103A.
  - The extent of porphyrin metallation in Na_3Citr-Ag hydrosol/porphyrin system is a function of Na_3Citr concentration (Fig. 75A): the higher the Na_3Citr concentration; the lower the extent of porphyrin metallation – Table XXXVIII.
- In H_3Citr-Ag hydrosol/porphyrin systems:
  - pH decrease stemming from the H_3Citr concentration increase highly influences the porphyrin-Ag NP surface interaction; especially in the case of non-charged porphyrins; because if the protonation proceeds a non-charged porphyrin becomes positively charged and, as a cation, it can easily interact with citrate anions bound on NP surfaces (Fig. 103B).

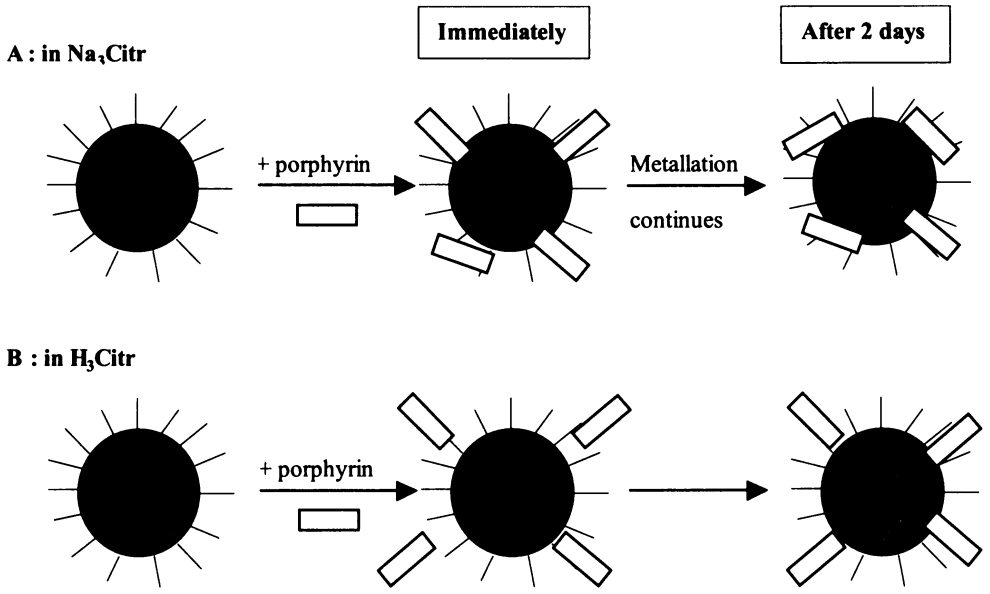

Fig. 103: Schematic depiction of the role of citrates in (A) neutral and/or (B) acidic ambient in the citrate-hydrosol/porphyrin systems . Ag NP (full grey circles) chemically modified by citrate anions (black lines) are able to interact with porphyrin molecules (open rectangles):
(A) in neutral ambient - due to their positive charges on substituents (TMPyP) and/or due to the N-atoms of their substituents (TAPP, APTPP, TPyP). A partial metallation occurs immediately or within the two-days evolution.
(B) In acidic ambient– the ionic interaction between citrate anions (stemming from dissociated citric acid molecules) and the protonized porphyrin molecules on their substituents (cations) and/or diacid forms of porphyrins reveals immediately. Porphyrins can further approach the Ag NP surface during the two-days period, however, no metallation proceeds in acidic ambient.
Therefore, porphyrins can be lying on Ag NP surfaces in neutral ambient (i.e. can be metallated); while they can be adsorbed edge-on on Ag NP surfaces in acidic ambient (i.e. cannot be metallated).

Table XXXVIII: Summary of results of SERRS spectral probing of Na_3Citr-Ag hydrosols by porphyrins

Porphyrin	Measured immediately	Measured after 2 days	Order of porphyrins according to their metallation allowance
TMPyP	Na_3Citr concentration increase = metallation decrease; except of the $Na_3Citr(1x10^{-2}M)$-Ag hydrosol/TMPyP system	Na_3Citr concentration increase = metallation decrease; except of the $Na_3Citr(1x10^{-2}M)$-Ag hydrosol/TMPyP system	2
TPyP	Na_3Citr concentration increase = metallation decrease	Na_3Citr concentration increase = metallation decrease	3
TAPP	Na_3Citr concentration increase = metallation decrease; except of the $Na_3Citr(1x10^{-5}M)$-Ag hydrosol/TAPP system	Na_3Citr concentration increase = metallation decrease; no exception further	1
APTPP	almost no metallation	Na_3Citr concentration increase = metallation decrease	4
TMPP	no metallation	hardly any metallation; except of the $Na_3Citr(1x10^{-5}M)$-Ag hydrosol/TMPP system	5

- Ag(0) adsorption sites have been encountered in $H_3Citr(1x10^{-5}$ M)-Ag hydrosol systems as witnessed by Ag(0)-TMPyP detection (Fig. 76).
- SERRS spectral features of diacid forms of TPyP, TAPP, APTPP and probably also of TMPP have been detected. Their relative contributions to the SERRS signal have increased with the

increasing H_3Citr concentration in the system, i.e. with decreasing pH. Porphyrins can be ordered as it follows with respect to their ability to form the diacid form:

TAPP >> APTPP > TMPP > TPyP, TMPyP.

The reason why some porphyrins can and the others cannot create the diacid form under the same conditions lies in different pK_a values of pronation of the N-atomes in the center of the porphine cycle. This difference is induced by the different character and number of substituents (aminophenyl, methoxyphenyl, or pyridyl) on the porphine cycle.

- The interaction between a particular porphyrin species and citrate-modified Ag NPs surface as probed for: TMPyP, TPyP, TAPP, APTPP, and TMPP, is governed by:
  A) peripheral substituent of the porphyrin macrocycle
     (i) positive or without charge,
     (ii) the presence (or absence) of terminal groups strongly interacting with Ag NPs surface
     - among the strongly interacting (argentophilic):
       1. flexibility or rigidity of bonding of the terminal group (flexible = e.g. phenyl-NH_2, and rigid = e.g. pyridyl);
       2. number of the terminal group in porphyrin structure.

  B) pH: neutral/acidic → particular pH:
     (i) the protonation of terminal groups at the particular system pH: phenyl-NH_2 > py;
     (ii) the possibilities of protonation of the N-atoms in the center of the porphyrin macrocycle;
     (iii) a partial protonation of the free $-COO^-$ group of adsorbed citrate to –COOH does not appear to be too significant (i.e. is difficult to determine), does not correspond to pK_a values for free non-adsorbed citrate/citric acid.
- Finally, the following new possibilities for SERRS spectral detection of porphyrins are offered by the employment of Na_3Citr-Ag hydrosols and H_3Citr-Ag hydrosols as substrates:
  (1) In $Na_3Citr(1x10^{-4}$ M)-Ag hydrosol/TMPyP, $Na_3Citr(1x10^{-3}$ M)-Ag hydrosol/TMPyP and H_3Citr-Ag hydrosol/TMPyP systems, the tetracationic porphyrin TMPyP is detected as an unperturbed, native free base porphyrin species; as opposed to the w-Ag hydrosol/TMPyP system, in which the metallated Ag-TMPyP species is detected. Since TMPyP is currently tested as an efficient photosensitizer for the photodynamic therapy of cancer, its selective detection, e.g. in tissue extracts, can be important for following the photosensitizers presence in important organ tissue (liver, kidney etc.). In that case; detection of the native free base species is highly important for the achievement of the selectivity of its detection in the presence of metalloporphyrins, particularly hem.
  (2) In $Na_3Citr(1x10^{-5}$ M)-Ag hydrosol/TPyP and $Na_3Citr(1x10^{-4}$ M)-Ag hydrosol/TPyP systems, the neutral porphyrin TPyP is detected predominantly in its native, free base form, yielding SERRS spectra with a substantially higher signal/noise ratios than that obtained from the w-Ag hydrosol/TPyP system. In addition to that, there are some indicies (namely, the limitation to the low Na_3Citr concentration in the system, the absence of any charged group which would enable porphyrin-citrate electrostatic attraction, and , simultaneously, no TPyP metallation) that TPyP is probably attached to Ag NP surface by the strongly argentophilic N-atoms of pyridyl peripheral substituent(s). In other words, TPyP is adsorbed edge-on, i.e. in a perpendicular orientation to the Ag NPs surface.
  A possibility of the edge-on adsorption of a neutral species containing pyridine moieties on Ag NPs surfaces in the $Na_3Citr(1x10^{-5}$ M)-Ag hydrosol has been demonstrated for bpy by detection of Ag^+-bpy surface species.
  This indicates that at low citrate coverages of Ag NPs, there are still some adsorption sites available for bpy (or TPyP) adsorption. Alternatively, the citrate coverage is still low enough to enable the penetration of the adsorbate with strongly argentophilic pyridine moieties to approach the surface and replace the citrate ions.
  Ag NPs modified by low coverages of adsorbed citrate ions and edge-on adsorbed TPyP would be employed for Ag NPs assembling into dimers and small aggregates using the TPyP molecules as linkers.
  (3) In $H_3Citr(1x10^{-2}$ M)-Ag hydrosol/TAPP system, the originally neutral porphyrin is converted into a hexacationic species $[H_6TAPP]^{4+}$ (by protonation at low pH) which is efficiently attracted to adsorbed citrate ions. An additional advantage of the $H_3Citr(1x10^{-2}$ M)-Ag hydrosol is the presence of compact aggregates of intergrown NPs, in which the numerous intersticies act as "hot spots" (after laser light excitation). Both factors probably contribute to the very low concentration value of the SERRS spectral detection limit of TAPP in this system, which is $1x10^{-10}$ M or lower.

Conclusions

(I) The results of the systematic investigations presented in this Thesis indicate that overall process of LA/NF of Ag target in aqueous media (pure water or aqueous solutions of ionic/molecular species) by ns laser pulses can be viewed as an interplay of the following processes:

1. transport of material (Ag) from the Ag target into the aqueous ablation medium (LA),
2. agglomeration of atoms, ions and clusters in the aqueous medium – nanocrystal (NP) growth,
3. stabilization of NP (nanocrystals) by build-up of electric bilayer,
4. fragmentation of NP (nanocrystals),
5. aggregation of NPs into aggregates of closely spaced or nearly touching particles,
6. aggregation of Ag NPs into aggregates – additional growth and interpenetration of Ag NPs.

(II) Our results show that these processes are largely interrelated. In particular, the following manifestations of interrelations of the processes have been encountered:

(a) Provided that the electric bilayer stabilizing the NPs is build efficiently in the progress of the LA/NF (3.), the process of NP aggregation (5.) is prevented due to electrostatic repulsion between the negatively charged outer parts of the electric bilayers enveloping the NPs. The outer part of the electric bilayer is constituted by anions which compensate the positive charges of Ag^+ ad-atoms present on Ag NP surfaces (under aerobic conditions).

In this Thesis, it has been demonstrated that introduction of ionic/molecular species into the aqueous ablation ambient principally affects the progress and outcome of LA/NF process (chiefly via this process (3.)). Nevertheless, it has also been demonstrated that the effect of some ions, namely chlorides is more complicated, (e.g. also pH dependent) and governs also occurrence of processes (6).

(b) Furthermore, it has been demonstrated for citrate ions that their presence and concentration in neutral ablation medium during LA/NF affects the efficiency of LA process (1.), which for all the citrate concentrations in the $1x10^{-5}$ M – $1x10^{-2}$ M range, is higher than for LA/NF in pure water. The efficiencies of LA step (1.) of the overall LA/NF process in pure water and in citrate solutions have been directly evaluated via determination of total Ag content in the aqueous ablation ambient after accomplishment of the LA/NF process and thus expressed in terms of the total amount of ablated Ag.

While the mechanisms of ion action during the LA process (1.) may be highly complicated and requires further investigation, a rather simple explanation of this effect based on a higher re-absorption of 1064 nm laser pulses prior to their impact on the Ag target by the w-Ag hydrosol (in which larger particles absorbing at 1064 nm are present) than by the citrate-Ag hydrosol (in which such particles are absent) is also possible.

(c) The increase of laser pulse energy, with which LA/NF is performed, results into an increase of the fraction of larger particles in the resulting Ag NP hydrosols. The effect decreases with the increased stabilization of Ag NPs, which has been achieved by introduction of stabilizing ionic species, in particular citrates in the neutral ablation medium and further decreases with their increasing concentration. Apparently, with the increase of laser pulse energy which corresponds to an increased efficiency of LA, i.e. more efficient transport of the material into solution (an evidence for that has been given in ref. 32), larger concentrations of stabilizing ions are required for production of small and well stabilized Ag NPs in the resulting Ag hydrosols.

Nevertheless, this straightforward correlation fails for chlorides at higher concentrations and in acidic ambient, and also for citrates in acidic ambient, most probably due to the processes of the compact aggregates formation (6.). More detailed conclusions about these processes are presented in [Paragraph (V)].

(III) Of the above listed processes, LA (1.) and NF (4.) are conditioned by laser pulse irradiation while the other processes can proceed both under illumination, and in the "dark". Therefore, in addition to the parameters previously employed for controlling of the above mentioned LA/NF process, namely laser pulse wavelength and energy per pulse, the continuous or step-wise performing of LA/NF emerges as another important parameter affecting the progress and outcome of the LA/NF.

The basic importance of this factor is demonstrated for LA/NF in water. In particular, more efficient formation and stabilization of small NPs during the step-wise LA/NF process involving the dark periods (in comparison to the LA/NF process performed with continuous irradiation) is attributed to more efficient redistribution of NPs due to continuous stirring and efficient electric bilayer build-up around the NPs during the "dark period".

Furthermore, it has been shown that the impact of this parameter is modified by the presence and action of ions intentionally introduced into the aqueous medium, and that it is different for ions strongly adsorbing on Ag NP surfaces (citrates) and those with strong ability of Ag^+ ions complexation (THS).

In particular, this parameter has virtually no importance when citrate ions are present in the neutral aqueous ablation medium (i.e. the results of the step-wise and continuously performed LA/NF were nearly the same in this case). This result is tentatively explained by strong stabilization of Ag NP by adsorbed citrate ions under irradiation (hence no dark periods are required for a more efficient stabilization of Ag NPs).

In contrast to that, this parameter has been found to affect markedly particularly the Ag NP aggregation process during LA/NF in aqueous THS solution. As an explanation, it is proposed that in the dark periods, THS ions cause perturbation of the electric bilayer around the NPs by extraction of Ag^+ ions [156] from Ag NP surfaces.

(IV) The effect of change of laser pulse wavelength from 1064 nm to 532 nm is different for each of the two major light-induced processes involved in LA/NF, i.e. for LA (1.) and NF (4.) performed in pure water. While LA proceeds more efficiently at 1064 nm, NF is more efficient at 532 nm. The observation is explained in the following manner: the absorption coefficient of bulk Ag (governing the efficiency of LA) is higher at 1064 nm than at 532 nm, while absorption of Ag NP (the determining factor for NF) is larger at 532 nm than at 1064 nm. As a result, a consecutive LA/NF procedure with 1064 nm and 532 nm has been tested and shown to be an optimal procedure for preparation of small Ag NPs hydrosols of low polydispersity.

(V) (a) The presence of OH^-, Cl^-, and citrate anions in the aqueous ablation medium in the course of LA/NF performed with 1064 nm laser pulses has been found to promote the formation of small NPs and their stabilization; nevertheless, with some ion-specificity and limitations.

In particular, in the case of chlorides, there is a threshold Cl^- concentration above which a destabilizing effect occurs. The threshold concentration is pH dependent and decreases at low pH values. The formation of compact aggregates of intergrown Ag NPs (6.) has been found to be responsible for these results. In consequence of that, the optimal concentration for maximal stabilization has been found to be dependent on laser pulse energy and to increase with the increasing energy per pulse value. Therefore, this optimal concentration appears to be affected by the efficiency of LA (1.) and NF (4.). This, in turn, indicates that the parameter governing the onset of compact aggregates formation is the coverage estimated according to [112] to be close to a monolayer of Ag NPs by adsorbed chlorides.

In the case of citrate ions presence in neutral ablation medium, the small NPs formation and stabilization increases monotonously with the increasing citrate concentration (in the $1x10^{-5}$ M – $1x10^{-2}$ M range). This concentration dependence is maintained for laser pulse energies values in the 200 - 400 mJ/pulse range. Therefore, it can be concluded that stabilization of Ag NPs by adsorbed citrates proceeds though an efficient build-up of electric bilayer enveloping the NPs (3.) and, in the overall range of citrate concentration, is not complicated by other processes, namely (6.).

Concerning citrate ions presence in acidic ablation medium, interference of processes (6.) has been encountered. While the lower stabilizing effect of citrates in acidic ambient can be well understood in terms of a partial protonation of anionic $-COO^-$ groups to neutral –COOH, which leads to a decrease of the electrostatic repulsion among the NPs in the hydrosol, it is not yet clear why processes (6.), rather than (5.) occur in this particular case.

Furthermore, the specificity of the stabilizing effect of OH^-, Cl^-, and/or citrate anions manifest itself also during aging of Ag hydrosols prepared by LA/NF in the presence of these ions in the aqueous ablation medium. The long-term (one or several weeks) stabilization effect of the anions increases in the sequence: $OH^- < Cl^-$ < citrate.

(b) The presence of Ag^+ cations and/or THS anions in the aqueous ablation medium leads to the decrease of the efficiency of small Ag NPs formation and, particularly, of their stabilization. The destabilization effects stem most probably from inefficient build-up of the electric bilayer around the NPs (namely for Ag^+), or its perturbation (for THS), which, in turn, allows the process of NP aggregation (5.) to progress during LA/NF.

(VI) The principal advantages of LA/NF of Ag target in aqueous ambient as a method of controlled preparation of Ag NP hydrosols targeted towards their further applications in plasmonics in general, and SERS/SERRS spectroscopy in particular, have been demonstrated in the following manner:

(a) Ag NP hydrosol containing chiefly small Ag NPs (5-35 nm) weakly stabilized most probably by OH^- or HCO_3^- ions (but sufficiently stable for further applications) have been prepared by LA/NF carried out subsequently with the ns laser pulses of 1064 nm and 532 nm wavelength in pure water and of ca 200 mJ/pulse and ca 60 mJ/pulse energies, respectively. These Ag NP hydrosols can be used for further applications either directly, or after treatment by selected agents. The conclusions about functioning of both the native and the treated hydrosols as substrates for SERS and SERRS spectroscopy are presented in [Paragraph (VII)].

(b) Two types of hydrosols of Ag NPs functionalized by adsorbed citrates have been prepared:

(i) Hydrosols of small Ag NPs well stabilized through their functionalization by adsorbed citrate ions (bidentatelly coordinated by two carboxylate groups to Ag NPs surface) have been prepared by LA/NF with ns laser pulses of 1064 nm wavelength and of 200 – 400 mJ/pulse energies in sodium citrate solutions of $1x10^{-5}$ M – $1x10^{-2}$ M concentrations.

(ii) Alternatively, hydrosols containing compact aggregates of touching and intergrown Ag NPs were obtained by LA/NF carried out (under the same conditions as in (i)) in citric acid solutions.

The conclusions about the possibilities and distinct advantages of application of these hydrosols of Ag NPs functionalized by citrate ions in various coverages (varied through variations of sodium citrate concentrations in the aqueous ablation media), in various protonation states and system pH (varied by the variations of citric acid

concentrations in the aqueous ablation medium) as substrates for SERRS of selected porphyrin species are presented in [Paragraph (VIII) and in Paragraph (IX)].

(c) Two types of hydrosols of Ag NPs functionalized by adsorbed chlorides have been prepared:

(i) Hydrosols of small Ag NPs efficiently stabilized by adsorbed chlorides resulted from LA/NF by ns laser pulses of 1064 nm wavelength using the following combinations of laser pulse energies and chloride concentrations ($1x10^{-4}$ M NaCl and ~200 mJ/pulse, $1x10^{-3}$ M NaCl and ~300 mJ/pulse).

(ii) Hydrosols of compact Ag NP aggregates containing touching and interpenetrating NPs result from LA/NF carried out by ns laser pulses of 1064 nm wavelengths in neutral chloride solutions with chloride concentrations $>1x10^{-3}$ M, and in acidic chloride solutions.

SERS spectral probing of these hydrosols by testing adsorbate 2,2'-bipyridine has shown that each of the hydrosols represents a different substrate for SERS spectroscopy. In particular, oxidized Ag^+ adsorption sites are the only ones available on surfaces of Ag NPs in hydrosols (i). In contrast to that, Ag(0) adsorption sites are available (probably in addition to Ag^+ sites) on surfaces of Ag NPs in hydrosols (ii).

In addition to that, compact aggregates of Ag NPs in hydrosols (ii) probably serve as very efficient light-amplifiers in the EM mechanism of SERS owing to the numerous intersticies between NPs, which, after laser irradiation in the SERS experiment, represent "hot spots", i.e. nano-scale locations of very strong optical fields. Large SERS enhancement are witnessed by very low concentration value of SERS spectral detection limit of bpy which is $1x10^{-7}$ M – $1x10^{-8}$ M.

(VII) SERS spectral testing of Ag NP hydrosols prepared by the optimized LA/NF procedure employing sequentially laser pulses of 1064 nm and 532 nm wavelengths, and of their chemical modifications via the action of Ag^+, BH_4^-, THS, and/or Cl^- ions has shown several possibilities of preparation of such substrates for SERS spectroscopy, on which Ag(0) adsorption sites (not encountered on commonly used, oxidized Ag NP surfaces) are available.

The formation of Ag(0) adsorption sites on Ag NP surfaces has been induced by treatment of Ag NP by agents containing BH_4^-, THS, and/or Cl^- ions, however, the mechanisms of Ag(0) adsorption sites formation are probably somewhat different for each of the agent.

In the case of THS, Ag(0) adsorption sites became available in consequence of extraction of Ag^+ ions from Ag NPs surfaces by THS and their complexation into water soluble complexes, as proposed in [156].

In the case of Cl^-, Ag(0) adsorption sites can possibly be located amidst those fully occupied by adsorbed chlorides, which causes a local change of Fermi level position of Ag.

Finally, the Ag(0) adsorption sites can be formed by reduction of Ag^+ sites by BH_4^-, which is a strong reducing agent. In this particular case, the existence of these adsorption sites can be gradually cancelled by addition of excess Ag^+ ions. Therefore, there is a possibility of reversible tuning of the presence (by BH_4^- action) or absence (by Ag^+ action) of Ag(0) adsorption sites which creates a situation similar to changes of applied potential on Ag electrodes.

(VIII) SERRS spectral probing of the Ag NP hydrosols, prepared by LA/NF with ns laser pulses of 1064 nm wavelength and of 300 mJ/pulse energy in sodium citrate or citric acid solutions of $1x10^{-5}$ M – $1x10^{-2}$ M concentration by the selected free base porphyrin species TMPyP, TPyP, TAPP, APTPP and TMPP, has shown that the adsorbed citrate ions (possibly partially protonized in acidic media) can play the following roles in adsorption of other molecular species, namely porphyrins:

(a) Molecular spacer, i.e. a species which is attached to Ag NPs surface (by two carboxylate groups) and possesses also free functional group (one free carboxylate group) suitable for attachment of other molecules into the vicinity of Ag NPs surface via a specific interaction (electrostatic attraction of positively charged species, such as cationic porphyrins as demonstrated for TMPyP). Positive charging of neutral porphyrins can be achieved by protonation of their macrocycle (i.e. diacid form formation) or peripheral substituents, as demonstrated for TPyP, TAPP, APTPP, and TMPP.

(b) Pre-orienting matrix inducing edge-on adsorption of other species possessing strongly argentophilic groups with the donor atom (e.g. N) fixed into a rigid arrangement (e.g. N of the pyridine heterocycle). Adsorbed citrates have been found to work as a pre-orienting matrix for edge-on adsorption of TPyP.

(c) The weaker adsorbate which is rejected (desorbed) from the Ag NP surface by more strongly adsorbing species. In the case of porphyrins, this process is conditioned by the formation of Ag-metalloporphyrin species as the thermodynamically more stable surface species. The rate of citrate substitution by a porphyrin is most probably dependent on peripheral substituents of the porphyrin, and has been found to be high for TAPP, which possesses four strongly argentophilic $-NH_2$ groups. These all can be bonded to Ag NP surfaces by the lone pair on N-atoms, while, simultaneously, the porphyrin macrocycle is oriented parallel to the Ag NP surface and is thus ready for metallation.

(IX) The most suitable and versatile substrate for SERRS is H_3Citr($1x10^{-2}$ M)-Ag hydrosol which allows for detection of positively charged (cationic TMPyP) as well as "neutral" porphyrin species (TPyP, TAPP, APTPP, TMPP) which become positively charged due to low pH. The positive charging results from protonation of either

their N-containing terminal group(s), or of N-atom in the center of porphyrin macrocycle (diacid form formation), or both.

In particular, TAPP is detected as a hexacationic species due to diacid form formation and protonation of all 4 amine groups ($NH_2 \rightarrow NH_3^+$). For this particular porhyrin, the concentration value of SERRS spectral detection limit is $1x10^{-10}$ M (or lower), and the SERRS signal is estimated to be about 30x higher than in the system with w-Ag hydrosol. Large SERRS enhancement are proposed to originate from the presence of compact aggregates in the substrate which, in specific cases such as the last mentioned system, can be complemented by formation of dimers and trimers of very closely spaced Ag NPs into which TAPP molecules are incorporated.

Other specific systems:

(a) $Na_3Citr(1x10^{-3}$ M)-Ag hydrosol, $Na_3Citr(1x10^{-4}$ M)-Ag hydrosol, and $H_3Citr(1x10^{-5}$ M)-Ag hydrosol are the most suitable substrates for the detection of TMPyP in its native free base form. In the system with the last mentioned substrate, Ag(0)-TMPyP surface species has been detected after 2 days of system aging.

(b) $Na_3Citr(1x10^{-5}$ M)-Ag hydrosol and $Na_3Citr(1x10^{-4}$ M)-Ag hydrosol are the substrates allowing for SERRS spectral detection of the native free base form of TPyP. In this system, the citrate-modified Ag NPs surface is proposed to serve as a pre-orienting matrix for edge-on adsorption of TPyP which represents a porphyrin species with four rigidly positioned, strongly argentophilic N-atoms of the peripheral pyridyl groups.

References and notes

[1] Maier, S. A. *Current Nanoscience* **2005**, *1*, 17.
[2] Moskovits, M. *J. Raman Spectr.* **2005**, *36*, 485.
[3] Baker, G. A., Moore, D. S. *Anal. Bioanal. Chem.* **2005**, *382*, 1751.
[4] McFarland, A. D., Van Duyne, R. P. *Nano Lett.* **2003**, *3*, 1057.
[5] Rotello, Vicent *Nanoparticle building blocks for nanotechnology, part 7: Plasmonic nanomaterials*, University of Massachussets, **2004**.
[6] Bohren, C.F. , Hufman, D.F. *Absorption and Scattering of Light by Small Particles*, Wiley&Sons, New York, **1983**.
[7] Maier, S. A., Brongersma, M. L., Kik, P. G., Meltzer, S., Requicha, A. A. G., Atwater, H. A. *Adv. Mater.* **2001**, *13*, 1501.
[8] Kelly K. L., Coronado, E., Zhao, L. L., Schatz, G. C. *J. Phys. Chem. B* **2003**, *107*, 668.
[9] Johansson, P., Xu, H., Käll, M. *Phys. Rev. B* **2005**, *72*, art. No. –035427.
[10] Fojtik, A., Henglein, A. *Ber. Bunsenges. Phys. Chem.* **1993**, *97*, 252.
[11] Procházka, M., Mojzeš, P., Štěpánek, J., Vlčková, B., Turpin, P-Y. *Anal. Chem.* **1997**, *69*, 5103.
[12] Bae, C. H., Nam, S. H., Park, S. M. *Applied Surface Science* **2002**, *197-198*.
[13] Srnová, I., Procházka, M., Vlčková, B., Štepánek, J., Malý, P. *Langmuir* **1998**, *14*, 4666.
[14] Mafuné, F., Kohno, J.-Y., Takeda, Y., Kondow, T. *J. PHys. Chem. B* **2003**, *107*, 12589.
[15] Cliffel, D. E.; Zamborini, F. P.; Gross, S. M.; Murray, R. W. *Langmuir* **2000**, *16*, 9699.
[16] von der Linde, D, Sokolowski-Tinten, K. *Applied Surface Science* **2000**, *154-155*, 1.
[17] von der Linde, D. et al. *J. Opt. Soc. Am. B* **1996**, *13*, 216.
[18] Semerok A., Chaléard, C., Detalle, V., Lacour, J.-L., Mauchien, P., Meynadier, P., Nouvellon, C., Sallé, B., Palianov, P., Perdrix, M., Petite, G. *Appl. Surf. Sci.* **1999**, *138-139*, 311.
[19] Kononenko T.V, Garnov, S. V., Klimentov, S. M., Konov, V. I., Loubnin, E. N., Dausinger, F., Raiber, A., Taut, C. *Appl.Surf.Sci* **1997**, *109/110*, 48.
[20] Ihlemann, J., Scholl, A., Schmidt, H., Wolff-Rottke, B. *Appl. Physics A* **1995**, *60*, 411.
[21] Momma, C. et al. *Opt. Commun.* **1996**, *129*, 134.
[22] Von Der Linde, D. et al. *Appl. Surf. Sci.* **1997**, *109–110*, 1.
[23] Phipps, C.R. et al. *J. Appl. Phys.* **1988**, *64*, 1083.
[24] Tsuji t., Kakita, T., Tsuji, M. *Applied Surface Science* **2003**, *206*, 314.
[25] Tsuji,T., Tsuboi, Y., Kitamura, N., Tsuji, M. *Appl. Surf. Sci.* **2004**, *229*, 365.
[26] Yoo, Y.H. et al. *J. Appl. Phys.* **2000**, *88*, 1638.
[27] Walton, A.J. et al. *Adv. Phys.* **1984**, *33*, 595.
[28] Zhu, S., Lu, Y. F., Hong, M. H. *Appl. Phys. Lett.* **2001**, *79*, 1396.
[29] Kabashin, A. V., Meunier, M. *J.Appl.Phys.* **2003**, *94*, 7941.
[30] Bruneau, S., Hermann, J., Dumitru, G., Sentis, M., Axente, E. *Appl.Surf.Sci* **2005**, *248*, 299.
[31] Tsuji, T., Iryo, K., Nishimura, Y., Tsuji, M. *J. Photochem. Photobio. A: Chemistry* **2001**, *145*, 201.
[32] Šmejkal, P., Pfleger, J.; Vlčková, B.; Dammer, O. *Journal of Physics - accepted.*
[33] Zhigilei, L. V.; Garrison, B. J. *Appl. Phys. A* **1999**, *69*, S75.
[34] Perez, D.; Lewis, L. J. *Phys. Rev. Lett.* **2002**, *89*, 255504.
[35] Bogaerts, A., Chen, Z., Gijbels, R., Vertes, A. *Spectrochim. Acta B* **2003**, *58*, 1867.
[36] Mafune´, F., Kohno, J.-y., Takeda, Y.,Kondow, T. *J. Phys. Chem. B* **2000**, *104*, 9111.
[37] Link, S.; Burda, C.; Mohamed, M. B.; Nikoobakht, B.; El-Sayed, M. A. *J. Phys. Chem. A* **1999**, *103*, 1165.
[38] Amoruso, S.; Ausanio, G.; Barone, A. C.; Bruzzese, R.; Gragnaniello, L.; Vitiello, M.; Wang, X. *J. PHys. B.: At. Mol. Opt. Phys.* **2005**, *38*, L329.
[39] Pereira, A.; Cros, A.; Delaporte, P.; Georgiou, S.; Manousaki, a.; Marine, W.; Sentis, M. *Appl. Phys. A* **2004**, *79*, 1433.
[40] Tsuji T., Iryo, K., Watanabe, N., Tsuji, M. *Applied Surface Science* **2002**, *202*, 80.
[41] Brause, R.; Möltgen, H.; Kleinermanns, K. *Applied Physics B, Laser and Optics* **2002**, *75*, 711.
[42] Hajiesmaeilbaigi, F.; Mohammadalipour, A.; Sabbaghzadeh, J.; Hoseinkhani, S.; Fallah, H. R. *Laser Phys. Lett.* **2006**, *3*, 252.
[43] Tarasenko, N. V.; Butsen, A. V.; Nevar, E. A. *Appl.Surf.Sci* **2005**, *247*, 418.
[44] Burakov, V. S.; Tarasenko, N. V.; Butsen, A. V.; Rozantsev, V. A.; Nedelko, M. I. *Eur. Phys. J. Appl. Phys.* **2005**, *30*, 107.
[45] Mafuné, F.; Kondow, T. *Chem. Phys. Lett.* **2003**, *372*, 199.
[46] Pfleger, J.; Šmejkal, P.; Vlčková, B.; Šlouf, M. *Proceedings of SPIE* **2003**, *5122*, 198.
[47] Sylvestre, J.-P.; Kabashin, A. V.; Sacher, E.; Meunier, M. *Appl. Phys. A: Materials Science & Processing* **2005**, *80*, 753.
[48] Zhao, C.; Qu, S.; Qiu, J.; Zhu, C.; Hirao, K. *Chemistry Letters* **2003**, *32*, 602.
[49] Šmejkal, P, Šišková, K., Vlčková, B., Pfleger, J., Šloufová, I., Šlouf, M., Mojzeš, P. *Spectrochim. Acta A* **2003**, *59*, 2321.

[50] Simakin, A. V.; Voronov, V. V.; Shafeev, G. A.; Brayner, R.; Bozon-Verduraz, F. *Chem. Phys. Lett.* **2001,** *348*, 182.
[51] Chen, Y.-H., Yeh, C.-S. *Colloids and Surfaces A: Physicochem. Eng. Aspects* **2002,** *197*, 133.
[52] Pyatenko, A.; Shimokawa, K.; Yamaguchi, M.; Nishimura, O.; Suzuki, M. *Appl. Phys. A* **2004,** *79*, 803.
[53] Compagnini, G.; Scalisi, A. A.; Puglisi, O. *J. AppL. Phys.* **2003,** *94*, 7874.
[54] Kurita, H.; Takami, A.; Koda, S. *Appl. Phys. Lett.* **1998,** *72*, 789.
[55] Mafuné, F.; Kohno, J.-y.; Takeda, Y.; Kondow, T. *J. Phys. Chem. B* **2001,** *105*, 9050.
[56] Mafuné, F.; Kohno, J.-y.; Takeda, Y.; Kondow, T. *J. Phys. Chem. B* **2002,** *106*, 7575.
[57] Mafuné, F.; Kohno, J.-y.; Takeda, Y.; Kondow, T. *J. Phys. Chem. B* **2002,** *106*, 8555.
[58] Mortier, T.; Verbiest, T.; Persoons, A. *Chem. Phys. Lett.* **2003,** *382*, 650.
[59] Takami, A.; Kurita, H.; Koda, S. *J. Phys. Chem. B* **1999,** *103*, 1226.
[60] Simakin, A. V.; Voronov, V. V.; Kirichenko, N. A.; Shafeev, G. A. *Appl. Phys. A* **2004,** *79*, 1127.
[61] Gill, M.; Perrie, W.; Papworth, A.; Fox, P.; O'Neill, W. *Proceedings of SPIE* **2005,** *5713*, 560.
[62] Sylvestre, J.-P.; Poulin, S.; Kabashin, A. V.; Sacher, E.; Meunier, M.; Luong, J. H. T. *J. Phys. Chem. B*, **2004**; *108*, 16864.
[63] Mafuné, F.; Kohno, J.-y.; Takeda, Y.; Kondow, T. *J. Phys. Chem. B* **2000,** *104*, 8333.
[64] Ong, T. S.; Lee, S. S.; Van, L. H.; Hong, M. H.; Chong, T. C. *Proceedings of SPIE* **2004,** *5662*, 67.
[65] Mafuné, F.; Kohno, J.-y.; Takeda, Y.; Kondow, T. *J. Phys. Chem. B* **2001,** *105*, 5114.
[66] Kabashin, A. V.; Meunier, M.; Kingston, C.; Luong, J. H. T. *J. Phys. Chem. B* **2003,** *107*, 4527.
[67] Šišková, K., Vlčková, B., Turpin, P-Y, Fayet, C, Hromádková'J and Šlouf,M *Journal of Physics - accepted.*
[68] Watanabe, A. *Bull Inst. Chem. Res. Kyoto. University* **1960,** *38*, 179.
[69] Kamat, P. V., Flumiani, M., Hartland, G. V. *J. Phys. Chem.* B **1998,** *102*, 3123.
[70] Linnert, T. et al. *Ber. Bunsen-Ges. Phys. Chem.* **1991**, *95*, 838.
[71] Ahmadi, T. S. et al. *J. Phys. Chem.* **1996,** *100*, 8053.
[72] Hodak,J. H. et al. *J. Phys. Chem.,B* **1998,***102,*6958.
[73] Šmejkal,P. Pfleger, J.; Šišková, K.; Vlčková, B.; Dammer, O.; Šlouf, M. *Appl. Phys. A* **2004,** *79*, 1307.
[74] Mafuné, F.; Kohno, J.-y.; Takeda, Y.; Kondow, t. *J. Am. Chem. Soc. Commun.* **2003,** *125*, 1686.
[75] Takeda, Y.; Kondow, T.; Mafuné, F. *Nucleosides Nucleotides Nucleic Acids* **2005,** *24*, 1215.
[76] Takeda, Y.; Kondow, T.; Mafuné, F. *J. Phys. Chem. B Condens Matter Mater Surf Interfaces Biophys.* **2006,** *110*, 2393.
[77] Kneipp, K., Kneipp, H., Itzkan, I., Dasari, R.R., Feld, M.S. *Chem. Rev.* **1999,** *99,* 2957.
[78] Kneipp, K.; Wang, Y.; Dasari, R. R.; Feld, M. S. *Applied Spectroscopy* **1995,** *49*, 780.
[79] Collin, R. *Field theory of guided waves*, 2nd ed., Wiley: New York, **1990**
[80] Barnes, W. L.; Dereoux, A.; Ebbesen, T. W. *Nature* **2003**, *424*, 824.
[81] Kreibig, U.; Vollmer, M. *Optical Properties of Metal Clusters*; Springer-Verlag: Berlin, **1995.**
[82] Kreibig, U.; Gartz, M.; Hilger, A.; Hovel, H. In *Fine Particles Science and Technology*; Pelizzatti, E., Ed.; Kluwer Academic Publishers: Boston, **1996**; p. 499.
[83] Mulvaney, P. *Semiconductor NanoclusterssPhysical, Chemical and Catalytic Aspects*; Kamat, P. V., Meisel, D., Eds.; Elsevier Science: Amsterdam, **1997**; p 99.
[84] Creighton, J. A.; Eadon, D. G. *J.Chem.Soc. Faraday Trans.* **1991,** *87*, 3881.
[85] Mie, G. *Ann. Phys.* **1908**, *25*, 377.
[86] Gans, R. *Ann. Phys.* **1912,** *37*, 881.
[87] Link, S.; El-Sayed, M. *J. Phys. Chem. B* **1999,** *103*, 8410.
[88] Perez-Juste, J.; Pastoriza-Santos, I.; Liz-Marzan, L. M.; Mulvaney, P. *Coord. Chem. Re*V. **2005**, *249*, 1870.
[89] Mulvaney, P. *Langmuir* **1996**, *12*, 788.
[90] Mulvaney, P., Liz-Marza´n, L. M. *Top. Curr. Chem.* **2003**, *226*, 225.
[91] Mock, J. J., Barbic, M., Smith, D. R.; Schultz, D. A.; Schultz, S. *J. Chem. Phys.* **2002,** *116*, 6755.
[92] Liz-Marzan, L. *Langmuir* **2006**, *22*, 32.
[93] Henglein, A. *J.Phys.Chem.* **1993**, *97*, 5457.
[94] Maxwell Garnett, J. C. *Philos. Trans. R. Soc.* **1904**, *203*, 385.
[95] Maxwell Garnett, J. C. *Philos. Trans. R. Soc.* **1906**, *205*, 237.
[96] Bruggeman, D. A. G. *Ann. Phys.* **1935**, *24*, 636.
[97] Michaels, A. M.; Jiang, J.; Brus, L. *J. Phys. Chem. B* **2000**, *104*, 11965.
[98] Linnert, T., Mulvaney, P., Henglein, A. *J. Phys. Chem.* **1993**, *97*,679.
[99] Gutierrez, M., Henglein, A. *J. Phys. Chem.* **1993**, *97*, 11368.
[100] Sánchez-Cortés, S., García-Ramos, J. V., Morcillo, G., Tinti, A. *Journal of Colloid and Interface Science* **1995,** *175*, 358.
[101] Grochala, W., Kudelski, A., Bukowska, J. *JRS* **1998,** *29*, 681.
[102] Wang, C.-y.; Liu, C.-y.; Wang, M.; Shen, T. *Spectrochim. Acta A* **1999,** *55*, 991.
[103] Doering, W. E.; Nie, S. *J.Phys.Chem. B* **2002,** *106*, 311.
[104] Srnová-Šloufová, I., Vlčková, B., Snoeck, T. L., Stufkens, D. J., Matějka, P. *Inorg. Chem.* **2000,** *39*, 3551.
[105] Ma et al. *Chem. Phys. Chem. Commun.* **2004**, *5*, 713.
[106] Vlčková, B., Šloufová, I. *Nano Letters*, **2002,** *2*, 121.

[107] Aravind, Nitzan, Metiu, *Surf.Sci.* **1981**, *110*, 189.
[108] Xu, H., Aizpurua, J., Käll, M., Apell, P. *Phys. Rev. E,* **2000**, *62*, 4318.
[109] Xu, H., Kall, M. *J. Phys. Chem. B* **2003**, *4*, 1001.
[110] Michl, M.; Vlčková, B.; Šloufová, I.; Mojzeš, P. *Can. J. Anal. Sci. Spectrosc.* **2003,** *48,* 1.
[111] Srnová–Šloufová, I, Šišková, K.,Vlčková, B., Štěpánek, J. *Proceedings of XVIIIth ICORS* **2002**, 277.
[112] Srnová-Šloufová, I., Šišková, K., Vlčková, B., Štěpánek, J. – manuscript submitted for Langmuir.
[113] Birke, R.L., Lombardi, J.K. *Advances in laser spectroscopy; eds. Heyden & Sons., London,* **1982**, 290.
[114] Kneipp, K.; Wang, Y.; Kneipp, H.; Perelman, L. T.; Itzkan, I.; Dasari, R. R.; Feld, M. S. *Physical Review Letters* **1997,** *78*, 1667.
[115] Aravind P.K, Metiu H. *J. Phys. Chem.* **1982**, *86*: 5076.
[116] Aravind P.K, Metiu H. *Surf. Sci.* **1983**; *124,* 506.
[117] Liver N, Nitzan A, Gersten JI. *Chem. Phys. Lett.* **1984**; *111,* 449.
[118] Xu, H.; Wang, X.-H.; Persson, M. P.; Xu, H. *Phys. Rev. Letters* **2004,** *93,* No-243002.
[119] Käll, M.; Xu, H.; Johansson, P. *JRS* **2005,** *36*, 510.
[120] Markel VA, Shalaev VM, Zhang P, HuynhW, Tay L, Haslett TL, Moskovits M. *Phys. Rev. B* **1999**; *59*, 10.
[121] Moskovits M, Tay LL, Yang J, Haslett T. *Topics Appl. Phys.* **2002**; *82,* 215.
[122] Avnir, D. *The fractal approach to heterogeneous chemistry; surfaces, colloids, polymers,* J. Wiley&Sons Ltd., New York, **1989**.
[123] Shalaev VM. *Springer Tracts Mod. Phys.* **200**, *158*, 1.
[124] Shalaev VM. *Topics Appl. Phys.* **2002**, *82,* 113.
[125] Wang DS, Kerker M. *Phys. Rev. B* **1981**, *24*, 1777.
[126] Wang DS, Kerker M. *Phys. Rev. B* **1982**, *25,* 2433.
[127] Creighton, J. A. *Proceedings of International Symposium on Progress in Surface Raman Spectroscopy – Theory, Techniques and Applications,* **2000,** 11.
[128] Moskovits, M. *J. Mol. Catal.* **1993**, *82*, 195.
[129] Kim, M.; Itoh, K. *J. Phys. Chem.* **1987**, *91*, 126.
[130] Šloufová, I. *PhD Thesis, Charles University, Prague,* **2000.**
[131] Srnová, I.; Vlčková, B.; Němec, I.; Šlouf, M.; Štěpánek, J. *J. Mol. Struct.* **1999**, *482-483*, 213.
[132] Siskova, K. *Diploma Thesis, Charles University, Prague* **2003**.
[133] Strukl, J. S.; Walter, J. L. *Spectrochim. Acta,* **1971**, *27A*, 209.
[134] Mallick, P. K.; Danzer, G. D.; Strommen, D. P.; Kincaid, J. R. *J. Phys. Chem.* **1988**, *92*, 5628.
[135] Cotton, T. M. *The application of SERS to biological systems in Spectroscopy of Surfaces, Wiley&Sons, Chichester,* **1988**, 90.
[136] Vlčková, B.; Matějka, P.; Šimonová, J.; Čermáková, K.; Pančoška, P.; Baumruk, V. *J.Phys.Chem.* **1993,** *97*, 9719.
[137] Šmejkal, P.; Vlčková, B.; Procházka, M.; Mojzeš, P.; Pfleger, J. *Journal of Molecular Structure* **1999,** *482-483*, 225.
[138] Šmejkal, P.; Vlčková, B.; Procházka, M.; Mojzeš, P.; Pfleger, J. *Vibrational Spectroscopy* **1999,** *19*, 243.
[139] Vlčková, B.; Šmejkal, P.; Michl, M.; Procházka, M.; Mojzeš, P.; Lednický, F. , Pfleger, J. *Journal of Inorganic Biochemistry* **2000,** *79*, 295.
[140] Monaco, R. R.; Zhao, M. *Int. J. Quant. Chem.* **1993**, *46*, 701.
[141] Šišková, K.,Vlčková,B.,Mojzeš, P. *J. Mol. Struct.* **2005**, *744–747*, 265.
[142] Procházka, M.; Turpin, P.-Y.; Štěpánek, J.; Vlčková, B. *J.Raman Spectrosc.* **2002,** *33*, 758.
[143] Blom, N.; Odo, J.; Nakamoto, K.; Strommen, D. P. *J.Phys.Chem.* **1986,** *90*, 2847.
[144] Stein, P.; Ulman, A.; Spiro, T. G. *J. Phys. Chem.* **1984,** *88*, 369.
[145] Creighton, J. A. *Spectroscopy of Surfaces*, Wiley&Sons, Chichester, **1988**, 37.
[146] Moskovits, M., Suh, J.S. *J. Phys. Chem.* **1984**, *88*, 5526.
[147] Čermáková, K; Šesták, O., Matějka, P., Baumruk, V., Vlčková B. *Collect. Czech. Chem. Commun.* **1993**, *58*, 2682.
[148] Roy, D., Furtak, T.E. *Chem.Phys.Lett.* **1986**, *124*, 299.
[149] Hildebrandt, P., Stockburger, M. *J.Phys.Chem.* **1984**, *88,* 5935.
[150] Cotton, T.M., Schultz, S.G., Van Duyne, R.P. *J.Am.Chem.Soc.* **1982**, *104*, 6528.
[151] Šmejkal, P., *PhD Thesis, Charles University, Prague* **2005**
[152] Šišková,K., Vlčková, B., Turpin, P-Y., Fayet, C. - manuscript in preparation.
[153] Neddersen, J; Chumanov, J.; Cotton, T. M. *Appl. Spectrosc.* **1993,** *47*, 1959.
[154] Hanzlíková, J.; Procházka, M.; Štěpánek, J.; Bok, J.; Baumruk, V.; Anzenbacher, J., P. *J.Raman Spectrosc.* **1998,** *29*, 575.
[155] Procházka, M.; Mojzeš, P.; Vlčková, B.; Turpin, P.-Y. *J.Phys.Chem.* **1997,** *101*, 3161.
[156] Procházka, M.; Vlčková, B.; Štěpánek, J.; Turpin, P.-Y. *Langmuir* **2005,** *21*, 2956.
[157] Procházka, M.; Štěpánek, J.; Turpin, P.-Y.; Bok, J. *J. Phys.Chem. B* **2002,** *106*, 1543.
[158] Hecht, D.; Strehblow, H.H. *J. Electroanal. Chem.* **1997**, *440,* 211.
[159] Lee, P. C.; Meisel, D. *J. Phys. Chem.* **1982,** *86*, 3391.

[160] The pH calculation of H_3Citr solutions: with respect to the fact that neither of three pK_a values for citric acid can be neglected (pK_{a1}=3.13 , pK_{a2}=4.76 , pK_{a3}=6.40), the three equations should be taken into account:

$$K_1 = \frac{[H_2Citr^-]*[H_3O^+]}{[H_3Citr]},\ K_2 = \frac{[HCitr^{2-}]*[H_3O^+]}{[H_2Citr^-]},\ K_3 = \frac{[Citr^{3-}]*[H_3O^+]}{[HCitr^{2-}]}.$$

The initial citric acid concentration introduced into the solution is then present in forms of all its possible anions and in non-dissociated form as described by the following equation:

$$c_{citr} = [H_3Citr] + [H_2Citr^-] + [HCitr^{2-}] + [Citr^{3-}].$$

Furthermore, the electroneutrality of the solution should be obeyed and thus

$$[H_3O^+] = [H_2Citr^-] + \frac{1}{2}[HCitr^{2-}] + \frac{1}{3}[Citr^{3-}] + [OH^-].$$

The hydroxyl anions are coming from water autoprotolysis which is the last required equation

$$K_w = [H_3O^+]*[OH^-].$$

From six above written equations, the one equation for $[H_3O^+]$ can be expressed

$$\frac{1}{K_1K_2K_3}[H_3O^+]^5 + \frac{1}{K_2K_3}[H_3O^+]^4 + \left(\frac{1}{K_3} - \frac{K_w}{K_1K_2K_3} - \frac{c_{citr}}{K_2K_3}\right)[H_3O^+]^3 + \left(1 - \frac{K_w}{K_2K_3} - \frac{c_{citr}}{2*K_3}\right)[H_3O^+]^2 + \left(-\frac{K_w}{K_3} - \frac{c_{citr}}{3}\right)[H_3O^+] - K_w = 0$$

Then, this equation can be solved for the studied citric acid concentrations (c_{citr}=1x10^{-5} M;1x10^{-4} M;1x10^{-3} M; 1x10^{-2} M) by considering K_{a1}, K_{a2}, K_{a3} of citric acid and K_w = 1x10^{-14}, using the numerical calculation in MatLab program.

[161] Vohlídal, J., Julák, A., Štulík, K., *Chemické a analytické tabulky*, GRADA Publishing **1999**.

[162] Tongwen, X., Weihua, Y., *Chemical Engineering and Processing* **2002,** *41,* 519.

[163] Kobayashi; Y., Itoh, K.; *J.Phys.Chem.* **1985**, *89*, 5174.

[164] According to a very rough approximation that (i) the pyridyl groups of TPyP have nearly the same value of K_a as free pyridine (6.6x10^{-6}) for which the appropriate reaction can be written as:

$C_5H_5N^+$-H → $H^+ + C_5H_5N$

$$K_a = \frac{[C_5H_5N]*[H^+]}{[C_5H_5N^+H]};$$

and (ii) considering that all TPyP molecules are dissolved in solution, i.e. the maximal concentration value of pyridyl is 8x10^{-8} M (due to the fact that 4 pyridyl groups are encountered in each TPyP molecule):

$$c_{pyr} = [C_5H_5N] + [C_5H_5N^+H] = 8x10^{-8}.$$

Then, the concentration of protonized pyridyl groups can be calculated with respect to known pH values in H_3Citr-hydrosols (Table XXVI) according to this relation:

$$[C_5H_5N^+H] = \frac{c_{pyr}}{\left(\frac{K_a}{[H^+]} + 1\right)} = \frac{8x10^{-8}}{\left(\frac{6.6x10^{-6}}{10^{-pH}} + 1\right)}$$

As a result, the degree of protonization of pyridyl groups of TPyP in final systems can be estimated as:

$$\alpha = \frac{[C_5H_5N^+H]}{8x10^{-8}} * 100\%$$

While in the lowest citric acid concentration it is around 27%; in all other systems, the protonization of pyridyl groups is higher than 92% (the degree of protonization increases with H_3Citr concentration increase - more exactly: 92.5%, 98.6%, 99.6%, respectively). In other words, TPyP molecules should be more or less positively charged on their N atoms of substituents in citric acid-hydrosols.

[165] Akins, D. L.; Zhu, H.-R.; Guo, C. *J.Phys.Chem.* **1996,** *100*, 5420.

Abbreviations and terminology

Abbreviations:

APTPP = 5-(4-Aminophenyl)-10,15,20-triphenyl-21H,23H-porphine
BH_4^- = borohydride anions
bpy = 2,2'-bipyridine
EM mechanism = electromagnetic mechanism
FA = factor analysis
HR-TEM = high-resolution transmission electron microscopy
LA = laser ablation
LA/NF = laser ablation and nanoparticles fragmentation
LSPR = localized surface plasmon resonance
NCA = normal coordinate analysis
NF = nanoparticles fragmentation
NP = nanoparticle
NPs = nanoparticles
py group(s) = pyridyl group(s)
PSD = particle size distribution
RS = Raman scattering
RRS = resonance Raman scattering
SERS = surface-enhanced Raman scattering
SERRS = surface-enhance resonance Raman scattering
SPE = surface plasmon extinction
SPR = surface plasmon resonance
TAPP = 5,10,15,20-Tetrakis(4-aminophenyl)-21H,23H-porphine
TEM = transmission electron microscopy
THS = $S_2O_3^{2-}$ = thiosulphate anions
TMPP = 5,10,15,20-Tetra(4-methoxy-phenyl)-21H,23H-porphine
TMPyP = H_2TMPyP = 5,10,15,20-Tetrakis(1-methyl-4-pyridyl)-21H,23H-porphine
TPyP = 5,10,15,20-Tetra(4-pyridyl)-21H,23H-porphine

Terminology:

Adsorbate = a chemical species adsorbing on Ag nanoparticle surfaces
Agent = a chemical species influencing nanoparticles properties
Hydrosol = nanoparticles dispersed in aqueous solution
Organosol = nanoparticles dispersed in organic solution
Sol = (colloid) = solution containing nanoparticles
Ultrapure water = deionized water

– ***used throughout this Thesis:***

Ag NP hydrosol = Ag hydrosol = silver nanoparticles dispersed in aqueous solution (in general)
Agent(concentration)-Ag hydrosol = Ag NP hydrosol prepared by LA/NF in the presence of a particular agent of the concentration value (in the final system) marked in parenthesis;
- contains Ag NPs with chemically modified surfaces
w-Ag hydrosol = Ag NP hydrosol prepared by LA/NF in the presence of ultrapure water
System = the solution of Ag NP hydrosol with a particular type and amount of the selected agent, or adsorbate, or both:
Ag hydrosol/agent
Ag hydrosol/adsorbate
Ag hydrosol/agent/adsorbate
Ag hydrosol/adsorbate/agent
Agent-Ag hydrosol/adsorbate(concentration) = the addition of a particular adsorbate of the concentration (in the final system)marked in parenthesis to the Ag hydrosol prepared by LA/NF in the presence of a particular agent